# TABLE OF CONTENTS


| Section | Title | Page |
|---|---|---|
| 4.0 | REACTOR | |
| 4.1 | SUMMARY DESCRIPTION | 4.1-1 |
| 4.2 | MECHANICAL DESIGN | 4.2-1 |
| 4.2.1 | Fuel | 4.2-2 |
| 4.2.1.1 | Design Bases | 4.2-2 |
| 4.2.1.2 | Design Description | 4.2-5 |
| 4.2.1.3 | Design Evaluation | 4.2-9 |
| 4.2.1.4 | Tests and Inspections | 4.2-18 |
| 4.2.2 | Reactor Vessel Internals | 4.2-22 |
| 4.2.2.1 | Design Bases | 4.2-22 |
| 4.2.2.2 | Description and Drawings | 4.2-23 |
| 4.2.2.3 | Design Loading Conditions | 4.2-26 |
| 4.2.2.4 | Design Loading Categories | 4.2-27 |
| 4.2.2.5 | Design Criteria Basis | 4.2-28 |
| 4.2.3 | Reactivity Control System | 4.2-29 |
| 4.2.3.1 | Design Bases | 4.2-29 |
| 4.2.3.2 | Design Description | 4.2-32 |
| 4.2.3.3 | Design Evaluation | 4.2-42 |
| 4.2.3.4 | Tests, Verification, and Inspections | 4.2-52 |
| 4.2.3.5 | Instrumentation Applications | 4.2-55 |
| 4.3 | NUCLEAR DESIGN | 4.3-1 |
| 4.3.1 | DESIGN BASES | 4.3-1 |
| 4.3.1.1 | Fuel Burnup | 4.3-2 |
| 4.3.1.2 | Negative Reactivity Feedbacks (Reactivity Coefficient) | 4.3-2 |
| 4.3.1.3 | Control of Power Distribution | 4.3-3 |
| 4.3.1.4 | Maximum Controlled Reactivity Insertion Rate | 4.3-4 |
| 4.3.1.5 | Shutdown Margins With Vessel Head in Place | 4.3-4 |
| 4.3.1.6 | Shutdown Margin for Refueling | 4.3-5 |
| 4.3.1.7 | Stability | 4.3-5 |
| 4.3.1.8 | Anticipated Transients Without Trip | 4.3-6 |
| 4.3.2 | Description | 4.3-6 |
| 4.3.2.1 | Nuclear Design Description | 4.3-6 |
| 4.3.2.2 | Power Distributions | 4.3-8 |
| 4.3.2.3 | Reactivity Coefficients | 4.3-19 |
| 4.3.2.4 | Control Requirements | 4.3-23 |
| 4.3.2.5 | Control | 4.3-25 |
| 4.3.2.6 | Control Rod Patterns and Reactivity Worth | 4.3-27 |
| 4.3.2.7 | Criticality of Fuel Assemblies | 4.3-28 |
| 4.3.2.8 | Stability | 4.3-33 |
| 4.3.2.9 | Vessel Irradiation | 4.3-38 |

## TABLE OF CONTENTS


| Section | Title | Page |
|---|---|---|
| 4.3.3 | Analytical Methods | 4.3-38 |
| 4.3.3.1 | Fuel Temperature (Doppler) Calculations | 4.3-39 |
| 4.3.3.2 | Macroscopic Group Constants | 4.3-40 |
| 4.3.3.3 | Spatial Few-Group Diffusion Calculations | 4.3-41 |
| **4.4** | **THERMAL AND HYDRAULIC DESIGN** | **4.4-1** |
| 4.4.1 | Design Bases | 4.4-1 |
| 4.4.1.1 | Departure from Nucleate Boiling Design Basis | 4.4-1 |
| 4.4.1.2 | Fuel Temperature Design Basis | 4.4-2 |
| 4.4.1.3 | Core Flow Design Basis | 4.4-2 |
| 4.4.1.4 | Hydrodynamic Stability Design Bases | 4.4-3 |
| 4.4.1.5 | Other Considerations | 4.4-3 |
| 4.4.2 | Description | 4.4-3 |
| 4.4.2.1 | Summary Comparison | 4.4-3 |
| 4.4.2.2 | Fuel and Cladding Temperatures | 4.4-4 |
| 4.4.2.3 | Critical Heat Flux Ratio or Departure from Nucleate Boiling Ratio and Mixing Technology | 4.4-6 |
| 4.4.2.4 | Flux Tilt Considerations | 4.4-13 |
| 4.4.2.5 | Void Fraction Distribution | 4.4-14 |
| 4.4.2.6 | Core Coolant Flow Distribution | 4.4-14 |
| 4.4.2.7 | Core Pressure Drops and Hydraulic Loads | 4.4-14 |
| 4.4.2.8 | Correlation and Physical Data | 4.4-15 |
| 4.4.2.9 | Thermal Effects of Operational Transients | 4.4-17 |
| 4.4.2.10 | Uncertainties in Estimates | 4.4-18 |
| 4.4.2.11 | Plant Configuration Data | 4.4-20 |
| 4.4.3 | EVALUATION | 4.4-20 |
| 4.4.3.1 | Core Hydraulics | 4.4-20 |
| 4.4.3.2 | Influence of Power Distribution | 4.4-22 |
| 4.4.3.3 | Core Thermal Response | 4.4-24 |
| 4.4.3.4 | Analytical Techniques | 4.4-24 |
| 4.4.3.5 | Hydrodynamic and Flow Power Coupled Instability | 4.4-26 |
| 4.4.3.6 | Temperature Transient Effects Analysis | 4.4-28 |
| 4.4.3.7 | Potentially Damaging Temperature Effects During Transients | 4.4-29 |
| 4.4.3.8 | Energy Release During Fuel Element Burnout | 4.4-29 |
| 4.4.3.9 | Deleted | 4.4-30 |
| 4.4.3.10 | Fuel Rod Behavior-Effects from Coolant Flow Blockage | 4.4-30 |
| 4.4.4 | Testing and Verification | 4.4-31 |
| 4.4.4.1 | Tests Prior to Initial Criticality | 4.4-31 |
| 4.4.4.2 | Initial Power and Plant Operation | 4.4-31 |
| 4.4.4.3 | Component and Fuel Inspections | 4.4-32 |
| 4.4.5 | Instrumentation Application | 4.4-32 |
| 4.4.5.1 | Incore Instrumentation | 4.4-32 |
| 4.4.5.2 | Overtemperature and Overpower $^{a}T$ Instrumentation | 4.4-32 |
| 4.4.5.3 | Instrumentation to Limit Maximum Power Output | 4.4-33 |

## LIST OF TABLES


| Section | Title |
|---|---|
| Table 4.1-1 | Reactor Design Comparison Table |
| Table 4.1-2 | Analytic Techniques In Core Design |
| Table 4.1-3 | Design Loading Conditions For Reactor Core Components |
| Table 4.2-1 | Maximum Deflections Allowed for Reactor Internal Support Structures |
| Table 4.3-1 | Reactor Core Description (First Cycle) |
| Table 4.3-2 | Nuclear Design Parameters (First Cycle) |
| Table 4.3-3 | Reactivity Requirements for Rod Cluster Control Assemblies |
| Table 4.3-4 | Deleted by Amendment 40 |
| Table 4.3-5 | Axial Stability Index For A Pressurized Water Reactor Core With A 12 Foot Active Core Height |
| Table 4.3-6 | Typical Neutron Flux Levels (N/Cm2-Sec) At Full Power |
| Table 4.3-7 | Comparison Of Measured And Calculated Doppler Defects |
| Table 4.3-8 | Saxton Core II Isotopics Rod My, Axial Zone 6 |
| Table 4.3-9 | Critical Boron Concentrations, HZP, BOL |
| Table 4.3-10 | Comparison of Measured and Calculated Rod Worth |
| Table 4.3-11 | Comparison of Measured and Calculated Moderator Coefficients at HZP, BOL |
| Table 4.3-12 | Watts Bar Spent Fuel Storage Rack Design Basis Fuel Assembly Specifications |
| Table 4.3-13 | Deleted by Amendment 92 |
| Table 4.3-14 | Deleted by Amendment 92 |
| Table 4.3-15 | Deleted By Amendment 92 |
| Table 4.3-16 | Deleted By Amendment 92 |
| Table 4.4-1 | Thermal and Hydraulic Comparison Table |
| Table 4.4-2 | Deleted by Amendment 73 |
| Table 4.4-3 | Void Fractions At Nominal Reactor Conditions With Design Hot Channel Factors |
| Table 4.4-4 | Deleted by Amendment 73 |

## LIST OF TABLES

**Section** **Title**

THIS PAGE INTENTIONALLY BLANK

## LIST OF FIGURES


| Section | Title |
|---|---|
| Figure 4.2-1 | Fuel Assembly Cross Section 17 x 17 |
| Figure 4.2-2 | 17 x 17 Vantage 5H Recage Fuel Assembly |
| Figure 4.2-3 | Fuel Rod Schematic |
| Figure 4.2-4 | Mid Grid Expansion Joint Design-Plan View |
| Figure 4.2-5 | Elevation View of Mid Grid Guide Thimble Joint |
| Figure 4.2-6 | Guide Thimble to Bottom Nozzle Joint |
| Figure 4.2-7 | Top Grid to Nozzle Attachment |
| Figure 4.2-8 | Deleted by Amendment 73 |
| Figure 4.2-9 | Deleted by Amendment 73 |
| Figure 4.2-10 | Lower Core Support Assembly (Core Barrel Assembly) |
| Figure 4.2-11 | Upper Core Support Structure |
| Figure 4.2-12 | Support Column |
| Figure 4.2-13 | Plan View of Upper Core Support Structure |
| Figure 4.2-14 | Full Length Rod Cluster Control and Drive Rod Assembly with Interfacing Components |
| Figure 4.2-15 | Full Length Rod Cluster Control Assembly Outline |
| Figure 4.2-16 | Full Length Absorber Rod |
| Figure 4.2-17 | Deleted by Amendment 40 |
| Figure 4.2-18 | Burnable Absorber Assembly (Typical) |
| Figure 4.2-19 | Burnable Absorber Rod-Cross Section |
| Figure 4.2-19a | Wet Annular Burnable Absorber |
| Figure 4.2-20 | Primary Source Assembly (Typical) |
| Figure 4.2-21 | Encapsulated Secondary Source Assembly (Typical) |
| Figure 4.2-22 | Thimble Plug Assembly (Typical) |
| Figure 4.2-23 | Full Length Control Rod Drive Mechanism |
| Figure 4.2-24 | Full Length Control Rod Drive Mechanism Schematic |
| Figure 4.2-25 | Deleted by Amendment 40 |
| Figure 4.2-26 | Nominal Latch Clearance at Minimum and Maximum Temperature |
| Figure 4.2-27 | Control Rod Drive Mechanism Latch Clearance Thermal Effect |
| Figure 4.2-28 | Schematic Representation of Reactor Core Model |
| Figure 4.3-1 | Fuel Loading Arrangement, Cycle 1 |
| Figure 4.3-2 | Typical Production and Consumption of Higher Isotopes |
| Figure 4.3-3 | Typical Boron Concentratioll versus First Cycle Burnup With and Without Burnable Absorber Rods. |
| Figure 4.3-4 | Replaced By Figures 4.3-4a and 4.3-4b |
| Figure 4.3-4a | Burnable Absorber Rod Arrangement within an Assembly, Cycle 1 |
| Figure 4.3-4b | Burnable Absorber Rod Arrangement within an Assembly, Cycle 1 |
| Figure 4.3-5 | Burnable Absorber Loading Pattern, Cycle 1 |
| Figure 4.3-6 | Normalized Power Density Distribution at Beginning of Life, Unrodded Core, Hot Full Power, No Xenon for Cycle 1 |
| Figure 4.3-7 | Normalized Power Density Distribution at Beginning of Life, Unrodded Core, Hot Full Power, Equilibrium Xenon for Cycle 1 |
| Figure 4.3-8 | Normalized Power Density Dlistribution at Beginning of Life, Bank D 17% Inserted, Hot Full Power, Equilibrium Xenon for Cycle 1 |

## LIST OF FIGURES


| Section | Title |
|---|---|
| Figure 4.3-9 | Normalized Power Density Distribution at Middle of Life, Unrodded Core, Hot Full Power, Equllibrium Xenon for Cycle 1 |
| Figure 4.3-10 | Normalized Power Density Distribution at End of Life, Unrodded Core, Hot Full Power, Equilibrium Xenon for Cycle 1 |
| Figure 4.3-11 | Normalized Power Density Distribution at End of Life, Bank D 17% Inserted, Hot Full Power, Equilibrium Xenon for Cycle 1 |
| Figure 4.3-12 | Rodwise Power Distribution in a Typical Assembly Near Beginning of Life, Hot Full Power, Equilibrium Xenon, Unrodded Core |
| Figure 4.3-13 | Rodwise Power Distribution in a Typical Assembly Near End of Life, Hot Full Power, Equilibrium Xenon, Unrodded Core |
| Figure 4.3-14 | Typical Axial Power Shapes Occurring at Beginning of Life |
| Figure 4.3-15 | Typical Axial Power Shape:s Occurring at Middle of Life |
| Figure 4.3-16 | Typical Axial Power Shapes Occurring at End of Life |
| Figure 4.3-17 | Comparison of Assembly Axial Power Distribution With Core Average Axial Distribution, Bank D Slightly Inserted, Typical |
| Figure 4.3-18 | Flow Chart for Determining Spike Model |
| Figure 4.3-19 | Predicted Power Spike Due to Single Non-flattened Gap in the Adjacent Fuel (Typical) |
| Figure 4.3-20 | Power Spike Factor as a Function of Axial Position |
| Figure 4.3-21 | Normalized Maximum $F_Q$ x Power Versus Axial Height During Normal Operation |
| Figure 4.3-22 | Peak Linear Power During Control Rod Malfunction Overpower Transients |
| Figure 4.3-23 | Peak Linear Power During Boration/Dilution Overpower Transients (Typical) |
| Figure 4.3-24 | Comparison Between Calculated and Measured Relative Fuel Assembly Power Distribution (Typical) |
| Figure 4.3-25 | Comparison of Calculated and Measured Axial Shape (Typical) |
| Figure 4.3-26 | Measured Values of $F_Q$ for Full Power Rod Configurations (Typical) |
| Figure 4.3-27 | Doppler Temperature Coefficient at BOL and EOL Cycle 1, (Typical) |
| Figure 4.3-28 | Doppler - Only Power Coefficient - BOL, EOL, Cycle 1, (Typical) |
| Figure 4.3-29 | Doppler - Only Power Defect - BOL, EOL, Cycle 1, (Typical) |
| Figure 4.3-30 | Moderator Temperature Coefficient - BOL, Cycle 1, No Rods, (Typical) |
| Figure 4.3-31 | Moderator Temperature Coefficient - EOL, Cycle 1, (Typical) |
| Figure 4.3-32 | Moderator Temperature Coefficient as a Function of Boron Concentration - BOL Cycle 1, No Rods, (Typical) |
| Figure 4.3-33 | Moderator Temperature Coefficient During Cycle 1 at HFP, ARO Equilibrium Xenon, Critical Boron Condition, Typical |
| Figure 4.3-34 | Total Power Coefficient - BOL, EOL, Cycle 1, (Typical) |
| Figure 4.3-35 | Total Power Defect BOL, EOL, Cycle 1, Typical |
| Figure 4.3-36 | Rod Cluster Control Assembly Pattern |

## LIST OF FIGURES


| Section | Title |
|---|---|
| Figure 4.3-37 | Accidental Simultaneous Withdrawal of Two Control Banks EOL, HZP, Banks D and B Moving in the Same Plane, (Typical) |
| Figure 4.3-38 | Deleted by Amendment 73 |
| Figure 4.3-39 | Deleted by Amendment 73 |
| Figure 4.3-40 | Axial Offset versus Time PWR Core with a 12 ft. Height and 121 Assemblies |
| Figure 4.3-41 | XY Xenon Test Thermocouple Response Quadrant Tilt Difference versus Time |
| Figure 4.3-42 | Calculated and Measured Doppler Defect and Coefficients at BOL Two-Loop Plant, 121 Assemblies, 12 -felot Core |
| Figure 4.3-43 | Comparison of Calculatedancl Measured Boron Concentration for 2-Loop Plant, 121 Assemblies, 12-foot Core |
| Figure 4.3-44 | Comparison of Calculated and Measured $C_B$ 2-Loop with 121 Assemblies, l2-Foot Core |
| Figure 4.3-45 | Comparison of Calculated and Measured $C_B$ in 3-Loop Plant, 157 Assemblies, 12 -Foot Core |
| Figure 4.3-46 | Minimum Required Burnup for Unrestricted Storage of Spent Fuel of Various Initial Enrichments |
| Figure 4.3-47 | Minimum Required Burnup for 2x2 Checkerboard Arrangement of 2 Spent Fuel Assemblies with 2 New Fuel Assemblies of 5% Enrichment (Maximum) |
| Figure 4.3-48 | Spent Fuel Storage Rack $k^{oo}$ vs Temperature |
| Figure 4.3-49 | Spent Fuel Storage Rack $k^{oo}$ vs Water Density |
| Figure 4.4-1 | Peak Fuel Average and Surface Temperatures During Fuel Rod Lifetime versus Linear Power |
| Figure 4.4-2 | Peak Fuel Centerline Temperature During Fuel Rod Lifetime versus Linear Power |
| Figure 4.4-3 | Thermal Conductivity of $UO_2$ (Data Corrected to 95% Theoretical Density) |
| Figure 4.4-4 | Deleted by Amendment 73 |
| Figure 4.4-5 | Comparison of Measured versus Predicted Critical Heat Flux for the WRB-1 Correlation |
| Figure 4.4-6 | Deleted by Amendment 73 |
| Figure 4.4-7 | Deleted by Amendment 73 |
| Figure 4.4-8 | TDC Versus Reynolds Number for 26" Grid Spacing |
| Figure 4.4-9 | Normalized Radial Flow and Enthalpy Distribution at 4-ft. Elevation |
| Figure 4.4-10 | Normalized Radial Flow and Enthalpy Distribution at 8-ft. Elevation |
| Figure 4.4-11 | Normalized Radial Flow and Enthalpy Distribution at 12-ft. Elevation Core Exit |
| Figure 4.4-12 | Void Fraction Versus Thenoodynamic Quality $H-H_{SAT}/Hg-H_{SAT}$ |
| Figure 4.4-13 | Deleted by Amendment 73 |

## LIST OF FIGURES


| Section | Title |
|---|---|
| Figure 4.4-14 | Deleted by Amendment 73 |
| Figure 4.4-15 | Deleted by Amendment 73 |
| Figure 4.4-16 | Deleted by Amendment 73 |
| Figure 4.4-17 | Deleted by Amendment 46 |
| Figure 4.4-18 | Deleted by Amendment 46 |
| Figure 4.4-19 | Deleted by Amendment 46 |
| Figure 4.4-20 | Deleted by Amendment 63 |
| Figure 4.4-21 | Deleted by Amendment 63 |
| Figure 4.4-22 | Distribution of In-Core Instrumentation |
| Figure 4.4-23 | Typical DNBR Evaluation of 100% Power Shapes at Conditions Representative of Loss of Flow |

# 4.0 REACTOR

## 4.1 SUMMARY DESCRIPTION

This chapter describes 1) the mechanical components of the reactor and reactor core including the fuel rods and fuel assemblies, reactor internals, and the control rod drive mechanisms (CRDMs), 2) the nuclear design, and 3) the thermal-hydraulic design.

The reactor core is comprised of an array of fuel assemblies which are identical in mechanical design, but different in fuel enrichment. The reference design described herein employs three enrichments in a three-region core, whereas more enrichments may be employed for a particular refueling scheme.

The fuel design being described contains the structural features of the VANTAGE 5H (V5H) design with Standard (STD) fuel rods. The discussion in this chapter will refer to this design as the V5H.

The core is cooled and moderated by light water at a pressure of 2,250 psia in the Reactor Coolant System. The moderator coolant contains boron as a neutron absorber. The concentration of boron in the coolant is varied as required to control relatively slow reactivity changes including the effects of fuel burnup. Additional boron, in the form of burnable absorber rods, is employed as needed to decrease the moderator temperature coefficient and to control the power distribution.

Two hundred and sixty-four STD fuel rods are mechanically joined in a square array to form a fuel assembly. The fuel rods are supported in intervals along their length by grid assemblies which maintain the lateral spacing between the rods throughout the design life of the assembly. The grid assembly consists of an "egg-crate" arrangement of interlocked straps. The straps contain spring fingers and dimples for fuel rod support as well as coolant mixing vanes. The fuel rods consist of slightly enriched uranium dioxide ceramic cylindrical pellets contained in slightly cold worked Zircaloy-4 tubing which is plugged and seal welded at the ends to encapsulate the fuel. All fuel rods are pressurized with helium during fabrication to reduce stresses and strains to increase fatigue life.

The center position in the assembly is reserved for the incore instrumentation, while the remaining 24 positions in the array are equipped with guide thimbles joined to the grids and the top and bottom nozzles. Depending upon the position of the assembly in the core, the guide thimbles are used as channels for insertion of rod cluster control assemblies (RCCAs), neutron source assemblies, and burnable absorber rods. Otherwise, the guide thimbles are fitted with plugging devices to limit bypass flow.

The bottom nozzle is a box-like structure which serves as a bottom structural element of the fuel assembly and directs the coolant flow distribution to the assembly.

The top nozzle assembly functions as the upper structural element of the fuel assembly in addition to providing a partial protective housing for the RCCA or other components.

The RCCAs each consist of a group of individual neutron absorber rods fastened at the top end to a common hub or spider assembly. These assemblies contain full length neutron absorber material to control the reactivity of the core under operating conditions.

The CRDMs are of the magnetic jack type. Control rods are positioned by electro-mechanical (solenoid) action utilizing gripper latches, which engage grooved drive rods which in turn are coupled to the RCCAs. The CRDMs are so designed that upon a loss of electrical power to the coils, the RCCA is released and falls by gravity to shutdown the reactor.

The components of the reactor internals are divided into three parts consisting of the lower core support structure (including the entire core barrel and neutron shield pad assembly), the upper core support structure and the in-core instrumentation support structure. The reactor internals support the core, maintain fuel alignment, limit fuel assembly movement, maintain alignment between fuel assemblies and CRDMs, direct coolant flow past the fuel elements and to the pressure vessel head, provide gamma and neutron shielding, and provide guides for the incore instrumentation.

The nuclear design analyses and evaluation establish physical locations for control rods and burnable absorbers as well as physical parameters such as fuel enrichments and boron concentration in the coolant. This ensures that the reactor core has inherent characteristics which together with corrective actions of the reactor control and emergency cooling systems, provide adequate reactivity control. This control is maintained even if the highest reactivity worth RCCA is stuck in the fully withdrawn position (Stuck Rod Criterion).

The thermal-hydraulic design analyses and evaluation establish coolant flow parameters which assure that adequate heat transfer is provided between the fuel clad and the reactor coolant. The thermal design takes into account local variations in dimensions, power generation, flow distribution and mixing. The mixing vanes incorporated in the fuel assembly spacer grid design induce additional flow mixing between the various flow channels within a fuel assembly as well as between adjacent assemblies.

Instrumentation is provided to monitor the nuclear, thermal-hydraulic, and mechanical performance of the reactor and to provide inputs to automatic control functions.

Table 4.1-1 presents a comparison of the principal nuclear, thermal-hydraulic and mechanical design parameters between Watts Bar Units 1 and 2 and the W. B. McGuire Nuclear Station Units 1 and 2 (Docket Nos. 50-369 and 50-370).

The effects of fuel densification were evaluated with the methods described in Section 4.2.1.

The analysis techniques employed in the core design are tabulated in Table 4.1-2. The loading conditions considered in general for the core internals and components are tabulated in Table 4.1-3. Specific or limiting loads considered for design purposes of the various components are listed as follows: fuel assemblies in Section 4.2.1.1.2;

reactor internals in Section 4.2.2.3 and Table 5.2-2; neutron absorber rods, burnable absorber rods, neutron source rods and thimble plug assemblies in Section 4.2.3.1.3; and CRDMs in Section 4.2.3.1.4. The dynamic analyses, input forcing functions, and response loadings are presented in Section 3.9.

## REFERENCES

*(1)* Deleted by Amendment 73.

## Table 4.1-1 Reactor Design Comparison Table
(Page 1 of 3)

| | THERMAL AND HYDRAULIC DESIGN PARAMETERS | WATTS BAR | W. B. McGUIRE[d] UNITS 1 AND 2 |
|---|---|---|---|
| 1. | Reactor Core Heat Output, MWt | 3411 | 3411 |
| 2. | Reactor Core Heat Output, $10^6$ BTU/hr | 11,641.7 | 11,641.7 |
| 3. | Heat Generated in Fuel, % | 97.4 | 97.4 |
| 4. | System Pressure, Nominal, psia | 2250 | 2250 |
| 5. | System Pressure, Minimum Steady State, psia | 2204 | 2220 |
| 6. | Minimum Departure from Nucleate Boiling Ratio for Design Transients | >1.31 | >1.30 |
| | **COOLANT FLOW** | | |
| 7. | Total Thermal Flow Rate, $10^6$ $1b_m$/hr | 144.7 | 144.8 |
| 8. | Effective Flow Rate for Heat Transfer, $10^4$ lb/hr | 131.7 | 133.9 |
| 9. | Effective Flow Area for Heat Transfer, $ft^2$ | 51.3 | 51.1 |
| 10. | Average Velocity Along Fuel Rods, ft/sec | 15.4 | 16.6 |
| 11. | Average Mass Velocity, $10^6$ $lb_m$/hr-$ft^2$ | 2.57 | 2.62 |
| | **COOLANT TEMPERATURE, °F** | | |
| 12. | Nominal Inlet | 559.0 | 559.1 |
| 13. | Average Rise in Vessel | 58.4 | 58.2 |
| 14. | Average Rise in Core | 63.5 | 62.5 |
| 15. | Average in Core | 592.5 | 592.0 |
| 16. | Average in Vessel | 588.2 | 588.2 |
| | **HEAT TRANSFER** | | |
| 17. | Active Heat Transfer, Surface Area, $ft^2$ | 59,700 | 59,700 |
| 18. | Average Heat Flux, BTU/hr-$ft^2$ | 189,800 | 189,800 |
| 19. | Maximum Heat Flux for Normal Operation, BTU/hr-$ft^2$ | 455,520 | 440,300 |
| 20. | Average Thermal Output, kW/ft | 5.45[c] | 5.44 |
| 21. | Maximum Thermal Output for Normal Operation, kW/ft | 13.1 | 12.6 |
| 22. | Maximum Thermal Output at Maximum Overpower Trip Point (118% power), kW/ft | 21.1[a] | 18.0[a] |

**Table 4.1-1 Reactor Design Comparison Table**
**(Page 2 of 3)**

| | THERMAL AND HYDRAULIC DESIGN PARAMETERS | WATTS BAR | W. B. McGUIRE[d] UNITS 1 AND 2 |
|---|---|---|---|
| 23. | Heat Flux Hot Channel Factor, FQ | 2.4[b] | 2.32[b] |
| 24. | Peak Fuel Central Temperature at 100% Power,EF | 3160 | 3250 |
| 25. | Peak Fuel Central Temperature at Maximum Thermal Output for Maximum Overpower Trip Point, EF | 4500 | 4150 |
| | **CORE MECHANICAL DESIGN PARAMETERS** | | |
| | **FUEL ASSEMBLIES** | | |
| 26. | Design | RCC Canless | RCC Canless |
| 27. | Number of Fuel Assemblies | 193 | 193 |
| 28. | UO2 Rods per Assembly | 264 | 264 |
| 29. | Rod Pitch, in | 0.496 | 0.496 |
| 30. | Overall Dimensions, in | 8.426 x 8.426 | 8.426 x 8.426 |
| 31. | Fuel Weight (as UO2), lb | 222,645 | 222,739 |
| 32. | Clad Weight, lb | 46,994 | 50,913 |
| 33. | Number of Grids per Assembly | 8 | 8 - Type R |
| 34. | Loading Technique | 3 region modified checkerboard | 3 region modified checkerboard |
| | **FUEL RODS** | | |
| 35. | Number | 50,952 | 50,952 |
| 36. | Outside diameter, in | 0.374 | 0.374 |
| 37. | Diametral Gap, in | 0.0065 | 0.0065 |
| 38. | Clad Thickness, in | 0.0225 | 0.0225 |
| 39. | Clad Material | Zircaloy-4 | Zircaloy-4 |
| | **FUEL PELLETS** | | |
| 40. | Material | UO2 Sintered | UO2 Sintered |
| 41. | Density (% of Theoretical) | 94.5 | 95 |
| 42. | Diameter, in | 0.3225 | 0.3225 |
| 43. | Length, in | 0.530 | 0.530 |

## Table 4.1-1 Reactor Design Comparison Table
**(Page 3 of 3)**

| | | | |
|---|---|---|---|
| | **CORE MECHANICAL DESIGN PARAMETERS** | | |
| | **ROD CLUSTER CONTROL ASSEMBLIES** | | |
| 44. | Neutron Absorber, Full Length | B4C with Ag-In-Cd tips | Ag-In-Cd |
| 45. | Neutron Absorber, Part Length | N/A | N/A |
| 46. | Cladding Material | Type 304 SS-Cold Worked | Type 304 SS-Cold Worked |
| 47. | Clad Thickness, in | 0.0385 | 0.0185 |
| 48. | Number of Full Length Clusters | 57 | 53 |
| 49. | Number of Absorber Rods per Cluster | 24 | 24 |
| | **CORE STRUCTURE** | | |
| 50. | Core Barrel, I.D./O.D, in | 148.0/152.5 | 148.0/152.5 |
| 51. | Thermal Shield | Neutron Pad Design | Neutron Pad Design |
| | **STRUCTURE CHARACTERISTICS** | | |
| 52. | Core Diameter, in (Equivalent) | 132.7 | 132.7 |
| 53. | Core Height, in (Active Fuel) | 143.7 | 143.7 |
| | **REFLECTOR THICKNESS AND COMPOSITION** | | |
| 54. | Top - Water plus Steel, in | ~10 | ~10 |
| 55. | Bottom - Water plus Steel, in | ~10 | ~10 |
| 56. | Side - Water plus Steel in | ~15 | ~15 |
| 57. | H2O/U Molecular Ratio Core, Lattice (Cold) | 2.41 | 2.41 |
| | **FEED ENRICHMENT, W/O** | | |
| 58. | Region 1 | 2.10 | 2.10 |
| 59. | Region 2 | 2.60 | 2.60 |
| 60. | Region 3 | 3.10 | 3.10 |

Notes:

a. See Section 4.3.2.2.6

b. This is the value of FQ for normal operation.

c. Based on densified active fuel length (143.7 inches)

d. Cycle 1

## Table 4.1-2 Analytic Techniques In Core Design
**(Page 1 of 2)**

| Analysis | Technique | Computer Code | Section Referenced |
|---|---|---|---|
| Mechanical Design of Core Internals | | | |
| Loads, Deflections, and Stress Analysis | Static and Dynamic Modeling | Blowdown code, FORCE, Finite element structural analysis code, and others | 3.7.2.1<br>3.9.1<br>3.9.3 |
| Fuel Rod Design | | | |
| Fuel Performance Characteristics (temperature, internal pressure, clad stress, etc.) | Semi-empirical thermal model of fuel rod with consideration of fuel density changes, heat transfer, fission gas release, etc. | Westinghouse fuel design model | 4.2.1.3.1<br>4.3.3.1<br>4.4.2.2<br>4.4.3.4.2 |
| Nuclear Design | | | |
| 1. Cross Sections and Group Constants | Microscopic data<br>Macroscopic constants for homogenized core regions<br>Group constants for control rods with self-shielding | Modified ENDF/B library LEOPARD/ CINDER type or PHOENIX-P<br>HAMMER-AIM | 4.3.3.2<br>4.3.3.2<br>4.3.3.2 |
| 2. X-Y and X-Y-Z Power Distributions, Fuel Depletion, Critical Boron Concentrations, X-Y and X-Y-Z Xenon Distributions, Reactivity Coefficients | 2-D and 3-D, 2-Group Diffusion Theory | TURTLE<br>PALADON (2D OR 3D)<br>ANC (2D OR 3D)<br>THURTLE | 4.3.3.3 |
| Nuclear Design (Continued) | | | |
| 3. Axial Power Distributions, Control Rod Worths, and Axial Xenon Distribution | 1-D, 2-Group Diffusion Theory | APOLLO | 4.3.3.3 |
| 4. Fuel Rod Power | Integral Transport Theory | LASER | 4.3.3.1 |

## Table 4.1-2 Analytic Techniques In Core Design
**(Page 2 of 2)**

| Analysis | Technique | Computer Code | Section Referenced |
|---|---|---|---|
| 5. Effective Resonance Temperature | Monte Carlo Weighting Function | REPAD | |
| Thermal-Hydraulic Design | | | |
| 1. Steady-state | Subchannel analysis of local fluid conditions in rod bundles, including inertial and cross flow resistance terms, solution progresses from core-wide to hot assembly to hot channel | THINC-IV | 4.4.3.4.1 |
| 2. Transient Departure from Nucleate Boiling Analysis | Subchannel analysis of local fluid conditions in rod bundles during transients by including accumulation terms in conservation equations; solution is based on a five-channel model which simulates the whole core, including the hot assembly and hot subchannel | THINC-I (THINC-III) | 4.4.3.4.1 |

**Table 4.1-3 Design Loading Conditions For Reactor Core Components**

| | |
|---|---|
| 1. | Fuel Assembly Weight |
| 2. | Fuel Assembly Spring Forces |
| 3. | Internals Weight |
| 4. | Control Rod Trip (equivalent static load) |
| 5. | Differential Pressure |
| 6. | Spring Preloads |
| 7. | Coolant Flow Forces (static) |
| 8. | Temperature Gradients |
| 9. | Differences In Thermal Expansion |
| | a. Due to temperature differences |
| | b. Due to expansion of different materials |
| 10. | Interference Between Components |
| 11. | Vibration (mechanically or Hydraulically induced) |
| 12. | One Or More Loops Out Of Service |
| 13. | All Operational Transients Listed in Table 5.2-2 |
| 14. | Pump Overspeed |
| 15. | Seismic Loads (operation basis earthquake and design basis earthquake) |
| 16. | Blowdown Forces (injection transients for the cold and hot leg break) |

THIS PAGE INTENTIONALLY BLANK

## 4.2 MECHANICAL DESIGN

The plant conditions for design are divided into four categories in accordance with their anticipated frequency of occurrence and risk to the public: Condition I - Normal Operation and Operational Transients; Condition II - Faults of Moderate Frequency; Condition III - Infrequent Faults; Condition IV - Limiting Faults.

The reactor is designed so that its components meet the following performance and safety criteria:

*(1)* The mechanical design of the reactor core components and their physical arrangement, together with corrective actions of the reactor control, protection and emergency cooling systems (when applicable) assure that:

*(a)* Fuel damage [(1)] is not expected during Condition I and Condition II events. It is not possible, however, to preclude a very small number of rod failures. These are within the capability of the plant cleanup system and are consistent with plant design bases.

*(b)* The reactor can be brought to a safe state following a Condition III event with only a small fraction of fuel rods damaged although sufficient fuel damage might occur to preclude resumption of operation without considerable outage time.

*(c)* The reactor can be brought to a safe state and the core can be kept subcritical with acceptable heat transfer geometry following transients arising from Condition IV events.

*(2)* The fuel assemblies are designed to accommodate expected conditions for handling during assembly inspection and refueling operations, and shipping loads.

*(3)* The fuel assemblies are designed to accept control rod insertions in order to provide the required reactivity control for power operations and reactivity shutdown conditions.

*(4)* All fuel assemblies have provisions for the insertion of incore instrumentation necessary for plant operation.

*(5)* The reactor internals, in conjunction with the fuel assemblies, direct reactor coolant through the core to achieve acceptable flow distribution and to restrict bypass flow so that the heat transfer performance requirements can be met for all modes of operation. In addition, the internals provide core support and distribute coolant flow to the pressure vessel head so that the temperature differences between the vessel flange and head do not result in leakage from the flange during the Condition I and II events. Required inservice inspection can be carried out as the internals are removable and provide access to the inside of the pressure vessel.

---

*(1)* Fuel damage as used here is defined as penetration of the fission product barrier (i.e., the fuel rod clad).

## 4.2.1 Fuel

### 4.2.1.1 Design Bases

The fuel rod and fuel assembly design bases are established to satisfy the general performance and safety criteria presented in Section 4.2 and specific criteria noted below.

#### 4.2.1.1.1 Fuel Rods

The integrity of the fuel rods is ensured by designing to prevent excessive fuel temperatures, excessive internal rod gas pressures due to fission gas releases, and excessive cladding stresses and strains. This is achieved by designing the fuel rods so that the following conservative design bases are satisfied during Condition I and Condition II events over the fuel lifetime:

*(1)* Fuel Pellet Temperatures - The center temperature of the hottest pellet is to be below the melting temperature of the $UO_2$ (melting point of 5,080°F[1] unirradiated and decreasing by 58°F per 10,000 MWD/MTU). While a limited amount of center melting can be tolerated, the design conservatively precludes center melting. A calculated fuel centerline temperature of 4700°F has been selected as an overpower limit to assure no fuel melting. This provides sufficient margin for uncertainties as described in Sections 4.4.1.2 and 4.4.2.10.l.

*(2)* Internal Gas Pressure - The internal pressure of the lead rod (maximum internal pressure) in the reactor will be limited to a value below that which could cause, (1) the diametral gap to increase due to outward cladding creep during steady state operation and, (2) extensive DNB propagation to occur.

Reference [23] shows that the DNB propagation criteria is satisfied.

*(3)* Clad Stress - The effective clad stress is less than that which would cause general yield of the clad. While the clad has some capability for accommodating plastic strain, the yield strength has been accepted as a conservative design basis limit.

Radial, tangential, and axial stress components due to pressure differential and fuel clad contact pressure are combined into an effective stress using the maximum-distortion-energy theory. The Von Mises criterion is used to evaluate if the yield strength has been exceeded. Von Mises criterion states that an isotropic material under multiaxial stress will begin to yield plastically when the effective stress (i.e., combined stress using maximum-distortion-energy theory) becomes equal to the material yield stress in simple tension as determined by a uniaxial tensile test. Since general yielding is to be

prohibited, the volume average effective stress determined by integrating across the clad thickness is increased by an allowance for local non-uniformity effects before it is compared to the yield strength. The yield strength correlation is that appropriate for irradiated clad since the irradiated properties are attained at low exposure whereas the fuel/clad interaction conditions which can lead to minimum margin to the design basis limit always occurs at much higher exposure.

*(4)* Clad Tensile Strain - The clad tensile strain is less than one percent. This limit is consistent with proven practice.

*(5)* Strain Fatigue - The cumulative strain fatigue cycles are less than the design strain fatigue life. This basis is consistent with proven practice.

The STD fuel rods are designed for extended burnup operation using the NRC approved Westinghouse extended burnup design methods, models and criteria in References [25], [26], and [27]. The detailed fuel rod design establishes such parameters as pellet size and density, clad-pellet diametral gap, gas plenum size, and helium pre-pressure. The design also considers effects such as fuel density changes, fission gas release, clad creep, and other physical properties which vary with burnup.

Irradiation testing and fuel operational experience has verified the adequacy of the fuel performance and design bases. This is discussed in references [2], [3], and [27]. Fuel experience and testing results, as they become available, are used to improve fuel rod design and manufacturing processes and assure that the design bases and safety criteria are satisfied.

#### 4.2.1.1.2 Fuel Assembly Structure

Structural integrity of the fuel assemblies is assured by setting limits on stresses and deformations due to various loads and by determining that the assemblies do not interfere with the functioning of other components. Three types of loads are considered.

*(1)* Non-operational loads such as those due to shipping and handling.

*(2)* Normal and abnormal loads which are defined for Conditions I and II.

*(3)* Abnormal loads which are defined for Conditions III and IV.

These criteria are applied to the design and evaluation of the top and bottom nozzles, the guide thimbles, and grids and the thimble joints.

The design bases for evaluating the structural integrity of the fuel assemblies are:

*(1)* Non-operational - dimensional stability, under specified g loading.

*(2)* Normal Operation and Operational Transients (Condition I) and Faults of Moderate Frequency (Condition II).

For the normal operating and upset conditions (Conditions I and II, respectively), the fuel assembly component structural design criteria are classified into two material categories, namely austenitic steels and zircaloy. The stress categories and strength theory presented in the ASME Boiler and Pressure Vessel Code, Section III, are used as a general guide. The maximum shear-theory (Tresca criterion) for combined stresses is used to determine the stress intensities for the austenitic steel components. The stress intensity is defined as the numerically largest difference between the various principal stresses in a three dimensional field. The design stress intensity value ($S_m$) for austenitic steels, such as nickel-chromium-iron alloys, is given by the lowest of the following:

*(a)* 1/3 of the specified minimum tensile strength or 2/3 of the specified minimum yield strength at room temperature;

*(b)* 1/3 of the tensile strength or 90% of the yield strength at operating temperature but not to exceed 2/3 of the specified minimum yield strength at room temperature.

The stress intensity limits for the austenitic steel components are given below. All stress nomenclature is per the ASME Boiler and Pressure Vessel Code, Section III.

**Stress Intensity Limits**

| Categories | Limit |
|---|---|
| General Primary Membrane Stress Intensity | $S_m$ |
| Local Primary Membrane Stress Intensity | 1.5 $S_m$ |
| Primary Membrane plus Bending Stress Intensity | 1.5 $S_m$ |
| Total Primary plus Secondary Stress Intensity | 3.0 $S_m$ |

The zircaloy structural components which consist of guide thimbles, six inner grids, instrument tube, and fuel tubes are in turn subdivided into two categories because of material differences and functional requirements. The fuel tube design criteria is covered separately in Section 4.2.1.1.1. The maximum stress theory is also used to evaluate the guide thimble design. For conservative purposes, the zircaloy unirradiated properties are used to define the stress limits.

*(3)* Infrequent Faults (Condition III) and Limiting Faults (Condition IV).

Abnormal loads during Conditions III or IV - worst cases represented by combined seismic and blowdown loads.

*(a)* Deflections or failures of components cannot interfere with the reactor shutdown or emergency cooling of the fuel rods.

*(b)* The fuel assembly structural component stresses under faulted conditions are evaluated using primarily the methods outlined in Appendix F of the ASME Boiler and Pressure Vessel Code, Section III. Since the current analytical methods utilize linear elastic analysis, the stress allowables are defined as the smaller value of 2.4 $S_m$ or 0.70 $S_u$ for primary membrane and 3.6 $S_m$ or 1.05 $S_u$ for primary membrane plus primary bending. For the austenitic steel fuel assembly components, the stress intensity is defined in accordance with the rules described in the previous section for normal operating conditions. For the zircaloy components the stress intensity limits are set at two-thirds of the material yield strength, $S_y$, at reactor operating temperature. This results in zircaloy stress intensity limits being the smaller of 1.6 $S_y$ or 0.70 $S_u$ for primary membrane and 2.4 $S_y$ or 1.05 $S_u$ for primary membrane plus bending. For conservative purposes, the zircaloy unirradiated properties are used to define the stress limits.

The grid component strength criteria are based on experimental tests. The limit is established at $P_c$, where $P_c$ is the experimental collapse load determined at the 95% confidence level on the true mean, as taken from the distribution of grid crush test measurements.

### 4.2.1.2 Design Description

The VANTAGE 5H fuel assembly [28] and STD fuel rod design data are given in Table 4.3-1.

Two hundred and sixty four STD fuel rods, twenty four guide thimble tubes, and one instrumentation thimble tube are arranged within a supporting structure to form a fuel assembly. The instrumentation thimble is located in the center position and provides a channel for insertion of an incore neutron detector, if the fuel assembly is located in an instrumented core position. The guide thimbles provide channels for insertion of either a rod cluster control assembly, a neutron source assembly, a burnable absorber assembly or a plugging device, depending on the position of the particular fuel assembly in the core. Figure 4.2-1 shows a cross-section of the fuel assembly array, and Figure 4.2-2 shows a fuel assembly full length outline. The fuel rods are loaded into the fuel assembly structure so that there is clearance between the fuel rod ends and the reconstitutable top nozzle (RTN) and debris filter bottom nozzle (DFBN).

Each fuel assembly is installed vertically in the reactor vessel and stands upright on the lower core plate, which is fitted with alignment pins to locate and orient the assembly. After all fuel assemblies are set in place, the upper support structure is installed. Alignment pins, built into the upper core plate, engage and locate the upper

ends of the fuel assemblies. The upper core plate then bears downward against the fuel assembly top nozzle via the holddown springs to hold the fuel assemblies in place.

#### 4.2.1.2.1 Fuel Rods

The STD fuel rods consist of uranium dioxide ceramic pellets contained in slightly cold worked Zircaloy-4 tubing which is plugged and seal welded at the ends to encapsulate the fuel. A schematic of the fuel rod is shown in Figure 4.2-3. The fuel pellets are right circular cylinders consisting of slightly enriched uranium dioxide powder which has been compacted by cold pressing and then sintered to the required density. The ends of each pellet are dished slightly to allow greater axial expansion at the center of the pellets.

To avoid overstressing of the cladding or seal welds, void volume and clearances are provided within the rods to accommodate fission gases released from the fuel, differential thermal expansion between the cladding and the fuel, and fuel density changes during burnup. Shifting of the fuel within the cladding during handling or shipping prior to core loading is prevented by a stainless steel helical spring which bears on top of the fuel. During assembly the pellets are stacked in the cladding to the required fuel height, the spring is then inserted into the top end of the fuel tube and the end plugs pressed into the ends of the tube and welded. All fuel rods are internally pressurized with helium during the welding process in order to minimize compressive clad stresses and creep due to coolant operating pressures. The helium pre-pressurization may be different for each fuel region. Fuel rod pressurization is dependent on the planned fuel burnup as well as other fuel design parameters and fuel characteristics (particularly densification potential). The fuel rods are designed such that (1) the internal gas pressure of the lead rod will not exceed the value which causes the fuel-clad diametral gap to increase due to outward cladding creep during steady state operation, (2) extensive DNB propagation will not occur, (3) the cladding stress-strain limits (Section 4.2.1.1.1) are not exceeded for Condition I and II events, and (4) clad flattening will not occur during the fuel core life.

#### 4.2.1.2.2 Fuel Assembly Structure

The fuel assembly structure consists of a bottom nozzle, top nozzle, guide thimbles and grids, as shown in Figure 4.2-2.

**Bottom Nozzle**

The debris filter bottom nozzle (DFBN) is a box-like structure which serves as a bottom structural element of the fuel assembly and directs the coolant flow distribution to the assembly. The nozzle is designed to reduce the possibility of fuel rod damage attributed to debris-induced fretting. The square nozzle is fabricated from Type 304 stainless steel and consists of a perforated plate and four angle legs with bearing plates as shown in Figure 4.2-2. The legs form a plenum for the inlet coolant flow to the fuel assembly. The plate acts to prevent a downward ejection of the fuel rods from the fuel assembly. The bottom nozzle is fastened to the fuel assembly guide tubes by integral deformable locking cap screws which penetrate through the nozzle and mate with an inside fitting in each guide tube as shown in Figure 4.2-6.

Coolant flow through the fuel assembly is directed from the plenum in the bottom nozzle upward through the penetrations in the plate to the channels between the fuel rods. The penetrations in the plate are positioned between the rows of the fuel rods.

Axial loads (holddown) imposed on the fuel assembly and the weight of the fuel assembly are transmitted through the bottom nozzle to the lower core plate. Indexing and positioning of the fuel assembly is controlled by alignment holes in two diagonally opposite bearing plates which mate with locating pins in the lower core-plate. Any lateral loads on the fuel assembly are transmitted to the lower core plate through the locating pins.

**Top Nozzle**

The top nozzle assembly functions as the upper structural element of the fuel assembly in addition to providing a partial protective housing for the rod cluster control assembly or other components. It consists of an adapter plate, enclosure, top plate, and pads. The assembly has holddown springs mounted as shown in Figure 4.2-2. The springs and bolts are made of Inconel-718 and Inconel-600, respectively, whereas other components are made of Type 304 stainless steel.

The square adapter plate is provided with round and obround penetrations to permit the flow of coolant upward through the top nozzle. The ligaments in the plate cover the tops of the fuel rods and prevent their upward ejection from the fuel assembly. The enclosure is a metal shroud which sets the distance between the adapter plate and the top plate. The top plate has a large square hole in the center to permit access for the control rods and the control rod spiders. Holddown springs are mounted on the top plate and are fastened in place by bolts and clamps located at two diagonally opposite corners. On the other two corners, integral pads are positioned which contain alignment holes for locating the upper end of the fuel assembly.

In the VANTAGE 5H reconstitutable top nozzle design, a stainless steel nozzle insert is mechanically connected to the top nozzle adapter plate by means of a pre-formed circumferential bulge near the top of the insert. The insert engages a mating groove in the wall of the adapter plate thimble tube thru-hole. The insert has four (4) equally spaced axial slots which allow the insert to deflect inwardly at the elevation of the bulge, thus permitting the installation or removal of the nozzle. The insert bulge is positively held in the adapter plate mating groove by placing a lock tube with a uniform ID identical to that of the thimble tube into the insert.

To remove the top nozzle, a tool is first inserted through a lock tube and expanded radially to engage the bottom edge of the tube. An axial force is then exerted on the tool which overrides the local lock tube deformations and withdraws the lock tube from the insert. After the lock tubes have been withdrawn, the nozzle is removed by raising it off the upper slotted ends of the nozzle inserts which deflect inwardly under the axial lift load. With the top nozzle removed, direct access is provided for fuel rod examinations or replacement. Reconstitution is completed by the remounting of the nozzle and the insertion of lock tubes. The design bases and evaluation of the reconstitutable top nozzle are given in Section 2.3.2 in Reference [28].

### Guide Thimble and Instrument Tube

The guide thimbles are structural members which also provide channels for the neutron absorber rods, burnable absorber rods, neutron source rods, or thimble plugs. Each one is fabricated from Zircaloy-4 tubing having two different diameters. The larger diameter at the top provides a relatively large annular area to permit rapid insertion of the control rods during a reactor trip as well as to accommodate the flow of coolant during normal operation. The lower portion of the guide thimbles has a reduced diameter to produce a dashpot action near the end of the control rod travel during a reactor trip. Four holes are provided on the thimble tube above the dashpot to reduce the rod drop time. The dashpot is closed at the bottom by means of an end plug which is provided with a small flow port to avoid fluid stagnation in the dashpot volume during normal operation and to accommodate the outflow of water from the dashpot during a reactor trip. The lower end of the guide thimble is fitted with an end plug which is then fastened into the bottom nozzle by an integral locking cap screw. In the VANTAGE 5H design, the top end of the guide thimbles are fastened to a tubular nozzle insert sleeve by three expansion swages. The inserts engage into mating grooves in the top nozzle adapter plate as shown in Figure 4.2-7.

For the VANTAGE 5H design, each grid is fastened to the guide thimble assemblies to create an integrated structure. The fastening method depicted in Figures 4.2-4 and 4.2-5 is used for all but the top and bottom grids in the VANTAGE 5H assembly.

An expanding tool is inserted into the inner diameter of the Zircaloy thimble tube at the elevation of stainless steel sleeves that have been brazed/welded into the Inconel grid assembly. In the VANTAGE 5H design, these mid grid sleeves are made of Zircaloy and are laser welded to the Zircaloy grid assemblies. The multi-lobed tool forces the thimble and sleeve outward to a predetermined diameter, thus joining the two components.

The bottom grid assembly is joined to the assembly as shown in Figure 4.2-6. The stainless steel insert is attached to the bottom grid and later captured between the guide thimble end plug and the bottom nozzle by means of a stainless steel thimble screw.

The described methods of grid fastening are standard and have been used successfully since the introduction of Zircaloy guide thimbles in 1969.

The central instrumentation tube of each fuel assembly is constrained by seating in counterbores in each nozzle. This tube is a constant diameter and guides the incore neutron detectors. Sufficient diametral clearance exists for the flux thimble to traverse the tube without binding. Instrumentation tubes are expanded at the top and mid grids in the same manner as the previously discussed expansion of the guide thimbles to the grids.

### Grid Assemblies

The fuel rods, as shown in Figure 4.2-2, are supported at intervals along their length by structural grid assemblies which maintain the lateral spacing between the rods.

Each fuel rod is supported laterally within each grid cell by a combination of support dimples and springs (six support locations per cell; i.e, four dimples and two springs). The magnitude of grid spacing spring force on the fuel rods is set high enough to minimize possible fretting, without overstressing the cladding at the contact points. All grid assemblies allow axial thermal expansion of the fuel rods without imposing restraint sufficient to develop buckling or distortion.

The top and bottom (non-mixing vanes) grids are made of Inconel 718 strap materials, chosen for its strength and high corrosion resistance. The six intermediate (mixing vane) grids of the VANTAGE 5H design are made of Zircaloy straps (chosen for its low neutron absorption properties). Inner straps include mixing vanes which project into the coolant stream and promote mixing of the coolant in the high heat flux region of the assemblies.

All grid assemblies consist of individual slotted straps assembled in an interlocking "egg-crate" arrangement. Zircaloy grid strap joints and grid/sleeve joints are fabricated by laser welding, whereas all Inconel grid joints are brazed. The outside straps on all grids contain mixing vanes which, in addition to their mixing function, aid in guiding the grids and fuel assemblies past projecting surfaces during handling or during loading and unloading of the core.

### 4.2.1.3 Design Evaluation

### 4.2.1.3.1 Fuel Rods

The STD fuel rods are designed to assure the design bases are satisfied for Condition I and II events. This assures that the fuel performance and safety criteria (Section 4.2) are satisfied.

**Materials - Fuel Cladding**

The desired fuel rod clad is a material which has a superior combination of neutron economy (low absorption cross section), high strength (to resist deformation due to differential pressures and mechanical interaction between fuel and clad), high corrosion resistance (to coolant, fuel and fission products), and high reliability. Zircaloy-4 has this desired combination of clad properties. As shown in reference [3], there is considerable PWR operating experience on the capability of Zircaloy as a clad material. Clad hydriding has not been a significant cause of clad perforation since current controls on fuel contained moisture levels were instituted[3].

Metallographic examination of irradiated commercial fuel rods has shown occurrences of fuel/clad chemical interaction. Reaction layers of < 1 mil in thickness have been observed between fuel and clad at limited points around the circumference. Westinghouse metallographic data indicates that this interface layer remains very thin even at high burnup. Thus, there is no indication of propagation of the layer and eventual clad penetration.

Stress corrosion cracking is another postulated phenomenon related to fuel/clad chemical interaction. Reactor tests have shown that in the presence of high clad

tensile stresses, large concentrations of iodine can chemically attack the Zircaloy tubing and can lead to eventual clad cracking. Westinghouse has no evidence that this mechanism is operative in commercial fuel.

**Materials - Fuel Pellets**

Sintered, high density uranium dioxide fuel chemically reacts only slightly with the clad, at core operating temperatures and pressures. In the event of clad defects, the high resistance of uranium dioxide to attack by water protects against fuel deterioration although limited fuel erosion can occur. As has been shown by operating experience and extensive experimental work, the thermal design parameters conservatively account for changes in the thermal performance of the fuel elements due to pellet fracture which may occur during power operation. The consequences of defects in the clad are greatly reduced by the ability of uranium dioxide to retain fission products including those which are gaseous or highly volatile. Observations from several operating Westinghouse PWRs [2] and [3] has shown that fuel pellets can densify under irradiation to a density higher than the manufactured values. Fuel densification and subsequent incomplete settling of the fuel pellets results in local and distributed gaps in the fuel rods.

An extensive analytical and experimental effort has been conducted by Westinghouse to characterize the fuel densification phenomenon and identify improvements in pellet manufacturing to eliminate or minimize this anomaly [5] and [3].

The effects of fuel densification have been taken into account in the nuclear and thermal hydraulic design of the reactor described in Sections 4.3 and 4.4, respectively.

**Materials - Strength Considerations**

One of the most important limiting factors in fuel element duty is the mechanical interaction of fuel and clad. This fuel/clad interaction produces cyclic stresses and strains in the clad, and these in turn deplete clad fatigue life. The reduction of fuel/clad interaction is therefore a principal goal of design. In order to achieve this goal and to enhance the cyclic operational capability of the fuel rod, the technology for using pre-pressurized fuel rods in Westinghouse PWRs has been developed.

Initially the gap between the fuel and clad is sufficient to prevent hard contact between the two. However, during power operation a gradual compressive creep of the clad onto the fuel pellet occurs due to the external pressure exerted on the rod by the coolant. Clad compressive creep eventually results in hard fuel/clad contact. During this period of fuel/clad contact, changes in power level could result in significant changes in clad stresses and strains. By using pre-pressurized fuel rods to partially offset the effect of the coolant external pressure, the rate of clad creep toward the surface of the fuel is reduced. Fuel rod pre-pressurization delays the time at which substantial fuel/clad interaction and hard contact occur and hence significantly reduces the number and extent of cyclic stresses and strains experienced by the clad both before and after fuel/clad contact. These factors result in an increase in the fatigue life margin of the clad and lead to greater clad reliability. If gaps should form in the fuel

stacks, clad flattening will be prevented by the rod pre-pressurization so that the flattening time will be greater than the fuel core life.

A two dimensional (r,θ) finite element model has been established to investigate the effects of radial pellet cracks on stress concentrations in the clad. Stress concentration, herein, is defined as the difference between the maximum clad stress in the θ direction and the mean clad stress. The first case has the fuel and clad in mechanical equilibrium and as a result the stresses in the clad are close to zero. In subsequent cases the pellet power is increased in steps and the resultant fuel thermal expansion imposes tensile stress in the clad. In addition to uniform clad stresses, stress concentrations develop in the clad adjacent to radial cracks in the pellet. These radial cracks have a tendency to open during a power increase but the frictional forces between fuel and clad oppose the opening of these cracks and result in localized increases in clad stress. As the power is further increased, large tensile stresses exceed the ultimate tensile strength of $U0_2$, additional cracks in the fuel are created which limits the magnitude of the stress concentration in the clad.

As part of the standard fuel rod design analysis, the maximum stress concentration evaluated from finite element calculations is added to the volume averaged effective stress in the clad as determined from one dimensional stress/strain calculations. The resultant clad stress is then compared to the temperature dependent Zircaloy yield stress.

**Steady-State Performance Evaluation**

In the calculation of the steady-state performance of a nuclear fuel rod, the following interacting factors must be considered:

*(1)* Clad creep and elastic deflection.

*(2)* Pellet density changes, thermal expansion, gas release, and thermal properties as a function of temperature and fuel burnup.

*(3)* Internal pressure as a function of fission gas release, rod geometry, and temperature distribution.

These effects are evaluated using an overall fuel rod design model[4]. The model modifications for time dependent fuel densification are given in reference [5]. With these interacting factors considered, the model determines the fuel rod performance characteristics for a given rod geometry, power history, and axial power shape. In particular, internal gas pressure, fuel and clad temperatures, and clad deflections are calculated. The fuel rod is divided lengthwise into several sections and radially into a number of annular zones. Fuel density changes, clad stresses, strains and deformations, and fission gas releases are calculated separately for each segment. The effects are integrated to obtain the internal rod pressure.

The initial rod internal pressure is selected to delay fuel/clad mechanical interaction and to avoid the potential for flattened rod formation. It is limited however, by the rod internal pressure design basis given in Section 4.2.1.1.1. The plenum height of the fuel

rod has been designed to ensure that the maximum internal pressure of the fuel rod will not exceed the value which would cause the fuel clad diametral gap to increase during steady-state operation.

The gap conductance between the pellet surface and the clad inner diameter is calculated as a function of the composition, temperature, and pressure of the gas mixture, and the gap size or contact pressure between clad and pellet. After computing the fuel temperature for each pellet annular zone, the fractional fission gas release is calculated based on local fuel temperature and burnup. The total amount of gas released is based on the average fractional release within each axial and radial zone and the gas generation rate which is a function of burnup. Finally, the gas released is summed over all zones and the pressure is calculated.

The model shows good agreement in fit for a variety of published and proprietary data on fission gas release, fuel temperatures and clad deflections [25,26]. Included in this spectrum are variations in power, time, fuel density, and geometry. The in-pile fuel temperature measurement comparisons used are referenced in Section 4.4.2.2.

Initially, the gap between the fuel and cladding is sufficient to prevent hard contact between the two. However, during power operation a gradual compressive creep of the cladding onto the fuel pellet occurs due to the external pressure exerted on the rod by the coolant. Cladding compressive creep eventually results in fuel/clad contact. During this period of fuel/clad contact, changes in power level could result in changes in cladding stresses and strains. By using prepressurized fuel rods to partially offset the effect of the coolant external pressure, the rate of cladding creep toward the surface of the fuel is reduced. Fuel rod prepressurization delays the time at which fuel/clad contact occurs and hence, significantly reduces the number and extent of cyclic stresses and strains experienced by the cladding both before and after fuel/clad contact. These factors result in an increase in the fatigue life margin of the cladding and lead to greater cladding reliability. If gaps should form in the fuel stacks, cladding flattening will be prevented by the rod pre-pressurization so that the flattening time will be greater then the fuel core life.

The clad stresses at a constant local fuel rod power are low. Compressive stresses are created by the pressure differential between the coolant pressure and the rod internal gas pressure. Because of the pre-pressurization with helium, the volume average effective stresses are always less than approximately 15,000 psi at the pressurization level used in this fuel rod design. Stresses due to the temperature gradient are not included in this average effective stress because thermal stresses are, in general, negative at the clad inside diameter and positive at the clad outside diameter and their contribution to the clad volume average stress is small. Furthermore, the thermal stress decreases with time during steady-state operation due to stress relaxation. The stress due to pressure differential is highest in the minimum power rod at the beginning-of-life (due to low internal gas pressure) and the thermal stress is highest in the maximum power rod (due to steep temperature gradient).

Tensile stresses could be created once the clad has come in contact with the pellet. These stresses would be induced by the fuel pellet swelling during irradiation. There

is very limited clad pushout after pellet-clad contact. Fuel swelling can result in small clad strains (< 1%) for expected discharge burnups but the associated clad stresses are very low because of clad creep (thermal and irradiation-induced creep). Furthermore, the 1 percent strain criterion is extremely conservative for fuel-swelling driven clad strain because the strain rate associated with solid fission products swelling is very slow (~5x $10^{-7}$ $hr^{-1}$). In-pile experiments[30] have shown that zircaloy tubing exhibits "super-plasticity" at slow strain rates during neutron irradiation. Uniform clad strains of >10% have been achieved under these conditions with no sign of plastic instability.

Pellet thermal expansion due to power increases is considered the only mechanism by which significant stresses and strains can be imposed on the clad. Power increases in commercial reactors can result from fuel shuffling (e.g., Region 3 positioned near the center of the core for Cycle 2 operation after operating near the periphery during Cycle 1), reactor power escalation following extended reduced power operation, and control rod movement. In the mechanical design model, lead rods are depleted using best estimate power histories as determined by core physics calculations. During the depletion, the amount of diametral gap closure is evaluated based upon the pellet expansion-cracking model, clad creep model, and fuel swelling model. At various times during the depletion the power is increased locally on the rod to the burnup dependent attainable power density as determined by core physics calculations. The radial, tangential, and axial clad stresses resulting from the power increases are combined into a volume average effective clad stress.

The von Mises criterion is used to evaluate if the clad yield stress has been exceeded. This criterion states that an isotropic material in multiaxial stress will begin to yield plastically when the effective stress exceeds the yield stress as determined by a uniaxial tensile test. The yield stress correlation is that for irradiated cladding since fuel/clad interaction occurs at high burnup. Furthermore, the effective stress is increased by an allowance, which accounts for stress concentrations in the clad adjacent to radial cracks in the pellet, prior to the comparison with the yield stress. This allowance was evaluated using a two-dimensional ($r,\Theta$) finite element model.

Slow transient power increases can result in large clad strains without exceeding the clad yield stress because of clad creep and stress relaxation. Therefore, in addition to the yield stress criterion, a criterion on allowable clad positive strain is necessary. Based upon high strain rate burst and tensile test data on irradiated tubing, 1% strain was determined to be the lower limit on irradiated clad ductility and thus adopted as a design criterion.

In addition to the mechanical design models and design criteria, Westinghouse relies on performance data accumulated through transient power test programs in experimental and commercial reactors, and through normal operation in commercial reactors.

It is recognized that a possible limitation to the satisfactory behavior of the fuel rods in a reactor which is subjected to daily load follow is the failure of the cladding by low cycle strain fatigue. During their normal residence time in reactor, the fuel rods may

be subjected to −1000 cycles or more with typical changes in power level from 50 to 100% of their steady-state values.

The assessment of the fatigue life of the fuel rod cladding is subjected to a considerable uncertainty due to the difficulty of evaluating the strain range which results from the cyclic interaction of the fuel pellets and claddings. This difficulty arises, for example, from such highly unpredictable phenomena as pellet cracking, fragmentation, and relocation. Nevertheless, since early 1968, Westinghouse has been investigating this particular phenomenon both analytically and experimentally. Strain fatigue tests on irradiated and nonirradiated hydrided Zr-4 claddings were performed which permitted a definition of a conservative fatigue life limit and recommendation of a methodology to treat the strain fatigue evaluation of the Westinghouse reference fuel rod designs.

However, Westinghouse is convinced that the final proof of the adequacy of a given fuel rod design to meet the load follow requirements can only come from in-pile experiments performed on actual reactors. The Westinghouse experience in load follow operation dates back to early 1970 with the load follow operation of the Saxton reactor. Successful load follow operation has been performed on Point Beach unit 1 (300 load follow cycles) and Point Beach unit 2 (150 load follow cycles). In both cases, there was no significant coolant activity increase that could be associated with the load follow mode of operation. Reference [3] provides the most recent experience with Westinghouse fuel rod designs.

The following paragraphs present briefly the Westinghouse analytical approach to strain fatigue.

A comprehensive review of the available strain-fatigue models was conducted by Westinghouse as early as 1968.

This included the Langer-O'Donnel model[9], the Yao-Munse model, and the Manson-Halford model. Upon completion of this review and using the results of the Westinghouse experimental programs discussed below, it was concluded that the approach defined by Langer-O'Donnel would be retained and the empirical factors of their correlation modified in order to conservatively bound the results of the Westinghouse testing program.

The Langer-O'Donnel empirical correlation has the following form:

$$S_a = \frac{E}{4\sqrt{N_f}} \ln \frac{(100)}{100 - RA} + S_e$$

where:

$S_a$ = 1/2 E $\Delta\varepsilon t$ = pseudo-stress amplitude which causes failure in $N_f$ cycles (lb/in$^2$)
$\varepsilon_t$ = total strain range (in/in)
E = Young's Modulus (lb/in$^2$)
$N_f$ = number of cycles to failure
RA = reduction in area at fracture in a uniaxial tensile test (%)
$S_e$ = endurance limit (lb/in$^2$)

Both RA and $S_e$ are empirical constants which depend on the type of material, the temperature and irradiation. The Westinghouse testing program was subdivided in the following subprograms:

*(1)* A rotating bend fatigue experiment on unirradiated Zircaloy-4 specimens at room temperature and at 725°F. Both hydrided and non-hydrided Zircaloy-4 cladding were tested.

*(2)* A biaxial fatigue experiment in gas autoclave on unirradiated Zircaloy-4 cladding, both hydrided and nonhydrided.

*(3)* A fatigue test program on irradiated cladding from the CVTR and Yankee Core V conducted at Battelle Memorial Institute.

The results of these test programs provided information on different cladding conditions including the effect of irradiation, of hydrogen level, and of temperature.

The Westinghouse design equations followed the concept for the fatigue design criterion according to the ASME Boiler and Pressure Vessel Code, Section III. Namely,

*(1)* The calculated pseudo-stress amplitude ($S_a$) has to be multiplied by a factor of 2 in order to obtain the allowable number of cycles ($N_f$).

*(2)* The allowable cycles for a given $S_a$ is 5% of $N_f$, or a safety factor of 20 on cycles.

The lesser of the two allowable number of cycles is selected. The cumulative fatigue life fraction is then computed as:

$$\sum_{1}^{k} \frac{n_k}{N_{fk}} \leq 1$$

where:

$n_k$ = number of diurnal cycles of mode k.

The potential effects of operation with waterlogged fuel are discussed in Section 4.4.3.6. Waterlogging is not considered to be a concern during operational transients.

**Rod Bowing**

Reference [10] presents the model used for evaluation of fuel rod bowing. To the present time this model has been used for bow assessment in 14 x 14, 15 x 15, and 17 x 17 type cores.

### 4.2.1.3.2 Fuel Assembly Structure

**Stresses and Deflections**

The potential sources of high stresses in the assembly are avoided by the design. For example, stresses in the fuel rod due to thermal expansion and zircaloy irradiation growth are limited by the relative motion of the rod as it slips over the grid spring and dimple surfaces. Clearances between the fuel rod ends and nozzles are provided so that Zircaloy irradiation growth will not result in end interferences. Stresses in the fuel assembly caused by tripping of the rod cluster control assembly have little influence on fatigue because of the small number of events during the life of an assembly. Assembly components and prototype fuel assemblies made from production parts have been subjected to structural tests to verify that the design bases requirements are met [7].

The fuel assembly design loads for shipping are established and accelerometers are permanently placed into the shipping cask to monitor, and detect fuel assembly accelerations that would result from loads in excess of the criteria. Past history and experience has indicated that loads which exceeded the allowable limits rarely occur. Exceeding the limits requires reinspection of the fuel assembly for damage. Tests on various fuel assembly components such as the grid assembly, sleeves, inserts and structure joints have been performed to assure that the shipping design limits do not result in impairment of fuel assembly function. The methodology for the seismic analysis of the fuel assembly is presented in References [7], [24], and [28].

**Dimensional Stability**

A prototype fuel assembly has been subjected to column loads in excess of those expected in normal service and faulted conditions [7][28].

The coolant flow channels are established and maintained by the structure composed of grids and guide thimbles. The lateral spacing between fuel rods is provided and controlled by the support dimples of adjacent grid cells. Contact of the fuel rods on the dimples is maintained through the clamping force of the grid springs. Lateral motion of the fuel rods is opposed by the spring force and the internal moments generated between the spring and the support dimples. Grid testing is discussed in References [7] and [28].

No interference with control rod insertion into thimble tubes will occur during a postulated loss of coolant accident transient due to fuel rod swelling, thermal expansion, or bowing. In the early phase of the transient following the coolant break, the high axial loads which potentially could be generated by the difference in thermal expansion between fuel clad and thimbles are relieved by slippage of the fuel rods through the grids. The relatively low drag force restraint on the fuel rods will only induce minor thermal bowing, which is not sufficient to close the fuel rod-to-thimble tube gap. This rod-to-grid slip mechanism occurs simultaneously with control rod drop. Subsequent to the control rod insertion the transient temperature increase of the fuel rod clad can result in swelling, which is sufficient to contact the thimbles.

**Vibration and Wear**

Fuel rod vibrations are basically flow induced. The effect of the flow induced vibration on the fuel assembly and individual fuel rods is minimal. The cyclic stress range associated with deflections of such small magnitude is insignificant and has no effect on the structural integrity of the fuel rod.

The reaction on the grid support due to vibration motions is also correspondingly small and definitely much less than the spring preload. Firm contact is therefore maintained. No significant wear of the clad or grid supports is expected during the life of the fuel assembly.

The conclusion that the effect of flow induced vibrations on the fuel assembly and fuel rod is minimal is based on test results and analysis documented in the Hydraulic Flow Test of the 17 x 17 Fuel Assembly report [20], which takes into consideration the condition normally encountered in reactor operation. Hydraulic flow test results of the VANTAGE 5H assembly are discussed in Reference [28].

### 4.2.1.3.3 Operational Experience

A discussion of fuel operating experience is given in Reference [3].

### 4.2.1.3.4 Test Rod and Test Assembly Experience

This experience is presented in Sections 8 and 23 of Reference [2] and in Reference [28], Addendum 1-A, Section D.

### 4.2.1.3.5 Evaluation of the Reactor Core for a Limited Displacement RPV Inlet Nozzle Break

The fuel assembly response resulting from the most limiting main coolant pipe break was analyzed using time history numerical techniques. Since the resulting vessel motion induces primarily lateral loads on the reactor core, a finite element model similar to the seismic model described in Reference [7] was used to assess the fuel assembly deflections and impact forces.

The reactor core finite element model which simulates the fuel assembly interaction during lateral excitation consists of fuel assemblies arranged in a planar array with inner assembly gaps. For Watts Bar Nuclear Plant, fifteen fuel assemblies which

correspond to the maximum number of assemblies across the core diameter were used in the model. The fuel assemblies and the reactor baffle support are represented by single beam elements as shown in Figure 4.2-28. The time history motion for the upper and lower core plates and the barrel at the upper core plate elevation are simultaneously applied to the simulated reactor core model as illustrated in Figure 4.2-28. The three time history motions were obtained from the analysis of the reactor vessel and internals.

The fuel assembly response, namely, displacements and grid impact forces, was obtained from the reactor core model using the core plate and barrel motions resulting from a limited displacement RPV inlet nozzle break. Examination of the fuel assembly response curves indicated that the initial motion was in the opposite direction with respect to the excitation motion. The reactor core motion then reverses resulting in impacting at the baffle wall opposite the pipe break. The maximum fuel assembly deflection occurred in a peripheral fuel assembly. The fuel assembly stresses resulting from this deflection were evaluated and indicated substantial margins compared to the allowable values.

The fuel assembly grid impact forces were also obtained from the reactor core time history response. The maximum impact force occurred at the peripheral fuel assembly location adjacent to the baffle wall directly opposite the pipe break. The grid impact forces were rapidly attenuated for fuel assembly positions inward from the peripheral fuel. The grid impact force for the peripheral fuel assembly adjacent to the baffle on the pipe break side of the reactor were slightly lower than those on the opposite side of the core. Only a small (outer) portion of the core experienced significant grid impact forces. The maximum grid impact forces are required to be less than the allowable grid crush strength. A calculation of the maximum LOCA and seismic grid impact forces, combined using the square root sum of the squares method (in accordance with NUREG 0800, Section 4.2, Appendix A), demonstrated that the maximum value is less than the allowable grid strength.

### 4.2.1.4 Tests and Inspections

#### 4.2.1.4.1 Quality Assurance Program

The Quality Assurance Program Plan of the Westinghouse Nuclear Fuel Division, as summarized in Reference [11], has been developed to serve the division in planning and monitoring its activities for the design and manufacture of nuclear fuel.

The program provides for control over all activities affecting product quality, commencing with design and development and continuing through procurement, materials handling, fabrication, testing and inspection, storage, and transportation. The program also provides for the indoctrination and training of personnel and for the auditing of activities affecting product quality through a formal auditing program.

Westinghouse drawings and product process, and material specifications identify the inspection to be performed.

### 4.2.1.4.2 Quality Control

Quality control philosophy is generally based on the following inspections being performed to a 95% confidence that at least 95% of the product meets specifications, unless otherwise noted.

*(1)* Fuel System Components and Parts

The characteristics inspected depend upon the component parts and include dimensional and visual examinations, audits of test reports, material certification, and non-destructive testing, such as X-Ray and ultrasonic.

All material used in the Watts Bar Nuclear Plant core is accepted and released by Quality Control.

*(2)* Pellets

Inspection is performed for dimensional characteristics such as diameter, density, length and squareness of ends. Additional visual inspections are performed for cracks, chips and surface conditions according to approved standards.

Density is determined in terms of weight per unit length and is plotted on zone charts used in controlling the process. Chemical analyses are taken on a specified sample basis throughout pellet production.

*(3)* Rod Inspection

Fuel rod, control rodlet, burnable absorber, and source rod inspection consists of the following non-destructive examination techniques and methods, as applicable.

*(a)* Leak Testing

Each rod is tested using a calibrated mass spectrometer with helium being the detectable gas.

*(b)* Enclosure Welds

All weld enclosures are ultrasonic tested or x-rayed. X-rays are taken in accordance with Westinghouse specifications meeting the requirements of ASTM-E-142.

*(c)* Dimensional

All rods are dimensionally inspected prior to final release. The requirements include such items as length, camber, and visual appearance.

*(d)* Plenum Dimensions

All of the fuel rods are inspected by gamma-scanning, fluoroscope, x-ray or other approved methods as discussed in Section 4.2.1.4.3 to insure proper plenum dimensions.

*(e)* Pellet-to-Pellet Gaps

All of the fuel rods are inspected by fluoroscope, gamma-scanning or other approved methods as discussed in Section 4.2.1.4.3 to insure that no significant gaps exist between pellets.

*(f)* Enrichment

All of the fuel rods are active gamma-scanned to verify enrichment control prior to acceptance for assembly loading.

*(g)* Traceability

Traceability of rods and associated rod components is established by Quality Control.

*(4)* Assemblies

Each fuel rod, control rod, burnable absorber, and source rod assembly is inspected for drawing and/or specification requirements.

*(5)* Other Inspections

The following inspections are performed as part of the routine inspection operation:

*(a)* Tool and gage inspection and control includes standardization to primary and/or secondary working standards. Tool inspection is performed at prescribed intervals on all serialized tools. Complete records are kept of calibration and conditions of tools.

*(b)* Audits are performed of inspection activities and records to assure that prescribed methods are followed and that records are correct and orderly maintained.

*(c)* Surveillance inspection where appropriate, and audits of outside contractors are performed to insure conformance with specified requirements.

*(6)* Process Control

To prevent the possibility of mixing enrichments during fuel manufacture and assembly, strict enrichment segregation and other process controls are exercised.

The $UO_2$ powder is kept in sealed containers. The contents are fully identified, both by descriptive tagging and pre-selected color coding. A Westinghouse identification tag completely describing the contents is affixed to the containers before transfer to powder storage. Isotopic content is confirmed by sample isotopic analysis.

Powder withdrawal from storage can be made by only one authorized group, which directs the powder to the correct pellet production line. All pellet production lines are physically separated from each other and pellets of only a single nominal enrichment and density are produced in a given production line at any given time.

Finished pellets are placed on trays identified with the same color code as the powder containers and transferred to segregated storage racks within the confines of the pelleting area. Samples from each pellet lot are tested for isotopic content and impurity levels prior to acceptance by Quality Control. Physical barriers prevent mixing of pellets of different nominal densities and enrichments in this storage area. Unused powder and substandard pellets are returned to storage in the original color coded containers.

Loading of pellets into the Zircaloy tubing is performed in isolated production lines and only one enrichment is loaded on a line at a time.

A serialized traceability code is placed on each fuel tube which identifies the contract and enrichment. The end plugs are inserted; the bottom end plug is permanently identified to the contract and enrichment; and inert welded to seal the tube. The fuel tube remains coded, and traceability identified until just prior to installation in the fuel assembly. The traceability code and end plug identification character provide a cross reference of the fuel contained in the fuel rods.

At the time of installation into an assembly, the traceability codes are removed and a matrix is generated to identify each rod in its position within a given assembly. After the fuel rods are installed, an inspector verifies that all fuel rods in an assembly carry the correct identification character describing the fuel enrichment and density for the core region being fabricated. The top nozzle is inscribed with a permanent identification number providing traceability to the fuel contained in the assembly.

Similar traceability is provided for burnable absorbers, source rods and control rodlets as required.

### 4.2.1.4.3 Tests and Inspections by Others

If any Tests and Inspections are to be performed on behalf of the fuel supplier, the quality control procedures, inspection plans, etc., to be utilized will be reviewed and approved by the fuel supplier to insure that they are equivalent to the description provided above and are performed properly to meet all requirements.

#### 4.2.1.4.4 Onsite Inspection

Surveillance of fuel and reactor performance is routinely conducted on Westinghouse reactors. Power distribution is monitored using the excore fixed and incore movable detectors. Coolant activity and chemistry is followed which permits early detection of any fuel clad defects. Depending on the results of this monitoring, fuel inspections are performed.

### 4.2.2 Reactor Vessel Internals

#### 4.2.2.1 Design Bases

The design bases for the mechanical design of the reactor vessel internals components are as follows:

*(1)* The reactor internals, in conjunction with the fuel assemblies, shall direct reactor coolant through the core to achieve acceptable flow distribution and to restrict bypass flow so that the heat transfer performance requirements are met for all modes of operation. In addition, required cooling for the pressure vessel head shall be provided so that the temperature differences between the vessel flange and head do not result in leakage from the flange during reactor operation.

*(2)* In addition to neutron shielding provided by the reactor coolant, neutron pads are provided to limit the exposure of the pressure vessel in order to maintain the required ductility of the material for all modes of operation.

*(3)* Provisions shall be made for installing in-core instrumentation useful for the plant operation and vessel material test specimens required for a pressure vessel irradiation surveillance program.

*(4)* The core internals are designed to withstand mechanical loads arising from the SSE and 1/2 SSE and pipe ruptures and meet the requirement of Item 5 below.

*(5)* The reactor shall have mechanical provisions which are sufficient to adequately support the core and internals and to assure that the core is intact with acceptable heat transfer geometry following transients arising from abnormal operating conditions.

*(6)* Following the design basis accident, the plant shall be capable of being shutdown and cooled in an orderly fashion so that fuel cladding temperature is kept within specified limits. This implies that the deformation of certain critical reactor internals must be kept sufficiently small to allow core cooling.

The functional limitations for the core structures during the design basis accident are shown in Table 4.2-1. To insure no column loading of rod cluster control guide tubes, the upper core plate deflection is limited to not exceed the value shown in Table 4.2-1.

Details of the dynamic analyses, input forcing functions, and response loadings are presented in Section 3.9.

### 4.2.2.2 Description and Drawings

The reactor vessel internals are described as follows:

The components of the reactor internals consist of the lower core support structure (including the entire core barrel and neutron pads), the upper core support structure and the in-core instrumentation support structure. The reactor internals support the core, maintain fuel alignment, limit fuel assembly movement, maintain alignment between fuel assemblies and control rod drive mechanisms, direct coolant flow past the fuel elements, direct coolant flow to the pressure vessel head, provide gamma and neutron shielding, and guides for the in-core instrumentation. The coolant flows from the vessel inlet nozzles down the annulus between the core barrel and the vessel wall and then into a plenum at the bottom of the vessel. It then reverses and flows up through the core support and through the lower core plate. The lower core plate is sized to provide the desired inlet flow distribution to the core. After passing through the core, the coolant enters the region of the upper support structure and then flows radially to the core barrel outlet nozzles and directly through the vessel outlet nozzles. A small portion of the coolant flows between the baffle plates and the core barrel to provide additional cooling of the barrel. Similarly, a small amount of the entering flow is directed into the vessel head plenum and exits through the vessel outlet nozzles.

All the major material for the reactor internals is Type 304 stainless steel. Parts not fabricated from Type 304 stainless steel include bolts and dowel pins which are fabricated from Type 316 stainless steel, and the radial support clevis insert and bolts which are fabricated of Inconel. The only stainless steel materials used in the reactor core support structures which have yield strengths greater than 90,000 pounds are the 403 series used for holddown springs. The use of these materials is compatible with the reactor coolant and is acceptable based on the 1971 ASME Boiler and Pressure Vessel Code, Case Number 1337.

All reactor internals are removable from the vessel for the purpose of their inspection as well as the inspection of the vessel internal surface.

#### Lower Core Support Structure

The major containment and support member of the reactor internals is the lower core support structure, shown in Figure 4.2-10. This support structure assembly consists of the core barrel, the core baffle, and the lower core plate and support columns, the neutron pads, and the core support which is welded to the core barrel. All the major material for this structure is Type 304 stainless steel. The lower core support structure is supported at its upper flange from a ledge in the reactor vessel and its lower end is restrained from transverse motion by a radial support system attached to the vessel wall. Within the core barrel are an axial baffle and a lower core plate, both of which are attached to the core barrel wall and form the enclosure periphery of the core. The lower core support structure and core barrel serve to provide passageways and direct

the coolant flow. The lower core plate is positioned at the bottom level of the core below the baffle plates and provides support and orientation for the fuel assemblies.

The lower core plate is a member through which the necessary flow distribution holes for each fuel assembly are machined. Fuel assembly locating pins (two for each assembly) are also inserted into this plate. Columns are placed between the lower core plate and the core support of the core barrel to provide stiffness and to transmit the core load to the core support. Adequate coolant distribution is obtained through the use of the lower core plate and core support.

Rectangular specimen guides in which material samples can be inserted and irradiated during reactor operation are welded to the neutron pads and extended to the top of the panels. These samples are held in the rectangular specimen guides by a preloaded spring device at the top and bottom.

Vertically downward loads from weight, fuel assembly preload, control rod dynamic loading, hydraulic loads and earthquake acceleration are carried by the lower core plate into the lower core plate support flange on the core barrel shell and through the lower support columns to the core support and thence through the core barrel shell to the core barrel flange supported by the vessel flange. Transverse loads from earthquake acceleration, coolant cross flow, and vibration are carried by the core barrel shell and distributed between the lower radial support to the vessel wall, and to the vessel flange. Transverse loads of the fuel assemblies are transmitted to the core barrel shell by direct connection of the lower core plate to the barrel wall and by upper core plate alignment pins which are welded into the core barrel.

The radial support system of the core barrel is accomplished by "key" and "keyway" joints to the reactor vessel wall. At six equally spaced points around the circumference, an Inconel clevis block is welded to the vessel inner diameter. Another Inconel block is bolted to each of these blocks, and has a "keyway" geometry. Opposite each of these is a "key" which is welded to the lower core support. At assembly, as the internals are lowered into the vessel, the keys engage the keyways in the axial direction. With this design, the internals are provided with a support at the furthest extremity, and may be viewed as a beam fixed at the top and simply supported at the bottom.

Radial and axial expansions of the core barrel are accommodated, but transverse movement of the core barrel is restricted by this design. With this system, cyclic stresses in the internal structures are within the ASME Section III limits. In the event of an abnormal downward vertical displacement of the internals following a hypothetical failure, energy absorbing devices limit the displacement of the core after contacting the vessel bottom head. The load is then transferred through the energy absorbing devices of the lower internals to the vessel.

The energy absorbers are mounted on a base plate which is contoured on its bottom surface to the reactor vessel bottom internal geometry. Their number and design are determined so as to limit the stresses imposed on all components except the energy absorber to less than yield.

Assuming a downward vertical displacement, the potential energy of the system is absorbed mostly by the strain energy of the energy absorbing devices.

**Upper Core Support Assembly**

The upper core support structure, shown in Figures 4.2-11, 4.2-12, and 4.2-13 consists of the upper support assembly and the upper core plate between which are contained support columns and guide tube assemblies. The support columns establish the spacing between the top support plate assembly and the upper core plate and are fastened at top and bottom to these plates. The support columns serve to transmit the fuel assembly holddown loads from the upper core plate to the upper support and thence to the vessel flange. They position the upper core plate and upper support which act as the boundaries for the flow plenum at the outlet of the core. A support column or flow downcomer is provided at each fuel assembly position that does not contain accommodation for a control rod with the exception of the peripheral low power fuel assembly locations. The fuel assemblies which do not have a support column or flow downcomer above them are located in front of the inlet and outlet nozzles of the vessel. The support columns also contain thermocouple supports. Figure 4.2-12 illustrates a typical support column.

The guide tube assemblies, (See Figures 4.2-11 and 4.2-14) shield and guide the control rod drive rods and control rods. They are fastened to the upper support and are guided by pins in the upper core plate for proper orientation and support. Additional guidance for the control rod drive rods is provided by the upper guide tube extension which is attached to the upper support.

The upper core support assembly, which is removed as a unit during refueling operation, is positioned in its proper orientation with respect to the lower support structure by slots in the upper core plate which engage flat-sided upper core plate alignment pins which are welded into the core barrel. At an elevation in the core barrel where the upper core plate is positioned, the flat-sided pins are located at angular positions of 90° from each other. As the upper support structure is lowered into the lower internals, the slots in the plate engage the flat-sided pins axial direction. Lateral displacement of the plate and of the upper support assembly is restricted by this design. Fuel assembly locating pins protrude from the bottom of the upper core plate and engage the fuel assemblies as the upper assembly is lowered into place. Proper alignment of the lower core support structure, the upper core support assembly, the fuel assemblies and control rods are thereby assured by this system of locating pins and guidance arrangement. The upper core support assembly is restrained from any axial movements by a large circumferential spring which rests between the upper barrel flange and the upper core support assembly. The spring is compressed when the reactor vessel head is installed on the pressure vessel.

Vertical loads from weight, earthquake acceleration, hydraulic loads and fuel assembly preload are transmitted through the upper core plate via the support columns to the upper support assembly and then into the reactor vessel head. Transverse loads from coolant cross flow, earthquake acceleration, and possible vibrations are distributed by the support columns to the upper support and upper core plate. The upper support plate is particularly stiff to minimize deflection.

**In-Core Instrumentation Support Structures**

The incore instrumentation support structures consist of an upper system to convey and support thermocouples penetrating the vessel through the head and a lower system to convey and support flux thimbles penetrating the vessel through the bottom (Figure 7.7-9 shows the Basic Flux-Mapping System).

The upper system utilizes the reactor vessel head penetrations. Instrumentation port columns are slip-connected to in-line columns that are in turn fastened to the upper support plate. These port columns protrude through the head penetrations. The thermocouples are carried through these port columns and the upper support plate at positions above their readout locations. The thermocouple conduits are supported from the columns of the upper core support system. The thermocouple conduits are 304 stainless steel tubes.

In addition to the upper incore instrumentation, there are reactor vessel bottom port columns which carry the retractable, cold worked stainless steel flux thimbles that are pushed upward into the reactor core. Conduits extend from the bottom of the reactor vessel down through the concrete shield area and up to a thimble seal line. The minimum bend radii are about 144 inches and the trailing ends of the thimbles (at the seal line) are extracted approximately 15 feet during refueling of the reactor in order to avoid interference within the core. The thimbles are closed at the leading ends and serve as the pressure barrier between the reactor pressurized water and the containment atmosphere.

Mechanical seals between the retractable thimbles and conduits are provided at the seal line. During normal operation, the retractable thimbles are stationary and move only during refueling or for maintenance, at which time a space of approximately 15 feet above the seal line is cleared for the retraction operation.

The incore instrumentation support structure is designed for adequate support of instrumentation during reactor operation and is rugged enough to resist damage or distortion under the conditions imposed by handling during the refueling sequence. These are the only conditions which affect the incore instrumentation support structure. Reactor vessel surveillance specimen capsules are covered in Section 5.4.3.6.

### 4.2.2.3 Design Loading Conditions

The design loading conditions that provide the basis for the design of the reactor internals are:

*(1)* Fuel Assembly Weight
*(2)* Fuel Assembly Spring Forces
*(3)* Internals Weight
*(4)* Control Rod Trip (equivalent static load)
*(5)* Differential Pressure
*(6)* Spring Preloads
*(7)* Coolant Flow Forces (static)

*(8)* Temperature Gradients
*(9)* Differences in thermal expansion
  *(a)* Due to temperature differences
  *(b)* Due to expansion of different materials
*(10)* Interference between components
*(11)* Vibration (mechanically or hydraulically induced)
*(12)* All operational transients listed in Table 5.2-2
*(13)* Pump over-speed
*(14)* Seismic loads (operation basis earthquake and design basis earthquake)
*(15)* Blowdown forces injection transients for the cold and hot leg break.

Combined seismic and blowdown forces are included in the stress analysis as a design loading condition by statistically combining the maximum amplitude of each force.

The main objectives of the design analysis are to satisfy allowable stress limits, to assure an adequate design margin, and to establish deformation limits which are concerned primarily with the functioning of the components. The stress limits are established not only to assure that peak stresses will not reach unacceptable values, but also limit the amplitude of the oscillatory stress component in consideration of fatigue characteristics of the materials. Both low and high cycle fatigue stresses are considered when the allowable amplitude of oscillation is established. Dynamic analysis on the reactor internals is provided in Section 3.9.

As part of the evaluation of design loading conditions, extensive testing and inspections are performed, from the initial selection of raw materials up to and including component installation and plant operation. Among these tests and inspections are those performed during component fabrication, plant construction, startup and check out, and during plant operation.

### 4.2.2.4 Design Loading Categories

The combination of design loadings fit into either the normal upset or faulted conditions as defined in the ASME Section III Code.

Loads and deflections imposed on components due to shock and vibration are determined analytically and experimentally in both scaled models and operating reactors. The cyclic stresses due to these dynamic loads and deflections are combined with the stresses imposed by loads from component weights, hydraulic forces and thermal gradients for the determination of the total stresses of the internals.

The reactor internals are designed to withstand stresses originating from various operating conditions as summarized in Table 5.2-2.

The scope of the stress analysis problem is very large requiring many different techniques and methods, both static and dynamic. The analysis performed depends on the mode of operation under consideration.

**Allowable Deflections**

For normal operating conditions, downward vertical deflection of the lower core support plate is negligible.

For the loss of coolant accident plus the 1/2 safe shutdown earthquake condition, the deflection criteria of critical internal structures are the limiting values given in Table 4.2-1. The corresponding no loss of function limits are included in Table 4.2-1 for comparison purposes with the allowed criteria.

The criteria for the core drop accident are based upon analyses which have been performed to determine the total downward displacement of the internal structures following a hypothesized core drop resulting from loss of the normal core barrel supports. The initial clearance between the secondary core support structures and the reactor vessel lower head in the hot condition is approximately one half inch. An additional displacement of approximately 3/4 inch would occur due to strain of the energy absorbing devices of the secondary core support; thus the total drop distance is about 1-1/4 inches which is not sufficient to permit the grips of the rod cluster control assembly to come out of the guide thimble in the fuel assemblies.

Specifically, the secondary core support is a device which will never be used, except during a hypothetical accident of the core support (core barrel, barrel flange, etc.). There are 4 supports in each reactor. This device limits the fall of the core and absorbs the energy of the fall which otherwise would be imparted to the vessel. The energy of the fall is calculated assuming a complete and instantaneous failure of the primary core support and is absorbed during the plastic deformation of the controlled volume of stainless steel, loaded in tension. The maximum deformation of this austenitic stainless piece is limited to approximately 15%, after which a positive stop is provided to insure support.

### 4.2.2.5 Design Criteria Basis

The basis for the design stress and deflection criteria is identified below:

**Allowable Stress**

The initial design of Watts Bar was before the establishment of Subsection NG of the ASME Code, and no specific stress report was written for this application. However, previous evaluations were performed using the January 1971 Draft of Section III of the ASME B & PV Code. Later work by the NSSS vendor, such as for the V5H fuel conversion, did make use of more recent versions of the ASME code. Essentially all the fabrication and inspection requirements of Subsection NG have been satisfied.

Exceptions to code requirements include 'code stamp' not being applied to the reactor internals and no specific stress report written for Watts Bar Nuclear Plant.

All of 10 CFR 50 Appendix B is complied with and the resulting stresses and deformations are below established limits.

## 4.2.3 Reactivity Control System

### 4.2.3.1 Design Bases

Bases for temperature, stress on structural members, and material compatibility are imposed on the design of the reactivity control components.

#### 4.2.3.1.1 Design Stresses

The reactivity control system is designed to withstand stresses originating from various operating conditions as summarized in Table 5.2-2.

Allowable Stresses For normal operating conditions, Section III of the ASME Boiler and Pressure Code is used. All pressure boundary components are analyzed as Class I components under Article NB-3000.

Dynamic Analysis The cyclic stresses due to dynamic loads from component weights, hydraulic forces and thermal gradients are used for the determination of the total stresses of the reactivity control system.

#### 4.2.3.1.2 Material Compatibility

Materials are selected for compatibility in a PWR environment, for adequate mechanical properties at room and operating temperature, for resistance to adverse property changes in a radioactive environment, and for compatibility with interfacing components.

#### 4.2.3.1.3 Reactivity Control Components

The reactivity control components are described below:

These components are the rod cluster control assemblies, control rod drive mechanisms, neutron source assemblies, burnable absorber assemblies, and thimble plug assemblies. Although the thimble plug assembly does not directly contribute to the reactivity control of the reactor, it is presented as a reactivity control system component in this document because it is needed to restrict bypass flow through those thimbles not occupied by absorber, source, or burnable absorber rods.

The design bases for each of the mentioned components are in the following paragraphs.

**Rod Cluster Control Assemblies (Absorber Rods)**

The following are considered design conditions under Article NB-3000 of the ASME Boiler and Pressure Vessel Code, Section III. The control rod which is cold rolled Type 304 stainless steel is the only non-code material used in the control rod assembly. The stress intensity limit $S_m$ for this material is defined at 2/3 of the 0.2% offset yield stress.

*(1)* The external pressure equal to the Reactor Coolant System operating pressure.

*(2)* The wear allowance equivalent to 1,000 reactor trips.

*(3)* Bending of the rod due to a misalignment in the guide tube.

*(4)* Forces imposed on the rods during rod drop.

*(5)* Loads caused by accelerations imposed by the control rod drive mechanism.

*(6)* Radiation exposure for maximum core life.

*(7)* Temperature effects at operating conditions.

The absorber materials temperatures shall not exceed 1454°F which is the lower melting point of the two absorber materials[22].

**Burnable Absorber Rods**

The burnable absorber rod clad is designed as a Class I component under Article NB-3000 of the ASME Boiler and Pressure Vessel Code, Section III, 1973 for Conditions I and II. For abnormal loads during Conditions III and IV, code stresses are not considered limiting. Failures of the burnable absorber rods during these conditions must not interfere with reactor shutdown or emergency cooling of the fuel rods.

The burnable absorber material is non-structural. The structural elements of the burnable absorber rod are designed to maintain the absorber geometry even if the absorber material is fractured. The rods are designed so that the absorber material is below its softening temperature. Borosilicate glass is accepted for use in burnable absorber rods if the softening temperature is 1510+18°F. The softening temperature is defined in ASTM C 338.In addition, the structural elements are designed to prevent excessive slumping.

The Westinghouse designed wet annular burnable absorber (WABA) is used in reload cores. Reference [29] verifies that the WABA design meets burnable absorber design criteria.

**Neutron Source Rods**

The neutron source rods are designed to withstand the following:

*(1)* The external pressure equal to the Reactor Coolant System operating pressure and

*(2)* An internal pressure equal to an initial pre-pressurization and the pressure generated by released gases over the source rod life.

**Thimble Plug Assembly**

The thimble plug assemblies satisfy the following:

*(1)* Accommodate the differential thermal expansion between the fuel assembly and the core internals,

*(2)* Maintain positive contact with the fuel assembly and the core internals.

*(3)* Limit the flow through each occupied thimble to acceptable design value.

### 4.2.3.1.4 Control Rod Drive Mechanisms

The control rod drive mechanisms (CRDMs) pressure housings are Class I components designed to meet the stress requirements for normal operating conditions of Section III of the ASME Boiler and Pressure Vessel Code. Both static and alternating stress intensities are considered. The stresses originating from the required design transients are included in the analysis.

A dynamic seismic analysis is required on the CRDMs when a seismic disturbance has been postulated to confirm the ability of the pressure housing to meet ASME Code, Section III allowable stresses.

**CRDM Operability at WBN is Assured by the Following Actions:**

*(1)* Since control rods fall into the core because of gravitational acceleration and loss of power to the grippers releases the control rods, the CRDM is a fail-safe component.

*(2)* Rod drop time measurements during startup perform verification of operability of control rod insertion.

*(3)* Rod drop capability under abnormal conditions has been demonstrated by:

*(a)* Prototype flow tests which were performed for flows in excess of 150% of design flow over a wide range of temperatures.

*(b)* Scram deflection tests on CRDM's.

*(c)* Scram deflection tests on guide tubes and fuel assemblies.

*(d)* In addition, a Westinghouse licensee has performed dynamic tests on a prototype CRDM which provides additional evidence of the ability to insert control rods during a seismic event.

The ability to insert control rods is assured by the fail-safe CRDM design employed. Rod drop time tests provide confirmation of acceptable control rod insertion performance. Furthermore, capability under abnormal conditions has been demonstrated by tests performed by Westinghouse and Westinghouse licensees. The results of these tests confirm operability under abnormal conditions.

**Control Rod Drive Mechanisms Operational Requirements**

The basic operational requirements for the CRDMs are:

*(1)* 5/8 inch step,

*(2)* 144 inch nominal travel,

*(3)* 360 pound maximum load,

*(4)* Step in or out at 45 inches/minute (72 steps/minute),

*(5)* Electrical power interruption shall initiate release of drive rod assembly,

*(6)* Trip delay time of less than 150 milliseconds - Free fall of drive rod assembly shall begin less than 150 milliseconds after power interruption no matter what holding or stepping action is being executed with any load and coolant temperature of 100°F to 550°F.

*(7)* 40 year design life with normal refurbishment.

### 4.2.3.2 Design Description

Reactivity control is provided by neutron absorbing rods and a soluble chemical neutron absorber (boric acid). The boric acid concentration is varied to control long-term reactivity changes such as:

*(1)* Fuel depletion and fission product buildup.

*(2)* Cold to hot, zero power reactivity change.

*(3)* Reactivity change produced by intermediate term fission products such as xenon and samarium.

*(4)* Burnable absorber depletion.

Chemical and volume control is covered in Section 9.3.4.

The rod cluster control assemblies provide reactivity control for:

*(1)* Shutdown.

*(2)* Reactivity changes due to coolant temperature changes in the power range.

*(3)* Reactivity changes associated with the power coefficient of reactivity.

*(4)* Reactivity changes due to void formation.

The first fuel cycle contains more excess reactivity than subsequent cycles due to the loading of all fresh (unburned) fuel. If soluble boron were the sole means of control, the moderator temperature coefficient would be positive. It is desirable to have a negative moderator temperature coefficient throughout the entire cycle in order to reduce possible deleterious effects caused by a positive coefficient during loss of coolant or loss of flow accidents. This is accomplished by installation of burnable absorber assemblies.

The neutron source assemblies provide a means of monitoring the core during periods of low neutron activity.

The most effective reactivity control components are the rod cluster control assemblies and their corresponding CRDM, which are the only kinetic parts in the reactor. Figure 4.2-14 identifies the rod cluster control and CRDM assembly, in addition to the arrangement of these components in the reactor relative to the interfacing fuel assembly and guide tube. In the following paragraphs, each reactivity control component is described in detail.

The guidance system for the control rod cluster is provided by the guide tube as shown in Figure 4.2-14. The guide tube provides two regimes of guidance: 1) In the lower section, a continuous guidance system provides support immediately above the core. This system protects the rod against excessive deformation and wear due to hydraulic loading. 2) The region above the continuous section provides support and guidance at uniformly spaced intervals.

The envelope of support is determined by the pattern of the control rod cluster as shown in Figure 4.2-15. The guide tube assures alignment and support of the control rods, spider body, and drive rod while maintaining trip times at or below required limits.

### 4.2.3.2.1 Reactivity Control Components

#### Rod Cluster Control Assembly

The rod cluster control assemblies are divided into two categories: control and shutdown. The control groups compensate for reactivity changes due to variations in operating conditions of the reactor, power and temperature variations. Two criteria have been employed for selection of the control group. First, the total reactivity worth must be adequate to meet the nuclear requirements of the reactor. Second, in view of the fact that these rods may be partially inserted at power operation, the total power peaking factor should be low enough to ensure that the power capability is met. The control and shutdown group provides adequate shutdown margin, which is defined as the amount of negative reactivity by which the core would be subcritical at hot shutdown if all rod cluster control assemblies are tripped, assuming that the highest worth assembly remains fully withdrawn and assuming no changes in xenon or boron concentration.

A rod cluster control assembly comprises a group of individual neutron absorber rods fastened at the top end to a common spider assembly, as illustrated in Figure 4.2-15.

The absorber materials used in the control rods are $B_4C$ (boron carbide) pellets plus silver-indium-cadmium alloy slugs which are essentially "black" to thermal neutrons. These materials have sufficient additional resonance absorption to significantly increase their worth. The $B_4C$ pellets are stacked on top of the extruded AG-IN-CD slugs and are sealed in stainless steel tubes to prevent them from coming in direct contact with the coolant. In construction, the $B_4C$ pellets and the silver-indium-cadmium slugs are inserted into cold-worked stainless steel tubing which is then sealed at the bottom and the top by welded end plugs as shown in Figure

4.2-16. Sufficient diametral and end clearance is provided to accommodate relative thermal expansions and material swelling.

The bottom plugs are made bullet-nosed to reduce the hydraulic drag during reactor trip and to guide smoothly into the dashpot section of the fuel assembly guide thimbles. The upper plug is threaded for assembly to the spider and has a reduced end section to make the joint more flexible.

The material used in the absorber rod end plugs is Type 308 stainless steel. The design stresses used for the Type 308 material are the same as those defined in the ASME Code, Section III, for Type 304 stainless steel. At room temperature the yield and ultimate stresses per ASTM-580 are exactly the same for the two alloys. In view of the similarity of the alloy composition, the temperature dependence of strength for the two materials is also assumed to be the same.

The allowable stresses used as a function of temperature are listed in Table 1.1-2 of Section III of the ASME Boiler and Pressure Vessel Code. The fatigue strength for the Type 308 material is based on the S-N curve for austenitic stainless steels in Figure 1.9-2 of Section III of the ASME Boiler and Pressure Vessel Code. There are no other applications of stressed wrought Type 308 stainless steel in the control rod assembly. The spider assembly is in the form of a central hub with radial vanes containing cylindrical fingers from which the absorber rods are suspended. Handling grooves and internal grooves for connection to the drive rod assembly are machined into the upper end of the hub. A coil spring inside the spider body absorbs the impact energy at the end of a trip insertion. The radial vanes are joined to the hub by tack weld and braze and the fingers are joined to the vanes by brazing. A centerpost which holds the spring and its retainer is threaded into the hub within the skirt and welded to prevent loosening in service. All components of the spider assembly are made from Types 304 and 306 stainless steel except for the retainer which is of 17-4 PH material and the springs which are Inconel-718.

The absorber rods are fastened securely to the spider to assure trouble free service. The rods are first threaded into the spider fingers and then pinned to maintain joint tightness, after which the pins are welded in place. The end plug below the pin position is designed with a reduced section to permit flexing of the rods to correct for small operating or assembly misalignments.

The overall length is such that when the assembly is withdrawn through its full travel the tips of the absorber rods remain engaged in the guide thimbles so that alignment between rods and thimbles is always maintained. Since, the rods are long and slender, they are relatively free to conform to any small misalignments with the guide thimble.

Provision is made in the design for the use of part length control rods. However, all control rods are full length and part length control rods will not be used. All accident analyses have been performed without part length control rods. Therefore, part length control rods are not specified in the Watts Bar Nuclear Plant design basis.

### Burnable Absorber Assembly

Each burnable absorber assembly consists of borosilicate or WABA burnable absorber rods attached to a hold down assembly. Conceptual burnable absorber assemblies (containing borosilicate absorber) are shown in Figure 4.2-18. WABA rods may be used in place of the borosilicate absorber rods.

The borosilicate absorber rods consist of borosilicate glass tubes contained within Type 304 stainless steel tubular cladding which is plugged and seal welded at the ends to encapsulate the glass. The glass is also supported along the length of its inside diameter by a thin-wall tubular inner liner. The top end of the liner is open to permit the diffused helium to pass into the void volume and the liner overhangs the glass. The liner has an outward flange at the bottom end to maintain the position of the liner with the glass. A typical borosilicate burnable absorber rod is shown in longitudinal and transverse cross-sections in Figure 4.2-19.

A WABA rod (Figure 4.2-19A) consists of annular pellets of alumina-boron carbide ($Al_20_3$-$B_4C$) burnable absorber material contained within two concentric zircaloy tubes. These zircaloy tubes, which form the inner and outer clad for the WABA rod, are plugged and welded at each end to encapsulate the annular stack of absorber material. The assembled rod is then internally pressurized to 650 psig and seal welded. The absorber stack lengths are positioned axially within the WABA rods by the use of zircaloy bottom-end spacers. An annular plenum is provided within the rod to accommodate the helium gas released from absorber material depletion during irradiation. The reactor coolant flows inside the inner tube and outside the outer tube of the annular rod. Further design details are given in Section 3.0 of Reference [29].

The burnable absorber rods are statically suspended and positioned in selected guide thimbles within the fuel assemblies. The absorber rods in each assembly are attached together at the top end of the rods to a holddown assembly by a flat, perforated retaining plate which fits within the fuel assembly top nozzle and rests on the adapter plate. The absorber rod assembly is held down and restrained against vertical motion through a spring pack which is attached to the plate and is compressed by the upper core plate when the reactor upper internals assembly is lowered into the reactor. This arrangement ensures that the absorber rods cannot be ejected from the core by flow forces. Each rod is permanently attached to the base plate by a nut which is crimped or brazed/welded into place.

The borosilicate rod cladding is slightly-cold-worked Type 304 stainless steel, and the WABA rod cladding is Zircaloy-4. All other structural materials are Type 304 or 308 stainless steel except for the springs which are Inconel-718. The borosilicate glass tube provides sufficient boron content to meet the criteria discussed in Section 4.3.1.

### Neutron Source Assembly

The purpose of the neutron source assembly is to provide base neutron level to ensure that the detectors are operational and responding to core multiplication neutrons. Since there is very little neutron activity during loading, refueling, shutdown, and approach to criticality, a neutron source is placed in the reactor to provide a positive

neutron count. During approach to criticality, at least 1/2 cps on the source range detectors attributable to neutrons is required. The detectors, called source range detectors, are used primarily when the core is subcritical and during special subcritical modes of operations.

The source assembly also permits detection of changes in the core multiplication factor during core loading, refueling, and approach to criticality. This can be done since the multiplication factor is related to an inverse function of the detector count rate. Therefore a change in the multiplication factor can be detected during addition of fuel assemblies while loading the core, a change in control rod positions, and changes in boron concentration.

Both primary and secondary neutron source rods are used. The primary source rod, containing a radioactive material, spontaneously emits neutrons during initial core loading and reactor startup. After the primary source rod decays beyond the desired neutron flux level, neutrons are then supplied by the secondary source rod. The secondary source rod contains a stable material, which must be activated by neutron bombardment during reactor operation. The activation results in the subsequent release of neutrons. This becomes a source of neutrons during periods of low neutron flux, such as during refueling and subsequent startups.

The reactor core employs four source assemblies; two primary source assemblies and two secondary source assemblies. Each primary source assembly contains one primary source rod and between zero and twenty-three burnable absorber rods. Each secondary source assembly contains a symmetrical grouping of six secondary source rods and between zero and eighteen burnable absorber rods. Locations not filled with a source or burnable absorber rod contain a thimble plug. Conceptual source assemblies are shown in Figures 4.2-20 and 4.2-21.

Neutron source assemblies are employed at diametrically opposite sides of the core. The assemblies are inserted into the guide thimbles in fuel assemblies at selected unrodded locations. The source assemblies contain a holddown assembly identical to that of the burnable absorber assembly.

The primary and secondary source rods both utilize the same cladding material as the absorber rods. The secondary source rods contain Sb-Be pellets stacked to a height of approximately 88 inches. The primary source rods contain capsules of californium (Pu-Be possible alternate) source material and alumina spacer rods to position the source material within the cladding. The rods in each assembly are permanently fastened at the top end to a holddown assembly, which is identical to that of the burnable absorber assemblies.

The other structural members are constructed of Type 304 stainless steel except for the springs. The springs exposed to the reactor coolant are wound from an age hardened nickel base alloy for corrosion resistance and high strength.

**Thimble Plug Assembly**

In order to limit bypass flow through the guide thimbles in fuel assemblies which do not contain either control rods, source rods, or burnable absorber rods, the fuel assemblies at those locations are fitted with thimble plug assemblies.

The thimble plug assemblies as shown in Figure 4.2-22 consist of a flat base plate with short rods suspended from the bottom surface and a spring pack assembly. The twenty-four short rods, called thimble plugs, project into the upper ends of the guide thimbles to reduce the bypass flow. Similar short rods are also used on the source assemblies and burnable absorber assemblies to plug the ends of all vacant fuel assembly guide thimbles. At installation in the core, the thimble plug assemblies interface with both the upper core plate and with the fuel assembly top nozzles by resting on the adaptor plate. The spring pack is compressed by the upper core plate when the upper internals assembly is lowered into place. Each thimble plug is permanently attached to the base plate by a nut which is locked to the threaded end of the plug by a small lock bar welded to the nut.

All components in the thimble plug assembly, except for the springs, are constructed from Type 304 stainless steel. The springs are wound from an age hardened nickel base alloy for corrosion resistance and high strength.

### 4.2.3.2.2 Control Rod Drive Mechanism (CRDM)

All parts of the CRDM that are exposed to reactor coolant are fabricated of metals which resist the corrosive action of the primary coolant. Three types of metals are used exclusively: stainless steels, nickelchrome-iron alloy and cobalt based alloys. In the case of stainless steels, only austenitic and martensitic stainless steels are used. The martensitic stainless steels are not used in the heat treated conditions which cause susceptibility to stress corrosion cracking or accelerated corrosion in the Westinghouse PWR water chemistry. These martensitic stainless steels are procured in accordance with ASME Code Case 1337-8 wherein the minimum tempering temperature is 1125°F.

The discussions provided in Sections 5.2.5, 5.2.5.1, 5.2.5.2, 5.2.5.3, 5.2.5.4, 5.2.5.5 and 5.2.5.6 concerning the processes, inspections and tests on austenitic stainless steel components to assure freedom from increased susceptibility to intergranular corrosion caused by sensitization, and the discussions provided in Sections 5.2.5.5 and 5.2.5.7 on the control of welding of austenitic stainless steels, especially control of delta ferrite, are applicable to the austenitic stainless steel components of the control rod drive mechanisms.

Wherever magnetic flux is carried by parts exposed to the main coolant, 400 series stainless steel is used. Cobalt based alloys are used for the pins and latch tips. Nickel-chrome-iron alloy is used for the springs of latch assemblies and Type 304 stainless steel is used for all pressure containing parts as listed in Table 5.2-8.

Hard chrome plating provides wear surfaces on the sliding parts and prevents galling between mating parts.

Position indicator assemblies slide over the control rod drive mechanism rod travel housings. Each assembly detects the drive rod position by means of 42 discrete coils that magnetically sense the entry and presence of the rod drive line through its center line over the normal length of the drive rod travel.

Control rod drive mechanisms are located on the dome of the reactor vessel. They are coupled to rod control clusters which have absorber material over the entire length of the control rods and derive their name from this feature. The control rod drive mechanism is shown in Figure 4.2-23 and schematically in Figure 4.2-24.

The primary function of the control rod drive mechanism is to insert or withdraw rod cluster control assemblies within the core to control average core temperature and to shutdown the reactor.

The full length control rod drive mechanism is a magnetically operated jack. A magnetic jack is an arrangement of three electromagnets which are energized in a controlled sequence by a power cycler to insert or withdraw rod cluster control assemblies in the reactor core in discrete steps. Rapid insertion of the rod cluster control assemblies occurs when electrical power is interrupted.

The control rod drive mechanism consists of four separate subassemblies. They are the pressure vessel, coil stack assembly, latch assembly, and the drive rod assembly.

*(1)* The pressure vessel includes a latch housing and a rod travel housing which are connected by a threaded, seal welded, maintenance joint which facilitates replacement of the latch assembly. The closure at the top of the rod travel housing is a threaded plug with a canopy seal weld for pressure integrity. This closure contains a threaded plug used for venting.

The latch housing is the lower portion of the vessel and contains the latch assembly. The rod travel housing is the upper portion of the vessel and provides space for the drive rod during its upward movement as the control rods are withdrawn from the core.

*(2)* The coil stack assembly includes the coil housings, an electrical conduit and connector, and three operating coils; 1) the stationary gripper coil, 2) the moveable gripper coil, and 3) the lift coil.

The coil stack assembly is a separate unit which is installed on the drive mechanism by sliding it over the outside of the latch housing. It rests on the base of the latch housing without mechanical attachment.

Energizing the operating coils causes movement of the pole pieces and latches in the latch assembly.

*(3)* The latch assembly includes the guide tube, stationary pole pieces, moveable pole pieces, and two sets of latches; 1) the moveable gripper latches and 2) the stationary gripper latches.

The latches engage grooves in the drive rod assembly. The moveable gripper latches are moved up or down in 5/8 inch steps by the lift pole to raise or lower the drive rod. The stationary gripper latches hold the drive rod assembly while the moveable gripper latches are repositioned for the next 5/8 inch step.

*(4)* The drive rod assembly includes a flexible coupling, a drive rod, a disconnect button, a disconnect rod, and a locking button.

The drive rod has 5/8 inch grooves which receive the latches during holding or moving of the drive rod. The flexible coupling is attached to the drive rod and provides the means for coupling to the rod cluster control assembly.

The disconnect button, disconnect rod, and locking button provide positive locking of the coupling to the rod cluster control assembly and permits remote disconnection of the drive rod.

The control rod drive mechanism is a trip design. Tripping can occur during any part of the power cycler sequencing if electrical power to the coils is interrupted.

The control rod drive mechanism is threaded and seal welded on an adaptor on top of the reactor vessel and is coupled to the rod cluster control assembly directly below.

The mechanism is capable of raising or lowering a 360 pound load, (which includes the drive rod-weight) at a rate of 45 inches/minute. Withdrawal of the rod cluster control assembly is accomplished by magnetic forces while insertion is by gravity.

The mechanism internals are designed to operate in 650°F reactor coolant. The pressure vessel is designed to contain reactor coolant at 650°F and 2500 psia. The three operating coils are designed to operate at 392°F with forced air cooling required to maintain that temperature.

The control rod drive mechanism shown schematically in Figure 4.2-24 withdraws and inserts a rod cluster control assembly as shaped electrical pulses are received by the operating coils. An ON or OFF sequence, repeated by silicon controlled rectifiers in the power programmer, causes either withdrawal or insertion of the control rod. Position of the control rod is measured by 42 discrete coils mounted on the position indicator assembly surrounding the rod travel housing. Each coil magnetically senses the entry and presence of the top of the ferromagnetic drive rod assembly as it moves through the coil center line.

During plant operation the stationary gripper coil of the drive mechanism holds the rod cluster control assembly in a static position until a stepping sequence is initiated, at which time the moveable gripper coil and lift coil is energized sequentially.

**Rod Cluster Control Assembly Withdrawal**

The rod cluster control assembly is withdrawn by repetition of the following sequence of events (refer to Figure 4.2-24):

*(1)* Movable Gripper Coil (B) - ON

The latch locking plunger raises and swings the movable gripper latches into the drive rod assembly groove. A 1/16 inch axial clearance exists between the latch teeth and the drive rod.

*(2)* Stationary Gripper Coil (A) - OFF

The force of gravity, acting upon the drive rod assembly and attached control rod, causes the stationary gripper latches and plunger to move downward 1/16 inch until the load of the drive rod assembly and attached control rod is transferred to the movable gripper latches. The plunger continues to move downward and swings the stationary gripper latches out of the drive rod assembly groove.

*(3)* Lift Coil (C) - ON

The 5/8 inch gap between the movable gripper pole and the lift pole closes and the drive rod assembly raises one step length (5/8 inch).

*(4)* Stationary Gripper Coil (A) - ON

The plunger raises and closes the gap below the stationary gripper pole. The three links, pinned to the plunger, swing and the stationary gripper latches into a drive rod assembly groove. The latches contact the drive rod assembly and lift it (and the attached control rod) 1/16 inch. The 1/16 inch vertical drive rod assembly movement transfers the drive rod assembly load from the movable gripper latches to the stationary gripper latches.

*(5)* Moveable Gripper Coil (B) - OFF

The latch locking plunger separates from the movable gripper pole under the force of a spring and gravity. Three links, pinned to the plunger, swing the three movable gripper latches out of the drive rod assembly groove.

*(6)* Lift Coil (C) - OFF

The gap between the movable gripper pole and lift pole opens. The movable gripper latches drop 5/8 inch to a position adjacent to a drive rod assembly groove.

*(7)* 7.Repeat Step 1

The sequence described above (Items 1 through 6) is termed as one step or one cycle. The rod cluster control assembly moves 5/8 inch for each step or cycle. The sequence is repeated at a rate of up to 72 steps per minute and the drive rod assembly (which has a 5/8 inch groove pitch) is raised 72 grooves per minute. The rod cluster control assembly is thus withdrawn at a rate up to 45 inches per minute.

**Rod Cluster Control Assembly Insertion**

The sequence for rod cluster control assembly insertion is similar to that for control rod withdrawal, except the timing of lift coil (C) ON and OFF is changed to permit lowering the control assembly.

*(1)* Lift Coil (C) - ON

The 5/8 inch gap between the movable gripper and lift pole closes. The movable gripper latches are raised to a position adjacent to a drive rod assembly groove.

*(2)* Moveable Gripper Coil (B) - ON

The latch locking plunger raises and swings the movable gripper latches into a drive rod assembly groove. A 1/16 inch axial clearance exists between the latch teeth and the drive rod assembly.

*(3)* Stationary Gripper Coil (A) - OFF

The force of gravity, acting upon the drive rod assembly and attached rod cluster control assembly, causes the stationary gripper latches and plunger to move downward 1/16 inch until the load of the drive rod assembly and attached rod cluster control assembly is transferred to the movable gripper latches. The plunger continues to move downward and swings the stationary gripper latches out of the drive rod assembly groove.

*(4)* Lift Coil (C) - OFF

The force of gravity and spring force separates the movable gripper pole from the lift pole and the drive rod assembly and attached rod cluster control assembly drop down 5/8 inch.

*(5)* Stationary Gripper (A) - ON

The plunger raises and closes the gap below the stationary gripper pole. The three links, pinned to the plunger, swing the three stationary gripper latches into a drive rod assembly groove. The latches contact the drive rod assembly and lift it (and the attached control rod) 1/16 inch. The 1/16 inch vertical drive rod assembly movement transfers the drive rod assembly load from the movable gripper latches to the stationary gripper latches.

*(6)* Movable Gripper Coil (B) - OFF

The latch locking plunger separates from the movable gripper pole under the force of a spring and gravity. Three links, pinned to the plunger, swing the three movable gripper latches out of the drive rod assembly groove.

*(7)* Repeat Step 1

The sequence is repeated, as for rod cluster control assembly withdrawal, up to 72 times per minute which gives an insertion rate of 45 inches per minute.

**Holding and Tripping of the Control Rods**

During most of the plant operating time, the control rod drive mechanisms hold the rod cluster control assemblies withdrawn from the core in a static position. In the holding mode, only one coil, the stationary gripper coil (A), is energized on each mechanism. The drive rod assembly and attached rod cluster control assemblies hang suspended from the three latches.

If power to the stationary gripper coil is cut off, the combined weight of the drive rod assembly and the rod cluster control assembly is sufficient to move the latches out of the drive rod assembly groove. The control rod falls by gravity into the core. The trip occurs as the magnetic field, holding the stationary gripper plunger half against the stationary gripper pole, collapses and the stationary gripper plunger half is forced down by the weight acting upon the latches. After the rod cluster control assembly is released by the mechanism, it falls freely until the control rods enter the dashpot section of the guide thimbles in the fuel assembly.

### 4.2.3.3 Design Evaluation

#### 4.2.3.3.1 Reactivity Control Components

The components are analyzed for loads corresponding to normal, upset, emergency and faulted conditions. The analysis performed depends on the mode of operation under consideration.

The scope of the analysis requires many different techniques and methods, both static and dynamic.

Some of the loads that are considered on each component where applicable are as follows:

*(1)* Control Rod Trip (equivalent static load)
*(2)* Differential Pressure
*(3)* Spring Preloads
*(4)* Coolant Flow Forces (static)
*(5)* Temperature Gradients
*(6)* Differences in thermal expansion
  *(a)* Due to temperature differences
  *(b)* Due to expansion of different materials
*(7)* Interference between components
*(8)* Vibration (mechanically or hydraulically induced)
*(9)* All operational transients listed in Table 5.2-2
*(10)* Pump Overspeed
*(11)* Seismic Loads (operation basis earthquake and design basis earthquake)
*(12)* Blowdown forces (injection transients for the cold and hot leg break)
*(13)* Material swelling

*(14)* Gas Generation Pressure

The main objective of the analysis is to satisfy allowable stress limits, to assure an adequate design margin, and to establish deformation limits which are concerned primarily with the functioning of the components. The stress limits are established not only to assure that peak stresses will not reach unacceptable values, but also to limit the amplitude of the oscillatory stress component in consideration of fatigue characteristics of the materials. Standard methods of strength of materials are used to establish the stresses and deflections of these components. The dynamic behavior of the reactivity control components has been studied using experimental test data [20] and experience from operating reactors.

The design of reactivity component rods provides sufficient cold void volume within the burnable absorber, source rods, and neutron absorber rods containing $B_4C$ to limit the internal pressures to a value which satisfies the criteria in Section 4.2.3.1. A gas plenum at the top of the absorber, source, and burnable absorber rods provides void volume for the pressure buildup. Void volume for the helium in the burnable absorber rods is also obtained through the use of glass in tubular form which provides a central void along the length of the rods. Helium gas is not released by the AG-IN-CD neutron absorber rod material but is released by the $B_4C$ absorber material. The internal pressure of source rods continues to increase from ambient until end of life. The stress analysis of reactivity component rods assumes 100% gas release to the rod void volume and satisfies the criteria in Section 4.2.3.1.

Based on available data for properties of the borosilicate glass and on nuclear and thermal calculations for the burnable absorber rods, gross swelling or cracking of the glass tubing is not expected during operation. Some minor creep of the glass at the hot spot on the inner surface of the tube could occur but would continue only until the glass came in contact with the inner liner. The wall thickness of the inner liner is sized to provide adequate support in the event of slumping and to collapse locally before rupture of the exterior cladding if unexpected large volume changes due to swelling or cracking should occur. The top of the inner liner is open to allow communication to the central void by the helium which diffuses out of the glass.

Sufficient diametral and end clearances have been provided in the neutron absorber, burnable absorber and source rods to accommodate the relative thermal expansions and material swelling between the enclosed material and the surrounding clad and end plugs. There is no bending or warping induced in the rods although the clearance offered by the guide thimble would permit a postulated warpage to occur without restraint on the rods. Bending, therefore, is not considered in the analysis of the rods. The radial and axial temperature profiles have been determined by considering gap conductance, thermal expansion, and neutron and/or gamma heating of the contained material as well as gamma heating of the clad. The maximum neutron absorber material temperature was found to be less than 850°F for the AG-IN-CD and less than 1200°F for the $B_4C$ pellets. The maximum temperatures occur axially at only the highest flux region. The maximum borosilicate glass temperature was calculated to be about 1200°F and takes place following the initial rise to power. The glass temperature then decreases rapidly for the following reasons: 1) reduction in power generation due

to $B_{10}$ depletion; 2) better gap conductance as the helium produced diffuses to the gap; and 3) external gap reduction due to borosilicate glass creep. Rod, guide thimble, and dashpot flow analysis performed indicates that the flow is sufficient to prevent coolant boiling and maintain clad temperatures at which the clad material has adequate strength to resist coolant operating pressures and rod internal pressures.

The Westinghouse designed wet annular burnable absorber (WABA) is used in reload cores. Reference [29] verifies that the WABA design meets burnable absorber design criteria.

There is significant operating experience with zircaloy guide thimbles in Westinghouse-designed reactor cores [3]. Reference [28] verifies that the zircaloy guide thimbles in the V5H fuel assembly skeleton comply with the design criteria.

Temperatures for thimbles at the bottom of the fuel assemblies range from approximately 530°F to 563°F. Mid-assembly temperatures reach a high of about 593°F while the maximum temperatures at the top of the assemblies are about 641°F.

Analysis on the rod cluster control spider indicates the spider is structurally adequate to withstand the various operating loads including the higher loads which occur during the drive mechanism stepping action and rod drop. Experimental verification of the spider structural capability has been completed.

The materials selected are considered to be the best available from the standpoint of resistance to irradiation damage and compatibility with the reactor environment. The materials selected partially dictate the reactor environment (e.g., Cl control in the coolant). The current design type reactivity controls exclusive of the $B_4C$ control rod assembly, have been in service for a number of years. Operational experience with Westinghouse-designed RCCAs is provided in Reference [3].

At high fluences the austenitic materials increase in strength with a corresponding decreased ductility (as measured by tensile tests) but energy absorption (as measured by impact tests) remains quite high. Corrosion of the materials exposed to the coolant is quite low and proper control of Cl and $O_2$ in the coolant will prevent the occurrence of stress corrosion. All of the austenitic stainless steel base materials used are processed and fabricated to preclude sensitization. Although the control rod spiders are fabricated by furnace brazing, the procedure used requires that the pieces be rapidly cooled so that the time-at-temperature is minimized. The time that is spent by the control rod spiders in the sensitization range, 800 - 1500°F, is not more than 0.2 hours, as a maximum, during fabrication to preclude sensitization. The 17-4 PH parts are all aged at the highest standard aging temperature of 1100°F to avoid stress corrosion problems exhibited by aging at lower temperatures.

Based on the following considerations, it is judged that the potential for interference with rod cluster control assembly movement due to unusual local corrosion phenomena of the Zircaloy guide thimbles is very low. Operational experience to date and limited PIE data on irradiated thimbles are in support of this conclusion.

*(1)* Gap Considerations

The minimum hot diametral gap in the reduced dash pot area of the thimble is smaller than the minimum hot diametral gap in the upper thimble area. Thus, the dashpot area constitutes the region of maximum interest relative to any possible effects of localized corrosion.

*(2)* Intrinsic Corrosion

Using conservative calculations of corrosion kinetics in the dashpot area of the thimble ($T_{coolant}$ = 600°F and t = 1500 calendar days) it was determined that approximately 0.44 mils of oxide would be found on the Zircaloy. Taking the Pilling-Bedworth ratio at 1.56, then:

$$\text{mils metal} = \frac{0.44 \text{ mils}}{1.56} = 0.28 \text{ mils}$$

and the decrease in tube inside diameter is:

$$2 \times (0.44 - 0.28) = 0.32 \text{ mils or } 0.00032 \text{ inches.}$$

This latter value is considered to be very small compared to the minimum hot gap and the risk of interference with rod movement due to inherent corrosion is considered negligibly low.

Corrosion of the stainless steel control rod clad is also considered negligible relative to potential for annulus blockage.

*(3)* Deformation Enhanced Corrosion and Hydriding

Maximum deformation in the expanded area of the thimble is taken to be less than 60%. Studies of the effect of cold work on Zircaloy alloys under both steam and water conditions show no significant effects attributable to residual cold work on corrosion or hydriding behavior[14,15]. Preliminary examinations of thimbles taken from the Point Beach reactor indicate essentially equivalent corrosion rates in both bulged and unbulged areas. Thus, it is judged appropriate to estimate maximum corrosion effects by utilization of normal corrosion and hydriding models for the nominal metallurgical condition of the thimble.

*(4)* Crevice Corrosion

Under certain conditions, the Zircaloy alloys are susceptible to serious caustic assisted corrosion. Since LiOH is used for pH control in the primary coolant, the potential for such corrosion exists in the Westinghouse design. Studies show that caustic assisted attack can occur in crevices with low LiOH concentrations, but only under conditions of nucleate boiling[16,17]. Other work where crud, $Cl^-$, $Fe^{++}$, and $F^-$ were tested under conditions with no heat transfer, indicated no specific attack in crevices although in 0.01 M LiF, a general overall attack of the Zircaloy was noted.

Since the Westinghouse design is conservatively designed to preclude nucleate boiling in the annulus of the sleeve and thimble, and the overall $Li^+$, $Cl^-$, $F^-$, etc., concentrations are controlled by the primary coolant specification, it is judged that crevice corrosion will not occur. Observations to date on irradiated thimbles support this expectation.

*(5)* Effects of Surface Contamination

The use of any materials containing compounds of elements which are suspected to be detrimental if permitted to contact a fuel assembly component is subjected to control by specification. Materials considered particularly detrimental to zircaloy are not used in the bulging operation. After fabrication, the completed fuel assembly is subjected to an aqueous cleaning operation. Tooling development studies, tests made to determine localized thinning, hydriding orientation studies relating to effects of plastic deformation, and limited post irradiation examination studies of expanded joints indicate no cases of significant surface contamination. These tests have not been formally documented. Taking all of these factors into account, and also the fact that the as received surface condition of the thimble tubing is controlled by purchase specification, it is judged that the risk of significant corrosion due to surface contamination is quite low.

Analysis of the rod cluster control assemblies show that if the drive mechanism housing ruptures, the rod cluster control assembly will be ejected from the core by the pressure differential of the operating pressure and ambient pressure across the drive rod assembly. The ejection is also predicted on the failure of the drive mechanism to retain the drive rod/rod cluster control assembly position. It should be pointed out that a drive mechanism housing rupture will cause the ejection of only one rod cluster control assembly with the other assemblies remaining in the core. Analysis also showed that a pressure drop in excess of 4000 psi must occur across a two-fingered vane to break the vane/spider body joint causing ejection of two neutron absorber rods from the core. Since the greatest pressure drop in the system is only 2250 psi, a pressure drop in excess of 4000 psi is not possible. Thus, the ejection of the neutron absorber rods is not possible.

Ejection of a burnable absorber or thimble plug assembly is conceivable based on the postulation that the hold down bar fails and that the base plate and burnable absorber rods are severely deformed. In the unlikely event that failure of the hold down bar occurs, the upward displacement of the burnable absorber assembly only permits the base plate to contact the upper core plate. Since this displacement is small, the major portion of the borosilicate glass tubing remains positioned within the core. In the case of the thimble plug assembly, the thimble plugs will partially remain in the fuel assembly guide thimbles thus maintaining a majority of the desired flow impedance. Further displacement or complete ejection would necessitate the square base plate and burnable absorber rods be forced, thus plastically deformed, to fit up through a smaller diameter hole. It is expected that this condition requires a substantially higher force or pressure drop than that of the hold down bar failure.

Experience with control rods, burnable absorber rods, and source rods are discussed in Reference [3].

The mechanical design of the reactivity control components provides for the protection of the active elements to prevent the loss of control capability and functional failure of critical components. The components have been reviewed for potential failure and consequences of a functional failure of critical parts. The results of the review are summarized below.

**Rod Cluster Control Assembly**

*(1)* The basic absorbing materials are sealed from contact with the primary coolant and the fuel assembly and guidance surfaces by a high quality stainless steel clad. Potential loss of absorber mass or reduction in reactivity control material due to mechanical or chemical erosion or wear is therefore reliably prevented.

*(2)* A breach of the cladding for a limited number of absorber rods for any postulated reason does not result in serious consequences. The $B_4C$ absorber is relatively inert and would still remain remote from high coolant velocity regions.

*(3)* The individually clad absorber rods are doubly secured to the retaining spider vane by a threaded joint and a welded lock pin. This joint has been qualified by functional testing and actual service in operating plants. It should also be noted that in several instances of control rod jamming caused by foreign particles, the individual rods at the site of the jam have borne the full capacity of the control rod drive mechanism and higher impact loads to dislodge the jam without failure. The conclusion to be drawn from this experience is that this joint is extremely insensitive to potential mechanical damage. A failure of the joint would result in the almost complete insertion of the individual rod into the core, during normal operating conditions. This results in reduced reactivity which is a fail safe condition.

*(4)* The spider finger braze joint by which the individual rods are fastened to the vanes has also experienced the service described above and been subjected to the same jam freeing procedures also without failure. A failure of this joint would also result in the almost complete insertion of the individual rod into the core, during normal operating conditions.

*(5)* The radial vanes are attached to the spider body, again by a brazed joint. The joints are designed to a theoretical strength in excess of that of the components joined.

It is a feature of the design that the guidance of the rod cluster control is accomplished by the inner fingers of these vanes. They are therefore the most susceptible to mechanical damage. Since these vanes carry two rods, failure of the vane-to-hub joint such as the isolated incidents at Connecticut-Yankee does not prevent the free insertion of the rod pair[3].

Neither does such a failure interfere with the continuous free operation of the drive line, also as experienced at Connecticut-Yankee[3].

Failure of the vane-to-hub joint of a single rod vane could potentially result in failure of the separated vane and rod to insert. This could occur only at withdrawal elevations where the spider is above the continuous guidance section of the guide tube (in the upper internals). A rotation of the disconnected vane could cause it to hang on one of the guide cards in the intermediate guide tube. Such an occurrence would be evident from the failure of the rod cluster control to insert below a certain elevation but with free motion above this point.

This possibility is considered extremely remote because the single rod vanes are subjected to only vertical loads and very light lateral reactions from the rods. The consequences of such a failure are not considered critical since only one drive line of the reactivity control system would be involved. This condition is readily observed and can be cleared at shutdown.

*(6)* The spider hub being of single unit cylindrical construction is very rugged and of extremely low potential for damage. It is difficult to postulate any condition to cause failure. Should some unforeseen event cause fracture of the hub above the vanes, the lower portion with the vanes and rods attached would insert by gravity into the core causing a reactivity decrease. The rod could then not be removed by the drive line, again a fail safe condition. Fracture below the vanes cannot be postulated since all loads, including scram impact, are taken above the vane elevation.

*(7)* The rod cluster control rods are provided a clear channel for insertion by the guide thimbles of the fuel assemblies. Providing this physical barrier between the fuel rod and the intended insertion channel protects against all fuel rod failures. Distortion of the fuel rods by bending cannot apply sufficient force to damage or significantly distort the guide thimble. Fuel rod distortion by swelling, though precluded by design, would be terminated by fracture before contact with the guide thimble occurs. If such were not the case, it would be expected that a force reaction at the point of contact would cause a slight deflection of the guide thimble. The radius of curvature of the deflected shape of the guide thimbles would be sufficiently large to have a negligible influence on rod cluster control insertion.

**Burnable Absorber Assemblies**

The burnable absorber assemblies are static temporary reactivity control elements. The axial position is assured by the hold down assembly which bears against the upper core plate. Their lateral position is maintained by the guide thimbles of the fuel assemblies.

The individual rods are shouldered against the underside of the retainer plate and securely fastened at the top by a threaded nut which is then crimped or locked in place by a welded pin. The square dimension of the retainer plate is larger than the diameter

of the flow holes through the core plate. Failure of the hold down bar or spring pack therefore does not result in ejection of the burnable absorber rods from the core.

The only incident that could potentially result in ejection of the burnable absorber rods is a multiple fracture of the retainer plate. This is not considered credible because of the light loads borne by this component. During normal operation the loads borne by the plate are approximately 5 pounds/rod or a total of 100 pounds distributed at the points of attachment. Even a multiple fracture of the retainer plate would result in jamming of the plate segments against the upper core plate, again preventing ejection. Excessive reactivity increase due to burnable absorber ejection is therefore prevented.

The burnable absorber rod is clad with the same type of stainless steel cladding as is used for the rod cluster control rods. The burnable absorber is a borosilicate glass tube which is maintained in position by a central hollow stainless steel tube. Burnable absorber rods are placed in static assemblies and are not subjected to motion which might damage the rods. Further, the guide thimbles of the fuel assembly afford protection from damage.

During thousands of rod years of accumulated borosilicate glass burnable absorber (BA) rod experience, there have been only six (6) occurrences of BA clad penetrations or probable penetration. These occurred on borosilicate glass rods that were either assembled on secondary source assemblies which are subjected to multiple core cycles, or on BA assemblies which also had undergone multi-cycle use.

In most of these cases(4) the rods were found to be fractured with all or part of the individual broken rods being stuck in the fuel assembly guide thimbles (Ref. Sec. 5.2, WCAP-8183, Rev. 15). This exposed the borosilicate glass to the primary coolant. The fuel assemblies with the stuck BA rods were recycled through one or more additional cycles with no operational problems. Based on these results, the consequences of breaching of the clad of borosilicate glass BAs were found to be minor and to pose no operational problems.

To further insure trouble free performance, present designs no longer use borosilicate glass BA rods attached to the secondary source assemblies. Recycling of regular glass BA assemblies is only done occasionally to improve core performance. The Westinghouse designed wet annular burnable absorber (WABA) is used in reload cores. Reference [29] verified that the WABA design meets burnable absorber design criteria.

**Drive Rod Assemblies**

All postulated failures of the drive rod assemblies either by fracture or uncoupling lead to the fail safe condition. If the drive rod assembly fractures at any elevation, that portion remaining coupled falls with, and is guided by the rod cluster control assembly. This results in a reactivity decrease.

## 4.2.3.3.2 Control Rod Drive Mechanism

**Material Selection**

All pressure retaining materials comply with Section III of the ASME Boiler and Pressure Vessel Code, and are fabricated from austenitic (Type 304) stainless steel.

Magnetic pole pieces are fabricated from Type 410 stainless steel. All non-magnetic parts, except pins and springs, are fabricated from Type 304 stainless steel. Haynes 25 is used to fabricate link pins. Springs are made from nickel-chrome-iron alloy. Latch arm tips are clad with Stellite-6 to provide improved wearability. Hard chrome plate and Stellite-6 are used selectively for bearing and wear surfaces.

At the start of the development program, a survey was made to determine whether a material better than Type 410 stainless steel was available for the magnetic pole pieces. Ideal material requirements are as follows:

*(1)* High magnetic saturation value

*(2)* High permeability

*(3)* Low coercive force

*(4)* High resistivity

*(5)* High curie temperature

*(6)* Corrosion resistant

*(7)* High impact strength

*(8)* Non-oriented

*(9)* High machinability

*(10)* Resistance to radiation damage

After a comprehensive material trade-off study was made it was decided that the Type 410 stainless steel was satisfactory for this application.

The cast coil housings require a magnetic material. Both low-carbon cast steel and ductile iron have been successfully tested for this application. The choice, made on the basis of cost, indicates that ductile iron will be specified on the control rod drive mechanism. The finished housings are zinc plated to provide corrosion resistance.

Coils are wound on bobbins of molded Dow Corning 302 material, with double glass-insulated copper wire. Coils are then vacuum-impregnated with silicon varnish. A wrapping of mica sheet is secured to the coil outside diameter. The result is a well-insulated coil capable of sustained operation at 200 degrees centigrade.

The drive shaft assembly utilizes a Type 410 stainless steel drive rod. The coupling is machined from Type 403 stainless steel. Other parts are Type 304 stainless steel with the exception of the springs which are nickel-chrome-iron alloy and the locking button which is Haynes 25.

**Radiation Damage**

As required by the equipment specification, the control rod drive mechanisms are designed to meet a radiation requirement of 10 rads/hour. Materials have been selected to meet this requirement. The above radiation level which amounts to 1.753 x $10^6$ rads in twenty years will not limit control rod drive mechanism life. Control rod drive mechanisms at Yankee Rowe, which have been in operation since 1960, have not experienced problems due to radiation.

**Positioning Requirements**

The mechanism has a step length of 5/8 inch which determines the positioning capabilities of the control rod drive mechanism. (Note: Positioning requirements are determined by reactor physics.)

**Evaluation of Material's Adequacy**

The ability of the pressure housing components to perform throughout the design lifetime as defined in the equipment specification is confirmed by the stress analysis report required by the ASME Boiler and Pressure Vessel Code, Section III. Internal components subjected to wear will withstand a minimum of 3,000,000 steps without refurbishment as confirmed by life tests. Latch assembly inspection is recommended after 2.0/2.5 x $10^6$ steps have been accumulated on a single control rod drive mechanism.

**Results of Dimensional and Tolerance Analysis**

With respect to the control rod drive mechanism system as a whole, critical clearances are present in the following areas:

*(1)* Latch assembly (Diametral clearances)

*(2)* Latch arm-drive rod clearances

*(3)* Coil stack assembly-thermal clearances

*(4)* Coil fit in coil housing

The following write-up defines clearances that are designed to provide reliable operation in the control rod drive mechanism in these four critical areas. These clearances have been proven by life tests and actual field performance at operating plants.

**Latch Assembly - Thermal Clearances**

The magnetic latch has several clearances where parts made of Type 410 stainless steel fit over parts made from Type 304 stainless steel. Differential thermal expansion is therefore important. Minimum clearances of these parts at 68°F is 0.011 inches. At the maximum design temperature of 650°F, minimum clearance is 0.0045 inches and at the maximum expected operating temperature of 550°F, is 0.0057 inches.

**Latch Arm - Drive Rod Clearances**

The control rod drive mechanism incorporates a load transfer action. The movable or stationary gripper latch is not under load during engagement, as previously explained, due to load transfer action.

Figure 4.2-26 shows latch clearance variation with the drive rod as a result of minimum and maximum temperatures. Figure 4.2-27 shows clearance variations over the design temperature range.

**Coil Stack Assembly - Thermal Clearances**

The assembly clearance of the coil stack assembly over the latch housing was selected so that the assembly could be removed under all anticipated conditions of thermal expansion.

At 70°F inside diameter of the coil stack is 7.308/7.298 inches. The outside diameter of the latch housing is 7.260/7.270 inches.

Thermal expansion of the mechanism due to operating temperature of the control rod drive mechanism results in minimum inside diameter of the coil stack being 7.310 inches at 222°F and the maximum latch housing diameter being 7.302 inches at 532°F.

Under extreme tolerance conditions listed above it is necessary to allow time for a 70°F coil housing to heat during a replacement operation.

Four stack assemblies were removed from four hot control rod drive mechanisms mounted on 11.035 inch centers on a 550°F test loop, allowed to cool, and then replaced without incident as a test to prove the preceding.

**Coil Fit in Coil Housing**

Control rod drive mechanism and coil housing clearances are selected so that coil heat up results in a close to tight fit. This is done to facilitate thermal transfer and coil cooling in a hot control rod drive mechanism.

## 4.2.3.4 Tests, Verification, and Inspections

### 4.2.3.4.1 Reactivity Control Components

Tests and inspections are performed on each reactivity control component to verify the mechanical characteristics. In the case of the rod cluster control assembly, prototype

testing has been conducted and both manufacturing tests/inspections and functional testing at the plant site are performed.

During the component manufacturing phase, the following requirements apply to the reactivity control components to assure the proper functioning during reactor operation:

*(1)* All materials are procured to specifications to attain the desired standard of quality.

*(2)* A spider from each braze lot is proof tested by applying a 5000 pound load to the spider body, so that approximately 208.3 pounds is applied to each finger. This proof load provides a bending moment at the spider body approximately equivalent to 1.4 times the load caused by the acceleration imposed by the control rod drive mechanism. All spiders are tested in this manner.

*(3)* All clad/end-plug welds are checked for integrity by visual inspection, x-ray, and helium leak check. All the seal welds in the neutron absorber rods, burnable absorber rods and source rods are checked in this manner.

*(4)* To assure proper fitup with the fuel assembly, the rod cluster control, burnable absorber and source assemblies are installed in the fuel assembly without restriction or binding in the dry condition with a force not to exceed 15 pounds. Also a straightness of 0.01 in/ft is required on the entire inserted length of each rod assembly, except burnable absorber rods, where the straightness requirement is 0.012 in/ft.

The rod cluster control assemblies are functionally tested, following initial core loading but prior to criticality to demonstrate reliable operation of the assemblies. Each assembly is operated one time at no flow/cold conditions and one time at full flow/hot conditions. The assemblies are also trip tested at full flow/hot conditions. Those assemblies whose trip times fall outside a certain tolerance will be tested an additional 3 times at full flow/hot conditions. Thus each assembly is adequately tested to verify that the assemblies are properly functioning.

### 4.2.3.4.2 Control Rod Drive Mechanisms

Quality assurance procedures during production of control rod drive mechanisms include material selection, process control, mechanism component tests and inspections during production and hydrotests.

After all manufacturing procedures had been developed, several prototype control rod drive mechanisms and drive rod assemblies were life tested with the entire drive line under environmental conditions of temperature, pressure and flow. All acceptance tests confirm the $3 \times 10^6$ step unrefurbished life capability of the control rod drive mechanism and drive rod assembly.

These tests include verification that the trip time achieved by the control rod drive mechanisms meet the design requirement from start of rod cluster control assembly motion to top of dashpot. This trip time requirement is confirmed for each control rod drive mechanism prior to initial reactor operation, as required by Technical Specifications.

It is expected that all control rod drive mechanisms will meet specified operating requirements for the duration of plant life with normal refurbishment. However, a technical specification pertaining to an inoperable rod cluster control assembly has been set.

If a rod cluster control assembly cannot be moved by its mechanism, adjustments in the boron concentration ensure that adequate shutdown margin would be achieved following a trip. Thus, inability to move one rod cluster control assembly can be tolerated. Therefore, the number of inoperable rod cluster control assemblies has been limited to one.

In order to demonstrate proper operation of the control rod drive mechanism and to ensure acceptable core power distributions during operation, partial rod cluster control assembly movement checks are performed on the rod cluster control assemblies during reactor critical operation. (Refer to Plant Technical Specifications). In addition, drop tests of the rod cluster control assemblies are performed after each refueling shutdown to demonstrate continued ability to meet trip time requirements.

The trip time requirement is confirmed for each control rod drive mechanism at hot, full flow conditions prior to reactor operation in accordance with Technical Specifications.

Mechanical performance of a full-scale $B_4C$ control rod cluster assembly at reactor operating temperature, pressure, and various flow conditions has been demonstrated in the Westinghouse D-loop test facility located at Forest Hills, Pennsylvania. The tests were conducted in a similar manner to those of the 17 x 17 fuel assembly and control rod, the results of which were previously reported in references [21] and [22].

There are no significant differences between the prototype control rod drive mechanisms and the production units. Design materials, tolerances and fabrication techniques (Section 4.2.3.3.2) are the same. Actual experience in operating

Westinghouse plants indicates excellent performance of control rod drive mechanisms.

All units are production tested prior to shipment to confirm ability of the control rod drive mechanism to meet design specification-operational requirements.

Each production control rod drive mechanism undergoes a production test as listed below:

| Test | Acceptance Criteria |
|---|---|
| Cold (ambient) hydrostatic | ASME Section III |
| Confirm step length and load transfer (stationary gripper to movable gripper or movablegripper to stationary gripper) | Step Length<br>5/8 + 0.015 inches axial movement<br>Load Transfer<br>0.047 inches nominal axial movement |
| Cold (ambient) performance<br>Test at Design load -<br>5 full travel excursions | Operating Speed<br>45 inches/minute<br>Trip Delay<br>Free fall of drive rod to begin within 150 msec |

### 4.2.3.5 Instrumentation Applications

Instrumentation for determining reactor coolant average temperature ($T_{avg}$) is provided to create demand signals for moving groups of rod cluster control assemblies to provide load follow (determined as a function of turbine impulse pressure) during normal operation and to counteract operational transients. The hot and cold leg resistance temperature detectors (RTDs) are described in Section 7.2. The location of the RTDs in each loop is shown on the flow diagrams in Chapter 5. The Reactor Control System which controls the reactor coolant average temperature by regulation of control rod bank position is described in Section 7.7.

Rod position indication instrumentation is provided to sense the actual position of each control rod so that the actual position of the individual rod may be displayed to the operator. Signals are also supplied by this system as input to the rod deviation comparator. The rod position indication system is described in Chapter 7.

The reactor makeup control system whose functions are to permit adjustment of the reactor coolant boron concentration for reactivity control (as well to maintain the desired operating fluid inventory in the volume control tank), consists of a group of instruments arranged to provide a manually preselected makeup composition that is

borated or diluted as required to the charging pump suction header or the volume control tank. This system, as well as other systems including boron sampling provisions that are part of the Chemical and Volume Control System, are described in Section 9.3.

When the reactor is critical, the normal indication of reactivity status in the core is the position of the control bank in relation to reactor power (as indicated by the Reactor Coolant System loop ΔT) and coolant average temperature.

These parameters are used to calculate insertion limits for the control banks to give warning to the operator of excessive rod insertion. Monitoring of the neutron flux for various phases of reactor power operation as well as of core loading, shutdown, startup, and refueling is by means of the Nuclear Instrumentation System. The monitoring functions and readout and indication characteristics for the following means of monitoring reactivity are included in the discussion on safety related display instrumentation in Section 7.5:

*(1)* Nuclear Instrumentation System

*(2)* Temperature Indicators

*(a)* $T_{average}$ (Measured)

*(b)* ΔT (Measured)

*(c)* Auctioneered $T_{average}$

*(d)* $T_{reference}$

*(3)* Demand Position of Rod Cluster Control Assembly Group

*(4)* Actual Rod Position Indicator.

**REFERENCES**

*(1)* Christensen, J. A., Allio, R. J., and Biancheria, A., "Melting Point of Irradiated $U0_2$," WCAP-6065, February 1965.

*(2)* Eggleston, F. T., "Safety Related Research and Development for Westinghouse Pressurized Water Reactors-Program Summaries, Winter 1976 -Summer 1978," WCAP-8768, Revision 2, October 1977.

*(3)* "Operational Experience with Westinghouse Cores," WCAP-8183 (Latest Revision).

*(4)* Supplemental information on fuel design transmitted from R. Salvatore, Westinghouse NES, to D. Knuth, AEC, as attachments to letters NS-SL-518 (12/22/73), NS-SL-521 (12/29/72), NS-SL-524 (12/29/72) and NS-SL-543

(1/12/73), (Westinghouse Proprietary); and supplemental information on fuel design transmitted from R. Salvatori, Westinghouse NES, to D. Knuth, AEC, as attachments to letters NS-SL-527 (1/2/73) and NS-SL-544 (1/12/73).

*(5)* Hellman, J. M., (Ed.), "Fuel Densification Experimental Results and Model for Reactor Operation," WCAP-8218-P-A (Proprietary) and WCAP-8219-A (Non-Proprietary), March 1975.

*(6)* Deleted by Amendment 73

*(7)* Gesinski, L., Chiang, D. and Nakazato, S., "Safety Analysis of the 17 x 17 Fuel Assembly for Combined Seismic and Loss of Coolant Accident," WCAP-8236 (Proprietary) and WCAP-8288 (Non-Proprietary), December 1973.

*(8)* Deleted by Amendment 63.

*(9)* O'Donnell, W. J. and Langer, B. F., "Fatigue Design Basis for Zircaloy Components," Nuclear Science and Engineering, 20,1-12, 1964.

*(10)* Cadek, F. F., Cerni, S., Hellman, J. M., Reavis, W. J., "Fuel Rod Bowing," WCAP 8691 (Proprietary) and WCAP 8692 (Non-Proprietary), December 1975.

*(11)* Woodson, N.D., Bakos, F. R., "Energy Systems Business Unit, Power Generation Business Unit, Quality Assurance Plan", WCAP 8370, Rev. 12A, April, 1992.

*(12)* Deleted by Amendment 73

*(13)* Deleted by Amendment 73

*(14)* Carver, M. D. and Antrim, C. W., "Zirconium Progress Report for the Period June 15 - September 15, 1956," USBM-U-210.

*(15)* Burns, W. A. and Maffei, H. P., "ASTM Special Technical Publication No. 368".

*(16)* Anderson, W. K. and McGoff, M. J., "Corrosion of Zircaloy in Crevices Under Nucleate Boiling Conditions," KAPL-2203, 1962.

*(17)* Berry, W. E., White, E. L., and Fink, F. W., "Zircaloy-4 Corrosion in Halide Solutions and at Crevices in High Temperature Water," BMI-1571, 1962.

*(18)* Deleted by Amendment 73

*(19)* Deleted by Amendment 73

*(20)* DeMario, E. E., "Hydraulic Flow Test of the 17 x 17 Fuel Assembly," WCAP 8278 (Proprietary) and WCAP 8279 (Non-Proprietary), February 1974.

*(21)* Cooper, F. W., Jr., "l7xl7 Drive Line Components Tests Phase IB, II, III, D-Loop-Drop and Deflection," WCAP-8446 (Proprietary) and WCAP-8449, December 1974.

*(22)* Skarita, J., (Ed.), "Hybrid $B_4C$ Absorber Control Rod Evaluation Report," WCAP-8846, September 1976.

*(23)* Risher, D. H., et. al., "Safety Analysis for the Revised Fuel Rod Internal Pressure Design Basis," WCAP-8963, November 1976 (Proprietary) and WCAP-8964, August 1977 (Non-proprietary).

*(24)* Gesinski, L.,et. al., "Safety Analysis of the 17 X 17 Fuel Assembly for Combined Seismic and Loss-of-Coolant Accident," WCAP-8288, Addendum 1, April 1974.

*(25)* Miller, J. V., (Ed.), "Improved Analytical Models Used in Westinghouse Fuel Rod Design Computations," WCAP-8720 (Proprietary) and WCAP-8785 (Non-Proprietary), October 1976.

*(26)* Weiner, R. A., et al, "Improved Fuel Performance Models for Westinghouse Fuel Rod Designs and Safety Evaluations," WCAP-10851-P-A (Proprietary) and WCAP-11873-A (Non-Proprietary), August 1988.

*(27)* Davidson, S. L., (Ed.), et al, "Extended Burnup Evaluation of Westinghouse Fuel," WCAP-10125-P-A (Proprietary) and WCAP-10126-A (Non-Proprietary), December 1985.

*(28)* Davidson, S. L., and Kramer, W. R., (Ed.), "Reference Core Report VANTAGE 5 Fuel Assembly," WCAP-10444-P-A and WCAP-10445-NP-A, September 1985, and Addendum 2A, February 1989.

*(29)* Skaritka, J., et al, "Westinghouse Wet Annular Burnable Absorber Evaluation Report," WCAP-10021-NP-A, Revision 1 (Non-Proprietary), October 1983.

*(30)* Watkins, B., and Wood, D. S., "The Significance of Irradiation-Induced Creep on Reactor Performance of a Zircaloy-2 Pressure Tube," Applications - Related Phenomena for Zirconium and its Alloys, ASTM STP 458. American Society for Testing and Materials, 1969, pp 226-240.

**Table 4.2-1 Maximum Deflections Allowed for Reactor Internal Support Structures**

| Component | Allowable Deflections (in) | No-Loss-Of Function Deflections (in) |
|---|---|---|
| Upper Barrel | | |
| radial inward | 4.1 | 8.2 |
| radial outward | 1.00 | 1.0 |
| Upper Package | 0.10 | 0.15 |
| Rod Cluster Guide Tubes | 1.00 | 1.75 |

THIS PAGE INTENTIONALLY BLANK

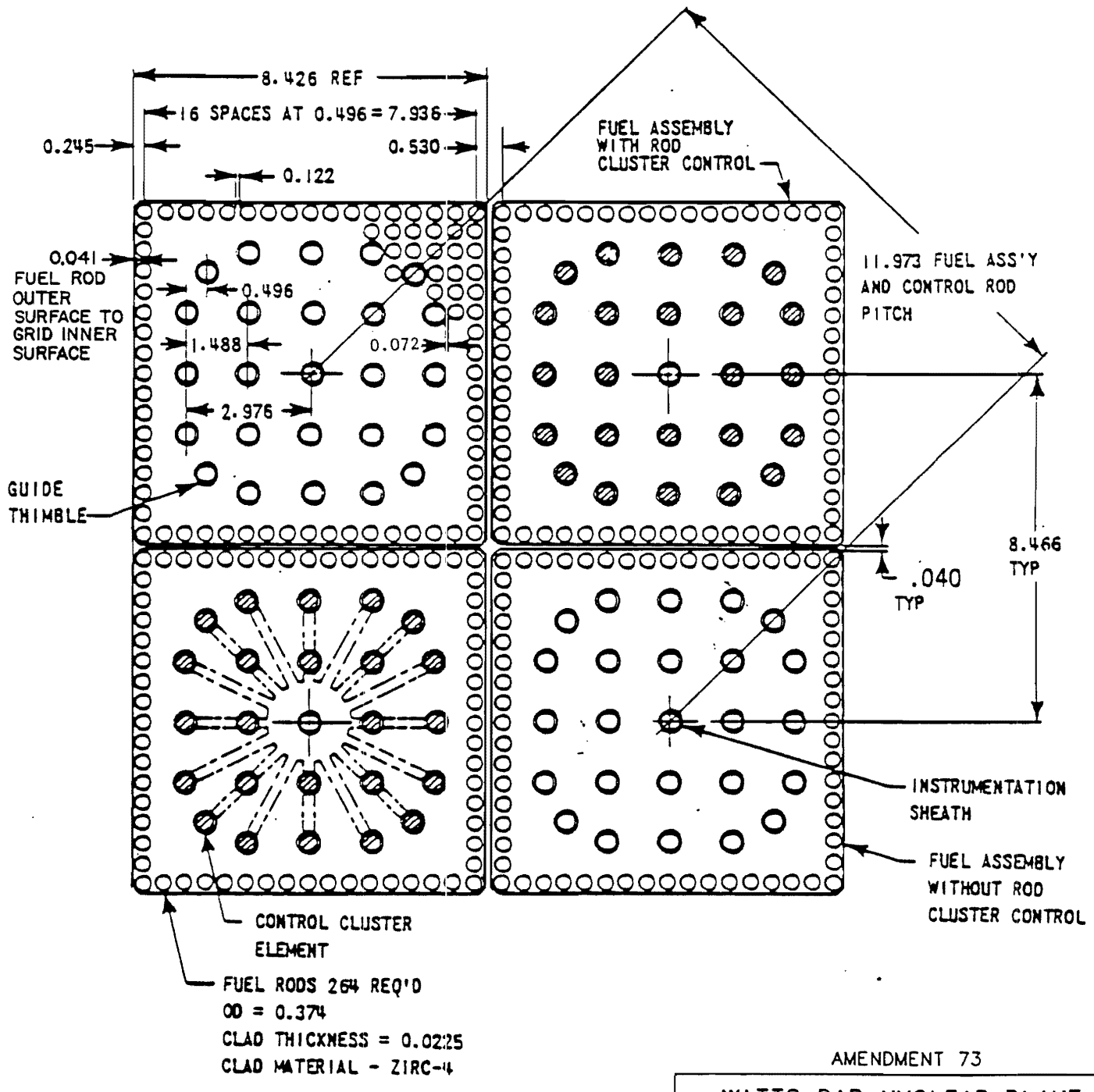


AMENDMENT 73

WATTS BAR NUCLEAR PLANT
FINAL SAFETY
ANALYSIS REPORT

Fuel Assembly Cross Section
17 x 17

FIGURE 4.2-1

**Figure 4.2-1 Fuel Assembly Cross Section 17 x 17**

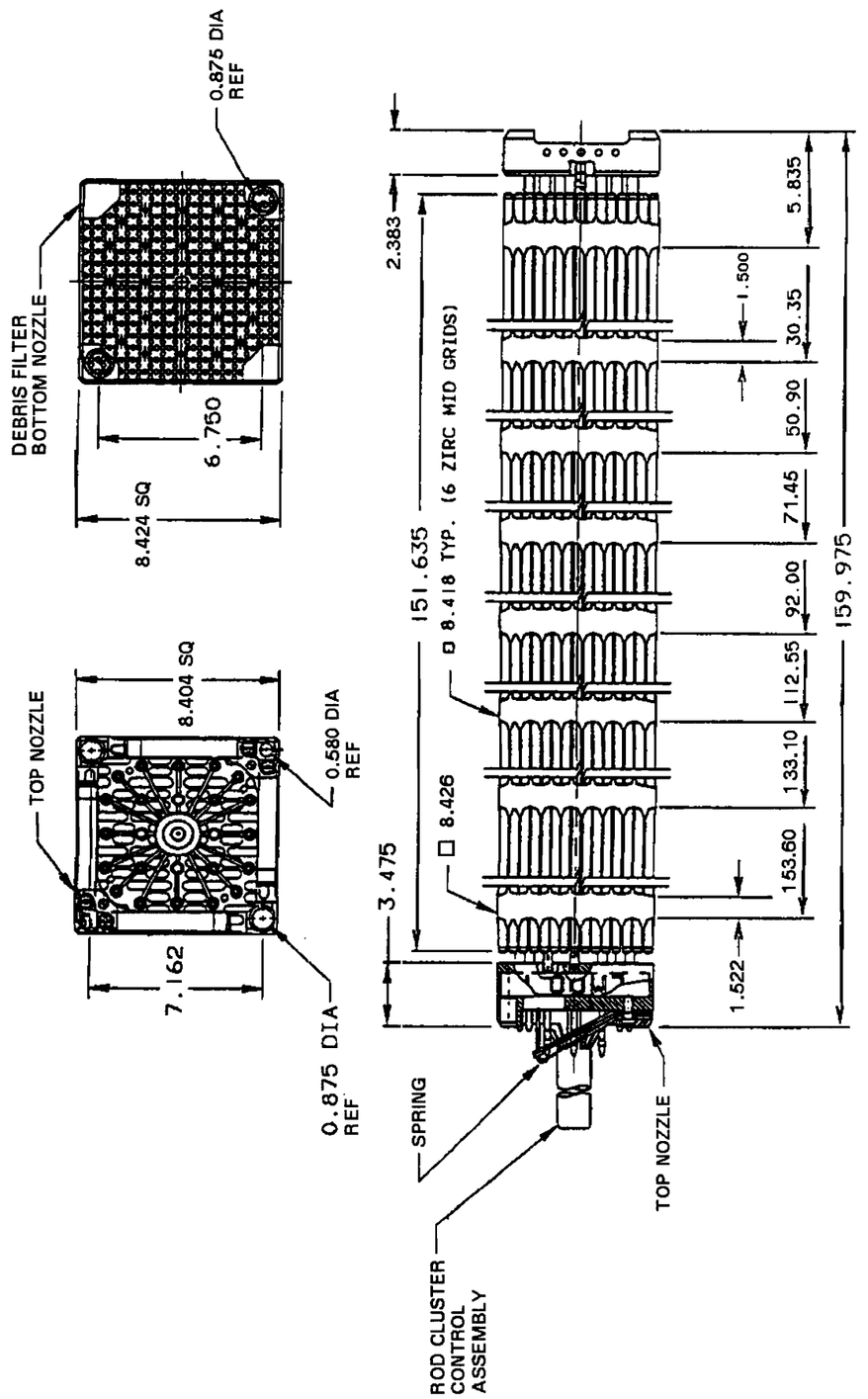


Figure 4.2-2 17 x 17 Vantage 5H Recage Fuel Assembly

AMENDMENT 73

WATTS BAR NUCLEAR PLANT
FINAL SAFETY
ANALYSIS REPORT

17 X 17 VANTAGE 5H
RECAGE FUEL ASSEMBLY
FIGURE 4.2-2

SCANNED DOCUMENT
THIS IS A SCANNED DOCUMENT MAINTAINED ON THE WBNP OPTIGRAPHICS SCANNER DATABASE

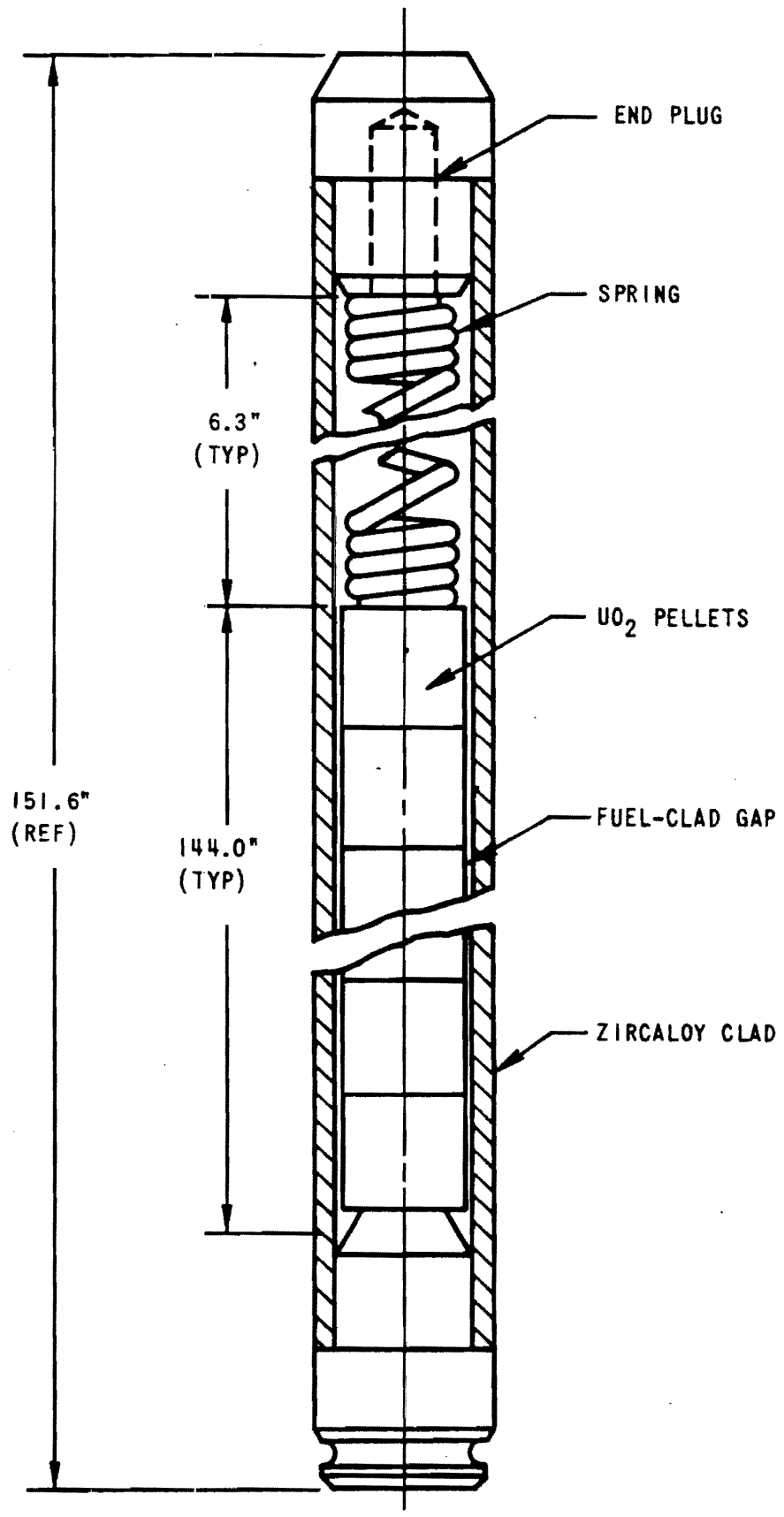


Figure 4.2-3 Fuel Rod Schematic

Figure 4.2-3 Fuel Rod Schematic

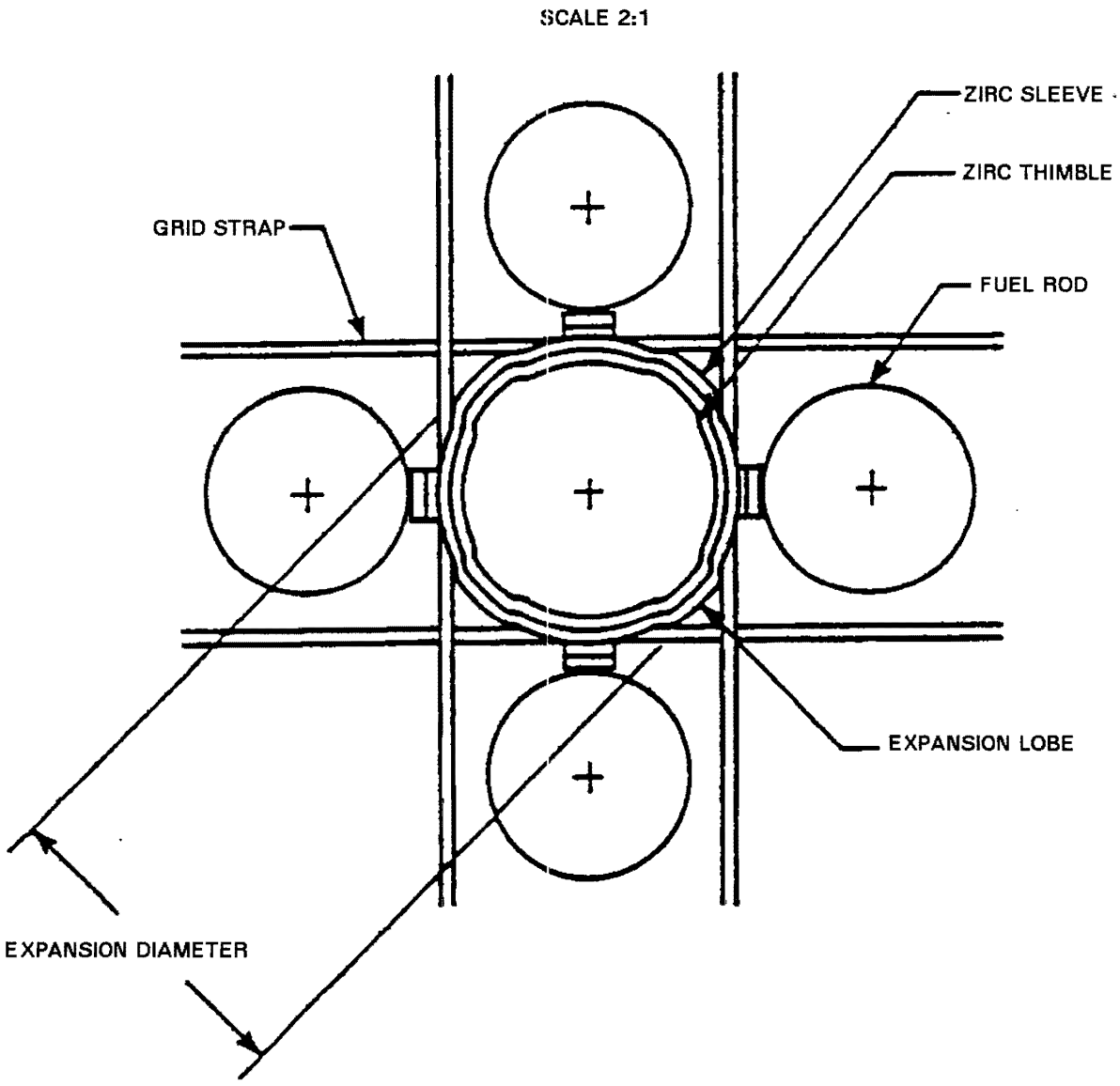


AMENDMENT 73

WATTS BAR NUCLEAR PLANT
FINAL SAFETY
ANALYSIS REPORT

MID GRID EXPANSION JOINT DESIGN
PLAN VIEW
FIGURE 4.2-4

SCANNED DOCUMENT
THIS IS A SCANNED DOCUMENT MAINTAINED ON THE WBNP OPTIGRAPHICS SCANNER DATABASE

**Figure 4.2-4 Mid Grid Expansion Joint Design-Plan View**

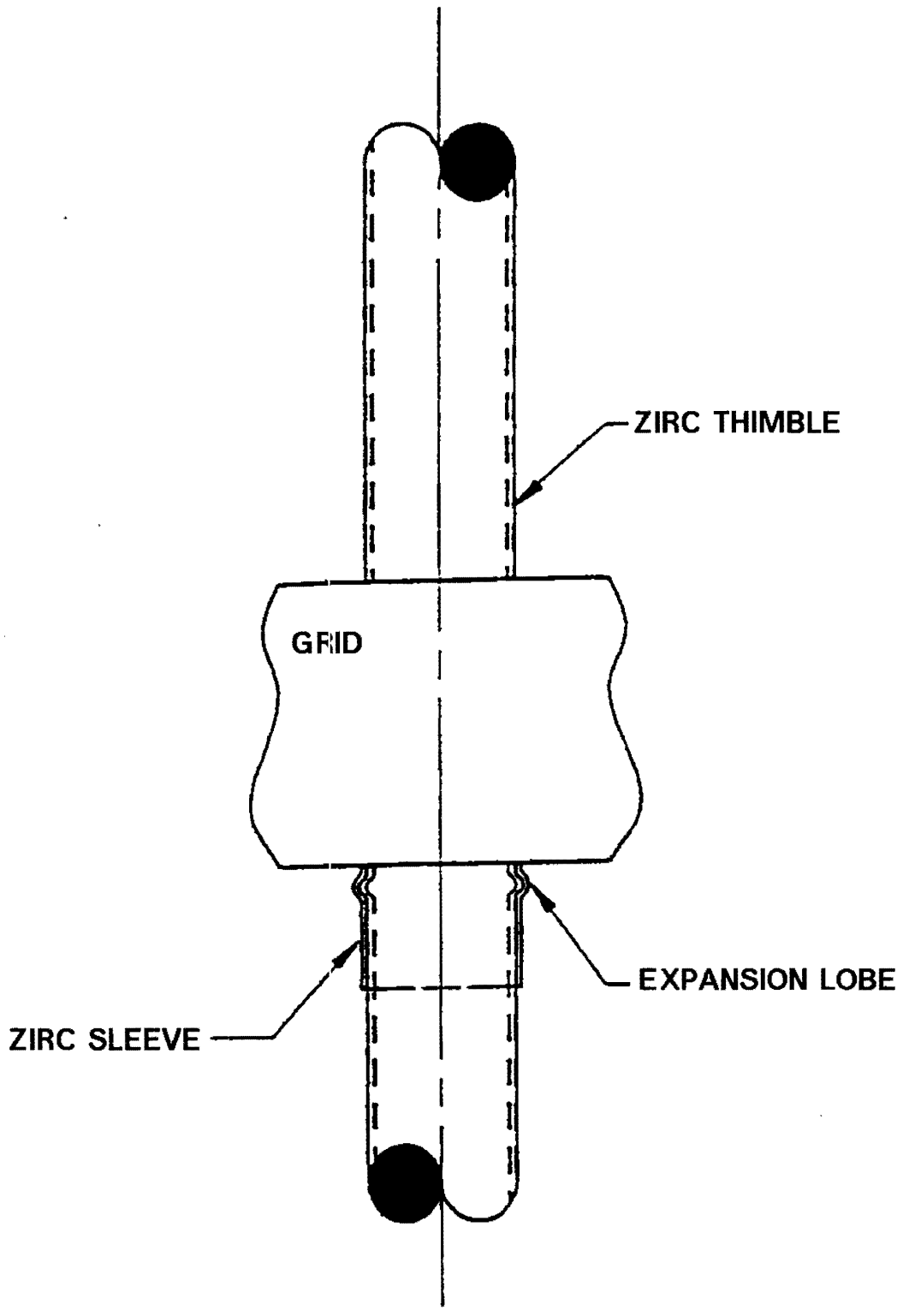


AMENDMENT 73

WATTS BAR NUCLEAR PLANT
FINAL SAFETY
ANALYSIS REPORT

ELEVATION VIEW OF MID GRID
GUIDE THIMBLE JOINT
FIGURE 4.2-5

SCANNED DOCUMENT
THIS IS A SCANNED DOCUMENT MAINTAINED ON
THE WBNP OPTIGRAPHICS SCANNER DATABASE

**Figure 4.2-5 Elevation View of Mid Grid Guide Thimble Joint**

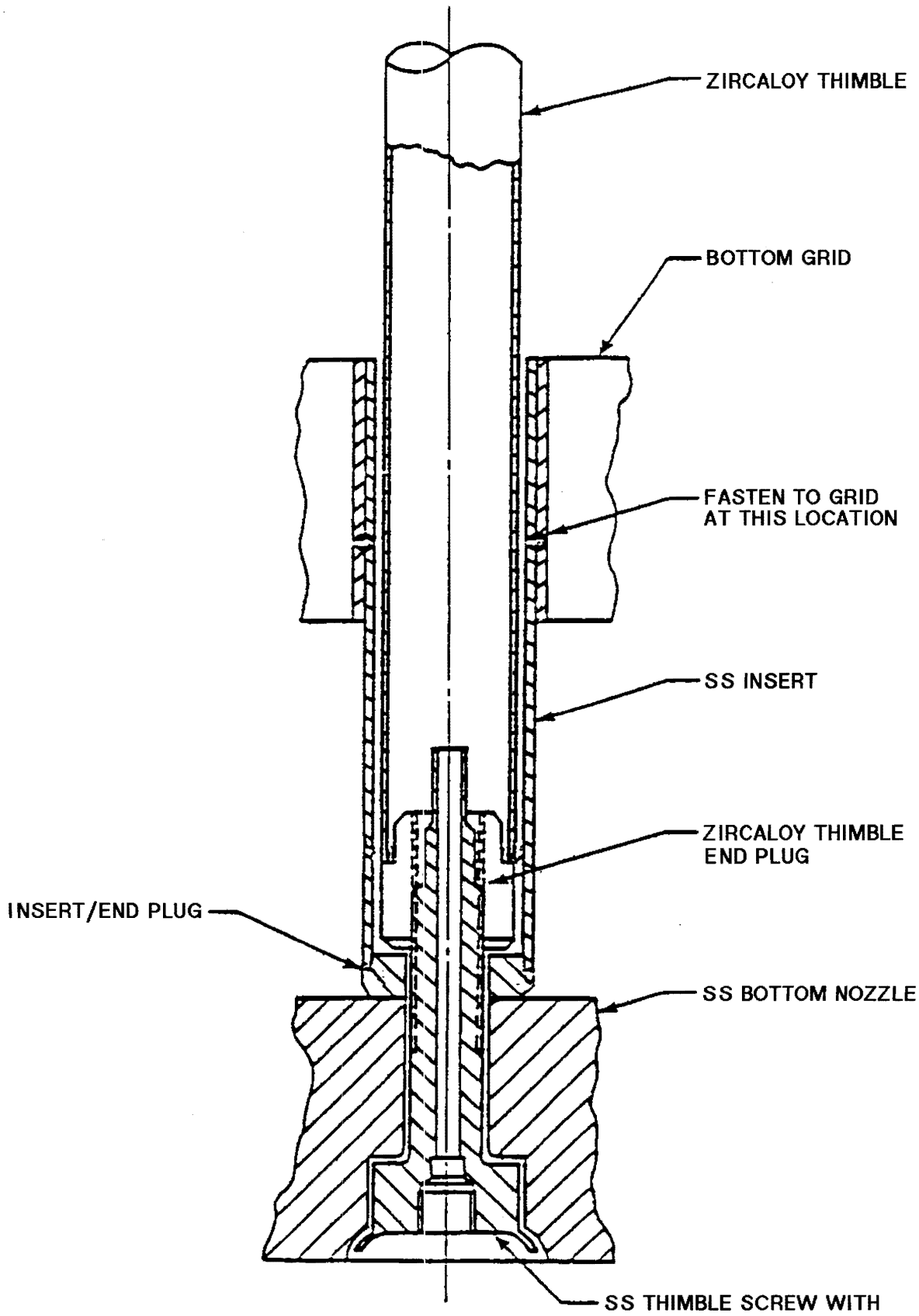


AMENDMENT 73

WATTS BAR NUCLEAR PLANT
FINAL SAFETY
ANALYSIS REPORT

GUIDE THIMBLE TO BOTTOM
NOZZLE JOINT
FIGURE 4.2-6

SCANNED DOCUMENT
THIS IS A SCANNED DOCUMENT MAINTAINED ON
THE WBNP OPTIGRAPHICS SCANNER DATABASE

**Figure 4.2-6 Guide Thimble to Bottom Nozzle Joint**

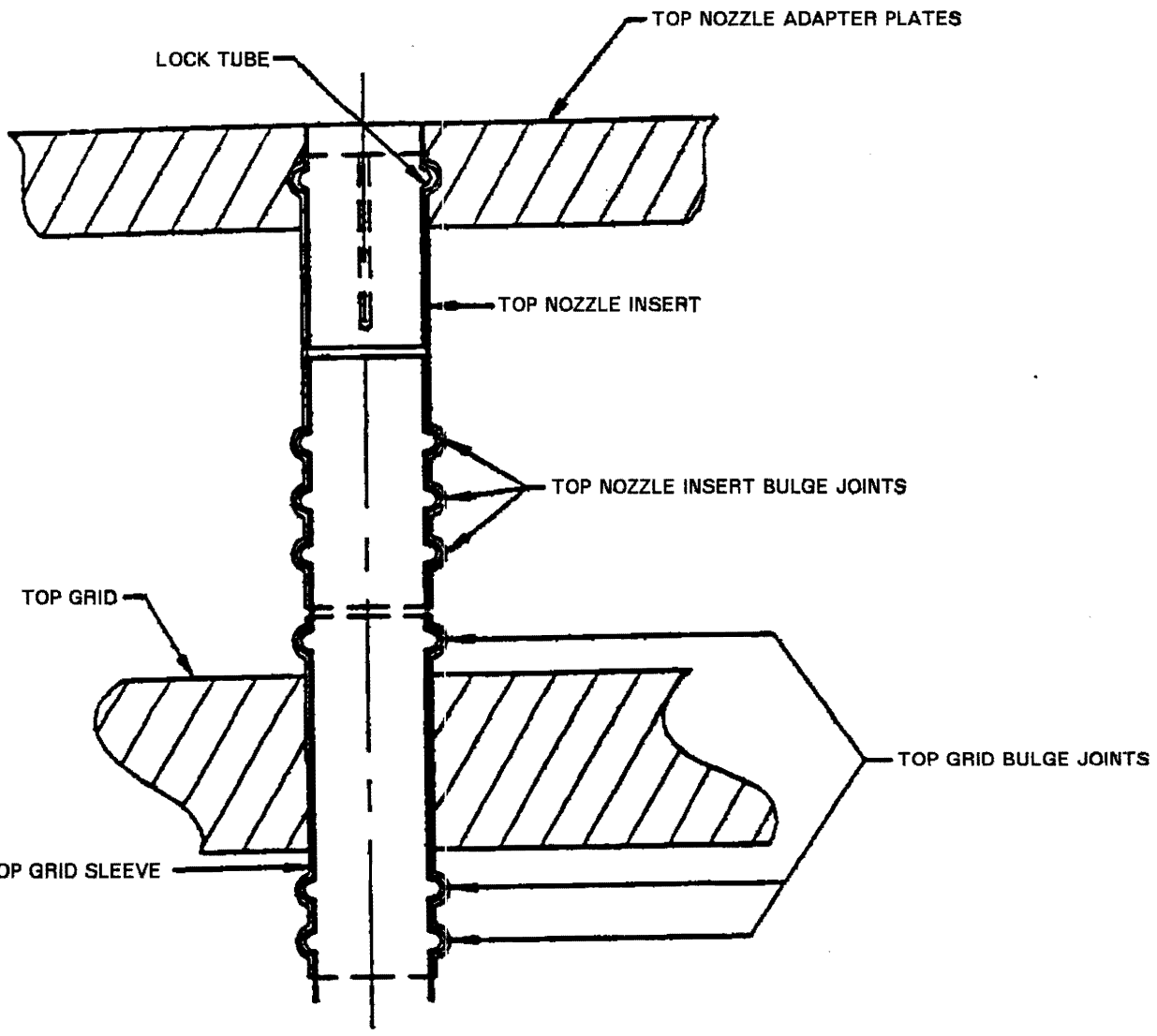


SCANNED DOCUMENT
THIS IS A SCANNED DOCUMENT MAINTAINED ON THE WBNP OPTIGRAPHICS SCANNER DATABASE

AMENDMENT 73

WATTS BAR NUCLEAR PLANT
FINAL SAFETY
ANALYSIS REPORT

TOP GRID TO NOZZLE ATTACHMENT
FIGURE 4.2-7

**Figure 4.2-7 Top Grid to Nozzle Attachment**

**Figure 4.2-8 Deleted by Amendment 73**

**Figure 4.2-9 Deleted by Amendment 73**

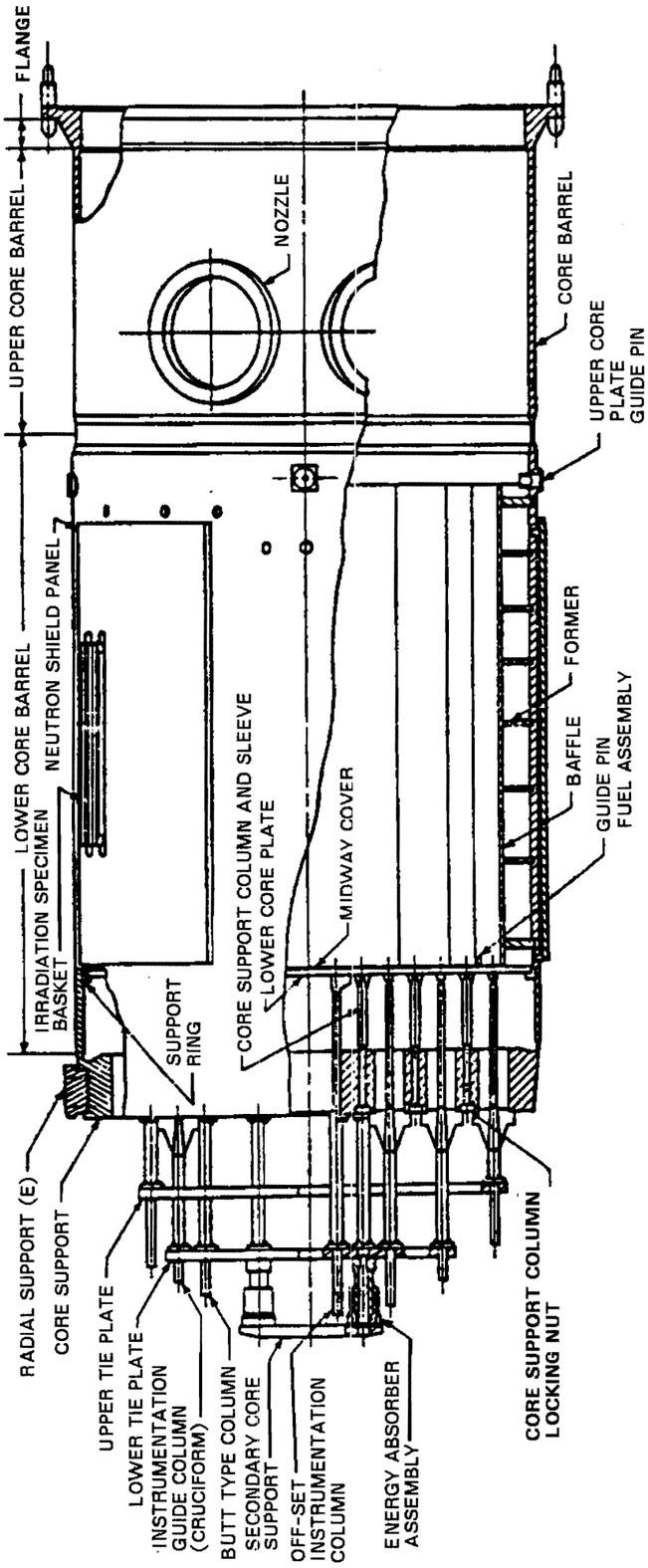


Figure 4.2-10 Lower Core Support Assembly (Core Barrel Assembly)

AMENDMENT 73

WATTS BAR NUCLEAR PLANT
FINAL SAFETY
ANALYSIS REPORT

LOWER CORE SUPPORT ASSEMBLY
(CORE BARREL ASSEMBLY)
FIGURE 4.2-10

SCANNED DOCUMENT
THIS IS A SCANNED DOCUMENT MAINTAINED ON THE WBNP OPTIGRAPHICS SCANNER DATABASE

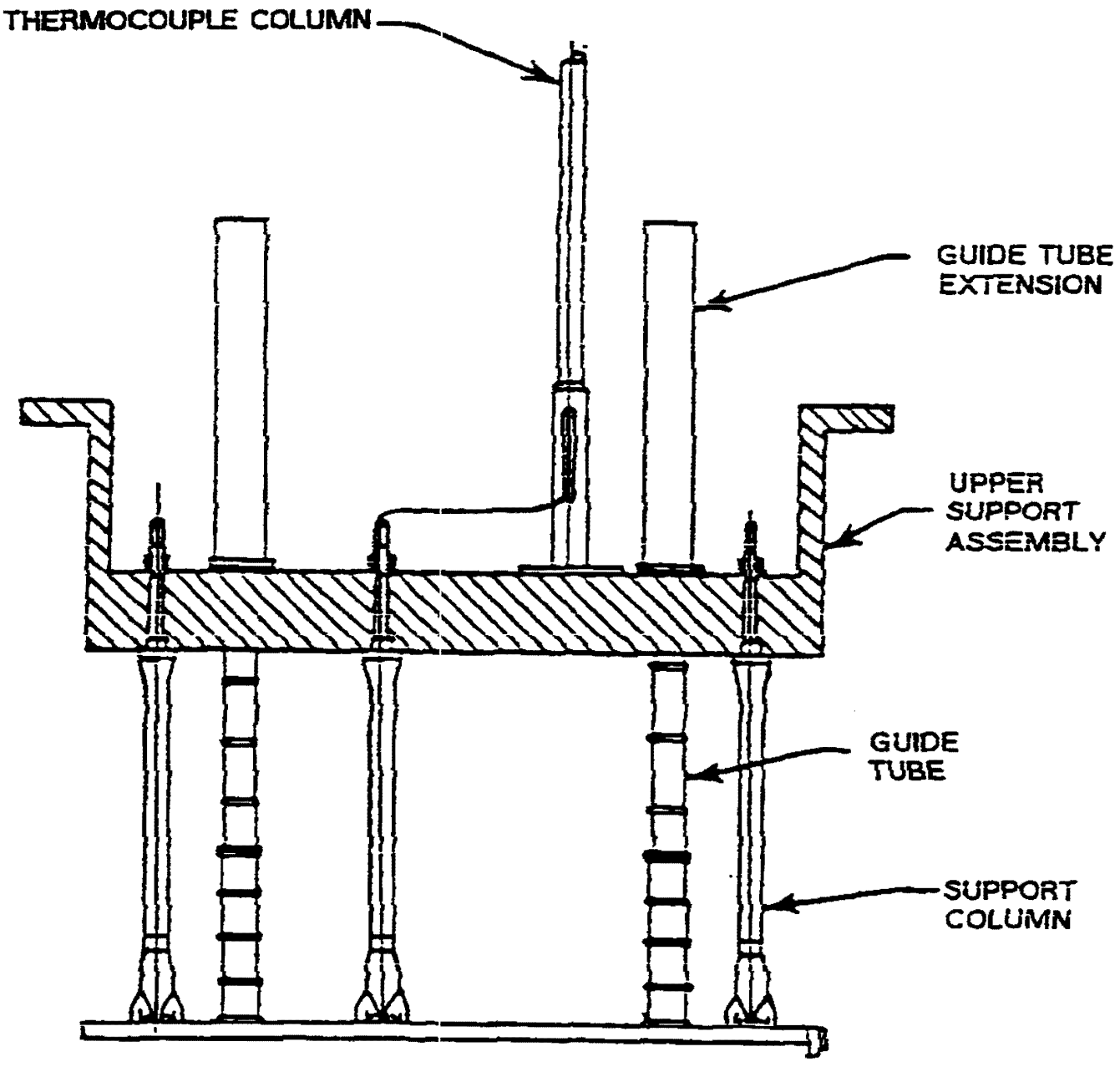


AMENDMENT 73

WATTS BAR NUCLEAR PLANT
FINAL SAFETY
ANALYSIS REPORT

UPPER CORE
SUPPORT STRUCTURE
FIGURE 4.2-11

SCANNED DOCUMENT
THIS IS A SCANNED DOCUMENT MAINTAINED ON THE WBNP OPTIGRAPHICS SCANNER DATABASE

**Figure 4.2-11 Upper Core Support Structure**

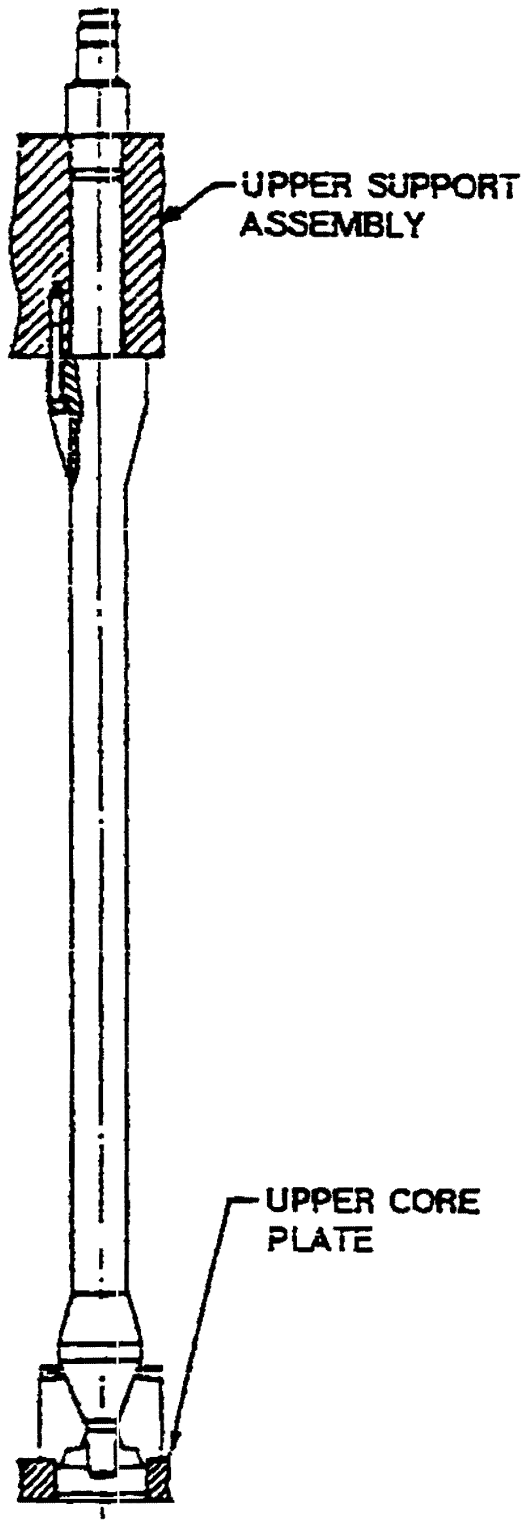


SCANNED DOCUMENT
THIS IS A SCANNED DOCUMENT MAINTAINED ON
THE WBNP OPTIGRAPHICS SCANNER DATABASE

AMENDMENT 73

WATTS BAR NUCLEAR PLANT
FINAL SAFETY
ANALYSIS REPORT

SUPPORT COLUMN
FIGURE 4.2-12

**Figure 4.2-12 Support Column**

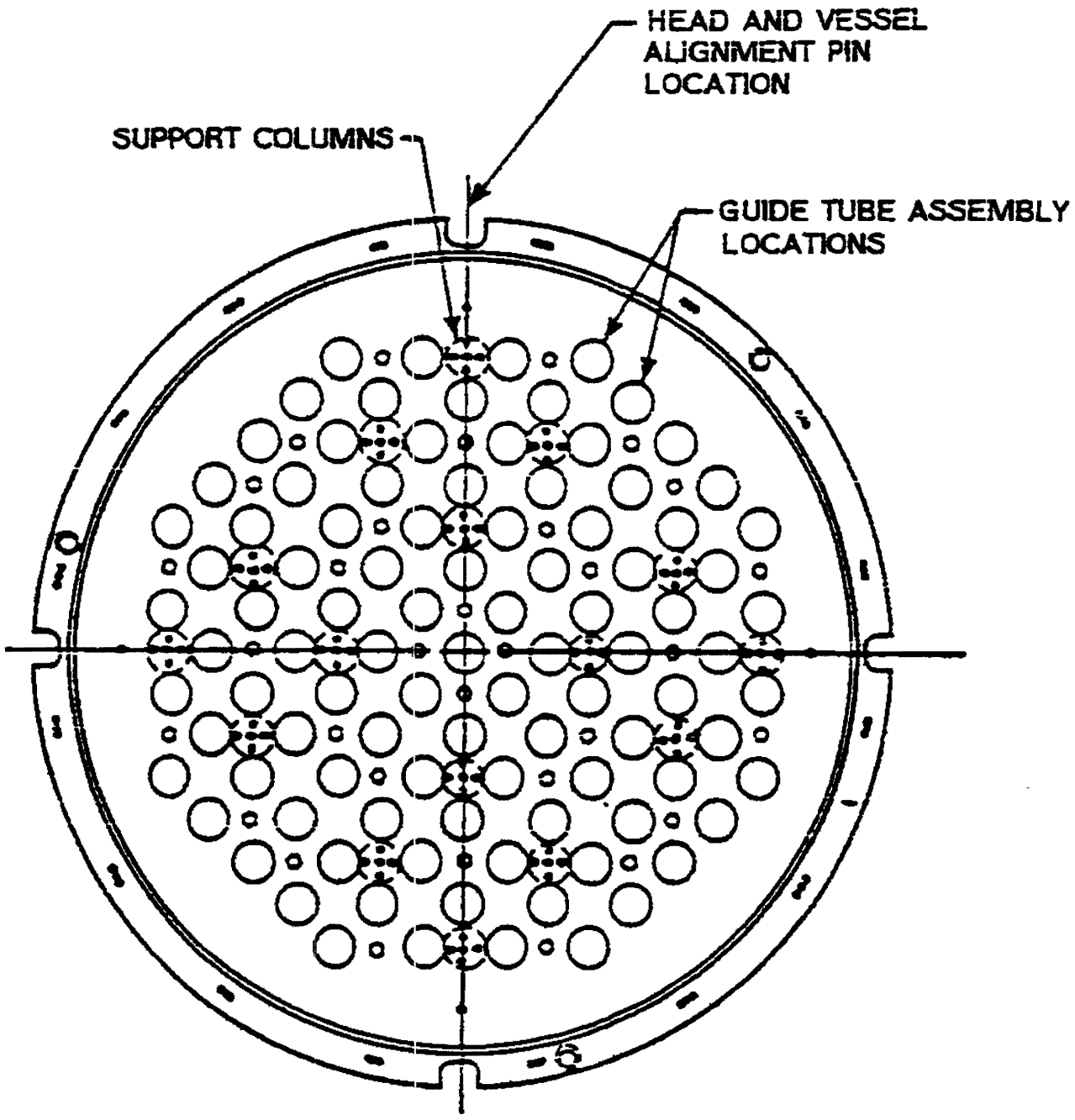


AMENDMENT 73

WATTS BAR NUCLEAR PLANT
FINAL SAFETY
ANALYSIS REPORT

PLAN VIEW
UPPER CORE
SUPPORT STRUCTURE
FIGURE 4.2-13

SCANNED DOCUMENT
THIS IS A SCANNED DOCUMENT MAINTAINED ON THE WBNP OPTIGRAPHICS SCANNER DATABASE

**Figure 4.2-13 Plan View of Upper Core Support Structure**

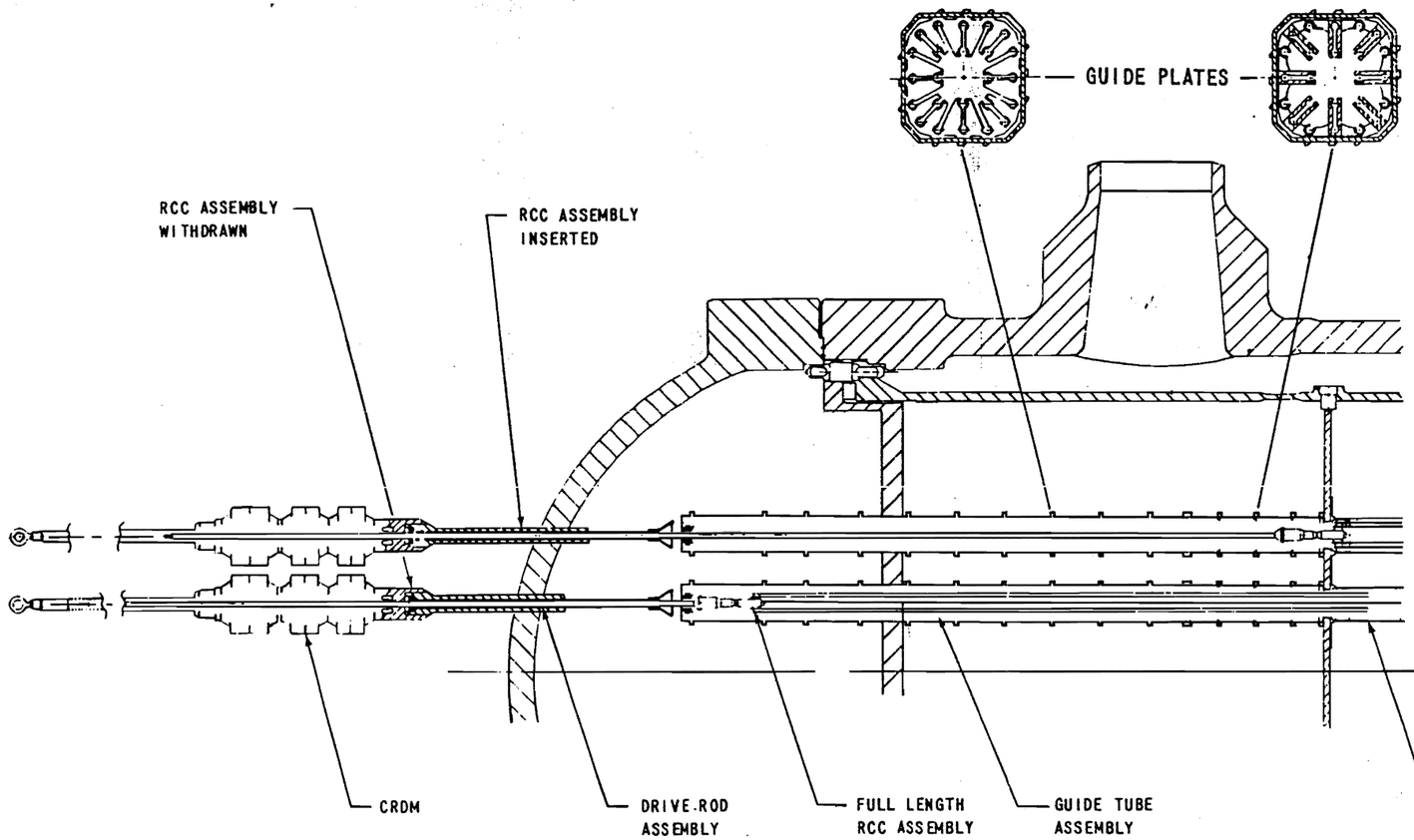


Figure 4.2-14 Full Length Rod Cluster Control and Drive Rod Assembly with Interfacing Components

Figure 4.2-14 Full Length Rod Cluster Control and Drive Rod Assembly with Interfacing Components

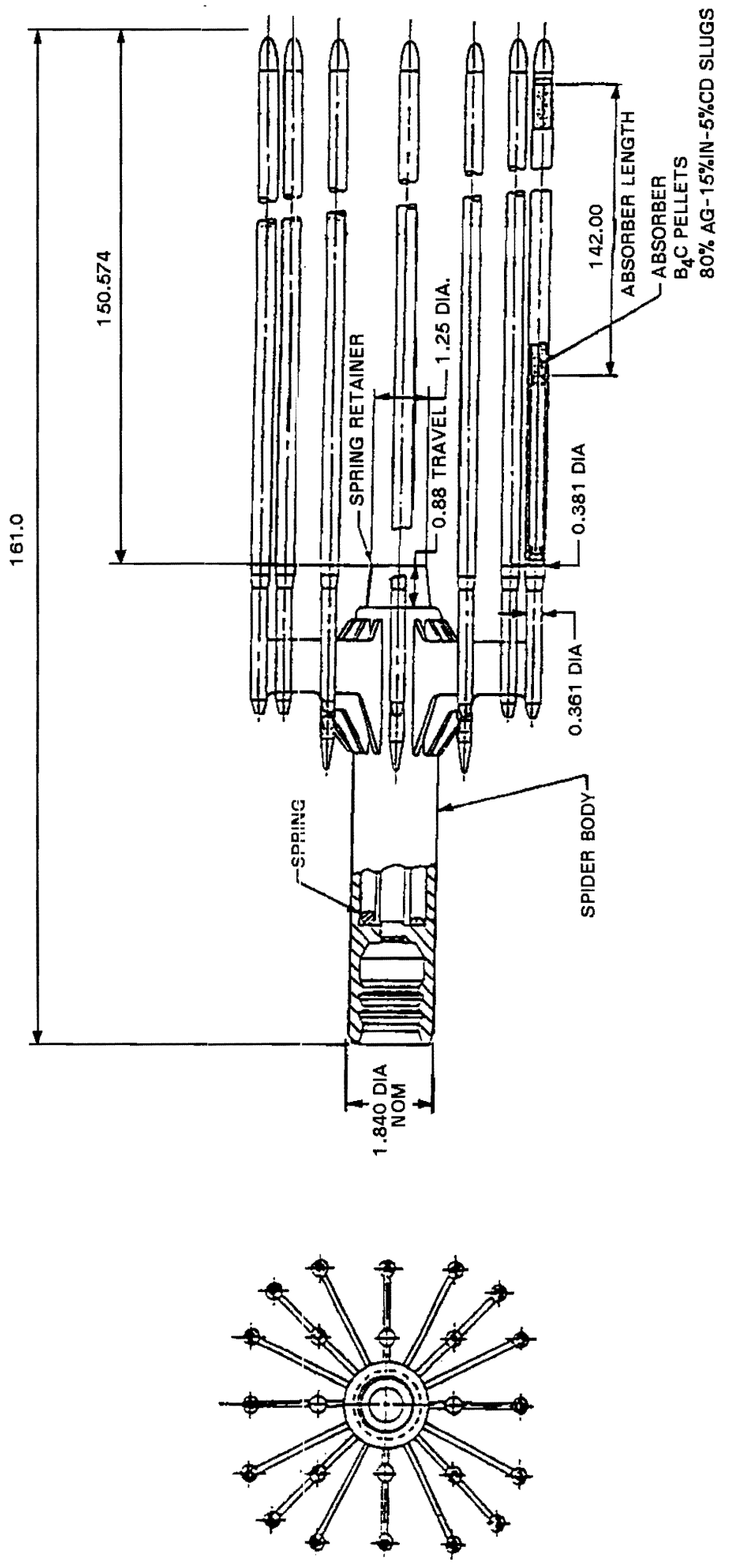




Figure 4.2-15 Full Length Rod Cluster Control Assembly Outline

AMENDMENT 73

WATTS BAR NUCLEAR PLANT
FINAL SAFETY
ANALYSIS REPORT

FULL LENGTH ROD CLUSTER
CONTROL ASSEMBLY OUTLINE
FIGURE 4.2-15

SCANNED DOCUMENT
THIS IS A SCANNED DOCUMENT MAINTAINED ON
THE WBNP OPTIGRAPHICS SCANNER DATABASE

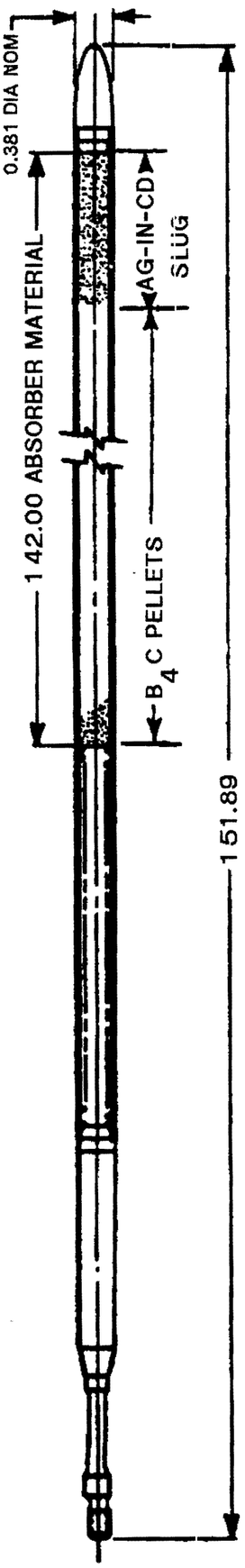


Figure 4.2-16 Full Length Absorber Rod

AMENDMENT 73

WATTS BAR NUCLEAR PLANT
FINAL SAFETY
ANALYSIS REPORT

FULL LENGTH ABSORBER ROD
FIGURE 4.2-16

SCANNED DOCUMENT
A SCANNED DOCUMENT MAINTAINED ON
NP OPTIGRAPHICS SCANNER DATABASE

**Figure 4.2-17 Deleted by Amendment 40**

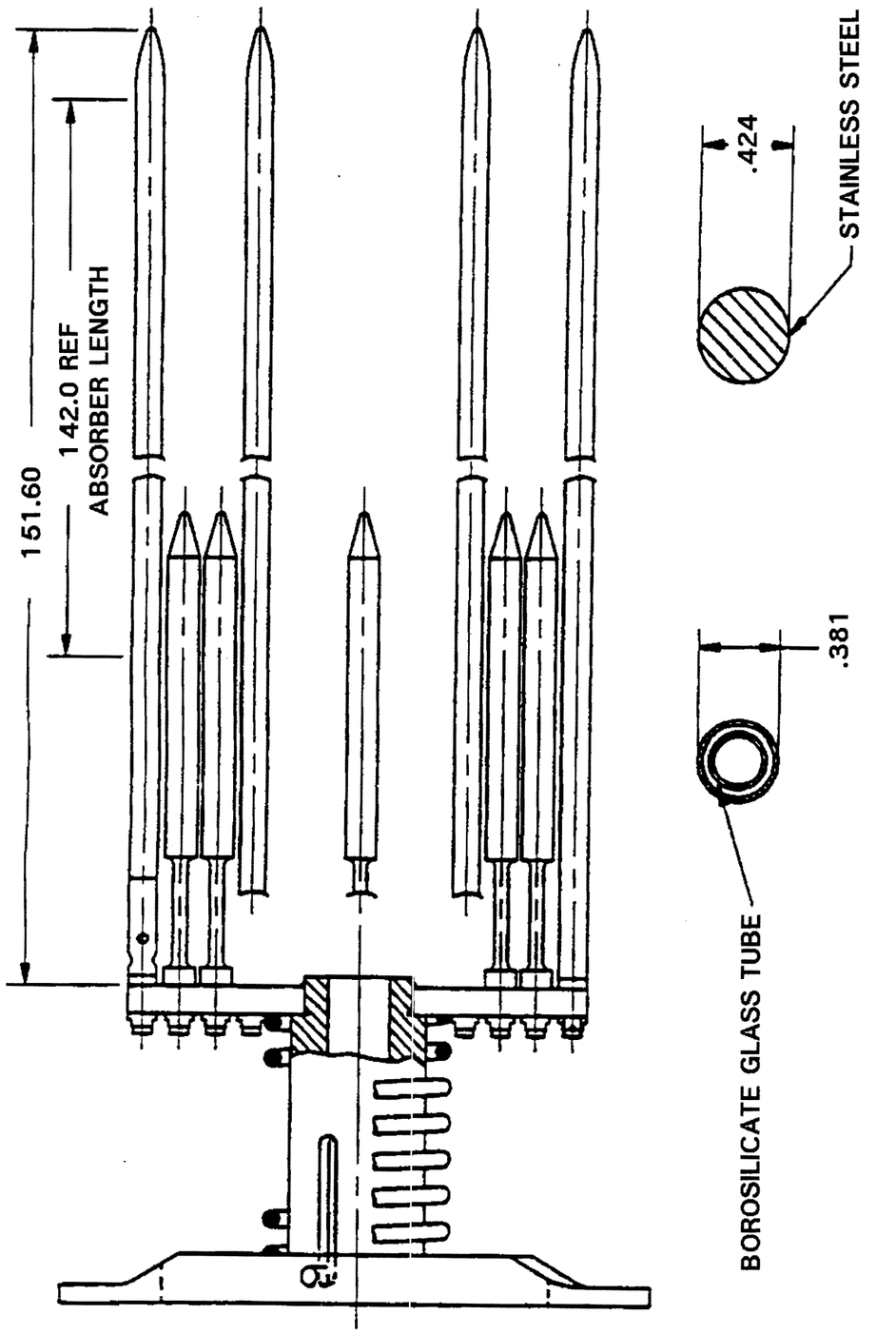


Figure 4.2-18 Burnable Absorber Assembly (Typical)

AMENDMENT 73

WATTS BAR NUCLEAR PLANT
FINAL SAFETY
ANALYSIS REPORT

BURNABLE ABSORBER ASSEMBLY
(TYPICAL)
FIGURE 4.2-18

SCANNED DOCUMENT
THIS IS A SCANNED DOCUMENT MAINTAINED ON
THE WBNP OPTIGRAPHICS SCANNER DATABASE

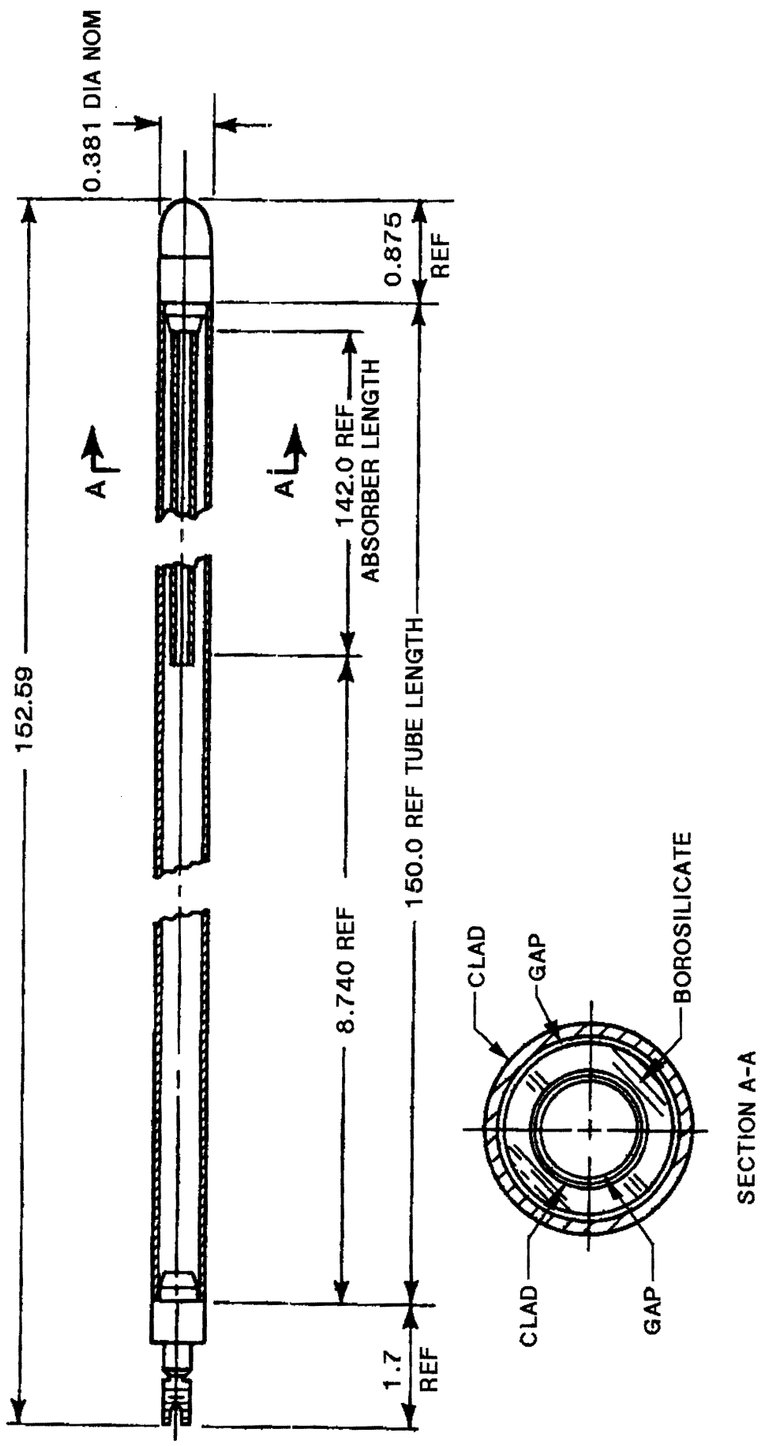


Figure 4.2-19 Burnable Absorber Rod-Cross Section

AMENDMENT 73

WATTS BAR NUCLEAR PLANT
FINAL SAFETY
ANALYSIS REPORT

BURNABLE ABSORBER ROD
- CROSS SECTION -
FIGURE 4.2-19

SCANNED DOCUMENT
THIS IS A SCANNED DOCUMENT MAINTAINED ON THE WBNP OPTIGRAPHICS SCANNER DATABASE

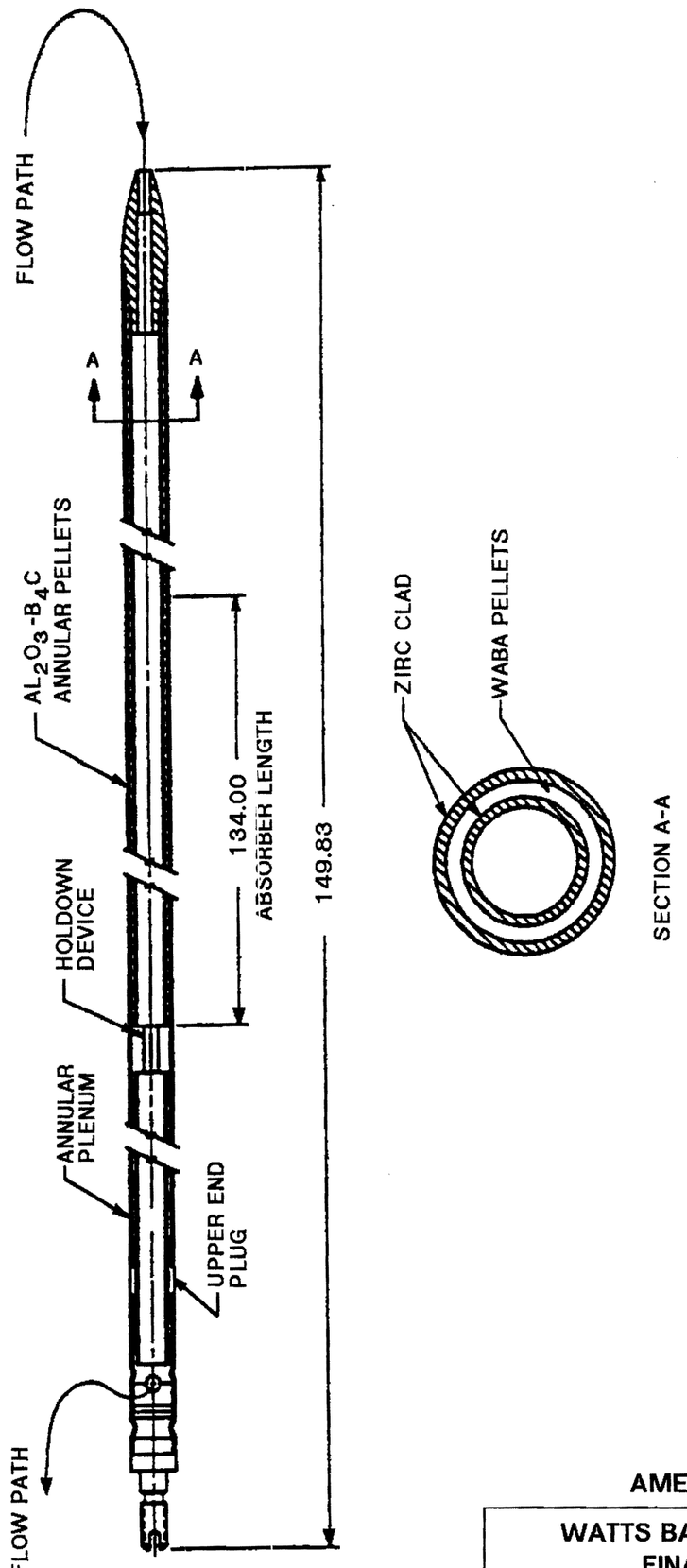


Figure 4.2-19a Wet Annular Burnable Absorber

AMENDMENT 73

WATTS BAR NUCLEAR PLANT
FINAL SAFETY
ANALYSIS REPORT

WET ANNULAR BURNABLE ABSORBER
FIGURE 4.2-19A

SCANNED DOCUMENT
THIS IS A SCANNED DOCUMENT MAINTAINED ON THE WBNP OPTIGRAPHICS SCANNER DATABASE

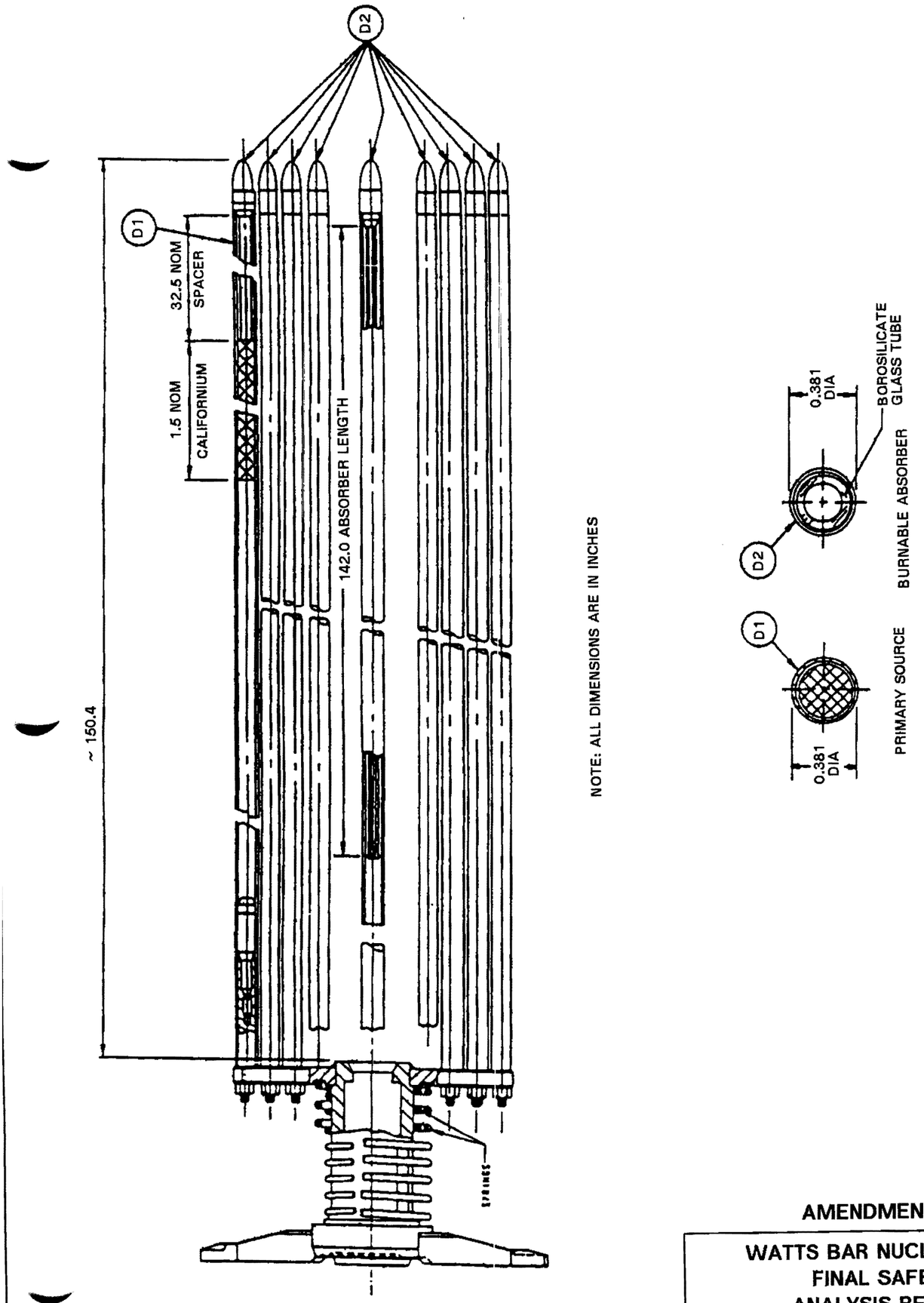


Figure 4.2-20 Primary Source Assembly (Typical)

AMENDMENT 73

WATTS BAR NUCLEAR PLANT
FINAL SAFETY
ANALYSIS REPORT

PRIMARY SOURCE ASSEMBLY
(TYPICAL)
FIGURE 4.2-20

SCANNED DOCUMENT
THIS IS A SCANNED DOCUMENT MAINTAINED ON
THE WBNP OPTIGRAPHICS SCANNER DATABASE

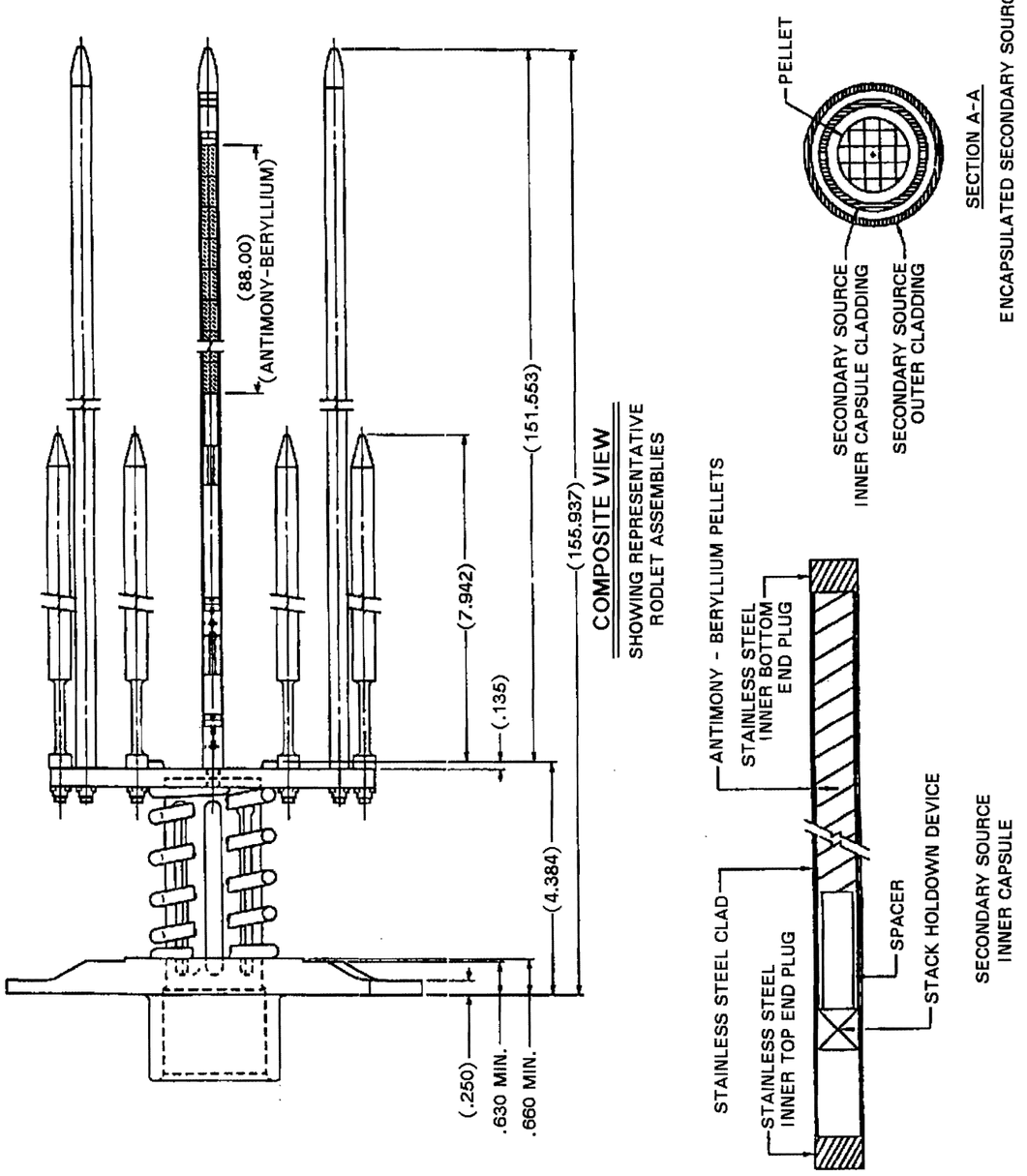


Figure 4.2-21 Encapsulated Secondary Source Assembly (Typical)

AMENDMENT 73

WATTS BAR NUCLEAR PLANT
FINAL SAFETY
ANALYSIS REPORT

ENCAPSULATED SECONDARY SOURCE
ASSEMBLY (TYPICAL)
FIGURE 4.2-21

SCANNED DOCUMENT
THIS IS A SCANNED DOCUMENT MAINTAINED ON
THE WBNP OPTIGRAPHICS SCANNER DATABASE

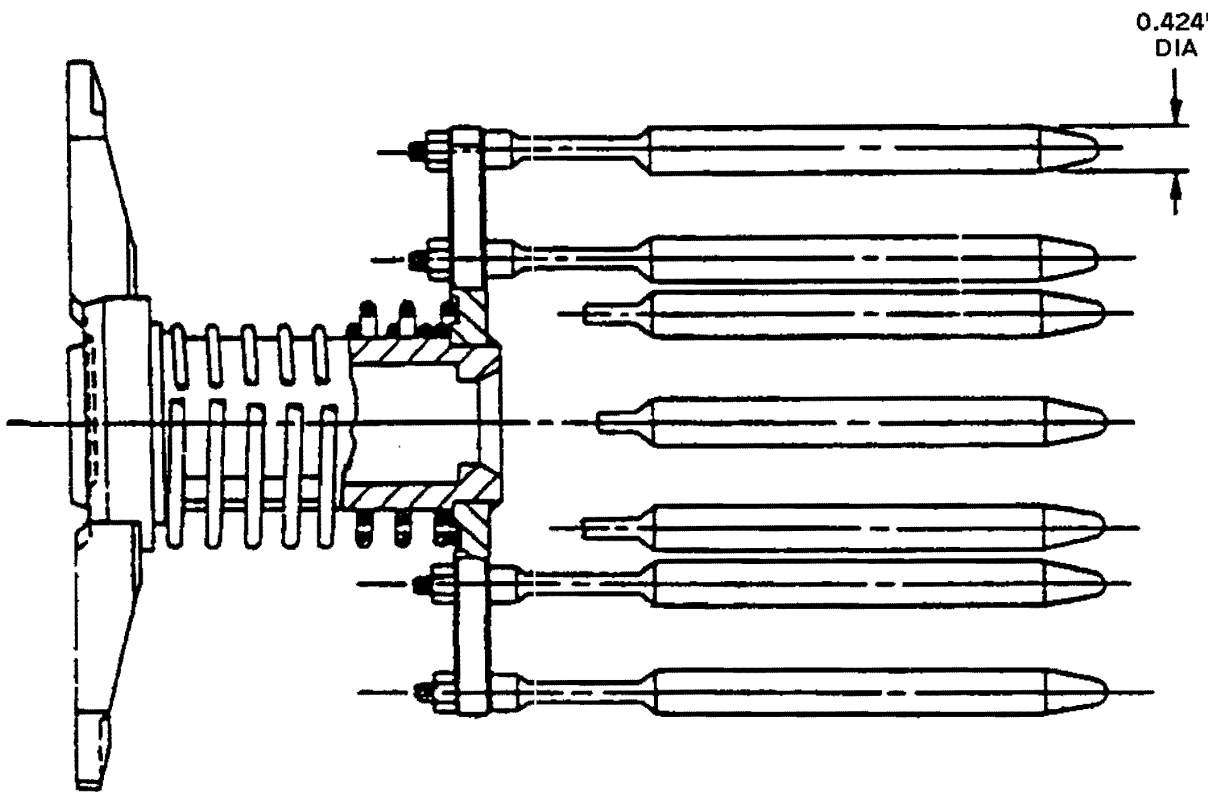


SCANNED DOCUMENT
THIS IS A SCANNED DOCUMENT MAINTAINED ON
THE WBNP OPTIGRAPHICS SCANNER DATABASE

AMENDMENT 73

WATTS BAR NUCLEAR PLANT
FINAL SAFETY
ANALYSIS REPORT

THIMBLE PLUG ASSEMBLY
(TYPICAL)
FIGURE 4.2-22

**Figure 4.2-22 Thimble Plug Assembly (Typical)**

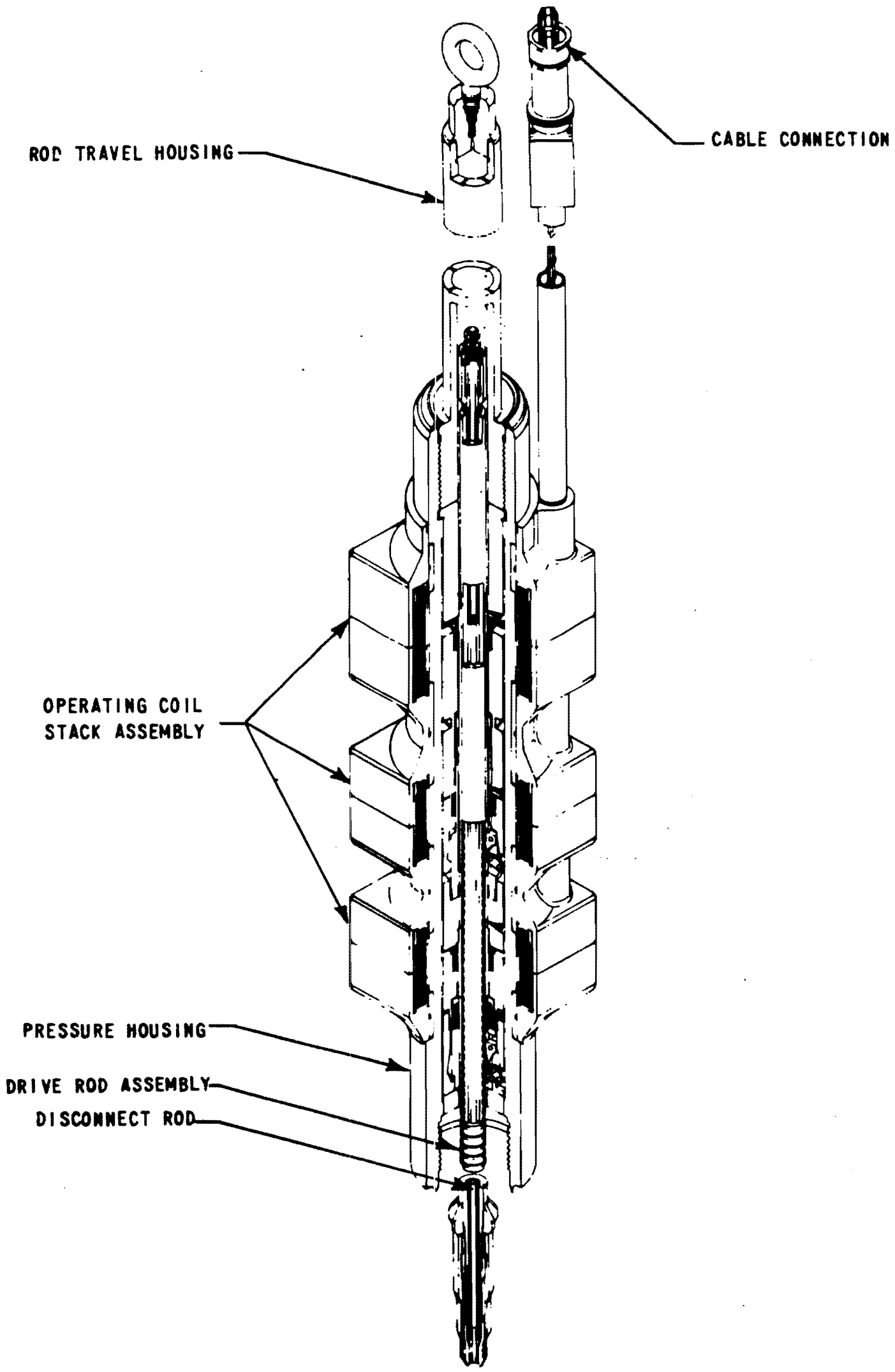


Figure 4.2-23 Full Length Control Rod Drive Mechanism

Figure 4.2-23 Full Length Control Rod Drive Mechanism

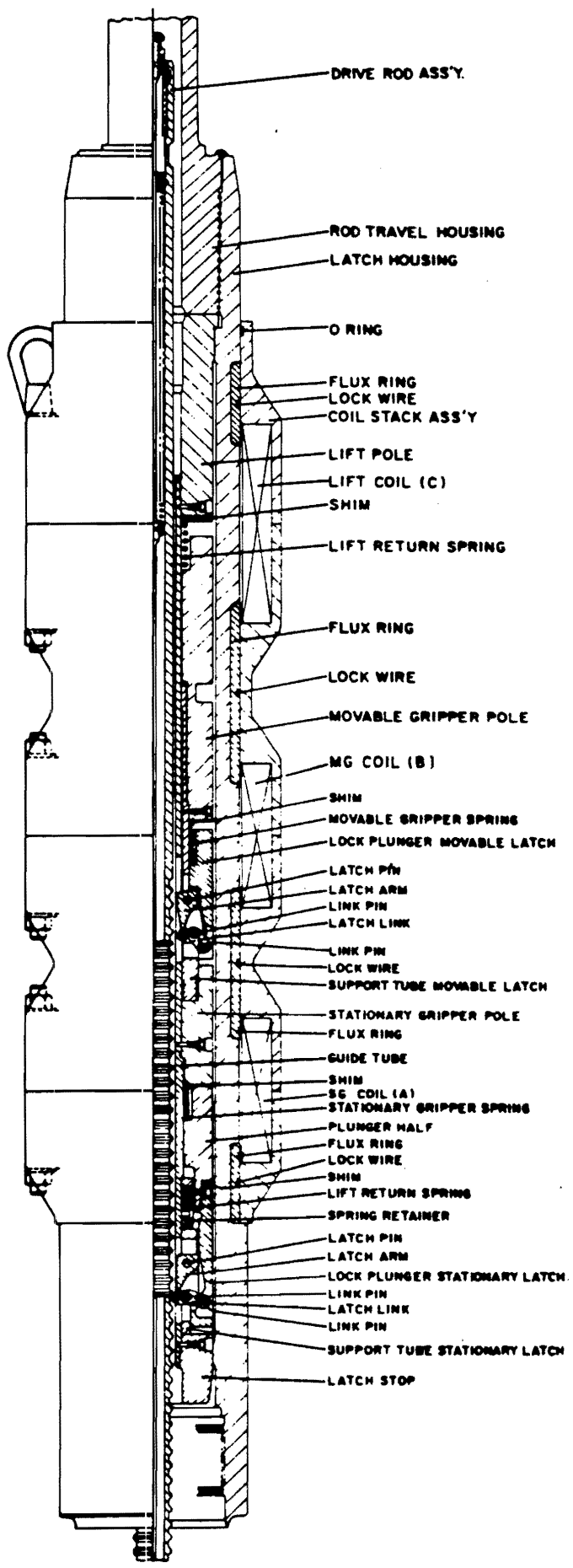


Figure 4.2-24 Full Length Control Rod Drive Mechanism Schematic

**Figure 4.2-24 Full Length Control Rod Drive Mechanism Schematic**

**Figure 4.2-25 Deleted by Amendment 40**

BEFORE LOAD TRANSFER

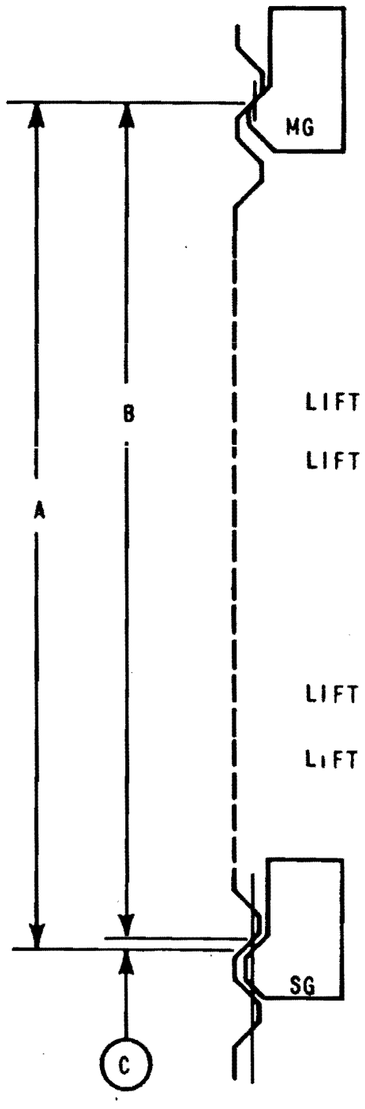


| | AT 70° | | |
|---|---|---|---|
| | A | B | C |
| LIFT COIL OFF | 15.640 | 15.625 | 0.015 |
| LIFT COIL ON | 16.265 | 16.250 | 0.015 |

| | AT 650° | | |
|---|---|---|---|
| | A | B | C |
| LIFT COIL OFF | 15.725 | 15.679 | 0.046 |
| LIFT COIL ON | 16.375 | 16.387 | 0.068 |

AFTER LOAD TRANSFER

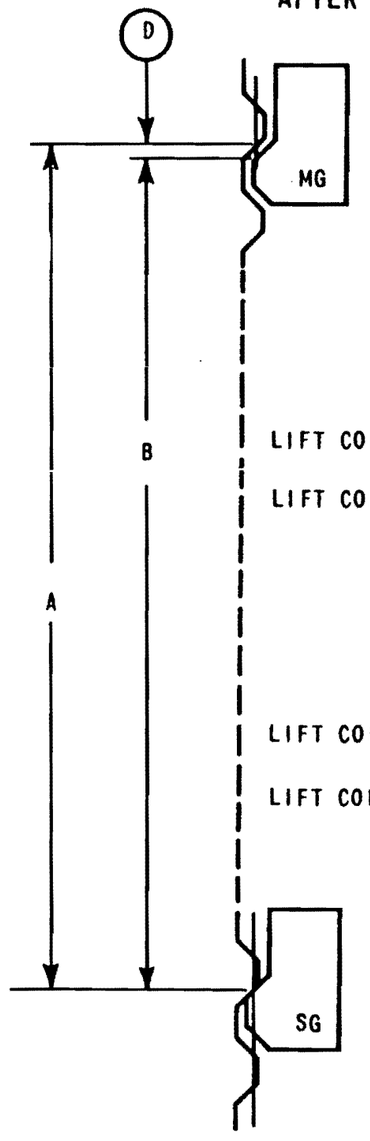


| | AT 70° | | |
|---|---|---|---|
| | A | B | D |
| LIFT COIL OFF | 15.625 | 15.578 | 0.047 |
| LIFT COIL ON | 16.258 | 16.203 | 0.047 |

| | AT 650° | | |
|---|---|---|---|
| | A | B | D |
| LIFT COIL OFF | 15.679 | 15.641 | 0.038 |
| LIFT COIL ON | 16.387 | 16.291 | 0.016 |

Figure 4.2-26 Nominal Latch Clearance at Minimum and Maximum Temperature

Figure 4.2-26 Nominal Latch Clearance at Minimum and Maximum Temperature

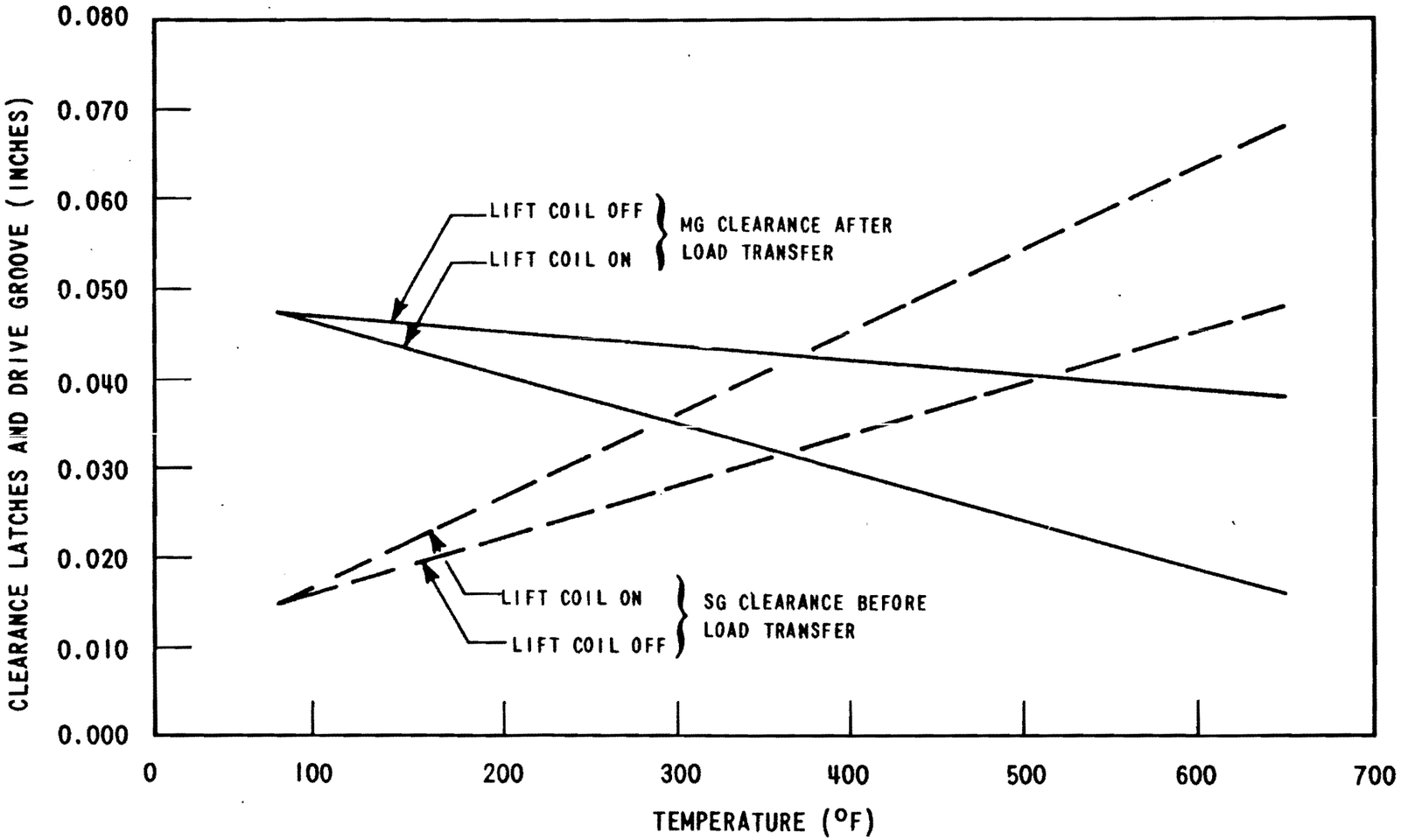


Figure 4.2-27 Control Rod Drive Mechanism Latch Clearance Thermal Effect

Figure 4.2-27 Control Rod Drive Mechanism Latch Clearance Thermal Effect

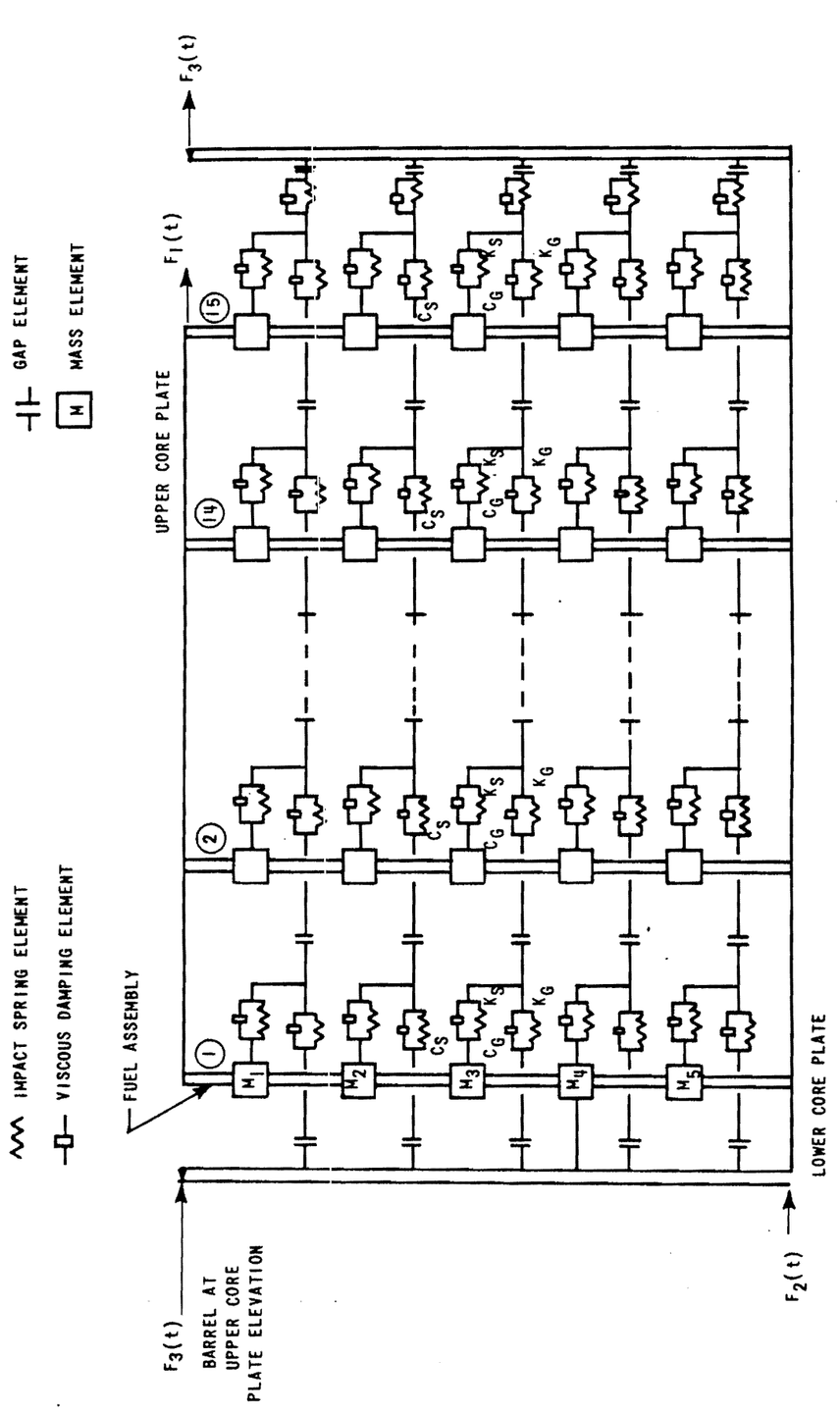


Figure 4.2-28 Schematic Representation of Reactor Core Model

**FIGURE 4.2-28 Schematic Representation of Reactor Core Model**

Added by Amendment 31

THIS PAGE INTENTIONALLY BLANK

## 4.3 NUCLEAR DESIGN

### 4.3.1 DESIGN BASES

This section describes the design bases and functional requirements used in the nuclear design of the fuel and reactivity control system and relates these design bases to the NRC General Design Criteria (GDC) presented in 10 CFR 50, Appendix A. Where appropriate, supplemental criteria such as the Final Acceptance Criteria for Emergency Core Cooling Systems are addressed. Before discussing the nuclear design bases it is appropriate to briefly review the four major categories ascribed to conditions of plant operation.

The full spectrum of plant conditions is divided into four categories, in accordance with the anticipated frequency of occurrence and risk to the public:

*(1)* Condition I - Normal Operation and Operational Transients

*(2)* Condition II - Faults of Moderate Frequency

*(3)* Condition III - Infrequent Faults

*(4)* Condition IV - Limiting Faults

In general the Condition I occurrences are accommodated with margin between any plant parameter and the value of that parameter which would require either automatic or manual protective action. Condition II incidents are accommodated with, at most, a shutdown of the reactor with the plant capable of returning to operation after corrective action. Fuel damage, defined as penetration of the fission product barrier, i.e., the fuel rod clad, is not expected during Condition I and Condition II events. It is not possible to preclude a very small number of rod failures for these events; however, the resulting fission product activity that would potentially result is within the design capability of the Chemical and Volume Control System (CVCS) and is consistent with the plant design bases.

Condition III incidents do not cause more than a small fraction of the fuel elements in the reactor to be damaged, although sufficient fuel element damage might occur to preclude immediate resumption of operation. The release of radioactive material due to Condition III incidents is not sufficient to interrupt or restrict public use of these areas beyond the exclusion radius. Furthermore, a Condition III incident does not, by itself, generate a Condition IV fault or result in a consequential loss of function of the reactor coolant or reactor containment barriers.

Condition IV occurrences are faults that are not expected to occur but are defined as limiting faults which must be designed against. Condition IV faults shall not cause a release of radioactive material that exceeds the limits of 10 CFR 100.

The core design power distribution limits related to fuel integrity are met for Condition I occurrences through conservative design and maintained by the action of the control system. The requirements for Condition II occurrences are met by providing an adequate protection system which monitors reactor parameters. The Control and Protection Systems are described in Chapter 7 and the consequences of Condition II, III and IV occurrences are given in Chapter 15.

### 4.3.1.1 Fuel Burnup

#### Basis

The fuel rod design basis is described in Section 4.2. The nuclear design basis is to install sufficient reactivity in the fuel to attain a region discharge burnup of 33,000 MWD/MTU for the first core and 48,000 MWD/MTU for the reload cores. The above, along with the design basis in Section 4.3.1.3, satisfies GDC-10.

#### Discussion

Fuel burnup is a measure of fuel depletion which represents the integrated energy output of the fuel (MWD/MTU) and is a convenient means for quantifying fuel exposure criteria.

The core design lifetime or design discharge burnup is achieved by installing sufficient initial excess reactivity in each fuel region and by following a fuel replacement program (such as that described in Section 4.3.2) that meets all safety related criteria in each cycle of operation.

Initial excess reactivity installed in the fuel, although not a design basis, must be sufficient to maintain core criticality at full power operating conditions throughout cycle life with equilibrium xenon, samarium, and other fission products present. The end of design cycle life is defined to occur when the chemical shim concentration is essentially zero with control rods present to the degree necessary for operational requirements (e.g., the controlling bank at the "bite" position). In terms of chemical shim boron concentration, this represents approximately 10 ppm with no control rod insertion.

A limitation on initial installed excess reactivity is not required other than as is quantified in terms of other design bases such as core negative reactivity feedback and shutdown margin discussed below.

### 4.3.1.2 Negative Reactivity Feedbacks (Reactivity Coefficient)

#### Basis

The fuel temperature coefficient will be negative and the moderator temperature coefficient of reactivity will be non-positive for power operating conditions, thereby providing negative reactivity feedback characteristics. The design basis meets GDC-11.

#### Discussion

When compensation for a rapid increase in reactivity is considered, there are two major effects. These are the resonance absorption effects (Doppler) associated with changing fuel temperature and the spectrum effect resulting from changing moderator density. These basic physics characteristics are often identified by reactivity coefficients. The use of slightly enriched uranium ensures that the Doppler coefficient of reactivity is negative. This coefficient provides the most rapid reactivity compensation. The core is also designed to have an overall negative moderator temperature coefficient of reactivity so that average coolant temperature or void content provides another, slower compensatory effect. The negative moderator temperature coefficient can be achieved through use of fixed burnable absorbers, integral fuel burnable absorbers (IFBAs), if present, and/or control rods which decrease the concentration of soluble boron required for reactivity control.

Restrictions on burnable absorber content (quantity and distribution) are not applied as a design basis other than as related to achieving a non-positive moderator temperature coefficient at power operating conditions as discussed in Section 4.3.2.

### 4.3.1.3 Control of Power Distribution

#### Basis

The nuclear design basis is that, with at least a 95% confidence level:

*(1)* The fuel will not be operated at a linear power greater than the average linear power multiplied by FQ(z)[1] under normal operating conditions including an allowance of 2% for calorimetric error and not including a power spike factor due to densification.

*(2)* Under abnormal conditions, including the maximum overpower condition, the fuel peak power will not cause melting as defined in Section 4.4.1.2.

*(3)* The fuel will not operate with a power distribution that violates the departure from nucleate boiling (DNB) design basis (i.e., the DNBR shall not be less than the safety analysis limits, as discussed in Section 4.4.1) under Condition I and II events including the maximum overpower condition.

*(4)* Fuel management will be such that rod powers and burnups are consistent with the assumptions in the fuel rod mechanical integrity analysis of Section 4.2.

The above basis meets GDC-10.

#### Discussion

Calculations of extreme power shapes which affect fuel design limits are performed with proven methods and verified frequently with measurements from operating reactors. The conditions under which limiting power shapes are assumed to occur are conservatively chosen with regard to any permissible operating state.

Even though there is good agreement between calculated peak power and measurements, a nuclear uncertainty margin is applied to the calculated peak local power. Such a margin is provided both for the analysis for normal operating states and for anticipated transients.

*(1)* FQ(z) is the heat flux hot channel factor and is specified in the Watts Bar Technical Specifications.

### 4.3.1.4 Maximum Controlled Reactivity Insertion Rate

#### Basis

The maximum reactivity insertion rate due to withdrawal of Rod Cluster Control Assemblies or by boron dilution is limited. This limit, expressed as a maximum reactivity change rate of 75 pcm/sec[1], is set such that peak heat generation rate and DNBR do not exceed the maximum allowable at overpower conditions. This satisfies GDC-25.

The maximum reactivity worth of control rods and the maximum rates of reactivity insertion employing control rods are limited so that a rod withdrawal or rod ejection accident will not cause rupture of the coolant pressure boundary or disruption of the core internals to a degree which would impair core cooling capacity (see Chapter 15).

Following any Condition IV event (rod ejection, steamline break, etc.) the reactor can be brought to the shutdown condition and the core will maintain acceptable heat transfer geometry. This satisfies GDC-28.

### Discussion

Reactivity addition associated with an accidental withdrawal of a control bank (or banks) is limited by the maximum rod speed (or travel rate) and by the worth of the bank(s). For the Watts Bar Nuclear Plant reactor the maximum control rod speed is 45 inches per minute and the maximum rate of reactivity change considering two control banks moving is less than 75 pcm/sec.

## 4.3.1.5 Shutdown Margins With Vessel Head in Place

### Basis

Minimum shutdown margin requirements as specified in the Watts Bar Technical Specifications are required in all power operating modes, hot standby, hot shutdown, and cold shutdown conditions.

In all analyses involving reactor trip, the single, highest worth Rod Cluster Control Assembly (RCCA) is postulated to remain untripped in its full-out position (stuck rod criterion). This satisfies GDC-26.

### Discussion

Two independent reactivity control systems are provided: control rods and soluble boron in the coolant. The control rod system can compensate for the reactivity effects of the fuel and water temperature changes accompanying power level changes over the range from full-load to no-load. The control rod system also provides the minimum shutdown margin under Condition I events and is capable of making the core subcritical rapidly enough to prevent exceeding acceptable fuel damage limits assuming that the highest worth control rod is stuck out upon trip. The boron system can compensate for all xenon burnout reactivity changes and will maintain the reactor in the cold shutdown condition. Thus, backup and emergency shutdown provisions are provided by a mechanical and a chemical shim control system which satisfies GDC-26.

*(1)* pcm = $10^{-5}$ $\Delta\rho$ (i.e., footnote in Table 4.3-2)

## 4.3.1.6 Shutdown Margin for Refueling

### Basis

When fuel assemblies are in the pressure vessel and the vessel head is not in place, $k_{eff}$ will be maintained at or below 0.95 with control rods and soluble boron. Further, the fuel will be maintained sufficiently subcritical that removal of all rod cluster control assemblies will not result in criticality.

### Discussion

ANS Standard N18.2 specifies a $k_{eff}$ not to exceed 0.95 in spent fuel storage racks and transfer equipment flooded with pure water and a $k_{eff}$ not to exceed 0.98 in normally dry new-fuel storage racks assuming optimum moderation. No criterion is given for the refueling operation, however a 5% margin, which is consistent with spent fuel storage and transfer and the new fuel storage, is adequate for the controlled and continuously monitored operations involved.

The boron concentration required to meet the refueling shutdown criteria is specified in the Technical Specifications. Verification that this shutdown criteria is met, including uncertainties, is achieved using standard design methods such as ARK [34] or PHOENIX-P/ANC [39] and TURTLE [9], PALADON [27], or ANC [38] codes. The subcriticality of the core is continuously monitored as described in the Technical Specifications.

## 4.3.1.7 Stability

### Basis

The core will be inherently stable to power oscillations at the fundamental mode. This satisfies GDC-12.

Spatial power oscillations, should they occur, can be reliably and readily detected and suppressed.

### Discussion

Oscillations of the total power output of the core, from whatever cause, are readily detected by the loop temperature sensors and by the nuclear instrumentation. The core is protected by these systems and a reactor trip would occur if power unacceptably increased, preserving the design margins to fuel design limits. The stability of the turbine/steam generator/ core systems and the reactor control system is such that total core power oscillations are not normally possible. The redundancy of the protection circuits ensures an extremely low probability of exceeding design power levels.

The core is designed so that diametral and azimuthal oscillations due to spatial xenon effects are self-damping and no operator action or control action is required to suppress them. The stability to diametral oscillations is so great that this excitation is highly improbable. Convergent azimuthal oscillations can be excited by prohibited motion of individual control rods. Such oscillations are observable and alarmed, when exceeding limits, using the excore detectors. Indications are also available from incore thermocouples and loop temperature measurements. Moveable incore detectors can be activated to provide more detailed information. These horizontal plane oscillations are self-damping by virtue of reactivity feedback effects designed into the core.

However, axial xenon and spatial power oscillations may occur late in core life. The control bank and excore detectors are provided for control and monitoring of axial power distributions. Assurance that fuel design limits are not exceeded is provided by reactor overpower $\Delta T$ and overtemperature $\Delta T$ (which uses the measured axial power imbalance as an input) trip functions.

## 4.3.1.8 Anticipated Transients Without Trip

The effects of anticipated transients with failure to trip are not considered in the design bases of the plant. Analysis has shown that the likelihood of such a hypothetical event is negligibly small. Furthermore, analysis of the consequences of a hypothetical failure to trip following anticipated transients has shown that no significant core damage would result and system peak pressures

would be limited such that the primary stress anywhere in the system boundary is less than the "emergency conditions" defined in the ASME Nuclear Power Plant Components Code, Section III, and no failure of the reactor coolant system would result [1].

## 4.3.2 Description

### 4.3.2.1 Nuclear Design Description

The reactor core consists of a specified number of fuel rods which are held in bundles by spacer grids and top and bottom fittings. The fuel rods are constructed of Zircaloy/ZIRLO™ cylindrical tubes containing $UO_2$ fuel pellets. The bundles, known as fuel assemblies, are arranged in a pattern which approximates a right circular cylinder.

Each fuel assembly contains a 17 x 17 rod array composed of 264 fuel rods, 24 guide thimbles and an incore instrumentation thimble. Figure 4.2-1 shows a cross sectional view of a 17 x 17 fuel assembly and the related thimble locations. Further details of the fuel assembly are given in Section 4.2.1.

Fuel assemblies of three different enrichments are used in the initial core loading to establish a favorable radial power distribution. Figure 4.3-1 shows the fuel loading pattern to be used in the first core. Two regions consisting of the two lower enrichments are interspersed so as to form a checkerboard pattern in the central portion of the core. The third region is arranged around the periphery of the core and contains the highest enrichment. The enrichments for the first core are shown in Table 4.3-1.

For reload cores, the exact pattern, initial and final positions of assemblies, and the number of fresh assemblies and their placement are dependent on the energy requirements for the next cycle, and the burnup and power histories of the previous cycle.

The core average enrichment is determined by the amount of fissionable material required to provide the desired core lifetime and energy requirements. The physics of the burnout process is such that operation of the reactor depletes the amount of fuel available due to the absorption of neutrons by the U-235 atoms and their subsequent fission. In addition, the fission process results in the formation of fission products, some of which readily absorb neutrons. These effects, depletion and the buildup of fission products, are partially offset by the buildup of plutonium from the non-fission absorption of neutrons in U-238, as shown in Figure 4.3-2 for the 17 x 17 fuel assembly. Therefore, at the beginning of any cycle, a reactivity reserve equal to the depletion of the fissionable fuel and the buildup of fission product absorbers over the specified cycle life must be 'built' into the reactor. This excess reactivity is controlled by removable neutron absorbing material in the form of boron dissolved in the primary coolant and burnable absorber rods or $ZrB_2$-coated fuel pellets in IFBAs (when present).

The concentration of boric acid in the primary coolant is varied to provide control and to compensate for long-term reactivity requirements. The concentration of the soluble neutron absorber is controlled by means of the Chemical and Volume Control System (CVCS) to compensate for reactivity changes due to fuel burnup, fission product buildup including xenon and samarium, burnable absorber depletion, and the cold-to-operating moderator temperature change. Rapid transient reactivity requirements and safety shutdown requirements are met with control rods.

As the boron concentration is increased, the moderator temperature coefficient becomes less negative. The use of a soluble absorber alone would result in a positive moderator coefficient at beginning-of-life for the first cycle. Therefore, burnable absorbers are used in the first core to

sufficiently reduce the soluble boron concentration to ensure that the moderator temperature coefficient is negative at power operating conditions. During operation the neutron absorber content in these rods is depleted thus adding positive reactivity to offset some of the negative reactivity from fuel depletion and fission product buildup. The depletion rate of the burnable absorber rods is not critical since chemical shim is always available and flexible enough to cover any possible deviations in the expected burnable poison depletion rate. Figure 4.3-3 is a graph of a typical core depletion with and without burnable absorber rods. Note that even at end-of-life conditions some residual poison remains in the burnable absorber rods resulting in a net decrease in the first cycle lifetime.

In addition to reactivity control, the burnable absorber rods are strategically located to provide a favorable radial power distribution. Figures 4.3-4a and 4.3-4b show the burnable absorber distribution within a fuel assembly for the several burnable absorber patterns used in a 17 x 17 array. The burnable absorber loading pattern is shown in Figure 4.3-5.

Tables 4.3-1 through 4.3-3 contain a summary of the reactor core design parameters for the first fuel cycle, including reactivity coefficients, delayed neutron fraction and neutron lifetimes. Sufficient information is included to permit an independent calculation of the nuclear performance characteristics of the core.

## 4.3.2.2 Power Distributions

The accuracy of power distribution calculations has been confirmed through approximately one thousand flux maps during some twenty years of operation under conditions very similar to those expected for Watts Bar. Details of this confirmation are given in Reference [2] and in Section 4.3.2.2.7.

### 4.3.2.2.1 Definitions

Power distributions are quantified in terms of hot channel factors. These factors are a measure of the peak pellet power within the reactor core and the total energy produced in a coolant channel, relative to the total reactor power output, and are expressed in terms of quantities related to the nuclear or thermal design, namely:

Power density is the thermal power produced per unit volume of the core (kW/liter).

Linear power density is the thermal power produced per unit length of active fuel (kW/ft). Since fuel assembly geometry is standardized, this is the unit of power density most commonly used. For all practical purposes, it differs from kW/liter by a constant factor which includes geometry and the fraction of the total thermal power which is generated in the fuel rod.

Average linear power density is the total thermal power produced in the fuel rods divided by the total active fuel length of all rods in the core.

Local heat flux is the heat flux at the surface of the cladding ($BTU\text{-}ft^{-2}\text{-}hr^{-1}$). For nominal rod parameters this differs from linear power density by a constant factor.

Rod power or rod integral power is the length integrated linear power density in one rod (kW).

Average rod power is the total thermal power produced in the fuel rods divided by the number of fuel rods (assuming all rods have equal length).

The hot channel factors used in the discussion of power distributions in this section are defined as follows:

$F_Q$, Heat Flux Hot Channel Factor, is defined as the maximum local heat flux on the surface of a fuel rod divided by the average fuel rod heat flux, allowing for manufacturing tolerances on fuel pellets and rods, and including fuel densification effects.

$F_Q^N$, Nuclear Heat Flux Hot Channel Factor, is defined as the maximum local fuel rod linear power density divided by the average fuel rod linear power density, assuming nominal fuel pellet and rod parameters.

$F_Q^E$, Engineering Heat Flux Hot Channel Factor, is the allowance on heat flux required for manufacturing tolerances. The engineering factor allows for local variations in enrichment, pellet density and diameter, surface area of the fuel rod, and eccentricity of the gap between pellet and clad. Statistically combined, the net effect is a factor of 1.03 to be applied to fuel rod surface heat flux.

$F_{\Delta H}^N$, Nuclear Enthalpy Rise Hot Channel Factor, is defined as the ratio of the integral of linear power along the rod with the highest integrated power to the average rod power.

Manufacturing tolerances, hot channel power distribution and surrounding channel power distributions are explicitly treated in the calculation of the DNBR described in Section 4.4.

It is convenient for the purposes of discussion to define subfactors of $F_Q$. However, design limits are set in terms of the total peaking factor.

$F_Q$ =Total peaking factor or heat flux hot-channel factor

$$= \frac{}{A}$$

Without densification effects,

$$F_Q = F_Q^N \times F_Q^E$$
$$= F_{XY}^N \times F_Z^N \times F_U^N \times F_Q^E$$

Where

$F_Q^N$ and $F_Q^E$ are defined above.

$F^N_U$ = the measurement uncertainty associated with a full core flux map with moveable detectors

$F^N_{XY}$ = ratio of peak power density to average power density in the horizontal plane of peak local power.

$F^N_Z$ = ratio of the power per unit core height in the horizontal plane of peak local power to the average value of power per unit core height. If the plane of peak local power coincides with the plane of maximum power per unit core height, then $F_Z^N$ is the core average axial peaking factor.

To include the allowances made for densification effects, which are height dependent, the following quantities are defined.

S(Z) = the allowance made for densification effects at height Z in the core.

See Section 4.3.2.2.5.

P(Z) = ratio of the power per unit core height in the horizontal plane at height Z to the average value of power per unit core height.

$F^N_{XY}(Z)$ = ratio of peak power density to average power density in the horizontal plane at height Z.

Then

$F_Q$=Total peaking factor

$$= \frac{\text{Maximum kW/ft}}{\text{Average kW/ft}}$$

Including densification effects,

$$F_Q = \max [F^N_{XY}(Z) \times P(Z)] \times S(Z) \times F^N_U \times F^E_Q$$

### 4.3.2.2.2 Radial Power Distributions

The power shape in horizontal sections of the core at full power is a function of the fuel assembly and burnable absorber loading patterns, the control rod pattern, and fuel burnup distribution. Thus, at any time in the cycle, any horizontal section of the core can be characterized as unrodded or with Bank D control rods. These two situations combined with burnup effects determine the radial power shapes which can exist in the core at full power. The effect on radial power shapes of power level, xenon, samarium and moderator density effects are considered also but these are quite small. The effect of nonuniform flow distribution is negligible. While radial power distributions in various planes of the core are often illustrated, the core radial enthalpy rise distribution as determined by the integral of power up each channel is of greater interest. Figures 4.3-6 through 4.3-11 show representative radial power distributions for one eighth of the core for representative operating conditions. These conditions are: 1) hot full power (HFP) at beginning-of-life (BOL), unrodded, no xenon, 2) HFP at BOL, unrodded, equilibrium xenon, 3) HFP at BOL, Bank D in 17%, equilibrium xenon, 4) HFP at middle-of-life (MOL), unrodded, equilibrium xenon, 5) HFP at end-of-life (EOL), unrodded, equilibrium xenon, and 6) HFP at EOL, Bank D in 17%, equilibrium xenon.

Since the position of the hot channel varies from time to time, a single reference radial design power distribution is selected for DNB calculations. This reference power distribution is conservatively chosen to concentrate power in one area of the core, minimizing the benefits of flow redistribution. Assembly powers are normalized to core average power.

### 4.3.2.2.3 Assembly Power Distributions

For the purpose of illustration, assembly power distributions from the BOL and EOL conditions corresponding to Figures 4.3-7 and 4.3-10, respectively, are given for the same assembly in Figures 4.3-12 and 4.3-13, respectively.

Since the detailed power distribution surrounding the hot channel varies from time to time, a conservatively flat assembly power distribution is assumed in the DNB analysis, described in Section 4.4, with the rod of maximum integrated power artificially raised to the design value of

$F^N_{\Delta H}$. Care is taken in the nuclear design of all fuel cycles and all operating conditions to ensure that a flatter assembly power distribution does not occur with limiting values of $F^N_{\Delta H}$.

### 4.3.2.2.4 Axial Power Distribution

The shape of the power profile in the axial direction is largely under the control of the operator through the manual operation of the control rods or automatic motion of the rods in response to manual operation of the CVCS. Nuclear effects which cause variations in the axial power shape include moderator density, Doppler effect on resonance absorption, spatial distribution of xenon, and burnup. Automatically controlled variations in total power output and rod motion are also important in determining the axial power shape at any time. Signals are available to the operator from the excore detectors which are long ion chambers outside the reactor vessel running parallel to the axis of the core. Separate signals are taken from the top and bottom halves of the chambers. The difference between top and bottom signals from each of four pairs of detectors is displayed on the control panel and called the flux imbalance, ΔI. Calculations of the core average peaking factor for many plants and measurements from operating plants under many operating situations are associated with either ΔI or axial offset in such a way that an upper bound can be placed on the peaking factor. For these correlations axial offset is defined as:

$$\text{axial offset} = \frac{\phi_t - \phi_b}{\phi_t + \phi_b} \quad 3$$

and $\phi_t$ and $\phi_b$ are the top and bottom detector current readings, respectively.

Representative axial power shapes from reference [3] for BOL, MOL, and EOL conditions are shown in Figures 4.3-14 through 4.3-16. These figures cover a wide range of axial offset, including values achieved by skewing xenon distributions.

The radial power distributions shown in Figures 4.3-8 and 4.3-11 involving the partial insertion of control rods represent a synthesis of power shapes from the rodded and unrodded planes. The applicability of the separability assumption upon which this procedure is based is ensured through extensive three-dimensional calculations of possible rodded conditions. As an example, Figure 4.3-17 compares the axial power distribution for several assemblies, at different distances from inserted control rods, with the core average axial distribution.

The only significant difference from the average occurs in the low power peripheral assemblies, thus, confirming the validity of the separability assumption.

### 4.3.2.2.5 Local Power Peaking

Fuel densification, which has been observed to occur under irradiation in several operating reactors, causes the fuel pellets to shrink both axially and radially. The pellet shrinkage combined with random hang-up of fuel pellets results in gaps in the fuel column when the pellets below the hung-up pellet settle in the fuel rod. The gaps vary in length and location in the fuel rod. Because of decreased neutron absorption in the vicinity of the gap, power peaking occurs in the adjacent fuel rods resulting in an increased power peaking factor. A quantitative measure of this local peaking is given by the power spike factor, S(Z), where Z is the axial location in the core.

The method used to compute the power spike factor is described in Reference [4] and is summarized in Figure 4.3-18. The information flow outlined in Figure 4.3-18 is as follows:

*(1)* The probability that an axial gap of a certain size will occur at a given location in the core is determined from fuel performance data.

*(2)* The magnitude of the power spike caused by a single axial gap of a certain size is determined from nuclear calculations as shown in Figure 4.3-19. This curve is valid for uranium fuel enrichments up to 5.0 wt/% U-235.

*(3)* For each axial interval to be analyzed, axial gap occurrence probabilities and the single event power spikes are entered into the DRAW computer code. The code produces a curve of power spike versus probability of exceeding power spike for each elevation in the core. The power census for a core is then statistically combined with the power spike probability curve to obtain a power spike penalty for the core such that less than one rod will exceed $F_Q^N$ at a 95% confidence level.

For fuel produced by a process other than those for which Reference [4] is applicable, specifications will be followed to ensure that the effects of densification will be no greater than has been allowed for in the design.

The specifications for qualifying the extent of densification will be based on the NRC report on fuel densification [30].

The power spike factor due to densification is assumed to be a local perturbation applicable to overpower transients. Thus, densification affects $F_Q$, but not $F_{\Delta H}^N$. The magnitude of the increased power peaking which increases from no effect at the bottom of the core to a few percent at the top of the core is shown in Figure 4.3-20. This curve is applicable for fuel pellets that have a density of at least 93.5 percent, and an enrichment of up to 5.0 wt/% U-235.

Results reported in Reference [5] show that the power spike penalty should not be included in determining the predicted $F_Q$.

### 4.3.2.2.6 Limiting Power Distributions

According to the ANSI classification of plant conditions (see Chapter 15), Condition I occurrences are those which are frequently or regularly expected in the course of power operation, maintenance, or maneuvering of the plant. As such, Condition I occurrences are accommodated with margin between any plant parameter and the value of that parameter which would require either automatic or manual protective action. Inasmuch as Condition I events frequently or regularly occur, they must be considered from the point of view of affecting the consequences of fault conditions (Conditions II, III, and IV). In this regard, analysis of each fault condition described is generally based on a conservative set of initial conditions corresponding to the most adverse set of conditions which can occur during Condition I operation.

The list of steady state and shutdown conditions, permissible deviations and operational transients is given in Section 15.1. Implicit in the definition of normal operation is proper and timely action by the reactor operator. That is, the operator follows recommended operating procedures for maintaining appropriate power distributions and takes any necessary remedial actions when alerted to do so by the plant instrumentation. Thus, as stated above, the worst or limiting power distribution which can occur during normal operation is to be considered as the starting point for analysis of Conditions II, III, and IV events.

Improper procedural actions or errors by the operator are assumed in the design as occurrences of moderate frequency (ANSI Condition II). Some of the consequences which might result are listed in Section 15.2. Therefore, the limiting power shapes which result from such Condition II events are those power shapes which deviate from the normal operating condition at the recommended axial offset band, e.g. due to lack of proper action by the operator during a xenon transient following a change in power level brought about by control rod motion. Power shapes which fall in this category are used for determination of the reactor protection system setpoints so as to maintain margin to overpower or DNB limits.

Reference [37] describes the methods for determining the limiting shape that can be created in Watts Bar's reactor core for the allowable ΔI operating space.

The means for maintaining power distributions within the required hot channel factor limits are described in the Watts Bar Technical Specifications. A complete discussion of power distribution control in Westinghouse PWRs is given in Reference [6].

Detailed information on the design constraints on local power density in a Westinghouse PWR, on the defined operating procedures and on the measures taken to preclude exceeding design limits is presented in the Westinghouse topical reports on peaking factors [8] and power distribution control and load following procedures [7]. The following paragraphs summarize these reports and describe the calculations used to establish the upper bound on peaking factors.

The calculations used to establish the upper bound on peaking factors, $F_Q$ and $F^N_{\Delta H}$, include all of the nuclear effects which influence the radial and/or

axial power distributions throughout core life for various modes of operation including load follow, reduced power operation, and axial xenon transients.

Radial power distributions are calculated for the full power condition, and fuel and moderator temperature feedback effects are included for the average enthalpy plane of the reactor. The steady state nuclear design calculations are done for normal flow with the same mass flow in each channel and flow redistribution effects neglected. The effect of flow redistribution is calculated explicitly where it is important in the DNB analysis of accidents. The effect of xenon on radial power distribution is small (compare Figures 4.3-6 and 4.3-7), but is included as part of the normal design process.

The core average axial profile, however, can experience significant changes which can occur rapidly as a result of rod motion and load changes and more slowly due to xenon redistribution. Several thousand cases are examined to determine the points of closest approach to axial power distribution limits. Since the properties of the nuclear design dictate what axial shapes can occur, boundaries on the limits of interest can be set in terms of the parameters which are readily observed in the plant. Specifically, the nuclear design parameters which are significant to the axial power distribution analysis are:

*(1)* Core power level

*(2)* Core height

*(3)* Coolant temperature and flow

*(4)* Coolant temperature program as a function of reactor power

*(5)* Fuel cycle lifetimes

*(6)* Rod bank worths

*(7)* Rod bank overlaps

Normal operation of the plant assumes compliance with the following conditions:

*(1)* Control rods in a single bank move together with no individual rod insertion differing by more than +12 steps (indicated) from the bank demand position;

*(2)* Control banks are sequenced with overlapping banks;

*(3)* The control bank insertion limits are not violated;

*(4)* Axial power distribution procedures, which are given in terms of flux difference control and control bank position, are observed.

The axial power distribution procedures referred to above are part of the required operating procedures which are followed in normal operation. Limits placed on the axial flux difference are designed to assure that the heat flux hot channel factor, $F_Q$, is maintained within acceptable limits. The constant axial offset control (CAOC) operating procedures described in Reference [7] require control of the axial flux difference at all power levels within a permissible operating band about a target value corresponding to the equilibrium full power value. The relaxed axial offset control (RAOC) procedures described in Reference [37] were developed to provide wider control bandwidths and, consequently, more operating flexibility. These wider operating limits, particularly at lower power levels, can increase plant availability by allowing quicker plant startups and increased maneuvering flexibility without trip or reportable occurrences.

Further operating flexibility is achieved by combining RAOC operation with an $F_Q$ surveillance technical specification. Monitoring $F_Q(z)$ and increasing the measured value for expected plant maneuvers is a convenient way of assuring that the plant operates below the $F_Q(z)$ limit, while retaining the intent of using a measured parameter to verify technical specification compliance.

In the standard CAOC analysis described in Reference [7], the generation of the normal operation power distributions is constrained by the rod insertion limits (RIL) and the ΔI band limits. The purpose of RAOC is to find the widest permissible ΔI-Power operating space by analyzing a wide range of ΔI. Therefore, the generation of normal operation power distributions is constrained only by RIL.

For a CAOC analysis, load follow simulations are performed covering the allowed CAOC operating space to generate a typical range of allowed axial xenon distributions which, in turn, are used to calculate axial power distributions in both normal operation and Condition II accident conditions. For a RAOC analysis, however, a reconstruction model described in Reference [37] is used as a more practical method to create axial xenon distributions covering the wider ΔI-Power operating space allowed with RAOC operation. Each resulting power shape is analyzed to determine if LOCA constraints are met or exceeded. The total peaking factor, $F^T_Q$, is determined using standard synthesis methods as described in Reference [7].

The calculated points are synthesized from axial calculations combined with radial factors appropriate for rodded and unrodded planes. In these calculations, the effects of xenon redistribution that occur following the withdrawal of a control bank (or banks) from a rodded region on the unrodded radial peak are obtained from two-dimensional X-Y calculations. A 1.03 factor, which is applied on the unrodded radial peak was obtained from calculations in which the xenon

distribution was preconditioned by the presence of control rods and then allowed to redistribute for several hours. A detailed discussion of this effect may be found in reference [7]. The calculated values have been increased by a factor of 1.05 for conservatism and a factor of 1.03 for the engineering factor $F_Q^E$.

The envelope drawn over the normalized maximum ($F_Q(z)$ H Power) points in Figure 4.3-21 represents an upper bound envelope on local power density versus elevation in the core. It should be emphasized that this envelope is a conservative representation of the bounding values of local power density. Expected values are considerably smaller and, in fact, less conservative bounding values may be justified with additional analysis or surveillance requirements. For example, Figure 4.3-21 bounds both BOL and EOL conditions but without consideration of radial power distribution flattening with burnup, i.e., both BOL and EOL points presume the same radial peaking factor. Inclusion of the burnup flattening effect would reduce the local power densities corresponding to EOL conditions which may be limiting at the higher core elevations.

Finally, as previously discussed, this upper bound envelope is based on procedures of load follow which require operation within an allowed axial offset range. These procedures are detailed in the Watts Bar Technical Specifications and are followed by relying only upon excore surveillance supplemented by the normal monthly full core map requirement and by computer based alarms on deviation and time of deviation from the allowed flux difference band.

Allowing for fuel densification effects, the average linear power at 3411 MWt is 5.45 kW/ft. The conservative upper bound value of normalized local power density, including uncertainty allowances, is $F_Q(Z)$, where K(Z) = 1, corresponding to a peak linear power at 102% power.

To determine reactor protection system setpoints, with respect to power distributions, three categories of events are considered, namely rod control equipment malfunctions, operator errors of commission and operator errors of omission. In evaluating these three categories of events, the core is assumed to be operating within the four constraints described above.

The first category comprises uncontrolled rod withdrawal (with rods moving in the normal bank sequence) for full-length banks. Also included are motions of the full-length banks below their insertion limits, which could be caused, for example, by uncontrolled dilution or primary coolant cooldown. Power distributions were calculated throughout these occurrences, assuming short term corrective action. That is, no transient xenon effects were considered to result from the malfunction. The event was assumed to occur from typical normal operating situations which include normal xenon transients. It was further assumed in determining the power distributions that total core power level would be limited to below 118 percent by reactor trip. Results are given in Figure 4.3-22 in units of kW/ft. The peak power density which can occur in such events, assuming reactor trip at or below 118 percent, is less than that required for center-line melt, including uncertainties and densification effects.

The second category, also appearing in Figure 4.3-22, assumes that the operator mispositions the rod bank in violation of the insertion limits and creates short term conditions not included in normal operating conditions.

The third category assumes that the operator fails to take action to correct a flux difference violation. The results shown on Figure 4.3-23 are $F_Q$ multiplied by 102% power including an allowance for calorimetric error. The peak linear power does not exceed 21.1 kW/ft including the above factors.

Since the peak kW/ft is below the above limit, no flux difference penalties are required for overpower protection. It should be noted that a reactor overpower accident is not assumed to

occur coincident with an independent operator error. Additional detailed discussion of these analyses is presented in reference [7].

The appropriate hot channel factors, $F_Q$ and $F^N_{\Delta H}$, for peak local power density and for DNB analysis at full power are based on analyses of possible operating power shapes addressed in the Technical Specifications.

The maximum allowable $F_Q$ can be increased with decreasing power as shown in the Watts Bar Technical Specifications. Increasing $F^N_{\Delta H}$ with decreasing power is permitted by the DNB protection setpoints and allows radial power shape changes with rod insertion to the insertion limits, as described in Section 4.4.3.2. The allowance for increased $F^N_{\Delta H}$ as a function of power is given in the Technical Specifications. This becomes a design basis criterion which is used for establishing acceptable control rod patterns and control bank sequencing. Likewise, fuel loading patterns for each cycle are selected with consideration of this design criterion. The worst values of $F^N_{\Delta H}$ for possible rod configurations occurring in normal operation are used in verifying that this criterion is met. Typical radial factors and radial power distributions are shown in Figures 4.3-6 through 4.3-11. The worst values generally occur when the rods are assumed to be at their insertion limits. Maintenance of axial offset control establishes rod positions which are above the allowed rod insertion limits, thus assuring margin to the $F_{\Delta H}$ criterion. Section 3.2 of Reference 8 discusses the determination of $F_{\Delta H}$. These limits are taken as input to the thermal hydraulic design basis, as described in Section 4.4.3.2.1.

When a situation is possible in normal operation which could result in local power densities in excess of those assumed as the precondition for a subsequent hypothetical accident, but which would not itself cause fuel failure, administrative controls and alarms are provided for returning the core to a safe condition. These alarms are described in detail in Chapter 7.

### 4.3.2.2.7 Experimental Verification of Power Distribution Analysis

This subject is discussed in depth in reference [2]. A summary of this report is given here.

In a measurement of total peaking factor, $F_Q$, with the movable detector system described in Sections 7.7.1 and 4.4.5 the following uncertainties have to be considered:

*(1)* Reproducibility of the measured signal

*(2)* Errors in the calculated relationship between detector current and local flux

*(3)* Errors in the calculated relationship between detector flux and peak rod power some distance from the measurement thimble

The appropriate allowance for category 1 above has been quantified by repetitive measurements made with several intercalibrated detectors by using the common thimble features of the incore detector system. This system allows more than one detector to access any thimble. Errors in category 2 above are quantified to the extent possible, by using the fluxes measured at one thimble location to predict fluxes at another location which is also measured. Local power distribution predictions are verified in critical experiments on arrays of rods with simulated guide thimbles, control rods, burnable absorbers, etc. These critical experiments provide quantification of errors of categories 2 and 3 above.

Reference [2] describes critical experiments performed at the Westinghouse Reactor Evaluation Center and measurements taken on two Westinghouse plants with incore systems of the same type as used in Watts Bar. The report concludes that the uncertainty associated with $F_Q$ (heat flux

hot channel factor) is 4.58% at the 95% confidence level with only 5% of the measurements greater than the inferred value. This is equivalent to a 1.645σ limit on a normal distribution and is the uncertainty to be associated with a full core flux map with movable detectors reduced with a reasonable set of input data incorporating the influence of burnup on the radial power distribution. The uncertainty is usually rounded up to 5%.

In comparing measured power distributions ( or detector currents) with the calculations for the same condition, it is not possible to isolate the detector reproduciblility. Thus a comparison between measured and predicted power distributions has to include some measurement error. Such a comparison is given in Figure 4.3-24 for one of the maps used in reference [2]. Since the first publication of the report, hundreds of maps have been taken on these and other reactors. The results confirm the adequacy of the 5% uncertainty allowance on $F_Q$.

A similar analysis for the uncertainty in $F^N_{\Delta H}$ (rod integral power) measurements results in an allowance of 3.65% at the equivalent of a 1.645σ confidence level. For historical reasons an 8% uncertainty factor is allowed in the nuclear design basis; that is the predicted rod integrals at full power must not exceed the design $F_H$ less 8%.

A measurement in the second cycle of a 121 assembly, 12 foot core is compared with a simplified one dimensional core average axial calculation in Figure 4.3-25. This calculation does not give explicit representation to the fuel grids.

The accumulated data on power distributions in actual operation is basically of three types:

*(1)* Much of the data is obtained in steady state operation at constant power in the normal operating configuration;

*(2)* Data with unusual values of axial offset are obtained as part of the excore detector calibration exercise, which is performed monthly;

*(3)* Special tests have been performed in load follow and other transient xenon conditions, which have yielded useful information on power distributions.

These data are presented in detail in reference [8]. Figure 4.3-26 contains a summary of measured values of $F_Q$ as a function of axial offset for five plants from that report.

### 4.3.2.2.8 Testing

A series of physics tests is performed on the first core. These tests and the criteria for satisfactory results are described in detail in Chapter 14. Since not all limiting situations can be created at beginning-of-life, the main purpose of the tests is to provide a check on the calculational methods used in the predictions for the conditions of the test. Tests performed at the beginning of each reload cycle are limited to verification of selected safety related parameters of the reload design.

### 4.3.2.2.9 Monitoring Instrumentation

The adequacy of instrument numbers, spatial deployment, required correlations between readings and peaking factors, calibration and errors are described in references [2], [6], and [8]. The relevant conclusions are summarized here in Sections 4.3.2.2.7 and 4.4.5.

Provided the limitations given in Section 4.3.2.2.6 on rod insertion and axial flux difference are observed, the excore detector system provides adequate on line monitoring of power

distributions. Further details of specific limits on the observed rod positions and flux difference are given in the Technical Specifications together with a discussion of their bases.

Limits for alarms, reactor trip, etc. are given in the Technical Specifications. Descriptions of the systems provided are given in Section 7.7.

### 4.3.2.3 Reactivity Coefficients

The kinetic characteristics of the reactor core determine the response of the core to changing plant conditions or to operator adjustments made during normal operation, as well as the core response during abnormal or accidental transients. These kinetic characteristics are quantified in reactivity coefficients. The reactivity coefficients reflect the changes in the neutron multiplication due to varying plant conditions such as power, moderator or fuel temperatures, or less significantly due to a change in pressure or void conditions. Since reactivity coefficients change during the life of the core, ranges of coefficients are employed in transient analysis to determine the response of the plant throughout life. The results of such simulations and the reactivity coefficients used are presented in Chapter 15. The reactivity coefficients are calculated on a core-wise basis by diffusion theory methods and with nodal analysis methods. The effect of radial and axial power distribution on core average reactivity coefficients is implicit in those calculations and is not significant under normal operating conditions. For example, a skewed xenon distribution which results in changing axial offset by 5%, changes the moderator and Doppler temperature coefficients by less than 0.01 pcm/°F and 0.03 pcm/°F, respectively. An artificially skewed xenon distribution which results in changing the radial $F_H$ by 3%, changes the moderator and Doppler temperature coefficients by less than 0.03 pcm/°F and 0.001 pcm/°F, respectively. The spatial effects are accentuated in some transient conditions, for example, in postulated rupture of the main steamline and rupture of the RCCA mechanism housing as described in Chapter 15.

The analytical methods and calculational models used in calculating the reactivity coefficients are given in Section 4.3.3. These models have been confirmed through extensive testing of more than thirty cores similar to Watts Bar; results of these tests are discussed in Section 4.3.3.

Quantitative information for calculated reactivity coefficients, including fuel-Doppler coefficient, moderator coefficients (density, temperature, pressure, void) and power coefficient is given in the following sections.

#### 4.3.2.3.1 Fuel Temperature (Doppler) Coefficient

The fuel temperature (Doppler) coefficient is defined as the change in reactivity per degree change in effective fuel temperature and is primarily a measure of the Doppler broadening of U-238 and Pu-240 resonance absorption peaks. Doppler broadening of other isotopes such as U-236, Np-237, etc, are also considered but their contributions to the Doppler effect is small. An increase in fuel temperature increases the effective resonance absorption cross sections of the fuel and produces a corresponding reduction in reactivity.

The fuel temperature coefficient is calculated by performing two group X-Y calculations using an updated version of the TURTLE code[9], the PALADON code [27], or the ANC code [38]. The moderator temperature is held constant and the power level is varied. Spatial variation of fuel temperature is taken into account by calculating the effective fuel temperature as a function of power density as discussed in Section 4.3.3.1.

A typical Doppler temperature coefficient is shown in Figure 4.3-27 as a function of the effective fuel temperature (at beginning-of-life and end-of-life conditions). The effective fuel temperature

is lower than the volume averaged fuel temperature since the neutron flux distribution is non-uniform through the pellet and gives preferential weight to the surface temperature. The Doppler-only contribution to the power coefficient, defined later, is shown in Figure 4.3-28 as a function of relative core power. The integral of the differential curve on Figure 4.3-28 is the Doppler contribution to the power defect and is shown in Figure 4.3-29 as a function of power level. The Doppler coefficient becomes more negative as a function of life as the Pu-240 content (i.e., resonance absorption) increases. However, the overall Doppler coefficient becomes less negative as the fuel temperature changes with burnup as described in Section 4.3.3.1. The upper and lower limits of Doppler coefficient used in accident analyses are given in Chapter 15.

## 4.3.2.3.2 Moderator Coefficients

The moderator coefficient is a measure of the change in reactivity due to a change in specific coolant parameters such as density, temperature, pressure or void. The coefficients so obtained are moderator density, temperature, pressure and void coefficients.

### Moderator Density and Temperature Coefficients

The moderator temperature (density) coefficient is defined as the change in reactivity per degree change in the moderator temperature. Generally, the effect of the changes in moderator density as well as the temperature are considered together. A decrease in moderator density means less moderation which results in a negative moderator coefficient. An increase in coolant temperature, keeping the density constant, leads to a hardened neutron spectrum and results in an increase in resonance absorption in U-238, Pu-240 and other isotopes. The hardened spectrum also causes a decrease in the fission to capture ratio in U-235 and Pu-239. Both of these effects make the moderator coefficient more negative. Since water density changes more rapidly with temperature as temperature increases, the moderator temperature (density) coefficient become more negative with increasing temperature.

The soluble boron used in the reactor as a means of reactivity control also has an effect on moderator density coefficient since the soluble boron density, as well as the water density, are decreased when the coolant temperature rises. An increase in the soluble boron concentration introduces a positive component in the moderator coefficient. If the concentration of soluble boron is large enough, the net value of the coefficient may be positive. With the burnable absorber rods present, however, the initial hot boron concentration is sufficiently low that the moderator temperature coefficient is negative at operating temperatures. The effect of control rods is to make the moderator coefficient more negative by reducing the required soluble boron concentration and by increasing the 'leakage' of the core.

With burnup, the moderator coefficient becomes more negative primarily as a result of boric acid dilution but also to a significant extent from the effects of the buildup of plutonium and fission products.

The moderator coefficient is calculated for the various plant conditions discussed above by performing two-group two or three dimensional calculations, varying the moderator temperature by +5°F about each of the mean temperatures, and the density changes consistent with the temperature. The moderator coefficient is shown as a function of core temperature and boron concentration for a typical unrodded and rodded core in Figures 4.3-30 through 4.3-32. The temperature range covered is from cold (–68°F) to about 600°F. The contribution due to Doppler coefficient (because of change in moderator temperature) has been subtracted from these results. Figure 4.3-33 shows the hot, full-power moderator temperature coefficient plotted as a function of first cycle lifetime for the just critical boron concentration condition based on the design boron letdown condition.

The moderator coefficients presented here are calculated on a core wise basis, since they are used to describe the core behavior in normal and accident situations when the moderator temperature changes can be considered to affect the whole core.

### Moderator Pressure Coefficient

The moderator pressure coefficient relates the change in moderator density, resulting from a reactor coolant pressure change, to the corresponding effect on neutron production. This coefficient is of much less significance in comparison with the moderator temperature coefficient. A change of 50 psi in pressure has approximately the same effect (in magnitude but opposite in sign) on reactivity as a half degree change in moderator temperature. This coefficient can be determined from the moderator temperature coefficient by relating change in pressure to the corresponding change in density. The moderator pressure coefficient is negative over a portion of the moderator temperature range at beginning-of-life (-0.004 pcm/psi, BOL) but is always positive at operating conditions and becomes more positive during life (+0.3 pcm/psi, EOL).

### Moderator Void Coefficient

The moderator void coefficient relates the change in neutron multiplication to the presence of voids in the moderator. In a PWR, this coefficient is not very significant because of the low void content in the coolant. The core void content is < 1/2% and is due to local or statistical boiling. The void coefficient varies from +50 pcm/percent void at BOL and at low temperatures to -250 pcm/percent void at EOL and at operating temperatures. The negative void coefficient at operating temperature becomes more negative with fuel burnup.

## 4.3.2.3.3 Power Coefficient

The combined effect of moderator temperature and fuel temperature change as the core power level changes is called the total power coefficient and is expressed in terms of reactivity change per percent power change. The power coefficient at BOL and EOL conditions is given in Figure 4.3-34.

It becomes more negative with burnup reflecting the combined effect of moderator and fuel temperature coefficients with burnup. The power defect (integral reactivity effect) at BOL and EOL is given in Figure 4.3-35.

## 4.3.2.3.4 Comparison of Calculated and Experimental Reactivity Coefficients

Section 4.3.3 describes the comparison of calculated and experimental reactivity coefficients in detail. Based on the data presented there, the accuracy of the current analytical model is:

+ or $\pm$ 0.2 percent $\Delta\rho$ for Doppler and power defect

+ or $\pm$ 2 pcm/$^{\circ}$F for the moderator coefficient

Experimental evaluation of the calculated coefficients is done during the physics startup tests described in Chapter 14.

## 4.3.2.3.5 Reactivity Coefficients Used in Transient Analysis

Table 4.3-2 gives the representative ranges of the reactivity coefficients. The limiting values are used as design limits in the transient analysis. The exact values of the coefficient used in the analysis depend on whether the transient of interest is examined at BOL or EOL, whether the most negative or the most positive (least negative) coefficients are appropriate, and whether

spatial nonuniformity must be considered in the analysis. Conservative values of coefficients, considering various aspects of analysis, are used in the transient analysis. This is described in Chapter 15.

The reactivity coefficients shown in Figures 4.3-27 through 4.3-35 are values calculated for a typical cycle. The limiting values shown in Table 4.3-2 are chosen to encompass the best estimate reactivity coefficients, including the uncertainties given in Section 4.3.3.3, over appropriate operating conditions. The coefficients appropriate for use in subsequent cycles depend on the cores operating history, the number and enrichment of fresh fuel assemblies, the loading pattern of burned and fresh fuel, and number and location of burnable absorbers. The need for a reevaluation of any accident in a subsequent cycle is contingent upon whether or not the coefficients for that cycle fall within the identified range used in the analysis presented in Chapter 15 with due allowance for the calculational uncertainties given in Section 4.3.3.3. Control rod requirements are given in Table 4.3-3 for the core described and for a hypothetical equilibrium cycle since these are markedly different. These latter numbers are provided for information only and their validity in a particular cycle would be an unexpected coincidence.

### 4.3.2.4 Control Requirements

To ensure the shutdown margin requirements stated in the Watts Bar Technical Specifications under conditions where a cooldown to ambient temperature is required, concentrated soluble boron is added to the coolant. Boron concentrations for several core conditions are listed in Table 4.3-2. For all core conditions, including refueling, the boron concentration is well below the solubility limit. The rod cluster control assemblies are employed to bring the reactor to the hot shutdown condition. The minimum required shutdown margin is given in the Watts Bar Technical Specifications.

The ability to accomplish the shutdown for hot conditions is demonstrated in Table 4.3-3 which compares the difference between the Rod Cluster Control Assembly (RCCA) reactivity available, with an allowance for the worst stuck rod, with that required for control and protection purposes. The shutdown margin includes an allowance of 10% on the total calculated rod worth minus the most reactive stuck rod for analytic uncertainties[36]. The largest reactivity control requirement appears at the end-of-life when the moderator temperature coefficient reaches its peak negative value as reflected in the larger power defect.

The control rods are required to provide sufficient reactivity to account for the power defect from full power to zero power and to provide the required shutdown margin. The reactivity addition resulting from power reduction consists of contributions from Doppler, variable average moderator temperature, flux redistribution, and reduction in void content, as discussed below.

#### 4.3.2.4.1 Doppler

The Doppler effect arises from the broadening of U-238 and Pu-240 resonance peaks with an increase in effective pellet temperature. This effect is most noticeable over the range of zero power to full power due to the large pellet temperature increase with power generation.

#### 4.3.2.4.2 Variable Average Moderator Temperature

When the core is shutdown to the hot zero power condition, the average moderator temperature changes from the equilibrium full load value determined by the steam generator and turbine characteristics (steam pressure, heat transfer, tube fouling, etc.) to the equilibrium no load value, which is based on the steam generator shell side design pressure. The design change in

temperature is conservatively increased by 4EF to account for the control dead band and measurement errors.

Since the moderator coefficient is negative, there is a reactivity addition with power reduction. The moderator coefficient becomes more negative as the fuel depletes because the boron concentration is reduced. This effect is the major contributor to the increased requirement at end-of-life.

#### 4.3.2.4.3 Redistribution

During full power operation, the coolant density decreases with core height, and this, together with partial insertion of control rods, results in less fuel depletion near the top of the core. Under steady state conditions, the relative power distribution will be slightly asymmetric towards the bottom of the core. On the other hand, at hot zero power conditions, the coolant density is uniform up the core, and there is no flattening due to Doppler. The result will be a flux distribution which at zero power can be skewed toward the top of the core. The reactivity insertion due to the skewed distribution is calculated with an allowance for the most adverse effects of xenon distribution.

#### 4.3.2.4.4 Void Content

A small void content in the core is due to nucleate boiling at full power. The void collapse coincident with power reduction makes a small reactivity contribution.

#### 4.3.2.4.5 Rod Insertion Allowance

At full power, the control bank is operated within a prescribed band of travel to compensate for small periodic changes in boron concentration, changes in temperature and very small changes in the xenon concentration not compensated for by a change in boron concentration. When the control bank reaches either limit of this band, a change in boron concentration is required to compensate for additional reactivity changes. Since the insertion limit is set by a rod travel limit, a conservatively high calculation of the inserted worth is made which exceeds the normally inserted reactivity.

#### 4.3.2.4.6 Burnup

Excess reactivity of approximately 10% $\Delta\rho$ (hot) is installed at the beginning of each cycle to provide sufficient reactivity to compensate for fuel depletion and fission product buildup throughout the cycle. This reactivity is controlled by the addition of soluble boron to the coolant and by burnable absorbers. The soluble boron concentration for several core configurations, the unit boron worth, and burnable absorber worth are given in Tables 4.3-1 and 4.3-2. Since the excess reactivity for burnup is controlled by soluble boron and/or burnable absorbers, it is not included in control rod requirements.

#### 4.3.2.4.7 Xenon and Samarium Concentrations

Changes in xenon and samarium concentrations in the core occur at a sufficiently slow rate, even following rapid power level changes, that the resulting reactivity change is controlled by changing the soluble boron concentration.

#### 4.3.2.4.8 pH Effects

Changes in reactivity due to a change in coolant pH, if any, are sufficiently small in magnitude and occur slowly enough to be controlled by the boron system. Further details are available in reference [10].

### 4.3.2.4.9 Experimental Confirmation

Following a normal shutdown, the total core reactivity change during cooldown with a stuck rod has been measured on a 121 assembly, 10-foot high core and a 121 assembly, 12-foot high core. In each case, the core was allowed to cooldown until it reached criticality simulating the steamline break accident. For the ten foot core, the total reactivity change associated with the cooldown is overpredicted by about 0.3% Δρ with respect to the measured result. This represents an error of about 5% in the total reactivity change and is about half the uncertainty allowance for this quantity. For the 12-foot core, the difference between the measured and predicted reactivity change was an even smaller 0.2% Δρ. These measurements and others demonstrate the ability of the methods described in Section 4.3.3 to accurately predict the total shutdown reactivity of the core.

### 4.3.2.5 Control

Core reactivity is controlled by means of a chemical shim dissolved in the coolant, Rod Cluster Control Assemblies, and burnable absorber rods as described below.

### 4.3.2.5.1 Chemical Shim

Boron in solution as boric acid is used to control relatively slow reactivity changes associated with:

*(1)* The moderator temperature defect in going from cold shutdown at ambient temperature to the hot operating temperature at zero power,

*(2)* The transient xenon and samarium concentrations, such as that following power changes or changes in RCCA position,

*(3)* The excess reactivity required to compensate for the effects of fissile inventory depletion and buildup of long-life fission products.

*(4)* The burnable absorber depletion.

The boron concentrations for various core conditions are presented in Table 4.3-2.

### 4.3.2.5.2 Rod Cluster Control Assemblies

The numbers of Rod Cluster Control Assemblies shown in Table 4.3-1 are used for shutdown and control purposes to offset fast reactivity changes associated with:

*(1)* The required shutdown margin in the hot zero power, stuck rod condition.

*(2)* The reactivity compensation as a result of an increase in power above hot zero power (power defect including Doppler, and moderator reactivity changes).

*(3)* Unprogrammed fluctuations in boron concentration, coolant temperature, or xenon concentration (with rods not exceeding the allowable rod insertion limits).

*(4)* Reactivity ramp rates resulting from load changes.

The allowed control bank reactivity insertion is limited at full power to maintain shutdown capability. The insertion limit is determined using conservative xenon distributions and axial

power shapes. As the power level is reduced, control rod reactivity requirements are also reduced and more rod insertion is allowed. The control bank position is monitored and the operator is notified by an alarm if the limit is approached. In addition, the Rod Cluster Control Assembly withdrawal pattern determined from these analyses is used in determining power distribution factors and in determining the maximum worth of an inserted Rod Cluster Control Assembly ejection accident. For further discussion, refer to the Technical Specifications on Rod Insertion Limits.

Power distribution, Rod Ejection and Rod Misalignment analyses are based on the arrangement of the shutdown and control groups of the Rod Cluster Control Assemblies shown in Figure 4.3-36. All shutdown rod cluster control assemblies are withdrawn before withdrawal of the control banks is initiated. In going from zero to 100% power, control banks B, C and D are withdrawn sequentially. The limits of rod positions and further discussion on the basis for rod insertion limits are provided in the Watts Bar Technical Specifications.

### 4.3.2.5.3 Burnable Absorbers

The burnable absorbers provide partial control of the excess reactivity available during the cycle. In doing so, burnable absorbers prevent the moderator temperature coefficient from being positive at normal operating conditions. They perform this function by reducing the requirement for soluble boron in the moderator. The burnable absorber rod pattern in the core together with the number of rods per assembly is shown in Figure 4.3-5, while the arrangements of burnable absorber rods within an assembly are displayed in Figures 4.3-4a and 4.3-4b. The reactivity worth of these rods is shown in Table 4.3-1. The boron in the rods is depleted with burnup but at a sufficiently slow rate so that the resulting critical concentration of soluble boron is such that the moderator temperature coefficient remains negative at all times for power operating conditions.

### 4.3.2.5.4 Peak Xenon Startup

Compensation for the peak xenon buildup is accomplished using the boron control system. Startup from the peak xenon condition is accomplished with a combination of rod motion and boron dilution. The boron dilution may be made at any time, including during the shutdown period, provided the shutdown margin is maintained.

### 4.3.2.5.5 Load Follow Control and Xenon Control

During load follow maneuvers, power changes are accomplished using control rod motion and dilution or boration by the boron system as required. Control rod motion is limited by the control rod insertion limits as provided in the Technical Specifications and discussed in FSAR Section 4.3.2.5.2. Reactivity changes due to the changing xenon concentration can be controlled by rod motion and/or changes in the soluble boron concentration.

### 4.3.2.5.6 Burnup

Control of the excess reactivity for burnup is accomplished using soluble boron and/or burnable absorbers. The boron concentration must be limited during operating conditions to ensure the moderator temperature coefficient is negative. Sufficient burnable absorbers are installed at the beginning of a cycle to give the desired cycle lifetime without exceeding the boron concentration limit. The practical minimum boron concentration is 10 ppm.

### 4.3.2.6 Control Rod Patterns and Reactivity Worth

The Rod Cluster Control Assemblies are designated by function as the control groups and the shutdown groups. The terms 'group' and 'bank' are used synonymously throughout this report to describe a particular grouping of control assemblies. The rod cluster assembly pattern is displayed in Figure 4.3-36. The control banks are labeled A, B, C and D and the shutdown banks are labeled SA, SB, SC and SD. Each bank, although operated and controlled as a unit, is comprised of two subgroups. The axial position of the Rod Cluster Control Assemblies may be controlled manually or automatically. The Rod Cluster Control Assemblies are all dropped into the core following actuation of reactor trip signals.

Two criteria have been employed for selection of the control groups. First the total reactivity worth must be adequate to meet the requirements specified in Table 4.3-3. Second, in view of the fact that these rods may be partially inserted at power operation, the total power peaking factor should be low enough to ensure that the power capability requirements are met. Analyses indicate that the first requirement can be met either by a single group or by two or more banks whose total worth equals at least the required amount. The axial power shape would be more peaked following movement of a single group of rods worth three to four percent delta-ρ; therefore, four banks (described as A, B, C and D in Figure 4.3-36) have been selected.

The position of control banks for criticality under any reactor condition is determined by the concentration of boron in the coolant. On an approach to criticality, boron is adjusted to ensure that criticality will be achieved with control rods above the insertion limit set by shutdown margin and other considerations (See Watts Bar Technical Specifications). Early in the cycle there may also be a withdrawal limit at low power to maintain a negative moderator temperature coefficient. Usual practice is to adjust boron to ensure that the rod position lies within the maneuvering band, that is, such that an escalation from zero power to full power does not require further adjustment of boron concentration.

Ejected rod worths are given in Table 15.4-12 for several different conditions.

Allowable deviations due to misaligned control rods are discussed in the Watts Bar Technical Specifications.

A representative calculation for two banks of control rods simultaneously withdrawn (Rod Withdrawal accident) is given in Figure 4.3-37.

Calculation of control rod reactivity worth versus time following reactor trip involves both control rod velocity and differential reactivity worth. Nuclear design provides reactivity worth versus rod position from a series of steady-state calculations at various control rod positions, assuming all rods out of the core as the initial position in order to minimize the initial reactivity insertion rate. To be conservative, the rod of highest worth is assumed stuck out of the core and the flux distribution (and thus reactivity importance) is assumed to be skewed to the bottom of the core

The shutdown groups provide additional negative reactivity to assure an adequate shutdown margin. Shutdown margin is defined as the amount of reactivity by which the core would be subcritical at hot shutdown if all rod cluster control assemblies are tripped, but assuming that the highest worth assembly remains fully withdrawn and no changes in xenon or boron take place. The loss of control rod worth due to the material irradiation is negligible since only bank D rods may be in the core under normal operating conditions (near full power).

The values given in Table 4.3-3 show that the available reactivity in withdrawn Rod Cluster Control Assemblies provides the design bases minimum shutdown margin allowing for the

highest worth cluster to be at its fully withdrawn position. An allowance for uncertainty in the calculated worth of N-1 rods is made before determination of the shutdown margin.

### 4.3.2.7 Criticality of Fuel Assemblies

Criticality of fuel assemblies outside the reactor is precluded by adequate design of fuel transfer and fuel storage facilities and by administrative control procedures. This section identifies those criteria important to criticality safety analyses.

#### New Fuel Storage

New fuel is normally stored dry in the new fuel storage vault. The design basis for preventing criticality within the new fuel storage vault is that, including uncertainties, there is a 95 percent probability at a 95 percent confidence level that the effective multiplication factor ($K_{eff}$) of the fuel assembly array will be less than 0.95 under full moderator density conditions and less than 0.98 under low water density (optimum moderation) conditions.

The new fuel rack criticality analysis demonstrated that this rack will meet the design basis limits for $K_{eff}$ for storage of Westinghouse 17x17 STANDARD and VANTAGE 5H fuel assemblies with nominal enrichments up to 4.3 wt/% U-235 utilizing all (130) available storage cell locations. The analysis also showed that nominal enrichments above 4.3 wt/% and up to 5.0 wt/% U-235 can be stored provided that only 120 specific cells of the 130 available locations are utilized. The remaining storage cells must remain empty. The allowed locations for the 120 usable cells is described in the new fuel storage rack criticality report.

The design method which ensures the criticality safety of fuel assemblies in the spent fuel storage rack uses the AMPX system of codes for cross-section generation and KENO IV for reactivity determination. The 227 energy group cross-section library that is the common starting point for all cross-sections used for the benchmarks and the storage rack analysis is generated from ENDF/B-V data. The NITAWL program includes, in this library, the self-shielded resonance cross-sections that are appropriate for each particular geometry. The Nordheim Integral Treatment is used. Energy and spatial weighting of cross-sections is performed by the XSDRNPM program which is a one-dimensional Sn transport theory code. These multigroup cross-section sets are then used as input to KENO IV which is a three dimensional Monte Carlo theory program designed for reactivity calculations.

Under normal conditions, the fresh fuel racks are maintained in a dry environment. The introduction of water into the fresh fuel rack area is the worst case accident scenario. The full density and low density optimum moderation cases are bounding accident situations which result in the most conservative fuel rack $k_{eff}$.

Other accidents can be postulated which would cause some reactivity increase (i. e., dropping a fuel assembly between the rack and wall or on top of the rack). For these other accident conditions, the double contingency principle of ANSI N16.1-1975 is applied. This states that one is not required to assume two unlikely, independent, concurrent events to ensure protection against a criticality accident. Thus, for these other accident conditions, the absence of a moderator in the fresh fuel storage racks can be assumed as a realistic initial condition since assuming its presence would be a second unlikely event. The maximum reactivity increase for these kinds of postulated accidents is less than 10% delta-K/K, and since the normal, dry fresh fuel rack reactivity is less than 0.70, these postulated accidents will not result in a $K_{eff}$ which is more limiting than the analyzed worst case accident scenarios of full density and optimum moderation water flooding.

Thus, using the method described above, the maximum $K_{eff}$ was determined to be less than 0.95, which meets the criteria stated in Section 4.3.1.6.

### Spent Fuel Storage - Wet

The high density spent fuel storage racks for WBN are designed to assure that the effective neutron multiplication factor ($k_{eff}$) is equal to or less that 0.95. Design calculations model the racks fully loaded with fuel of the highest anticipated reactivity, and with a margin for uncertainty in reactivity calculations including mechanical tolerances. Uncertainties are statistically combined, such that the final $k_{eff}$ will be equal to or less than 0.95 with a 95% probability at a 95% confidence level.

The layout of storage cells in the WBN spent fuel pool is shown in Figure 9.1-15. The criticality analysis of the WBN spent fuel pool configuration assures that the maximum $K_{eff}$ will be less than or equal to 0.95 with fuel up to 4.95 ± .05 wt% U-235 enrichment.

Analysis of the WBN spent fuel rack configuration [41],[42] was performed using the SCALE[43],[44],[45] system of codes for cross section generation and reactivity calculations, and CASMO[46],[47],[48],[49] was used for depletion calculations. The design basis fuel is a 17x17 Westinghouse VANTAGE-5H[50] assembly containing a maximum initial enrichment of 4.95 ± .05 wt% U-235. The calculations were performed with a moderator temperature of 4°C.

Margin for uncertainty in the reactivity calculations and manufacturing tolerances were included such that the final $k_{eff}$ for allowed storage configurations will be less than or equal to 0.95 with a 95% probability at a 95% confidence level. In order to store fuel with U-235 enrichment as high as 4.95 ± .05 wt%, administrative controls and burnup credit must be applied. Therefore, the analysis takes credit for the reactivity decrease due to burnup of the stored fuel and for administrative controls on fuel placement. Burnup in discharged fuel was treated using CASMO4, performing depletion calculation which explicitly describe the fission product nuclide concentration. This methodology incorporates approximately 40 of the most important fission products. The fission product nuclide concentrations obtained from the CASMO4 depletions were then modeled in three-dimensions using KEN05a.

The VANTAGE 5H fuel design[50] was modeled as the design basis fuel. The VANTAGE 5H design contains a smaller guide tube outer diameter and thus slightly increased neutron moderation compared with the Westinghouse Standard 17x17 fuel assembly. In addition, VANTAGE 5H fuel assemblies have zircaloy spacer grids as opposed to the more neutron-absorbing material Inconel found on the Standard 17x17 fuel assembly. As a result of these differences, VANTAGE 5H fuel has a higher reactivity for a given enrichment than Standard 17x17 fuel. Therefore, analysis of VANTAGE 5H fuel also covers storage of Standard 17x17 fuel. VANTAGE 5H fuel assembly data is provided in Table 4.3-12. The analysis model bounds the design basis fuel assembly using the data provided in Table 4.3-12 or a more conservative value depending on the specific calculation.

Starting in Cycle 2 with Reload 1, Watts Bar Unit 1 used the Westinghouse fuel assembly designated a Vantage+/Performance+(V+/P+). The V+/P+ fuel design is less reactive than the Vantage 5H fuel design at the same enrichment. The ZIRLO material used in the midgrids, fuel cladding and guide tubes has a slight reactivity penalty relative to ZIRC-4[56]. Therefore, the analysis of Vantage 5H also covers and is bounding for the V+/P+ fuel design. In addition, the analysis evaluated the Robust Fuel Assembly (RFA) design (also planned for use on Unit 2) and determined that the Vantage 5 design is bounding for the burnups of interest.

Analytical Technique and Results

The criticality analysis for the WBN racks were performed primarily with KENO5a, a three-dimensional Monte Carlo computer code, using the 238-group SCALE cross-section library and the Nordheim integral treatment for resonance shielding effects found in NITAWL. Depletion analyses were performed using CASMO4, a two-dimensional transport theory code incorporating approximately 40 of the most important fission products.

Analysis of the spent fuel racks confirmed that the racks can safely and conservatively accommodate storage of fuel up to 5 wt% U-235 enrichment with the following storage conditions:

*(1)* Fuel Assemblies with 3.8 WT% or less U-235 Initial enrichment may be stored without restrictions.

*(2)* Fuel assemblies with initial enrichment greater than 3.8 wt% U-235 and less than a maximum of 5.0 wt% (4.95 ± 0.05) may be stored in one of four arrangements with the limits specified below.

*(A)* Fuel assemblies may be stored in the racks without further restrictions provided the burnup of each assembly is in the acceptable domain identified in Figure 4.3-46, depending on the specified initial enrichment.

*(B)* New and spent fuel assemblies may be stored in a checkerboard arrangement of 2 new and 2 spent assemblies, provided the accumulated burnup of each spent assembly is in the acceptable domain identified in Figure 4.3-47, depending on the specified initial enrichment.

*(C)* New fuel assemblies may be stored in 4-cell arrays with 1 of the 4 cells remaining empty of fuel (containing only water or water with up to 75 percent by volume of non-fuel bearing material).

*(D)* New fuel assemblies with a minimum of 32 integral fuel burnable absorber (IFBA rods may be stored in the racks without further restrictions provided the loading of ZrB2 in the coating of each IFBA rod is a minimum of 1.25 x (1.9625 mg/in).

A water cell is less reactive than any cell containing fuel and therefore may be used at any location in the loading arrangements. A water cell is defined as a cell containing water or non-fissile material with no more than 75 percent of the water displaced.

The Technical Specifications include curves defining the limiting burnup for fuel of various initial enrichments for both unrestricted storage and checkerboard arrangements assuming the fresh fuel region is enriched to 4.95 ± 0.05 wt% U-235. The calculated maximum reactivity is 0.948, which is within the regulatory limit of keff of 0.95. This maximum reactivity includes calculational uncertainties and manufacturing tolerances (95% probability at the 95% confidence level), an allowance for uncertainty in depletion calculations, and the evaluated effect of the axial distribution in burnup. Fresh fuel of less than 4.95% enrichment would result in lower reactivities.

Accounting for biases and uncertainties, the maximum $k_{eff}$ values for the above spent fuel storage rack conditions are less than 0.95. The maximum $k_{eff}$ was determined as follows:

$$k_{eff} = k_{eff} \text{ (KENO)} + \text{BIASES} + \text{UNCERTAINTIES}$$

Biases include the CASMO and KENO method biases and a bias for the extrapolation of enrichment from the critical benchmark comparisons. The uncertainties include the KENO statistical uncertainty, the KENO and CASMO method uncertainties, and the mechanical tolerance uncertainty

The analyses conservatively do not take credit for presence of borated water, presence of discrete burnable absorbers, lower enrichment and higher burnup which would decrease reactivity. Other conservative assumptions include:

- Ignoring radial neutron leakage from the spent fuel storage racks
- Ignoring the presence of control rods
- Ignoring the presence of spent burnable absorber assemblies in storage
- Ignoring the higher water temperature of the spent fuel pool
- Maximizing burnable poison history effects
- Maximizing water density history effects
- Minimizing the $^{10}B$ content in the Boral

A water gap between two rack modules with Boral panels on both sides of the water gap (i.e., a flux trap), precludes any adverse interaction between the two modules.

The effect of various parameters on reactivity was determined to ensure the conservatism of the analysis. This was accomplished by performing sensitivity studies on these parameters with CASMO. Parameters evaluated were axial burnup distribution, water temperature/density, assembly placement, mechanical tolerances, poison loading, pellet density, cell dimensions/bow, borated water activity worth, Boral width tolerance, cell lattice spacing tolerance, stainless steel thickness tolerance, and fuel enrichment and density tolerance.

## Accident Analysis

Although credit for soluble poison normally present in the spent fuel pool water is permitted under abnormal or accident conditions (double contingency principle), most abnormal or accident conditions will not result in exceeding the limiting reactivity ($k_{eff}$ = 0.95) even in the absence of soluble poison. However, the inadvertent misplacement of a fresh fuel assembly in a location intended to be a water cell has the potential for exceeding the limiting reactivity and results in the worst-case accident scenario, should there be a concurrent loss of all soluble boron. Misplacement of a fuel assembly outside the periphery of a storage module, or a dropped assembly lying on the top of the rack would have a smaller reactivity effect. Under this worst-cast accident condition, calculations show that approximately 55 ppm of soluble boron would be sufficient to ensure that the limiting $k_{eff}$ of 0.95 is not exceeded. Assuring the presence of soluble boron during fuel handling operation will preclude the possibility of the simultaneous occurrence of the two independent accident conditions. Administrative controls require that the spend fuel pool boron concentration be monitored (to ensure at least 2000 ppm) during operations requiring fuel moves in the pool until verification is made of assembly locations.

## 4.3.2.8 Stability

### 4.3.2.8.1 Introduction

The stability of the PWR cores against xenon-induced spatial oscillations and the control of such transients are discussed extensively in references [6], [12], [13], and [14]. A summary of these reports is given in the following discussion and the design bases are given in Section 4.3.1.7.

In a large reactor core, xenon-induced oscillations can take place with no corresponding change in the total power of the core. The oscillation may be caused by a power shift in the core which occurs rapidly by comparison with the xenon-iodine time constants. Such a power shift occurs in the axial direction when a plant load change is made by control rod motion and results in a change in the moderator density and fuel temperature distributions. Such a power shift could occur in the diametral plane of the core as a result of abnormal control action.

Due to the negative power coefficient of reactivity, PWR cores are inherently stable to oscillations in total power. Protection against total power instabilities is provided by the Reactor Control System as described in Section 7.7. Hence, the discussion on the core stability is limited here to xenon-induced spatial oscillations.

### 4.3.2.8.2 Stability Index

Power distributions, either in the axial direction or in the X-Y plane, can undergo oscillations due to perturbations introduced in the equilibrium distributions without changing the total core power. The overtones in the current PWRs, and the stability of the core against xenon-induced oscillations can be determined in terms of the eigenvalues of the first flux overtones. Writing, either in the axial direction or in the X-Y plane, the eigenvalue of the first flux harmonic as:

$$\xi = b + ic, \qquad (4.3\text{-}1)$$

then b is defined as the stability index and $T = 2\pi/c$ as the oscillation period of the first harmonic. The time-dependence of the first harmonic $\delta\varphi$ in the power distribution can be represented as:

$$\delta\phi(t) = A\, e^{\xi t} = a e^{bt} \cos ct, \qquad (4.3\text{-}2)$$

where A and a are constants. The stability index can also be obtained approximately by:

$$b = \frac{1}{T} \ln \frac{A_{n+1}}{A_n} \qquad (4.3\text{-}3)$$

where $A_n$, $A_{n+1}$ are the successive peak amplitudes of the oscillation and T is the time period between the successive peaks.

### 4.3.2.8.3 Prediction of the Core Stability

The stability of the Watts Bar Nuclear Plant core (i.e., with 17 x 17 fuel assemblies) against xenon-induced spatial oscillations is expected to be equal to or better than that of earlier designs. The prediction is based on a comparison of the parameters which are significant in determining the stability of the core against the xenon-induced oscillations, namely

*(1)* the overall core size is unchanged and spatial power distributions will be similar,

*(2)* the moderator temperature coefficient is expected to be similar to or slightly more negative, and

*(3)* the Doppler coefficient of reactivity is expected to be equal to or slightly more negative at full power.

Analysis of both the axial and X-Y xenon transient tests, discussed in Section 4.3.2.8.5, shows that the calculational model is adequate for the prediction of core stability.

### 4.3.2.8.4 Stability Measurements

*(1)* Axial Measurements

Two axial xenon transient tests conducted in a PWR with a core height of 12 feet and 121 fuel assemblies is reported in reference [15], and will be briefly discussed here. The tests were performed at approximately 10% and 50% of cycle life.

Both a free-running oscillation test and a controlled test were performed during the first test. The second test at mid-cycle consisted of a free-running oscillation test only. In each of the free-running oscillation tests, a perturbation was introduced to the equilibrium power distribution through an impulse motion of the control Bank D and the subsequent oscillation was monitored to measure the stability index and the oscillation period.

In the controlled test conducted early in the cycle, the part length rods were used to follow the oscillations to maintain an axial offset within the prescribed limits. The axial offset of power was obtained from the excore ion chamber readings (which had been calibrated against the incore flux maps) as a function of time for both free-running tests as shown in Figure 4.3-40.

The total core power was maintained constant during these spatial xenon tests, and the stability index and the oscillation period were obtained from a least-square fit of the axial offset data in the form of Equation (4.3-2). The axial offset of power is the quantity that properly represents the axial stability in the sense that it essentially eliminates any contribution from even order

harmonics, including the fundamental mode. The conclusions of the tests are:

*(a)* The core was stable against induced axial xenon transients both at the core average burnups of 1550 MWD/MTU and 7700 MWD/MTU. The measured stability indices are -0.041 $hr^{-1}$ for the first test (Curve 1 of Figure 4.3-40) and -0.014 $hr^{-1}$ for the second test (Curve 2 of Figure 4.3-40). The corresponding oscillation periods are 32.4 hrs. and 27.2 hrs., respectively.

*(b)* The reactor core becomes less stable as fuel burnup progresses and the axial stability index was essentially zero at 12,000 MWD/MTU.

*(2)* Measurements in the X-Y Plane

*(3)* Two X-Y xenon oscillation tests were performed at a PWR plant with a core height of 12 feet and 157 fuel assemblies. The first test was conducted at a core average burnup of 1540 MWD/MTU and the second at a core average burnup of 12900 MWD/MTU. Both of the X-Y xenon tests show that the core was stable in the X-Y plane at both burnups. The second test shows that the core became more stable as the fuel burnup increased and all Westinghouse PWR's with 121 and 157 assemblies are expected to be stable throughout their burnup cycles. The results of these tests are applicable to the 193 assembly Watts Bar cores as discussed in Section 4.3.2.

*(4)* In each of the two X-Y tests, a perturbation was introduced to the equilibrium power distribution through an impulse motion of one RCCA located along the diagonal axis. Following the perturbation, the uncontrolled oscillation was monitored using the moveable detector and thermocouple system and the excore power range detectors. The quadrant tilt difference (QTD) is the quantity that properly represents the diametral oscillation in the X-Y plane of the reactor core in that the differences of the quadrant average powers over two symmetrically opposite quadrants essentially eliminates the contribution to the oscillation from the azimuthal mode. The QTD data were fitted in the form of Equation (4.3-2) through a least-square method. A stability index of $-0.076^{-1}$ hr with a period of 29.6 hours was obtained from the thermocouple data shown in Figure 4.3-41.

It was observed in the second X-Y xenon test that the PWR core with 157 fuel assemblies had become more stable due to an increased fuel depletion and the stability index was not determined.

### 4.3.2.8.5 Comparison of Calculations with Measurements

The analysis of the axial xenon transient tests was performed in an axial slab geometry using a flux synthesis technique. The direct simulation of the axial offset data was carried out using the PANDA Code [16]. The analysis of the X-Y xenon transient tests was performed in an X-Y geometry using a modified TURTLE [9] Code. Both the PANDA and TURTLE codes solve the two-group time-dependent neutron diffusion equation with time-dependent xenon and iodine

concentrations. The fuel temperature and moderator density feed back is limited to a steady-state model. All the X-Y calculations were performed in an average enthalpy plane.

The basic nuclear cross-sections used in this study were generated from a unit cell depletion program which has evolved from the codes LEOPARD[17] and CINDER[18]. The detailed experimental data during the tests including the reactor power level, enthalpy rise and the impulse motion of the control rod assembly, as well as the plant follow burnup data were closely simulated in the study.

The results of the stability calculation for the axial tests are compared with the experimental data in Table 4.3-5. The calculations show conservative results for both of the axial tests with a margin of approximately -0.01 $hr^{-1}$ in the stability index.

An analytical simulation of the first X-Y xenon oscillation test shows a calculated stability index of -0.081 $hr^{-1}$ in good agreement with the measured value of -0.076 $hr^{-1}$. As indicated earlier, the second X-Y xenon test showed that the core had become more stable compared to the first test and no evaluation of the stability index was attempted. This increase in the core stability in the X-Y plane due to increased fuel burnup is due mainly to the increased magnitude of the negative moderator temperature coefficient.

Previous studies of the physics of xenon oscillations, including three-dimensional analysis, are reported in the series of topical reports, references [12], [13] and [14]. A more detailed description of the experimental results and analysis of the axial and X-Y xenon transient tests is presented in reference [15] and Section I of reference [19].

### 4.3.2.8.6 Stability Control and Protection

The excore detector system is utilized to provide indications of xenon-induced spatial oscillations. The readings from the excore detectors are available to the operator and also form part of the protection system.

*(1)* Axial Power Distribution

For maintenance of proper axial power distributions, the operator maintains an axial offset within a prescribed operating band, based on the excore detector readings. Should the axial offset be permitted to move far enough outside this band, the protection limit will be reached and the power will be automatically cutback.

As fuel burnup progresses, twelve foot PWR cores become less stable to axial xenon oscillations . However, free xenon oscillations are not allowed to occur, except for special tests. The control rod banks are sufficient to dampen and control any axial xenon oscillations present. Should the axial offset be inadvertently permitted to move far enough outside the allowed band due to an axial xenon oscillation, or for any other reason, the protection limit on axial offset will be reached and the power will be automatically cut back.

*(2)* Radial Power Distribution

The core described herein is calculated to be stable against X-Y xenon induced oscillations at all times in life.

The X-Y stability of large PWR's has been further verified as part of the startup physics test program for PWR cores with 193 fuel assemblies. The measured X-Y stability of the cores with 157 and 193 assemblies was in good agreement with the calculated stability, as discussed in Sections 4.3.2.8.4 and 4.3.2.8.5. In the unlikely event that X-Y oscillations occur, back-up actions are possible and would be implemented, if necessary, to increase the natural stability of the core. This is based on the fact that several actions could be taken to make the moderator temperature coefficient more negative, which will increase the stability of the core in the X-Y plane.

Provisions for the protection against non-symmetric perturbations in the X-Y power distribution that could result from equipment malfunctions are made in the protection system design. This includes control rod drop, rod misalignment and asymmetric loss of coolant flow.

A more detailed discussion of the power distribution control in PWR cores is presented in reference [6] and [7].

### 4.3.2.9 Vessel Irradiation

A brief review of the methods and analyses used in the determination of neutron and gamma ray flux attenuation between the core and the pressure vessel is given below. A more complete discussion on the pressure vessel irradiation and surveillance program is given in Section 5.4.3.6.

The materials that serve to attenuate neutrons originating in the core and gamma rays from both the core and structural components consist primarily of the core baffle, core barrel, the neutron pads, and associated water annuli, all of which are within the region between the core and the pressure vessel.

In general, few group neutron diffusion theory codes are used to determine flux and fission power density distributions within the active core and the accuracy of these analyses is verified by in-core measurements on operating reactors. Region and rod-wise power sharing information from the core calculations is then used as source information in two-dimensional $S_n$ transport calculations which compute the flux distribution throughout the reactor.

The neutron flux distribution and spectrum in the various structural components vary significantly from the core to the pressure vessel. Representative values of the neutron flux distribution and spectrum are presented in Table 4.3-6. The values listed are based on time-averaged equilibrium cycle reactor core parameters and power distributions, and thus, are suitable for long term fluence (nvt) projections and for correlation with radiation damage estimates.

As discussed in Section 5.4.3.6, the irradiation surveillance program utilizes actual test samples to verify the accuracy of the calculated fluxes at the vessel.

## 4.3.3 Analytical Methods

Calculations required in nuclear design consist of three distinct types, which are performed in sequence:

*(1)* Determination of effective fuel temperatures

*(2)* Generation of macroscopic few-group parameters

*(3)* Space-dependent, few-group diffusion calculations

These calculations are carried out by computer codes which can be executed individually. However, at Westinghouse, most of the codes required have been linked to form an automated design sequence which minimizes design time, avoids errors in transcription of data, and standardizes the design methods.

### 4.3.3.1 Fuel Temperature (Doppler) Calculations

Temperatures vary radially within the fuel rod, depending on the heat generation rate in the pellet; the conductivity of the materials in the pellet, gap, and clad; and the temperature of the coolant.

The fuel temperatures for use in most nuclear design Doppler calculations are obtained from a simplified version of the Westinghouse fuel rod design model described in Section 4.2.1.3.1 which considers the effect of radial variation of pellet conductivity, expansion coefficient and heat generation rate, elastic deflection of the clad, and a gap conductance which depends on the initial fill gas, the hot open gap dimension, and the fraction of the pellet over which the gap is closed. The fraction of the gap assumed closed represents an empirical adjustment used to produce good agreement with observed reactivity data at beginning-of-life. Further gap closure occurs with burnup and contributes a positive component to the Doppler defect. For detailed calculations of the Doppler coefficient, such as for use in xenon stability calculations, a more sophisticated temperature model is used which accounts for the effects of fuel swelling, fission gas releases, and plastic clad deformation.

Radial power distributions in the pellet as a function of burnup are obtained from LASER[20] calculations.

The effective U-238 temperature for resonance absorption is obtained from the radial temperature distribution by applying a radially dependent weighting function. The weighting function was determined from REPAD[21] Monte Carlo calculations of resonance escape probabilities in several steady state and transient temperature distributions. In each case, a flat pellet temperature was determined which produced the same resonance escape probability as the actual distribution. The weighting function was empirically determined from these results.

The effective Pu-240 temperature for resonance absorption is determined by a convolution of the radial distribution of Pu-240 number densities from LASER burnup calculations and the radial weighting function. The resulting temperature is burnup dependent, but the difference between U-238 and Pu-240 temperatures, in terms of reactivity effects, is small.

The effective pellet temperature for pellet dimensional change is that value which produces the same outer pellet radius in a virgin pellet as that obtained from the temperature model. The effective clad temperature for dimensional change is its average value.

The temperature calculational model has been validated by plant Doppler defect data as shown in Table 4.3-7 and Doppler coefficient data as shown in Figure 4.3-42. Stability index measurements also provide a sensitive measure of the Doppler coefficient near full power (See Section 4.3.2.8). It can be seen that Doppler defect data is typically within 0.2% of prediction.

### 4.3.3.2 Macroscopic Group Constants

Macroscopic few-group constants and consistent microscopic cross sections (needed for feedback and microscopic depletion calculations) are generated for fuel cells by ARK[34] or PHOENIX-P[39]. ARK is a point model cell homogenization, neutron spectrum isotopic depletion program which evolved from the codes LEOPARD[17] and CINDER[18]. Normally a simplified approximation of the main fuel chains is used. However, where needed, a complete solution for significant isotopes in the fuel chains, from Th-232 to Cm-244, is available[22]. Microscopic fast and thermal cross section data are taken for the most part from the ENDF/B[23] library, with a few exceptions where other data provided better agreement with critical experiments, isotopic measurements, and plant critical boron values. The effect on the unit fuel cell of non-lattice components in the fuel assembly is obtained by supplying an appropriate volume fraction of these materials in an extra region, which is homogenized with the unit cell in the fast (MUFT) and thermal (SOFOCATE) flux calculations. In the thermal calculation, the fuel rod, clad, and moderator are homogenized by energy-dependent disadvantage factors derived from an analytical fit to integral transport theory results. Group constants for discrete burnable absorber cells, guide thimbles, instrument thimbles and interassembly gaps are generated in a manner analogous to the fuel cell calculation. Integral fuel burnable absorbers, if present, are modeled as a component of the fuel cladding. Reflector group constants are taken from infinite medium LEOPARD calculations. Baffle group constants are calculated from an average of core and radial reflector microscopic group constants for stainless steel.

Group constants for control rods are calculated in a linked version of the HAMMER[24] and AIM[25] codes to provide an improved treatment of self shielding in the broad resonance structure of these isotopes at epithermal energies relative to that available in LEOPARD.

Validation of the cross section method is based on analysis of critical experiments isotopic data as shown in Table 4.3-8, plant critical boron (CB) values at HZP, BOL, as shown in Table 4.3-9 and at HFP as a function of burnup as shown in Figures 4.3-43 through 4.3-45. Control rod worth measurements are shown in Table 4.3-10.

Confirmatory critical experiments on burnable absorbers are described in reference [26].

PHOENIX-P has been approved by the USNRC as an alternative to ARK and its related codes for the generation of macroscopic and microscopic few group cross sections for PWR analysis [39]. PHOENIX-P is a two-dimensional, multigroup, transport-based lattice code capable of providing all necessary data for PWR analysis.

PHOENIX-P employs a 42 energy group library derived mainly from the ENDF/B-VI files. This library was designed to capture the integral properties of the multigroup data properly during group collapse and to model important resonance parameters properly. It contains all neutronics data necessary for modelling fuel, fission products, cladding and structural materials, coolant, and control and burnable absorber materials present in PWRs.

Group constants for burnable absorber cells, control rod cells, guide thimbles and instrumentation thimbles, or other non-fuel cells, can be obtained directly from PHOENIX-P without any adjustments such as those required in the cell or 1D lattice codes.

### 4.3.3.3 Spatial Few-Group Diffusion Calculations

Spatial few-group diffusion calculations consist primarily of two-group X-Y calculations using an updated version of the TURTLE code, two-group, 2 or 3 dimensional calculations using

PALADON or ANC, two-group axial calculations using APOLLO, an advanced version of the PANDA code, and THURTLE[35], a three dimensional version of TURTLE.

Discrete X-Y calculations (1 mesh per cell) are carried out to determine critical boron concentrations and power distributions in the X-Y plane. An axial average in the X-Y plane is obtained by synthesis from unrodded and rodded planes or by three dimensional nodal calculations.

The moderator coefficient is evaluated by varying the inlet temperature in the same X-Y calculations used for power distribution and reactivity predictions.

Validation of the reactivity calculations is associated with the validation of the group constants themselves, as discussed in Section 4.3.3.2. Validation of the Doppler calculations is associated with the fuel temperature validation discussed in Section 4.3.3.1. Validation of the moderator coefficient calculations is obtained by comparison with plant measurements at hot zero power conditions as shown in Table 4.3-11.

Axial calculations are used to determine differential control rod worth curves (reactivity versus rod insertion) and axial power shapes during steady state and transient xenon conditions (flyspeck curve). Group constants are obtained from the three-dimensional nodal model by flux-volume weighting for each axial slice. Radial bucklings are determined by varying parameters in the buckling model while forcing the one dimensional model to reproduce the axial characteristics (axial offset, midplane power) of the three dimensional model.

Validation of the spatial codes for calculating power distributions involves the use of incore and excore detectors and is discussed in Section 4.3.2.2.7.

Based on comparison with measured data it is estimated that the accuracy of current analytical methods is:

± 0.2% Δρ for doppler defect

± 2 pcm/°F for moderator coefficient

± 50 ppm for critical boron concentration with depletion

± 3% for power distributions

± 0.2% Δρ for rod bank worth

± 4 pcm/step for differential rod worth

± 0.5 pcm/ppm for boron worth

± 0.1% Δρ for moderator defect

## REFERENCES

*(1)* "Westinghouse Anticipated Transients Without Reactor Trip Analysis," WCAP-8330, August, 1974.

*(2)* Spier, E. M., "Evaluation of Nuclear Hot Channel Factor Uncertainties," WCAP-7308-L-P, June 1988.

*(3)* McFarlane, A. F., "Core Power Capability In Westinghouse PWRs," WCAP-7267-L (Proprietary), October 1969 and WCAP-7809 (Non-Proprietary), December 1971.

*(4)* Hellman, J. M. (Ed), "Fuel Densification Experimental Results and Model for Reactor Application," WCAP-8218-P-A (Proprietary), March 1975 and WCAP-8219-A (Non-Proprietary), March 1975.

*(5)* Hellman, J. M., Olson, C. A., and Yang, J. W., "Effects of Fuel Densification Power Spikes on Clad Thermal Transients," WCAP-8359, July 1974.

*(6)* "Power Distribution Control of Westinghouse Pressurized Water Reactors," WCAP-7208 (Proprietary), September 1968 and WCAP-7811 (Non-Proprietary), December 1971.

*(7)* Morita, T., et al., "Power Distribution Control and Load Following Procedures," WCAP-8385 (Proprietary), September 1974 and WCAP-8403 (Non-Proprietary), September 1974.

*(8)* McFarlane, A. F., "Power Peaking Factors," WCAP-7912-P-A (Proprietary), January 1975 and WCAP-7912-A (Non-Proprietary), January 1975.

*(9)* Altomare, S. and Barry, R. F., "The TURTLE 24.0 Diffusion Depletion Code," WCAP-7213-P-A (Proprietary), February 1975 and WCAP-7758-A (Non-Proprietary), February 1975.

*(10)* Cermak, J. O., et al, "Pressurized Water Reactor pH-Reactivity Effect Final Report," WCAP-3696-8 (EURAEC-2074), October 1968.

*(11)* Not used.

*(12)* Poncelet, C. G., and Christie, A. M., "Xenon-Induced Spatial Instabilities in Large PWRs," WCAP-3680-20 (EURAEC-1974), March 1968.

*(13)* Skogen, F. B. and McFarlane, A. F., "Control Procedures for Xenon-Induced X-Y Instabilities in Large PWRs," WCAP-3680-21 (EURAEC-2111), February 1969.

*(14)* Skogen, F. B. and McFarlane, A. F., "Xenon-Induced Spatial Instabilities In Three-Dimensions," WCAP-3680-22 (EURAEC-2116), September 1969.

*(15)* Lee, J. C., "Axial Xenon Transient Tests at the Rochester Gas and Electric Reactor," WCAP-7964, June 1971.

*(16)* Barry, R. F., and Minton, F., "The PANDA Code," WCAP-7048-P-A (Proprietary) and WCAP-7757-A (Non-Proprietary), January 1975.

*(17)* Deleted by Amendment 92

*(18)* England, T. R., "CINDER - A One-Point Depletion and Fission Product Program," WAPD-TM-334, August 1962.

*(19)* Eggleston, F. T., "Safety Related Research and Development for Westinghouse Pressurized Water Reactors, Program Summaries," WCAP-8485, March 1975.

*(20)* Poncelet, C. G., "LASER - A Depletion Program for Lattice Calculations Based on MUFT and THERMOS," WCAP-6073, April 1966.

*(21)* Olhoeft, J. E., "The Doppler Effect for a Non-Uniform Temperature Distribution in Reactor Fuel Elements," WCAP-2048, July 1962.

*(22)* Nodvik, R. J., "Supplementary Report On Evaluation of Mass Spectrometric and Radiochemical Analyses of Yankee Core I Spent Fuel, Including Isotopes of elements Thorium Through Curium," WCAP-6086, August 1969.

*(23)* Drake, M. K. (Ed), "Data Formats and Procedure for the ENDF/B Neutron Cross Section Library," BNL-50274, ENDF-102, Vol. I, 1970.

*(24)* Suich, J. E., and Honeck, H. C., "The HAMMER System, Heterogeneous Analysis by Multigroup Methods of Exponentials and Reactors," DP-1064, January 1967.

*(25)* Flatt, H. P., and Buller, D. C., "AIM-5, A Multigroup, One Dimensional Diffusion Equation Code," NAA-SR-4694, March 1960.

*(26)* "Nuclear Design of Westinghouse Pressurized Water Reactors with Burnable Poison Rods," WCAP-7806 (Non-Proprietary), December 1971.

*(27)* Camden, T. M., et al, "PALADON - Westinghouse Nodal Computer Code," WCAP-9485 (Non-proprietary) and WCAP-9486 (Proprietary), December 1978.

*(28)* Nodvik, R. J., "Saxton Core II Fuel Performance Evaluation," WCAP-3385-56, Part II, "Evaluation of Mass Spectrometric and Radiochemical Analyses of Irradiated Saxton Plutonium Fuel," July 1970.

*(29)* Leamer, R. D., et al, "$PUO_2$ -$UO_2$ Fueled Critical", WCAP-3726-1, July 1967.

*(30)* Meyers, R. O., "The Analysis of Fuel Densification", Division of Systems Safety, USNRC, NUREG 0085, July 1976.

*(31)* Deleted by Amendment 92

*(32)* Deleted by Amendment 92

*(33)* Deleted by Amendment 73

*(34)* Raymond, M., et al., "ARK(C) - A Spectrum-Dependent Neutron Flux, Reactivity and Fuel Depletion Program For PWR Lattice Cells," WCAP-9523, August 1979.

*(35)* Beard, C. L., and Steitler, R. W., "THURTLE - Multidimensional Neutron Diffusion Theory Code," WCAP-8344, June 1974 (Westinghouse Proprietary).

*(36)* Henderson, W. B., "Results of the Control Rod Worth Program," WCAP-9217, October 1977.

*(37)* Miller, R. W., Pogorzelski, N. A., Vestovich, J. A., "Relaxation of Constant Axial Offset Control $F_Q$ Surveillance Technical Specification," WCAP-10216, August 1982.

*(38)* Liu, Y. S., et al., "ANC: A Westinghouse Advanced Nodal Code," WCAP-10965-P-A (Westinghouse Proprietary), December 1985.

*(39)* Nguyen, T. Q., et al., "Qualification of the PHOENIX-P/ANC Nuclear Design System for Pressurized Water Reactor Cores," WCAP-11596, November 1987.

*(40)* Deleted by Amendment 92

*(41)* Holtec International Report HI-961513, Revision 2, “Evaluation Of The Spent Fuel Storage Racks For The Watts Bar Nuclear Plant, “ October 1996.

*(42)* Holtec International Report HI-2012620, Revision 0, “Evaluation of the Effect of the Use of Tritium Producing Burnable Absorber Rods (TPBARs) on Fuel Storage Requirements,” January 2002

*(43)* NUREG/CR-0200, “Scale: A Modular Code System for Performing Standardized Computer Analyses for Licensing Evaluation,” (SCALE 3.1 version).

*(44)* NUREG/CR-200 (SCALE 4.3 Package), “NITAWL-S: Scale System Module for Performing Resonance Shielding and Working Library Production,” 1995.

*(45)* NUREG/V-0200 (SCALE 4.3 Package), “KENO 5a. An Improved Monte Carlo Criticality Program with Supergrouping,” 1995.

*(46)* CAM-009-UG, “CASMO-3: A Fuel Assembly Burnup Program - User’s Manual,” Revision 1, Malte Edenius, Ake Ahlin, Bengt H. Forssen, Studsvik/NFA-86/7.

*(47)* AE-RF-76-4158, Studsvik Report, “CASMO - A Fuel Assembly Burnup Program”.

*(48)* “CASMO - A Fast Transport Theory Depletion Code for LWR Analysis,” ANS Transactions, Vol 26, p. 604, 1977.

*(49)* CASMO-3, A Fuel Assembly Burnup Program, Users Manual, Studsvik/NFA-87/7, November 1986.

*(50)* WCAP - 10444-P-A, Addendum 2-A, "VANTAGE 5H Fuel Assembly," April 1988.

*(51)* Deleted by Amendent 92

*(52)* BAW-1484-7, M.N. Baldwin, G.S. Hoover, R.L. Eng, F.G. Welfare, "Critical Experiments Supporting Close Proximity Water Storage of Power Reactor Fuel," July 1979.

*(53)* PNL-2438, S.R.Bierman, B.M. Durst, E.D. Clayton, "Critical Separation Between Subcritical Clusters of 2.35 wt% U-235 Enriched $UO_2$ Rods in Water With Fixed Neutron Poisons," October 1977.

*(54)* PNL-2615, S.R. Bierman, B.M. Durst, E.D. Clayton, "Critical Separation Between Subcritical Clusters of 4.29 wt% U-235 Enriched $UO_2$ Rids ub Water With Fixed Neutron Poisons," NUREG/CR-0073, May 1978.

*(55)* Holtec International Report HI-91670, "Spent Fuel Pool Modification For Increased Storage Capacity," January 1993.

*(56)* VANTAGE + Fuel Assembly Reference Core Report," Westinghouse Electric Corporation, WCAP-12610-P-A, April 1995.

**Table 4.3-1 Reactor Core Description**
**(First Cycle)**
**(Page 1 of 2)**

| | |
|---|---|
| **Active Core** | |
| Equivalent Diameter, in | 132.7 |
| Active Fuel Height, in | 143.7 |
| Height-to-Diameter Ratio | 1.09 |
| Total Cross-Section Area, $ft^2$ | 96.06 |
| $H_2O/U$ Molecular Ratio, lattice (Cold) | 2.41 |
| **Reflector Thickness and Composition** | |
| Top - Water plus Steel, in | ~10 |
| Bottom - Water plus Steel, in | ~10 |
| Side - Water plus Steel, in | ~15 |
| **Fuel Assemblies** | |
| Number | 193 |
| Rod Array | 17 x 17 |
| Rods per assembly | 264 |
| Rod Pitch, in | 0.496 |
| Overall Transverse Dimensions, in | 8.426 x 8.426 |
| Fuel Weight (as $UO_2$), lb | 222,645 |
| Zircaloy Weight, lb | 53,000 |
| Number of Grids per Assembly | 8 |
| Composition of Grids | Inconel-718, Zircaloy 4 |
| Weight of Grids, lb | 3100 |
| Number of Guide Thimbles per Assembly | 24 |
| Composition of Guide Thimbles | Zircaloy 4 |
| Diameter of Guide Thimbles (upper part), in | 0.442 I.D. x 0.474 O.D. |
| Diameter of Guide Thimbles (lower part), in | 0.397 I.D. x 0.430 O.D. |
| Diameter of Instrument Guide Thimbles, in | 0.440 I.D. x 0.476 O.D. |
| **Fuel Rods** | |
| Number | 50,952 |
| Outside Diameter, in | 0.374 |
| Diameter Gap, in | 0.0065 |
| Clad Thickness | 0.0225 |
| Clad Material | Zircaloy-4 |

**Table 4.3-1 Reactor Core Description**
**(First Cycle)**
**(Page 2 of 2)**

| | |
|---|---|
| **Fuel Pellets** | |
| Material | $UO_2$ Sintered |
| Density (percent of Theoretical) | 94.5 |
| Fuel Enrichments, wt. % | |
| Region 1 | 2.10 |
| Region 2 | 2.60 |
| Region 3 | 3.10 |
| Diameter, in | 0.3225 |
| Length, in | 0.530 |
| Mass of $UO_2$ per Foot of Fuel Rod, lb/ft | 0.364 |
| **Rod Cluster Control Assemblies** | |
| Neutron Absorber | Ag-In-Cd $B_4C$ |
| Composition | 80%, 15%, 5% 100% |
| Diameter, in | 0.301 0.294 |
| Density, $lb/in^3$ | 0.367 0.0637 |
| Cladding Material | Type 304, Cold Worked Stainless Steel |
| Clad Thickness, in | 0.0385 0.0385 |
| Number of Clusters | |
| Full Length | 57 |
| Number of Absorber Rods per Cluster | 24 |
| Full Length Assembly Weight (dry) nominal, lb | 93 |
| **Burnable Poison Rods (First Core)** | |
| Number | 1708 |
| Material | Borosilicate Glass |
| Outside Diameter, in | 0.381 |
| Inner Tube, O.D., in | 0.181 |
| Clad Material | Stainless Steel |
| Inner Tube Material | Stainless Steel |
| Boron Loading (wt. % $B_2O_3$ in glass rod) | 12.5 |
| Weight of Boron-10 per foot of rod, lb/ft | 0.000419 |
| Initial Reactivity Worth, % $\Delta\rho$ | $\approx$ 8.59 (hot), $\approx$ 6.19 (cold) |
| **Excess Reactivity** | |
| Maximum Fuel Assembly k (Cold, Clean, Unborated Water) | 1.40 |
| Maximum Core Reactivity (Cold, Zero Power, Beginning of Cycle, Zero Soluble Boron) | 1.213 |

**Table 4.3-2 Nuclear Design Parameters (First Cycle)**
**(Page 1 of 2)**

| | | |
|---|---|---|
| **Core Average Linear Power, kW/ft, including densification effects** | | 5.45 |
| **Total Heat Flux Hot Channel Factor, $F_Q$** | | 2.40 |
| **Nuclear Enthalpy Rise Hot Channel Factor, $F^N_{\Delta H}$** | | 1.55 |
| **Reactivity Coefficients+** | **Design Limits** | **Best Estimates** |
| Doppler-only Power, Lower Curve Coefficients, pcm/% power++ | -19.4 to -12.6 | -16.5 to -9.3 |
| (See Figure 15.1-5), Upper Curve | -10.2 to -6.7 | -15.3 to -8.4 |
| Doppler Temperature coefficient pcm/°F++ | - 2.9 to -1.0 | -2.1 to -1.4 |
| Moderator Temperature Coefficient pcm/°F++ | 0 to -40 | 0.0 to -33.6 |
| Boron Coefficient, pcm/ppm++ | -16.0 to -6.0 | -12.2 to -8.5 |
| Rodded Moderator Density Coefficient, pcm/gm/cc++ | $\leq 0.43 \times 10^5$ | $\leq 0.34 \times 10^5$ |

\+ Uncertainties are given in Section 4.3.3.3

++ Note: 1 pcm = (percent mille) $10^{-5}$ Δρ, where Δρ is calculated from two statepoint values of $k_{eff}$ by $1n(K_2/K_1)$.

**Table 4.3-2 Nuclear Design Parameters (First Cycle)**
**(Page 2 of 2)**

| | | |
|---|---|---|
| **Control Rod Worths** | | |
| Rod Requirements | | See Table 4.3-3 |
| Maximum Bank Worth, pcm | | < 2000 |
| Maximum Ejected Rod Worth | | See Chapter 15 |
| Bank Worth, pcm++ | HZP, BOL, Xe free | HZP, EOL Eq, Xe |
| Bank D | 1417 | 1404 |
| Bank C | 1187 | 1204 |
| Bank B | 1573 | 1314 |
| Bank A | 1156 | 1128 |
| **Radial Factor (BOL to EOL)** | | |
| Unrodded | | 1.38 to 1.23 |
| D bank | | 1.55 to 1.36 |
| **Boron Concentrations (Beginning of Cycle)** | | |
| Zero Power, $k_{eff}$ = 0.99, Cold, Rod Cluster Control Assemblies Out | | 1407 |
| Zero Power, $k_{eff}$ = 0.99, Hot, Rod Cluster Control Assemblies Out | | 1416 |
| Design Basis Refueling Boron Concentration | | 2000 |
| Zero Power,$k_{eff} \leq 0.95$, Cold, Rod Cluster Control Assemblies In | | 1136 |
| Zero Power, $k_{eff}$ = 1.00, Hot, Rod Cluster Control Assemblies Out | | 1314 |
| Full Power, No xenon, $k_{eff}$ = 1.0, Hot, Rod Cluster Control Assemblies Out | | 1186 |
| Full Power, Equilibrium Xenon, $k_{eff}$ = 1.0, Hot Rod Cluster Control Assemblies Out | | 869 |
| Reduction with Fuel Burnup First Cycle, ppm/GWD/MTU** | | See Figure 4.3-3 |

** Gigawatt Day (GWD) = 1000 Megawatt Day (1000 MWD)

## Table 4.3-3 Reactivity Requirements for Rod Cluster Control Assemblies

| Reactivity Effects, percent | Beginning of Life (first Cycle) | End of Life (first Cycle) | End of Life (Equilibrium Cycle) |
|---|---|---|---|
| 1. Control requirements | | | |
| Fuel temperature (Doppler), % Δρ | 1.23 | 1.13 | 1.10 |
| Moderator temperature*, % Δρ | 0.44 | 1.05 | 1.40 |
| Redistribution, % Δρ | 0.50 | 0.95 | 0.97 |
| Rod Insertion Allowance, % Δρ | 1.40 | 0.60 | 0.70 |
| Cooldown to 537°F | 0.54 | 0.54 | 0.54 |
| 2. Total Control, % Δρ | 4.11 | 4.27 | 4.71 |
| 3. Estimated Rod Cluster Control Assembly Worth (57 Rods) | | | |
| a.All full length assemblies inserted, % Δρ | 9.97 | 9.31 | 8.50 |
| b.All but one (highest worth) assembly inserted, % Δρ | 8.36 | 8.05 | 7.30 |
| 4. Estimated Rod Cluster Control Assembly credit with 10 percent adjustment to accommodate uncertainties (3b - 10 percent), % Δρ | 7.52 | 7.24 | 6.57 |
| 5. Shutdown margin available (4-2), % Δρ | 3.41 | 2.98 | 1.86** |

* Includes void effects

** The design basis minimum shutdown is 1.6%

**Table 4.3-4 Deleted by Amendment 40**

**Table 4.3-5 Axial Stability Index For A Pressurized Water Reactor Core With A 12 Foot Active Core Height**

| Burnup (MWD/T) | $F_Z$ | $C_B$ (ppm) | Stability Index ($hr^{-1}$) Exp | Calc |
|---|---|---|---|---|
| 1550 | 1.34 | 1065 | -0.041 | -0.032 |
| 7700 | 1.27 | 700 | -0.014 | -0.006 |
| | | Difference: | +0.027 | +0.026 |

**Table 4.3-6 Typical Neutron Flux Levels (N/Cm$^2$-Sec) At Full Power**

| | E > 1.0 MeV | 0.111 MeV < E < 1.0 MeV | 0.3 eV < E < 0.111 MeV | E < 0.3 eV |
|---|---|---|---|---|
| Core Center | $9.98 \times 10^{13}$ | $1.11 \times 10^{14}$ | $2.17 \times 10^{14}$ | $5.36 \times 10^{13}$ |
| Core Outer Radius at Mid-Height | $4.24 \times 10^{13}$ | $4.85 \times 10^{13}$ | $9.52 \times 10^{13}$ | $2.21\ 10^{13}$ |
| Core Top, on Axis | $2.62 \times 10^{13}$ | $2.13 \times 10^{13}$ | $1.31 \times 10^{14}$ | $4.35 \times 10^{13}$ |
| Core Bottom, on Axis | $2.70 \times 10^{13}$ | $2.25 \times 10^{13}$ | $1.33 \times 10^{14}$ | $4.74 \times 10^{13}$ |
| Pressure Vessel Inner Diameter Azimuthal Peak, Core Mid-Height | $2.08 \times 10^{10}$ | $2.83 \times 10^{10}$ | $6.18 \times 10^{10}$ | $1.20 \times 10^{11}$ |

**Table 4.3-7 Comparison Of Measured And Calculated Doppler Defects**

| Plant | Fuel Type | Core Burnup (MWD/MTU) | Measured (pcm)* | Calculated (pcm) |
|---|---|---|---|---|
| 1 | Air-filled | 1800 | 1700 | 1710 |
| 2 | Air-filled | 7700 | 1300 | 1440 |
| 3 | Air and helium-filled | 8460 | 1200 | 1210 |

*pcm = $10^5$ x 1n ($k_2/k_1$)

**Table 4.3-8 Saxton Core II Isotopics**
**Rod My, Axial Zone 6**

| Atom Ratio | Measured* | 2σ Precision (%) | LEOPARD Calculation |
|---|---|---|---|
| U-234/U | $4.65 \times 10^{-5}$ | ± 29 | $4.60 \times 10^{-5}$ |
| U-235/U | $5.74 \times 10^{-3}$ | ± 0.9 | $5.73 \times 10^{-3}$ |
| U-236/U | $3.55 \times 10^{-4}$ | ± 5.6 | $3.74 \times 10^{-4}$ |
| U-238/U | 0.99386 | ± 0.01 | 0.99385 |
| Pu-238/Pu | $1.32 \times 10^{-3}$ | ± 2.3 | $1.222 \times 10^{-3}$ |
| Pu-239/Pu | 0.73971 | ±0.03 | 0.74497 |
| Pu-240/Pu | 0.19302 | ± 0.2 | 0.19102 |
| Pu-241/Pu | $6.014 \times 10^{-2}$ | ± 0.3 | $5.74 \times 10^{-2}$ |
| Pu-242/Pu | $5.81 \times 10^{-3}$ | ± 0.9 | $5.38 \times 10^{-3}$ |
| Pu/U** | $5.938 \times 10^{-2}$ | ± 0.7 | $5.970 \times 10^{-2}$ |
| Np-237/U-238 | $1.14 \times 10^{-4}$ | ± 15 | $0.86 \times 10^{-2}$ |
| Am-241/Pu-239 | $1.23 \times 10^{-2}$ | ± 15 | $1.11 \times 10^{-4}$ |
| Cm-242/Pu-239 | $1.05 \times 10^{-4}$ | ± 10 | $1.11 \times 10^{-4}$ |
| Cm-244/Pu-239 | $1.09 \times 10^{-4}$ | ± 20 | $0.98 \times 10^{-4}$ |

* Reported in Reference [28]

** Weight Ratio

**Table 4.3-9 Critical Boron Concentrations, HZP, BOL**

| Plant Type | Measured (ppm) | Calculated (ppm) |
|---|---|---|
| 2-Loop, 121 Assemblies 10 foot core | 1583 | 1589 |
| 2-Loop, 121 Assemblies 12 foot core | 1625 | 1624 |
| 2-Loop, 121 Assemblies 12 foot core | 1517 | 1517 |
| 3-Loop, 157 Assemblies 12 foot core | 1169 | 1161 |
| 3-Loop, 157 Assemblies 12 foot core | 1344 | 1319 |
| 4-Loop, 193 Assemblies 12 foot core | 1370 | 1355 |
| 4-Loop, 193 Assemblies 12 foot core | 1321 | 1306 |

**Table 4.3-10 Comparison of Measured and Calculated Rod Worth**

| 2-Loop Plant, 121 Assemblies, 10 foot core | Measured (pcm) | Calculated (pcm) |
|---|---|---|
| Group B | 1885 | 1893 |
| Group A | 1530 | 1649 |
| Shutdown Group | 3050 | 2917 |
| ESADA Critical*, 0.69" Pitch, 2 wt.% $PuO_2$, 8% $Pu^{240}$, 9 Control Rods | | |
| 6.21" rod separation | 2250 | 2250 |
| 2.07" rod separation | 4220 | 4160 |
| 1.38" rod separation | 4100 | 4010 |

* Reported in Reference [26]

**Table 4.3-11 Comparison of Measured and Calculated Moderator Coefficients at HZP, BOL**

| Plant Type/ Control Bank Configuration | Measured $\alpha_{iso}$* (pcm/°F) | Calculated $\alpha_{iso}$* (pcm/°F) |
|---|---|---|
| 3-Loop, 157 Assemblies 12 foot core | | |
| D at 160 steps | -0.50 | -0.05 |
| D in, C at 190 steps | -3.01 | -2.75 |
| D in, C at 28 steps | -7.67 | -7.02 |
| B, C, and D in | -5.16 | -4.45 |
| 2-Loop, 121 Asssemblies, 12 foot core | | |
| D at 180 steps | +0.85 | +1.02 |
| D in, C at 180 steps | -2.40 | -1.90 |
| C and D in, B at 165 steps | -4.40 | -5.58 |
| B, C, and D in, A at 174 steps | -8.70 | -8.12 |
| 4-Loop, 193 Assemblies 12 foot core | | |
| ARO | -0.52 | -1.2 |
| D in | -4.35 | -5.7 |
| D and C in | -8.59 | -10.0 |
| D, C and B in | -10.14 | -10.55 |
| D, C, B and A in | -14.63 | -14.45 |

* Isothermal coefficients, which include the Doppler effect in the fuel;

$$\alpha_{iso} = 10^5 \ln \frac{k_2}{k_1} / \Delta T^{\circ} F$$

## Table 4.3-12 Watts Bar Spent Fuel Storage Rack Design Basis Fuel Assembly Specifications

**Fuel Rod Data**

| | |
|---|---|
| Outside diameter, in. | 0.374 |
| Cladding thickness, in. | 0.0225 |
| Cladding inside diameter, in. | 0.329 |
| Cladding material | Zr-4 |
| Pellet density, %T.D. | 97.0 |
| Stack density, g $UO_2$/cc | 10.631 |
| Pellet diameter, in. | 0.3225 |
| Maximum enrichment, wt% U-235 | 4.95 ± 0.05 |

**Fuel Assembly Data**

| | |
|---|---|
| Fuel rod array | 17x17 |
| Number of fuel rods | 264 |
| Fuel rod pitch, in. | 0.496 |
| Number of control rod guide and instrument thimbles | 25 |
| Thimble O.D., in. (nominal) | 0.474 |
| Thimble I.D., in. (nominal) | 0.442 |

**Table 4.3-13 Deleted by Amendment 92**

**Table 4.3-14 Deleted by Amendment 92**

**Table 4.3-15 Deleted By Amendment 92**

**Table 4.3-16 Deleted By Amendment 92**

THIS PAGE INTENTIONALLY BLANK

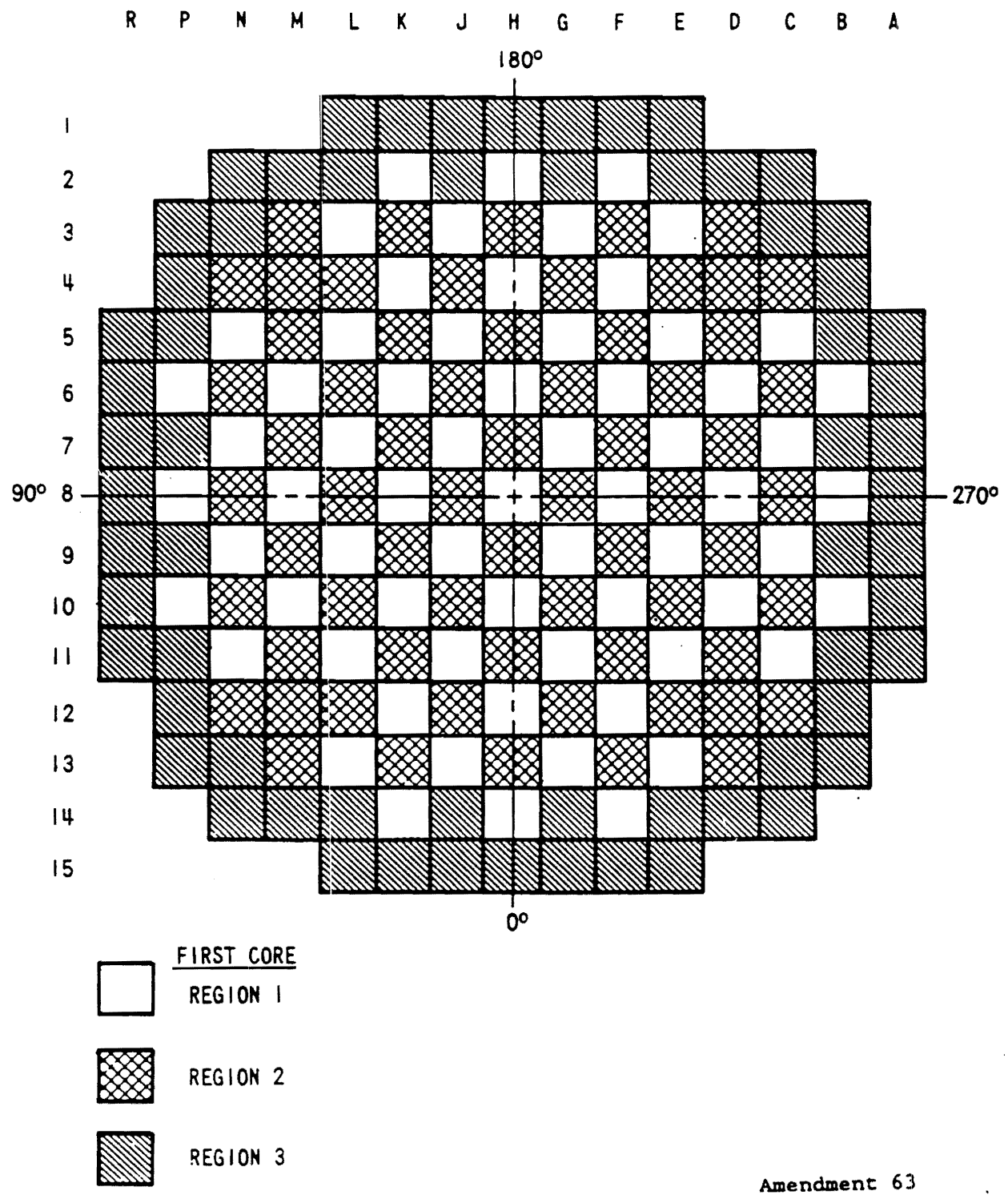


Figure 4.3-1. Fuel Loading Arrangement, Cycle 1

**Figure 4.3-1 Fuel Loading Arrangement, Cycle 1**

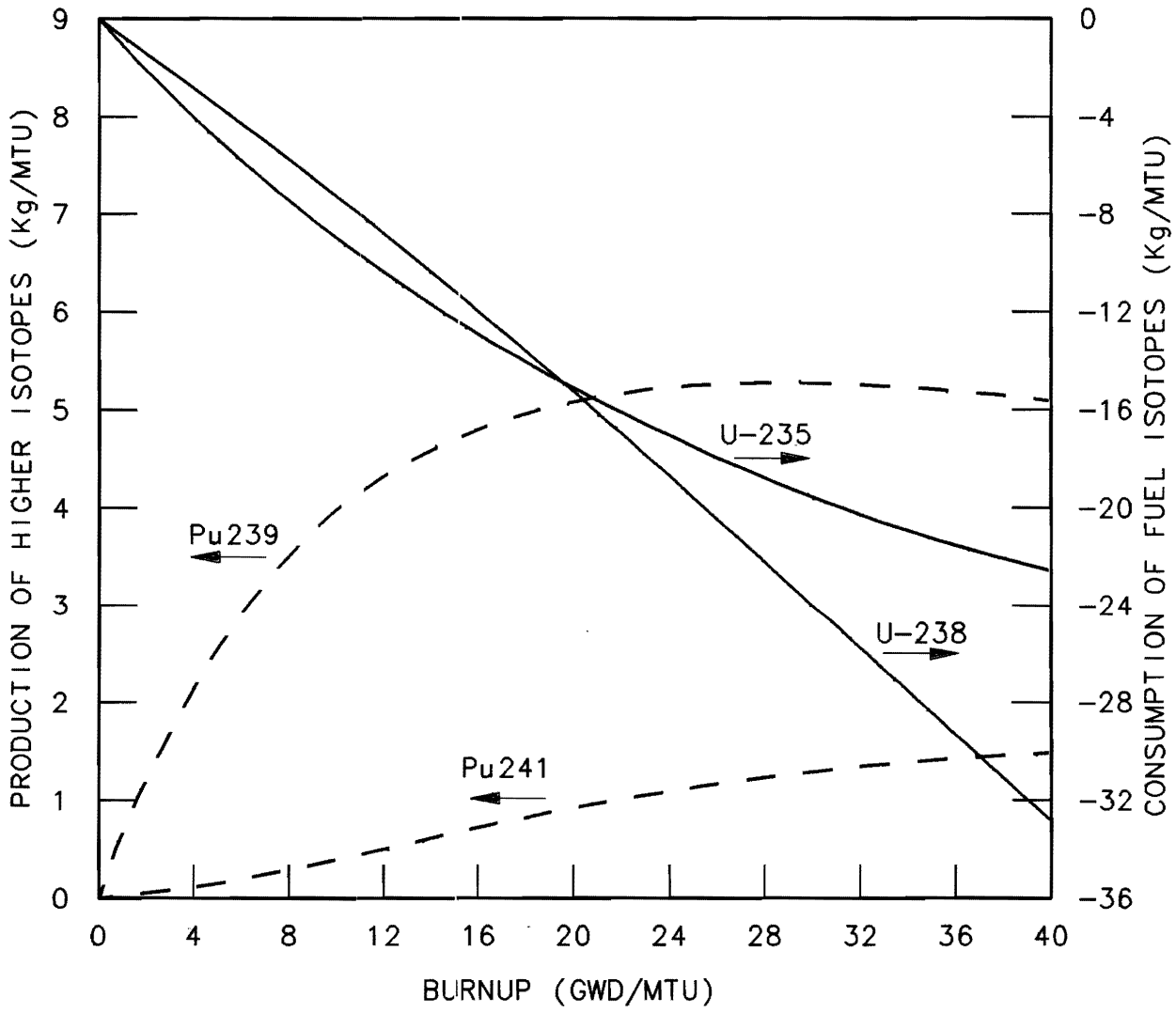


AMENDMENT 73

| WATTS BAR NUCLEAR PLANT FINAL SAFETY ANALYSIS REPORT |
|---|
| TYPICAL PRODUCTION AND CONSUMPTION OF HIGHER ISOTOPES |
| FIGURE 4.3-2 |

**Figure 4.3-2 Typical Production and Consumption of Higher Isotopes**

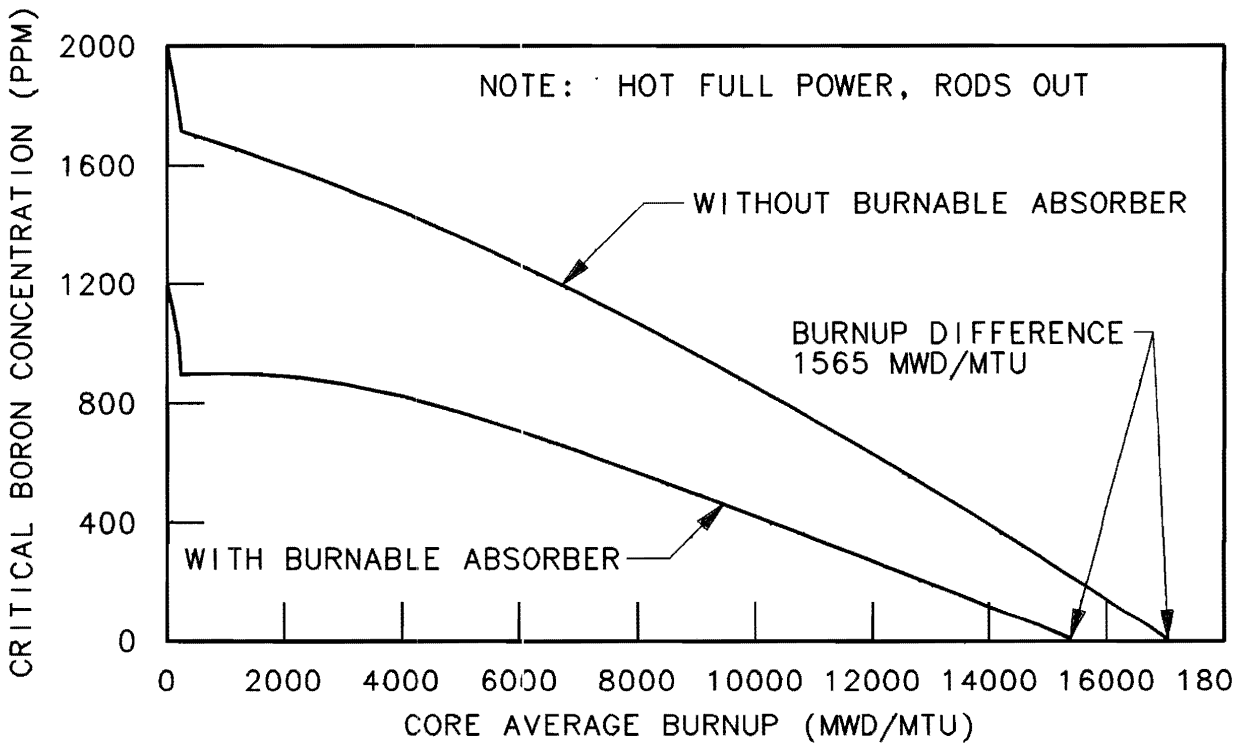


AMENDMENT 73

WATTS BAR NUCLEAR PLANT
FINAL SAFETY
ANALYSIS REPORT

TYPICAL BORON
CONCENTRATION VERSUS
FIRST CYCLE BURNUP WITH
AND WITHOUT BURNABLE
ABSORBER RODS

FIGURE 4.3-3

**Figure 4.3-3 Typical Boron Concentratioll versus First Cycle Burnup With and Without Burnable Absorber Rods.**

**Figure 4.3-4 Replaced By Figures 4.3-4a and 4.3-4b**

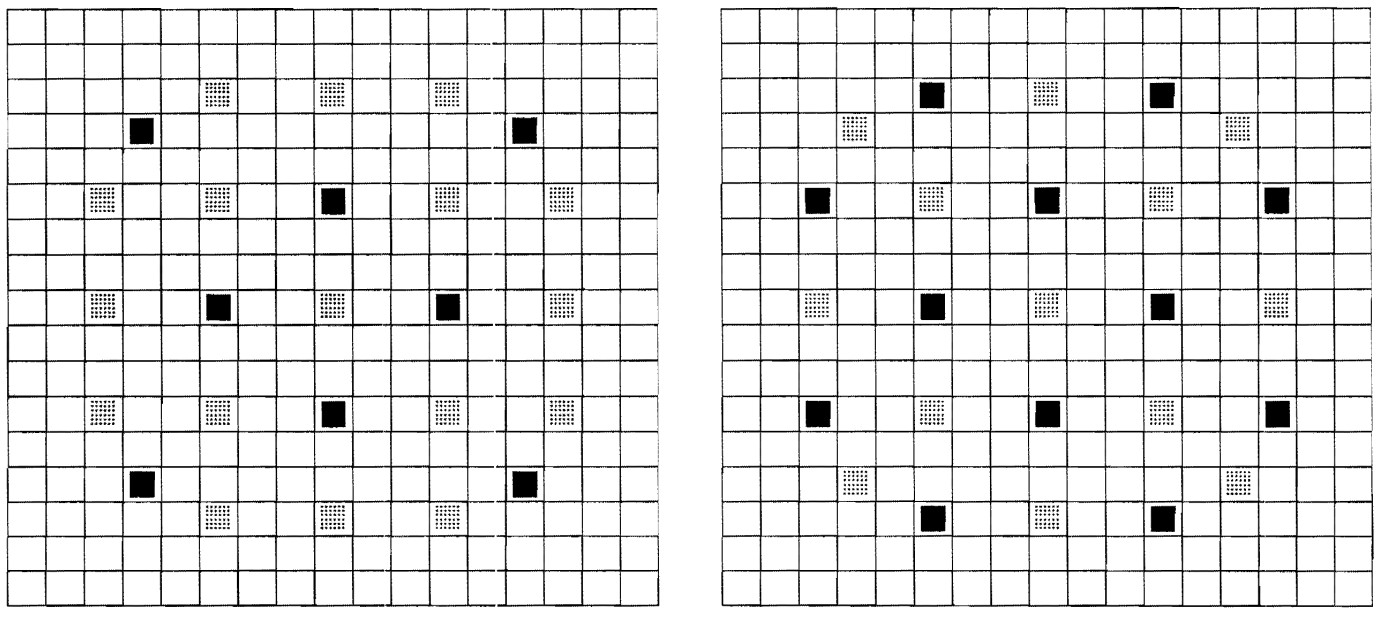


**Figure 4.3-4a Burnable Absorber Rod Arrangement within an Assembly, Cycle 1**

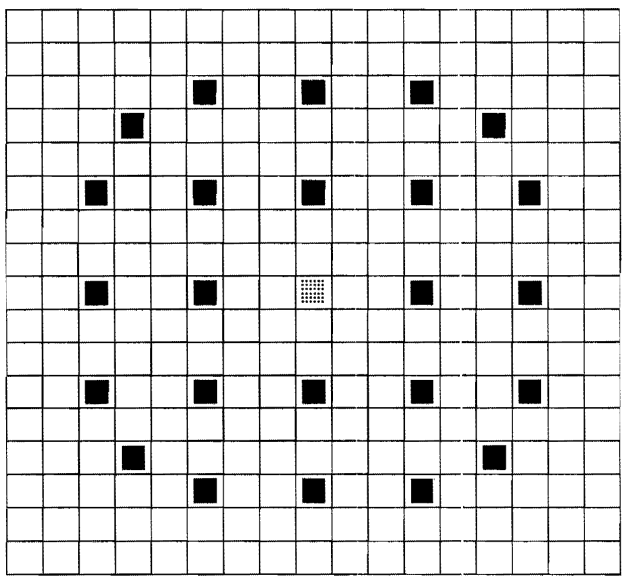

24 Burnable Absorber

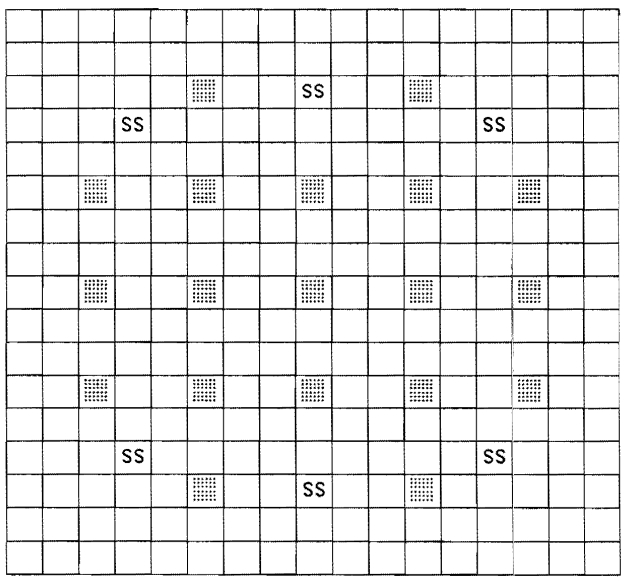


Secondary Source Assembly

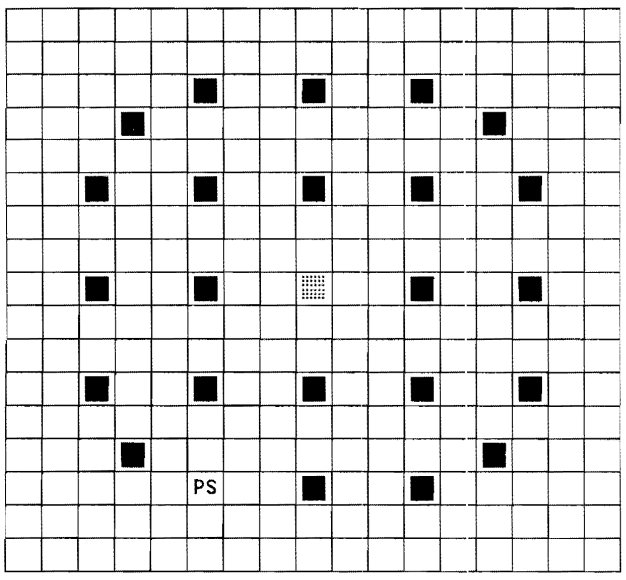


Primary Source Assembly

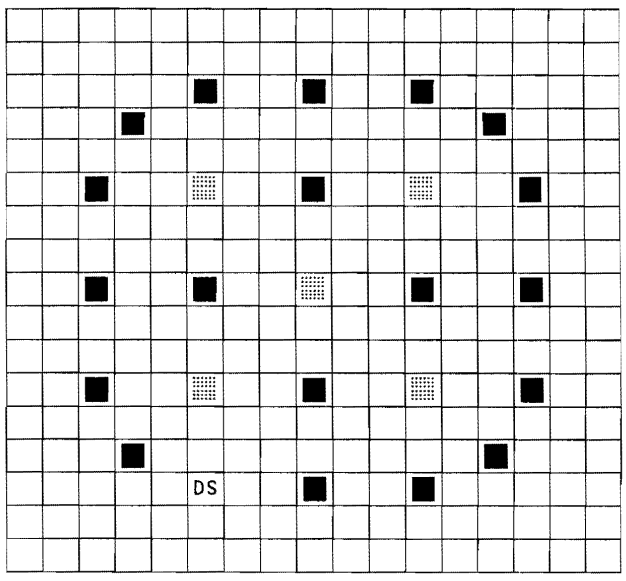


Depleted Primary Source Assembly

Amendment 73

| Legend |
|---|
| ⬚-Guide Tube or Instrument Tube |
| ■-Burnable Absorber Rod |
| SS-Secondary Source Rod |
| PS-Primary Source Rod |
| DS-Depleted Primary Source Rod |

| WATTS BAR<br>FINAL SAFETY ANALYSIS REPORT |
|---|
| BURNABLE ABSORBER ROD ARRANGEMENT WITHIN AN ASSEMBLY, CYCLE 1<br>FIGURE 4.3-4b |

**Figure 4.3-4b Burnable Absorber Rod Arrangement within an Assembly, Cycle 1**

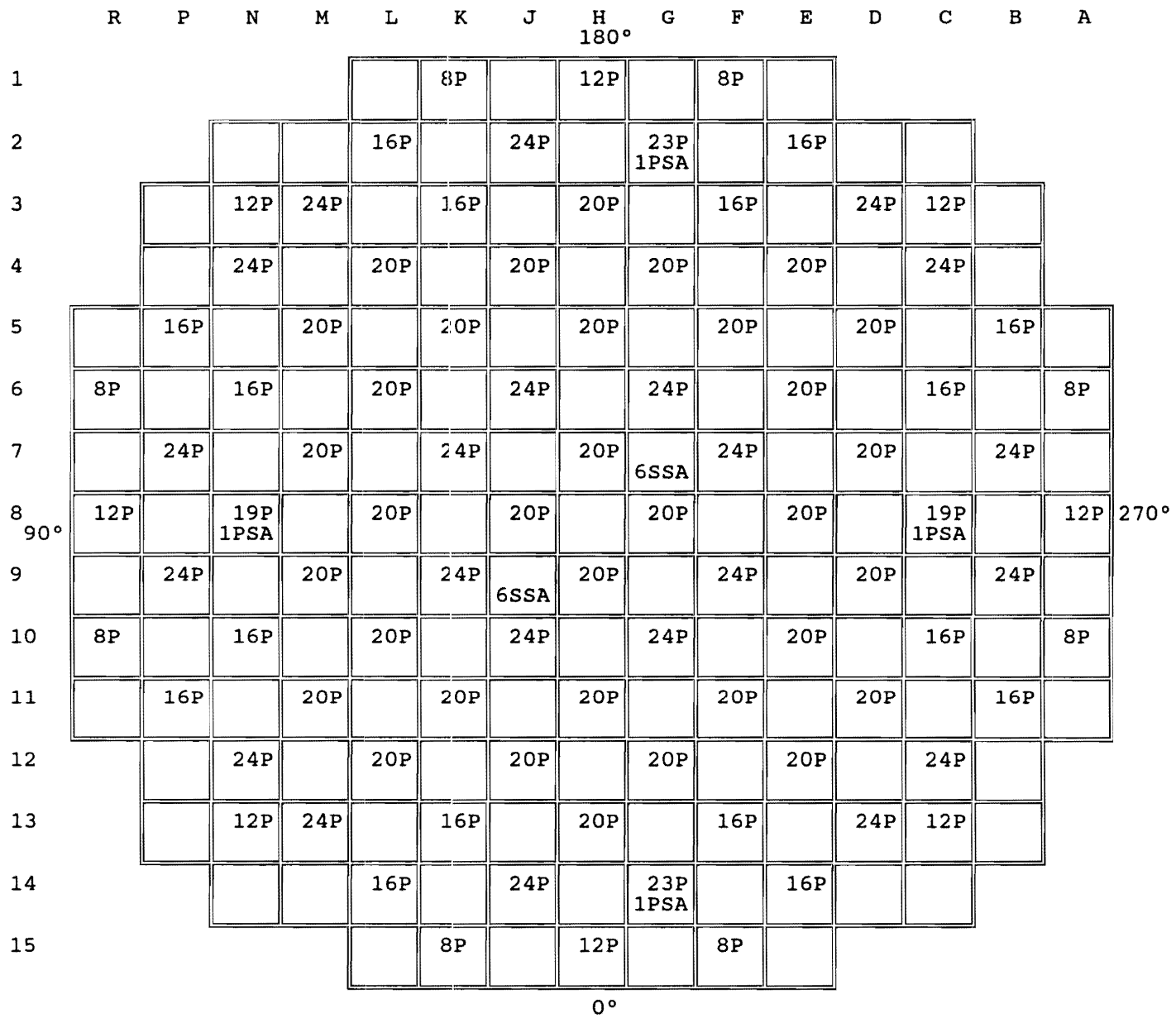


Amendment 73

| Legend |
|---|
| P-Burnable Absorber |
| SSA-Secondary Source Assembly |
| PSA-Primary Source Assembly |

| WATTS BAR FINAL SAFETY ANALYSIS REPORT |
|---|
| BURNABLE ABSORBER LOADING PATTERN, CYCLE 1 FIGURE 4.3-5 |

**Figure 4.3-5 Burnable Absorber Loading Pattern, Cycle 1**

| | H | G | F | E | D | C | B | A |
|---|---|---|---|---|---|---|---|---|
| 8 | 1.11 | | | | | | | |
| 9 | 1.02 | 1.10 | | | | | | |
| 10 | 1.10 | 0.97 | 1.13 | | | | | |
| 11 | 1.05 | 1.15 | 1.07 | 1.19 | | | | |
| 12 | 1.17 | 1.08 | 1.19 | 1.09 | 1.28 | | | |
| 13 | 1.06 | 1.16 | 1.13 | 1.13 | 0.88 | 0.88 | | |
| 14 | 1.05 | 1.02 | 1.06 | 0.99 | 0.88 | 0.58 | | |
| 15 | 0.75 | 0.85 | 0.75 | 0.61 | | | | |

CALCULATED FΔH = 1.40

Amendment 73

| LEGEND |
|---|
| VALUE REPRESENTS ASSEMBLY RELATIVE POWER |

| WATTS BAR<br>FINAL SAFETY ANALYSIS REPORT |
|---|
| NORMALIZED POWER DENSITY DISTRIBUTION AT BEGINNING OF LIFE, UNRODDED CORE, HOT FULL POWER, NO XENON FOR CYCLE 1<br>FIGURE 4.3-6 |

**Figure 4.3-6 Normalized Power Density Distribution at Beginning of Life, Unrodded Core, Hot Full Power, No Xenon for Cycle 1**

| | H | G | F | E | D | C | B | A |
|---|---|---|---|---|---|---|---|---|
| 8 | 1.15 | | | | | | | |
| 9 | 1.05 | 1.13 | | | | | | |
| 10 | 1.14 | 0.99 | 1.15 | | | | | |
| 11 | 1.07 | 1.17 | 1.09 | 1.20 | | | | |
| 12 | 1.18 | 1.09 | 1.20 | 1.09 | 1.26 | | | |
| 13 | 1.06 | 1.17 | 1.13 | 1.13 | 0.87 | 0.85 | | |
| 14 | 1.05 | 1.00 | 1.05 | 0.97 | 0.86 | 0.57 | | |
| 15 | 0.73 | 0.83 | 0.74 | 0.60 | | | | |

CALCULATED FΔH = 1.38

Amendment 73

| LEGEND |
|---|
| VALUE REPRESENTS ASSEMBLY RELATIVE POWER |

| WATTS BAR<br>FINAL SAFETY ANALYSIS REPORT |
|---|
| NORMALIZED POWER DENSITY DISTRIBUTION AT BEGINNING OF LIFE, UNRODDED CORE, HOT FULL POWER, EQUILIBRIUM XENON FOR CYCLE 1<br>FIGURE 4.3-7 |

**Figure 4.3-7 Normalized Power Density Distribution at Beginning of Life, Unrodded Core, Hot Full Power, Equilibrium Xenon for Cycle 1**

| | H | G | F | E | D | C | B | A |
|---|---|---|---|---|---|---|---|---|
| 8 | 1.11 | | | | | | | |
| 9 | 1.04 | 1.13 | | | | | | |
| 10 | 1.14 | 0.99 | 1.16 | | | | | |
| 11 | 1.06 | 1.17 | 1.09 | 1.20 | | | | |
| 12 | 1.15 | 1.09 | 1.21 | 1.08 | 1.22 | | | |
| 13 | 1.06 | 1.17 | 1.13 | 1.13 | 0.86 | 0.85 | | |
| 14 | 1.06 | 1.01 | 1.06 | 0.98 | 0.86 | 0.57 | | |
| 15 | 0.74 | 0.84 | 0.75 | 0.60 | | | | |

CALCULATED FΔH = 1.37

Amendment 73

| LEGEND |
|---|
| VALUE REPRESENTS ASSEMBLY RELATIVE POWER |

| WATTS BAR<br>FINAL SAFETY ANALYSIS REPORT |
|---|
| NORMALIZED POWER DENSITY DISTRIBUTION AT BEGINNING OF LIFE, BANK D 17% INSERTED, HOT FULL POWER, EQUILIBRIUM XENON FOR CYCLE 1<br>FIGURE 4.3-8 |

**Figure 4.3-8 Normalized Power Density Dlistribution at Beginning of Life, Bank D 17% Inserted, Hot Full Power, Equilibrium Xenon for Cycle 1**

| | H | G | F | E | D | C | B | A |
|---|---|---|---|---|---|---|---|---|
| 8 | 1.06 | | | | | | | |
| 9 | 1.13 | 1.06 | | | | | | |
| 10 | 1.07 | 1.12 | 1.07 | | | | | |
| 11 | 1.13 | 1.07 | 1.13 | 1.08 | | | | |
| 12 | 1.07 | 1.13 | 1.07 | 1.14 | 1.16 | | | |
| 13 | 1.13 | 1.07 | 1.13 | 1.05 | 1.06 | 0.99 | | |
| 14 | 1.01 | 1.10 | 0.98 | 1.01 | 0.86 | 0.61 | | |
| 15 | 0.77 | 0.79 | 0.74 | 0.59 | | | | |

CALCULATED FΔH = 1.23

Amendment 73

| LEGEND |
|---|
| VALUE REPRESENTS ASSEMBLY RELATIVE POWER |

| WATTS BAR<br>FINAL SAFETY ANALYSIS REPORT |
|---|
| NORMALIZED POWER DENSITY DISTRIBUTION AT END OF LIFE, UNRODDED CORE, HOT FULL POWER, EQUILIBRIUM XENON FOR CYCLE 1<br>FIGURE 4.3-10 |

**Figure 4.3-9 Normalized Power Density Distribution at Middle of Life, Unrodded Core, Hot Full Power, Equllibrium Xenon for Cycle 1**

| | H | G | F | E | D | C | B | A |
|---|---|---|---|---|---|---|---|---|
| 8 | 1.06 | | | | | | | |
| 9 | 1.13 | 1.06 | | | | | | |
| 10 | 1.07 | 1.12 | 1.07 | | | | | |
| 11 | 1.13 | 1.07 | 1.13 | 1.08 | | | | |
| 12 | 1.07 | 1.13 | 1.07 | 1.14 | 1.16 | | | |
| 13 | 1.13 | 1.07 | 1.13 | 1.05 | 1.06 | 0.99 | | |
| 14 | 1.01 | 1.10 | 0.98 | 1.01 | 0.86 | 0.61 | | |
| 15 | 0.77 | 0.79 | 0.74 | 0.59 | | | | |

CALCULATED FΔH = 1.23

Amendment 73

| LEGEND |
|---|
| VALUE REPRESENTS ASSEMBLY RELATIVE POWER |

| WATTS BAR<br>FINAL SAFETY ANALYSIS REPORT |
|---|
| NORMALIZED POWER DENSITY DISTRIBUTION AT END OF LIFE, UNRODDED CORE, HOT FULL POWER, EQUILIBRIUM XENON FOR CYCLE 1<br>FIGURE 4.3-10 |

**Figure 4.3-10 Normalized Power Density Distribution at End of Life, Unrodded Core, Hot Full Power, Equilibrium Xenon for Cycle 1**

| | H | G | F | E | D | C | B | A |
|---|---|---|---|---|---|---|---|---|
| 8 | 1.00 | | | | | | | |
| 9 | 1.11 | 1.06 | | | | | | |
| 10 | 1.07 | 1.12 | 1.08 | | | | | |
| 11 | 1.12 | 1.07 | 1.14 | 1.08 | | | | |
| 12 | 1.02 | 1.12 | 1.08 | 1.13 | 1.10 | | | |
| 13 | 1.12 | 1.07 | 1.13 | 1.05 | 1.05 | 0.99 | | |
| 14 | 1.02 | 1.12 | 0.99 | 1.02 | 0.86 | 0.61 | | |
| 15 | 0.79 | 0.81 | 0.75 | 0.60 | | | | |

CALCULATED FΔH = 1.23

Amendment 73

| LEGEND |
|---|
| VALUE REPRESENTS ASSEMBLY RELATIVE POWER |

| WATTS BAR<br>FINAL SAFETY ANALYSIS REPORT |
|---|
| NORMALIZED POWER DENSITY DISTRIBUTION AT END OF LIFE, BANK D 17% INSERTED, HOT FULL POWER, EQUILIBRIUM XENON FOR CYCLE 1<br>FIGURE 4.3-11 |

**Figure 4.3-11 Normalized Power Density Distribution at End of Life, Bank D 17% Inserted, Hot Full Power, Equilibrium Xenon for Cycle 1**

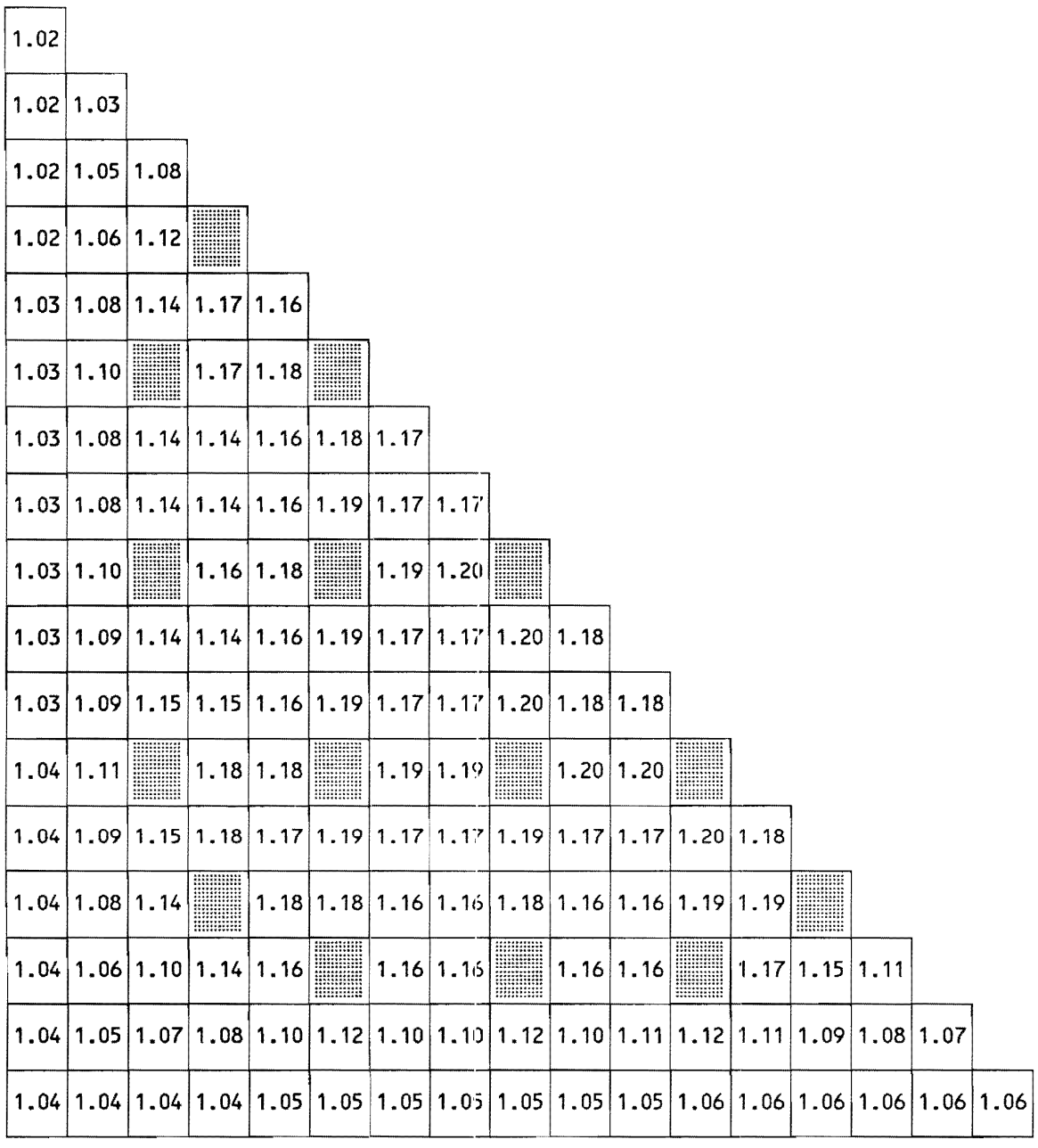


Amendment 73

| WATTS BAR<br>FINAL SAFETY ANALYSIS REPORT |
|---|
| RODWISE POWER DISTRIBUTION IN A TYPICAL ASSEMBLY NEAR BEGINNING OF LIFE, HOT FULL POWER, EQUILIBRIUM XENON, UNRODDED CORE<br>FIGURE 4.3-12 |

**Figure 4.3-12 Rodwise Power Distribution in a Typical Assembly Near Beginning of Life, Hot Full Power, Equilibrium Xenon, Unrodded Core**

| | | | | | | | | | | | | | | | | |
|---|---|---|---|---|---|---|---|---|---|---|---|---|---|---|---|---|
| 0.98 | | | | | | | | | | | | | | | | |
| 0.98 | 0.99 | | | | | | | | | | | | | | | |
| 0.98 | 1.00 | 1.03 | | | | | | | | | | | | | | |
| 0.99 | 1.02 | 1.07 | | | | | | | | | | | | | | |
| 1.00 | 1.03 | 1.09 | 1.11 | 1.09 | | | | | | | | | | | | |
| 1.01 | 1.06 | | 1.11 | 1.11 | | | | | | | | | | | | |
| 1.00 | 1.04 | 1.08 | 1.07 | 1.08 | 1.10 | 1.08 | | | | | | | | | | |
| 1.00 | 1.04 | 1.08 | 1.07 | 1.08 | 1.10 | 1.08 | 1.08 | | | | | | | | | |
| 1.01 | 1.06 | | 1.09 | 1.10 | | 1.10 | 1.10 | | | | | | | | | |
| 1.00 | 1.04 | 1.08 | 1.07 | 1.08 | 1.10 | 1.08 | 1.08 | 1.10 | 1.08 | | | | | | | |
| 1.00 | 1.04 | 1.08 | 1.07 | 1.08 | 1.10 | 1.08 | 1.08 | 1.10 | 1.08 | 1.08 | | | | | | |
| 1.01 | 1.06 | | 1.11 | 1.11 | | 1.10 | 1.10 | | 1.10 | 1.10 | | | | | | |
| 1.00 | 1.03 | 1.09 | 1.11 | 1.09 | 1.11 | 1.08 | 1.08 | 1.10 | 1.08 | 1.08 | 1.11 | 1.09 | | | | |
| 0.99 | 1.02 | 1.07 | | 1.11 | 1.11 | 1.07 | 1.07 | 1.09 | 1.07 | 1.07 | 1.11 | 1.11 | | | | |
| 0.98 | 1.00 | 1.03 | 1.07 | 1.09 | | 1.08 | 1.08 | | 1.08 | 1.08 | | 1.09 | 1.07 | 1.03 | | |
| 0.98 | 0.99 | 1.00 | 1.02 | 1.03 | 1.06 | 1.04 | 1.04 | 1.06 | 1.04 | 1.04 | 1.06 | 1.03 | 1.02 | 1.00 | 0.98 | |
| 0.98 | 0.98 | 0.98 | 0.99 | 1.00 | 1.01 | 1.00 | 1.00 | 1.01 | 1.00 | 1.00 | 1.01 | 1.00 | 0.99 | 0.98 | 0.98 | 0.98 |

Amendment 73

WATTS BAR
FINAL SAFETY ANALYSIS REPORT

RODWISE POWER DISTRIBUTION IN A TYPICAL ASSEMBLY NEAR END OF LIFE, HOT FULL POWER, EQUILIBRIUM XENON, UNRODDED CORE
FIGURE 4.3-13

**Figure 4.3-13 Rodwise Power Distribution in a Typical Assembly Near End of Life, Hot Full Power, Equilibrium Xenon, Unrodded Core**

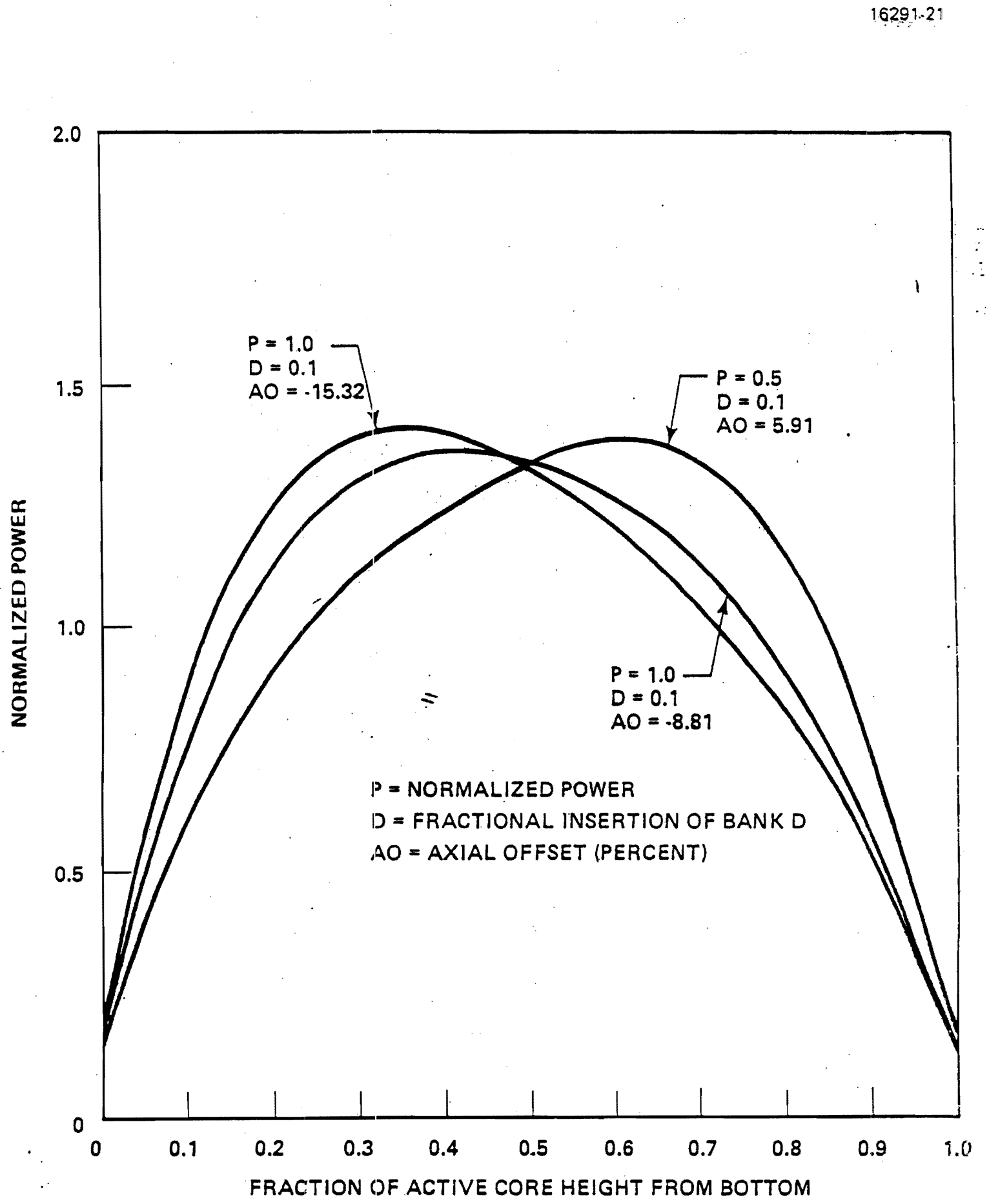


Figure 4.3-14. Typical Axial Power Shapes Occurring at Beginning of Life

Revised by Amendment 52

**Figure 4.3-14 Typical Axial Power Shapes Occurring at Beginning of Life**

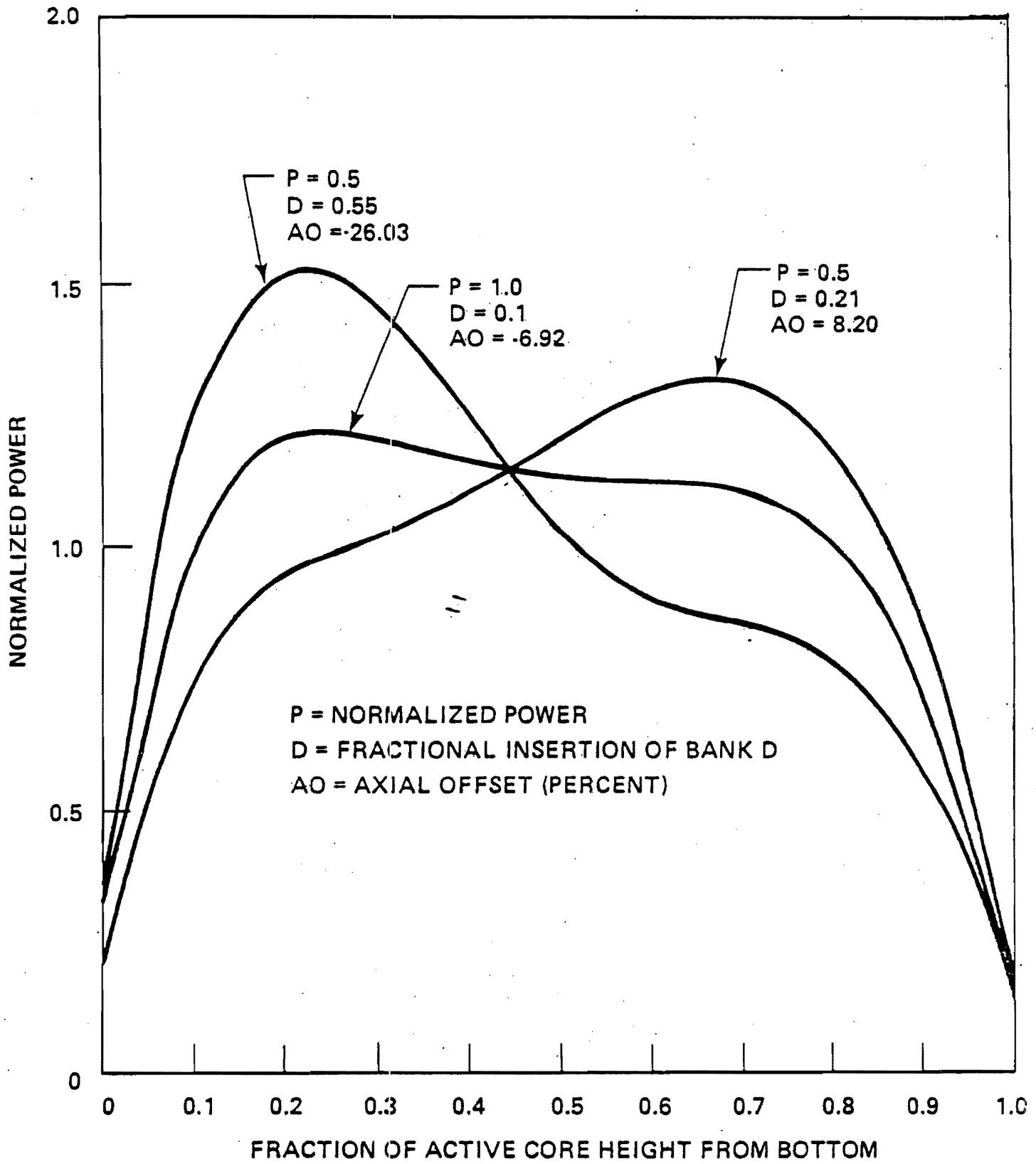


Figure 4.3-15. Typical Axial Power Shapes Occurring at Middle of Life

Revised by Amendment 52

**Figure 4.3-15 Typical Axial Power Shape:s Occurring at Middle of Life**

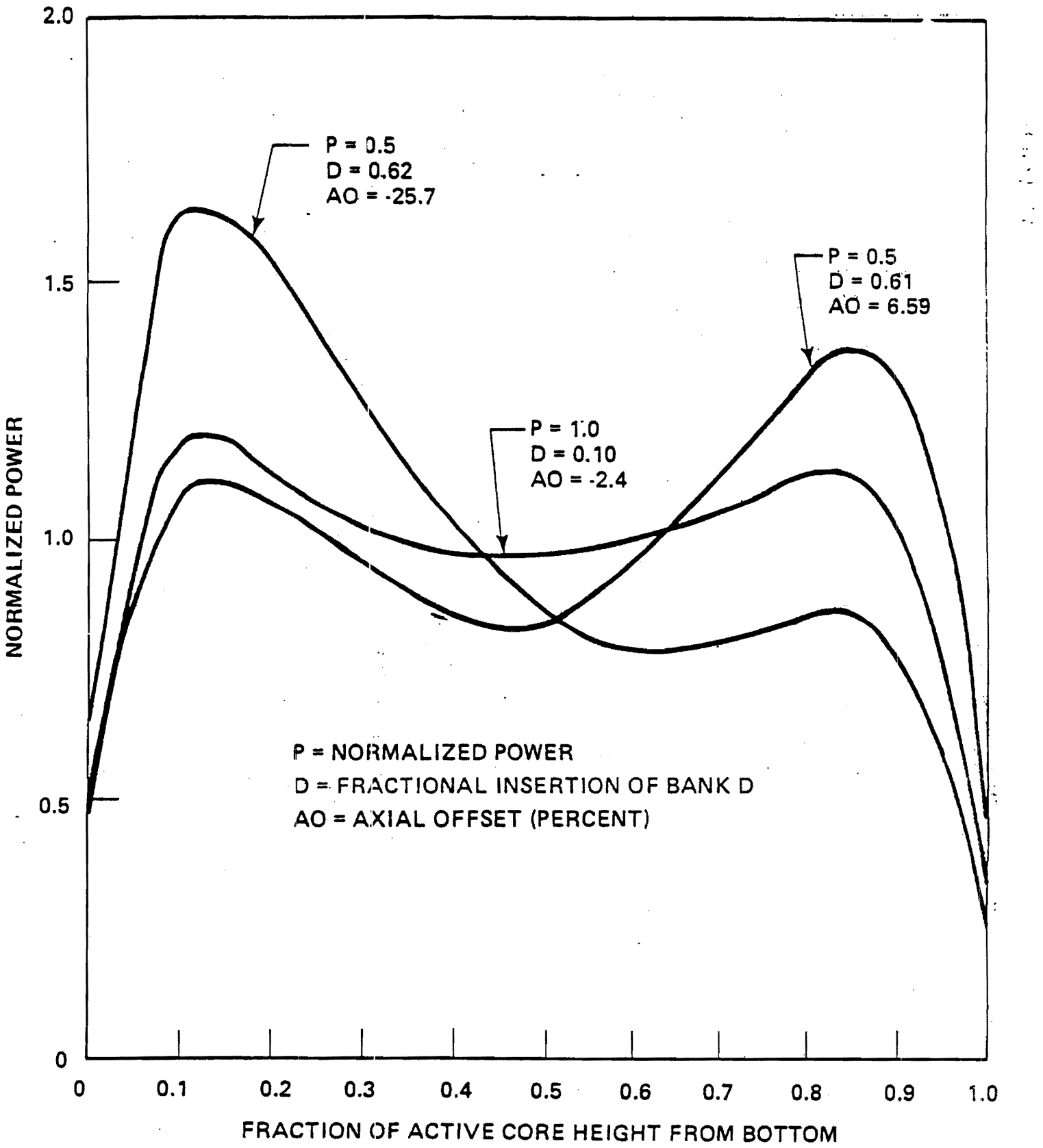


Figure 4.3-16. Typical Axial Power Shapes Occurring at End of Life

Revised by Amendment 52

**Figure 4.3-16 Typical Axial Power Shapes Occurring at End of Life**

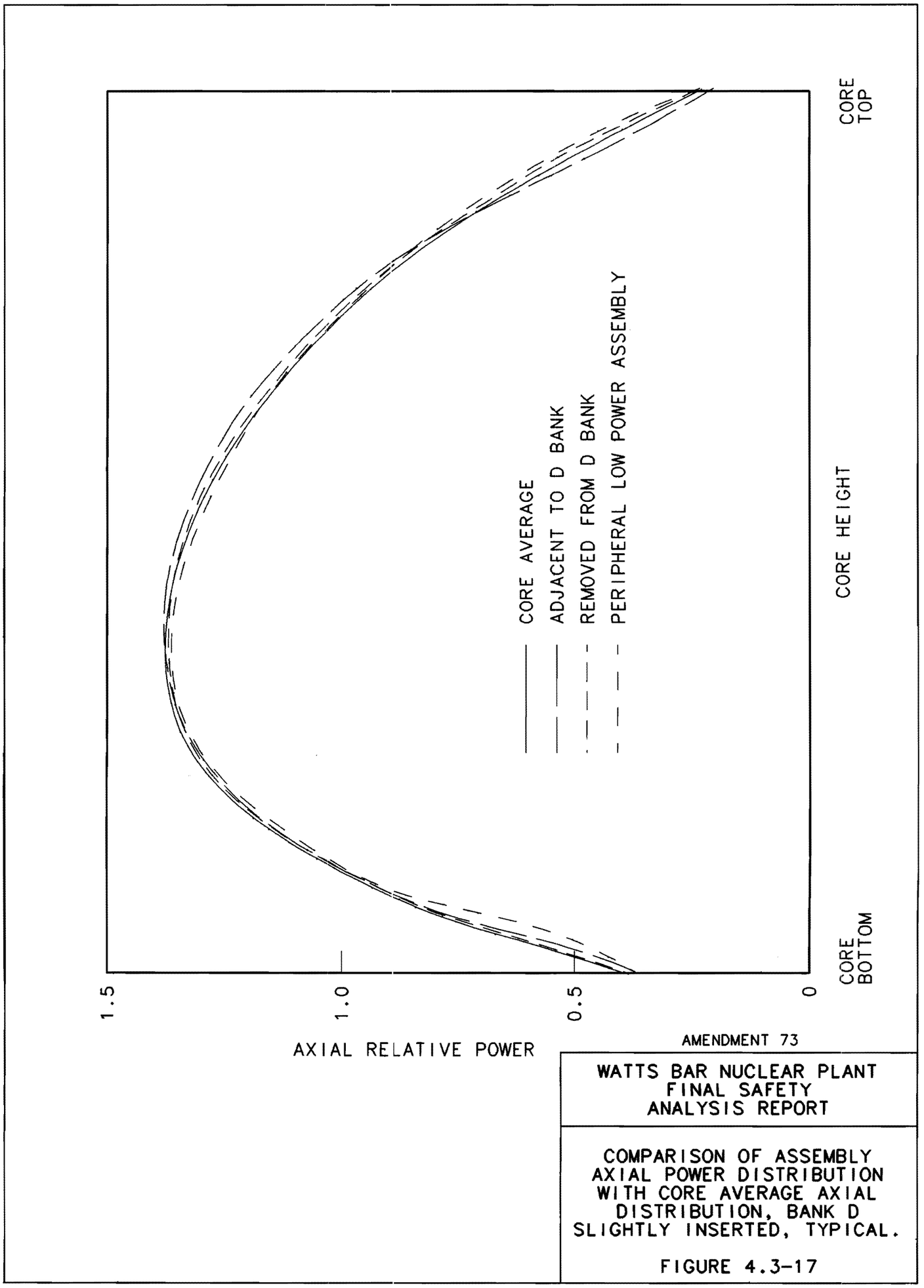


**Figure 4.3-17 Comparison of Assembly Axial Power Distribution With Core Average Axial Distribution, Bank D Slightly Inserted, Typical**

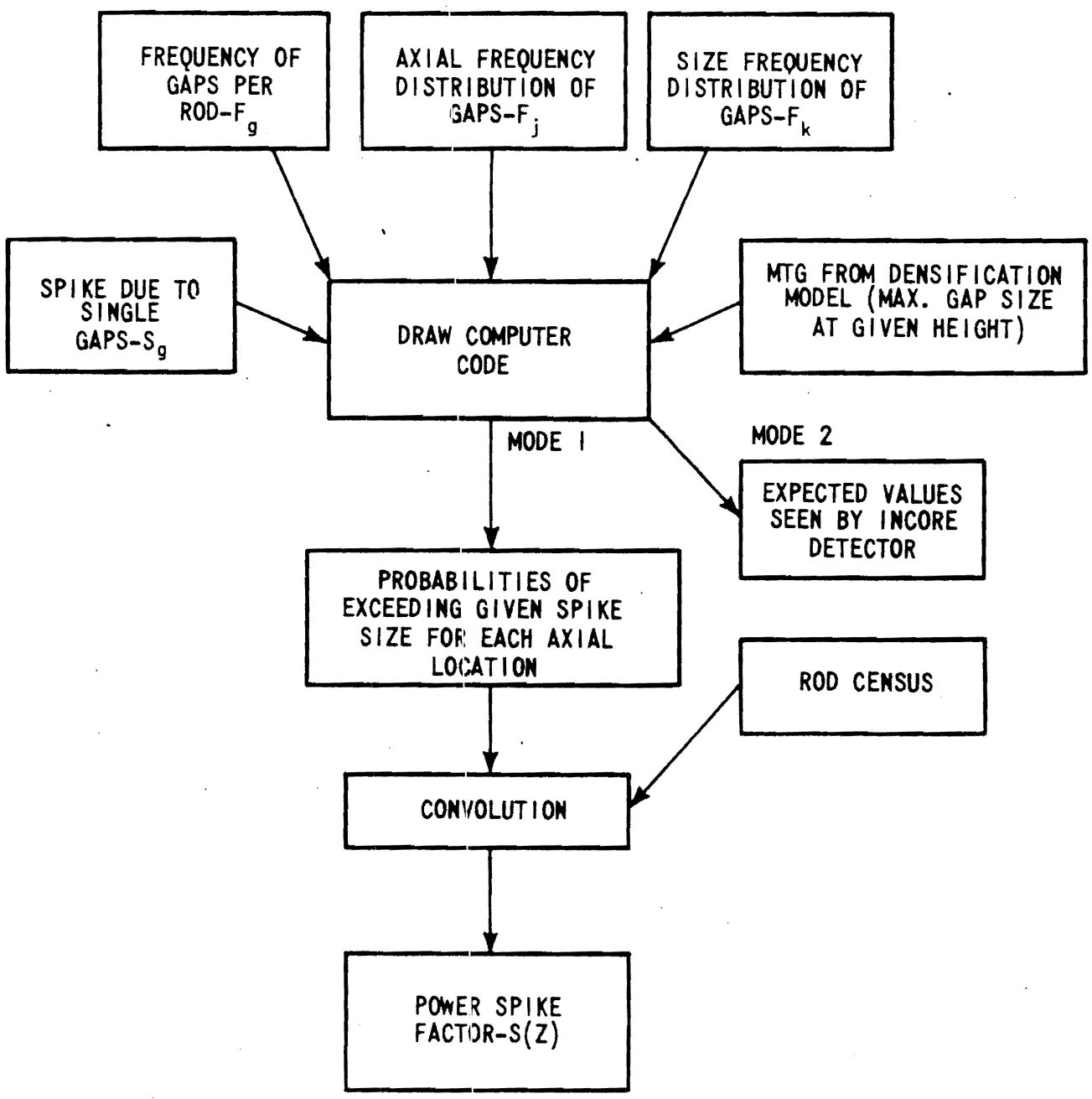


Figure 4.3-18 Flow Chart for Determining Spike Model

**Figure 4.3-18 Flow Chart for Determining Spike Model**

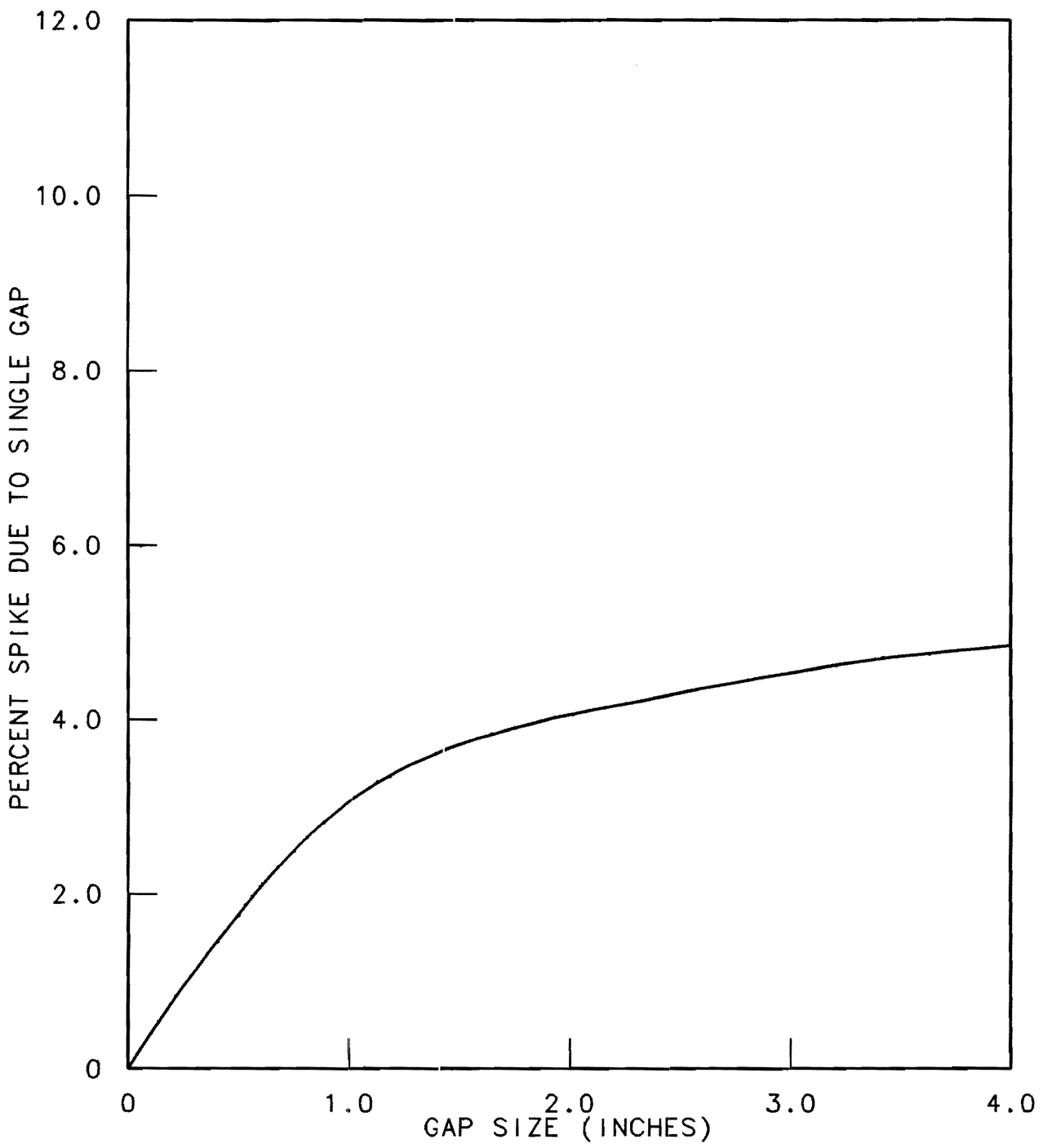


AMENDMENT 73

| |
|---|
| WATTS BAR NUCLEAR PLANT<br>FINAL SAFETY<br>ANALYSIS REPORT |
| PREDICTED POWER SPIKE<br>DUE TO SINGLE NONFLATTENED<br>GAP IN THE ADJACENT FUEL<br>(TYPICAL)<br><br>FIGURE 4.3–19 |

**Figure 4.3-19 Predicted Power Spike Due to Single Non-flattened Gap in the Adjacent Fuel (Typical)**

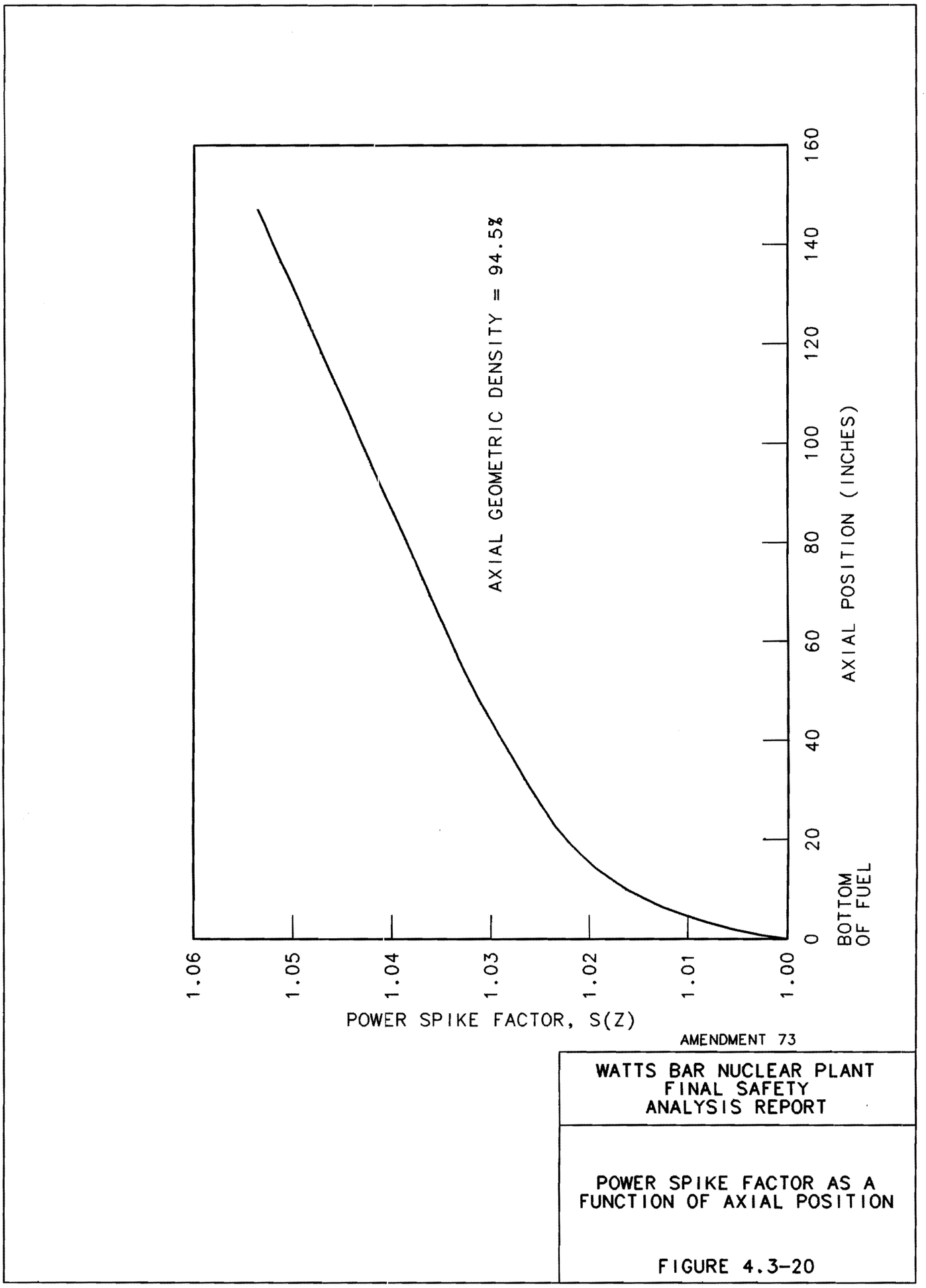


Figure 4.3-20 Power Spike Factor as a Function of Axial Position

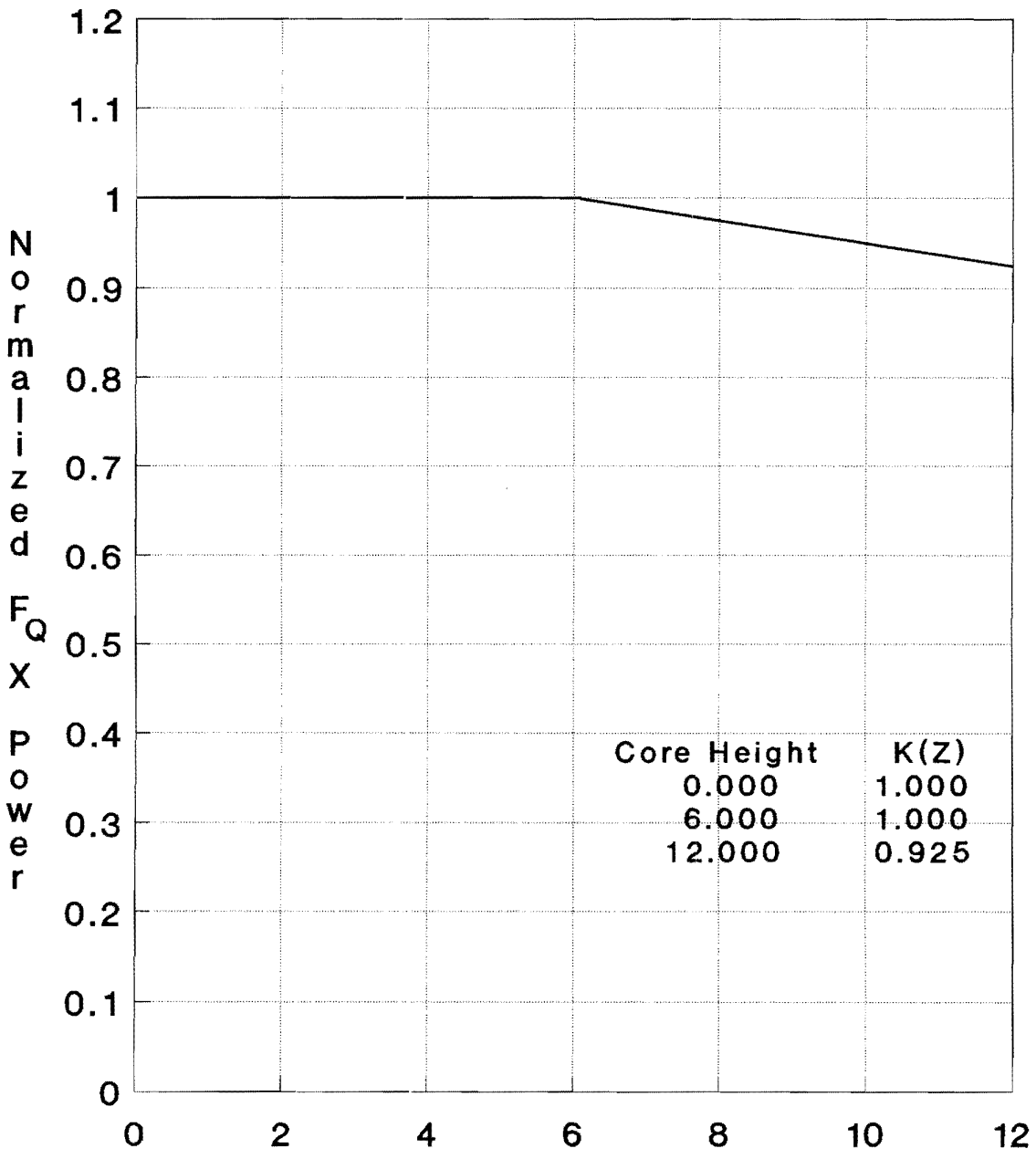


Note : K(Z) = Normalized $F_Q$ X Power

Amendment 73

| WATTS BAR<br>FINAL SAFETY ANALYSIS REPORT |
|---|
| NORMALIZED MAXIMUM $F_Q$ X POWER VERSUS AXIAL HEIGHT DURING NORMAL OPERATION<br>FIGURE 4.3-21 |

**Figure 4.3-21 Normalized Maximum $F_Q$ x Power Versus Axial Height During Normal Operation**

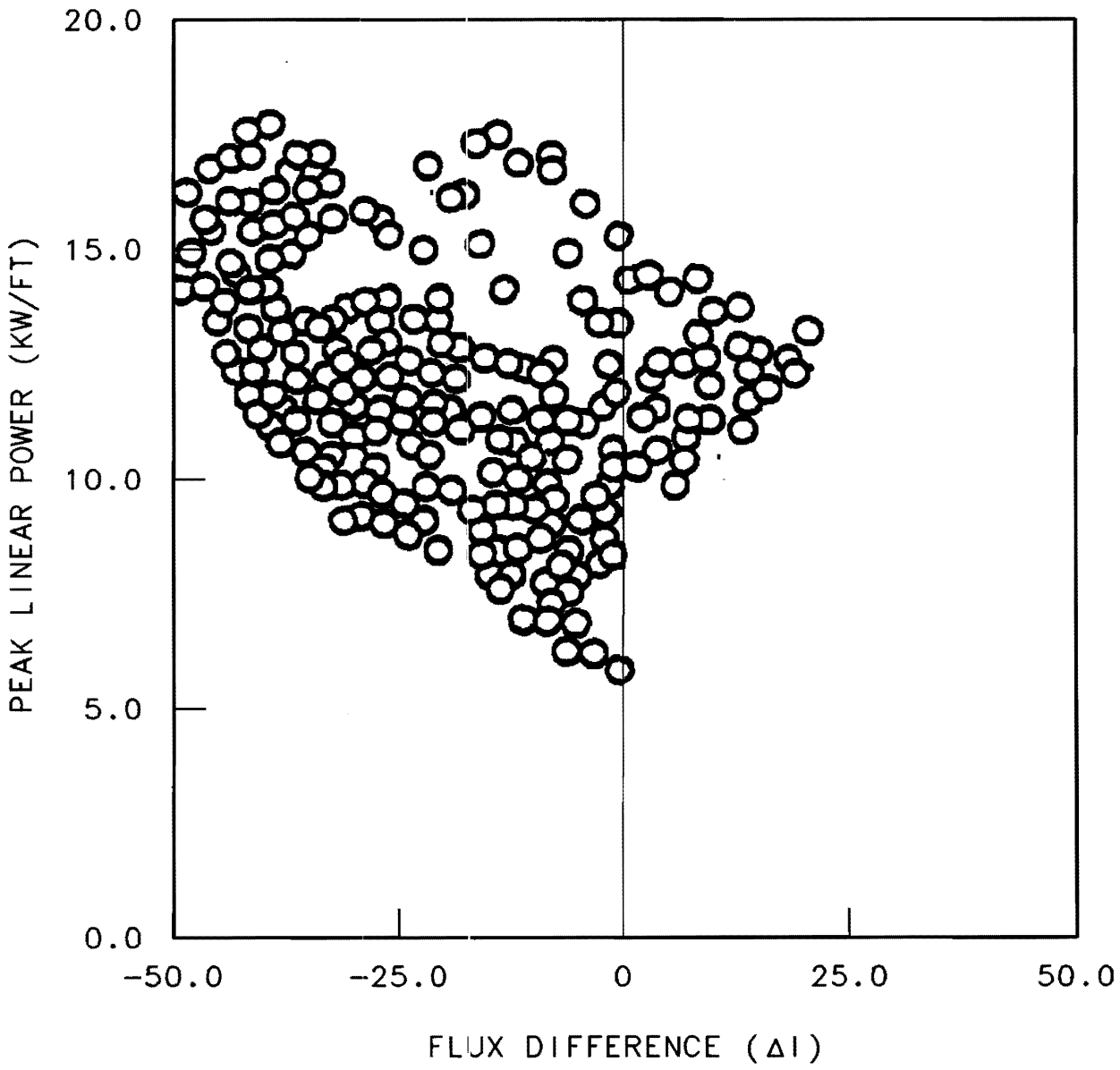


AMENDMENT 73

WATTS BAR NUCLEAR PLANT
FINAL SAFETY
ANALYSIS REPORT

PEAK LINEAR POWER DURING
CONTROL ROD MALFUNCTION
OVERPOWER TRANSIENTS

FIGURE 4.3-22

**Figure 4.3-22 Peak Linear Power During Control Rod Malfunction Overpower Transients**

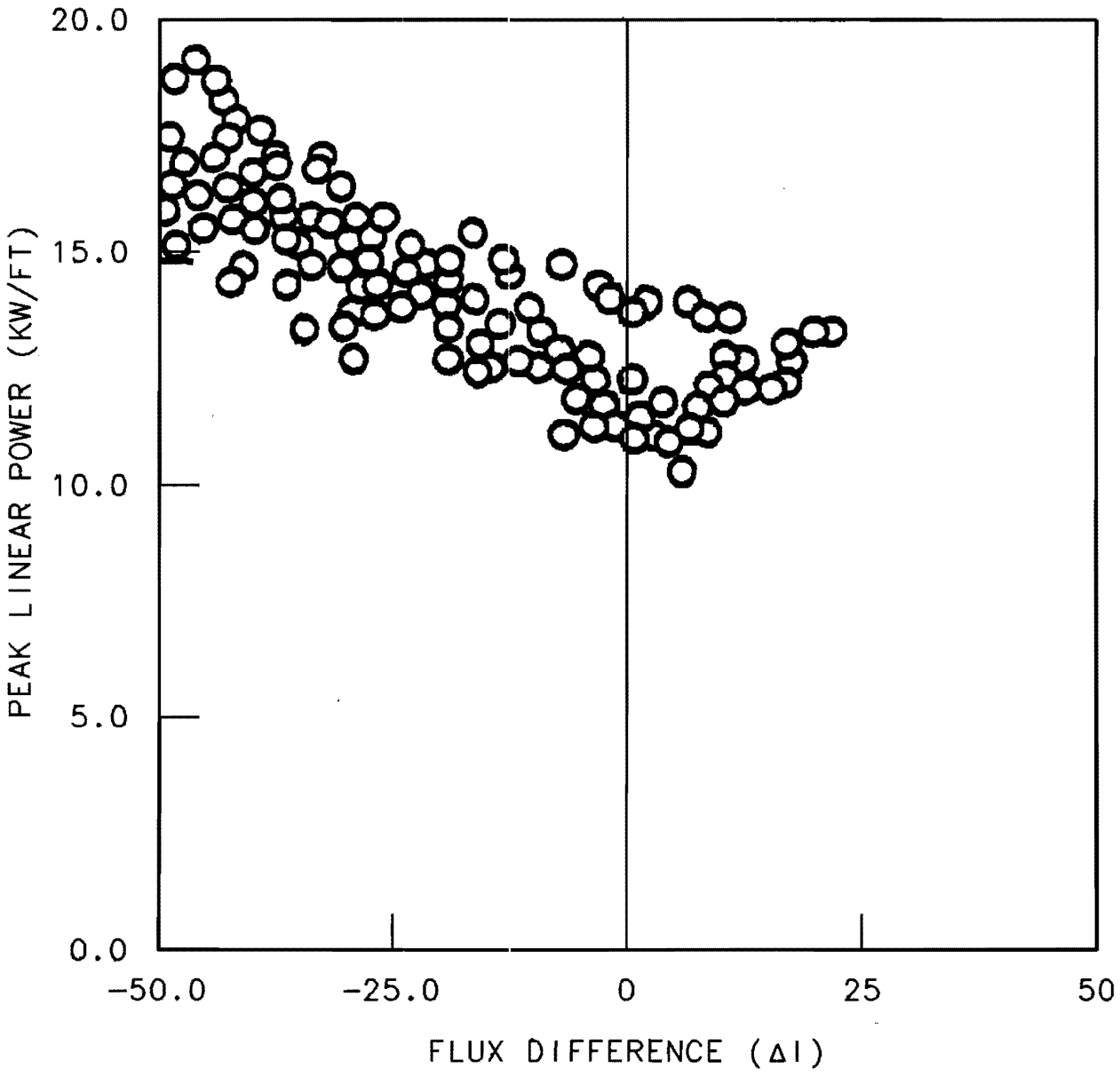


AMENDMENT 73

| WATTS BAR NUCLEAR PLANT FINAL SAFETY ANALYSIS REPORT |
|---|
| PEAK LINEAR POWER DURING BORATION/DILUTION OVERPOWER TRANSIENTS (TYPICAL) |
| FIGURE 4.3-23 |

**Figure 4.3-23 Peak Linear Power During Boration/Dilution Overpower Transients (Typical)**

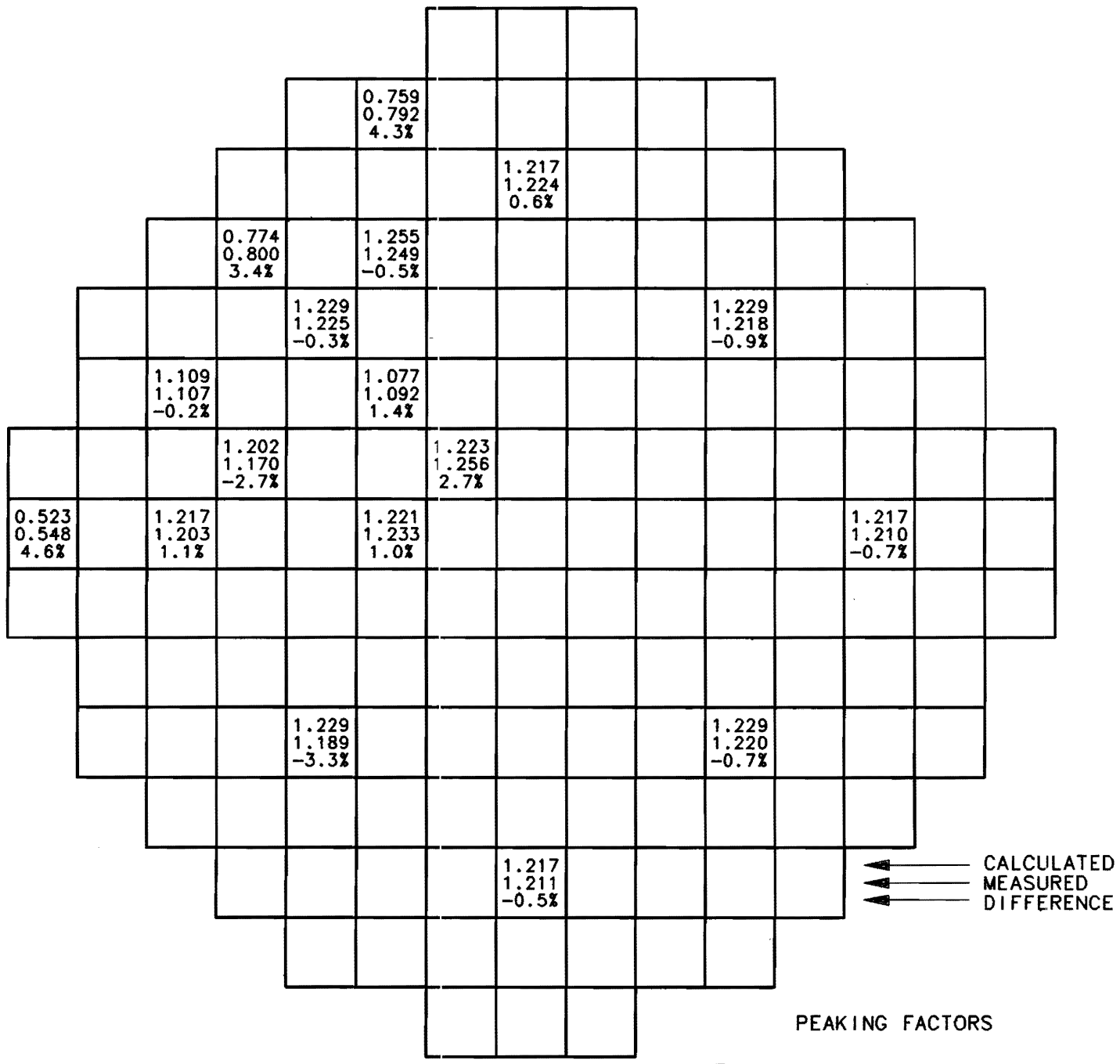


PEAKING FACTORS

$\bar{F}_Z = 1.5$

$F^N_{\Delta H} = 1.357$

$F^N_Q = 1.5$

AMENDMENT 73

WATTS BAR NUCLEAR PLANT
FINAL SAFETY
ANALYSIS REPORT

COMPARISON BETWEEN
CALCULATED AND MEASURED
RELATIVE FUEL ASSEMBLY
POWER DISTRIBUTION, (TYPICAL)

FIGURE 4.3-24

**Figure 4.3-24 Comparison Between Calculated and Measured Relative Fuel Assembly Power Distribution (Typical)**

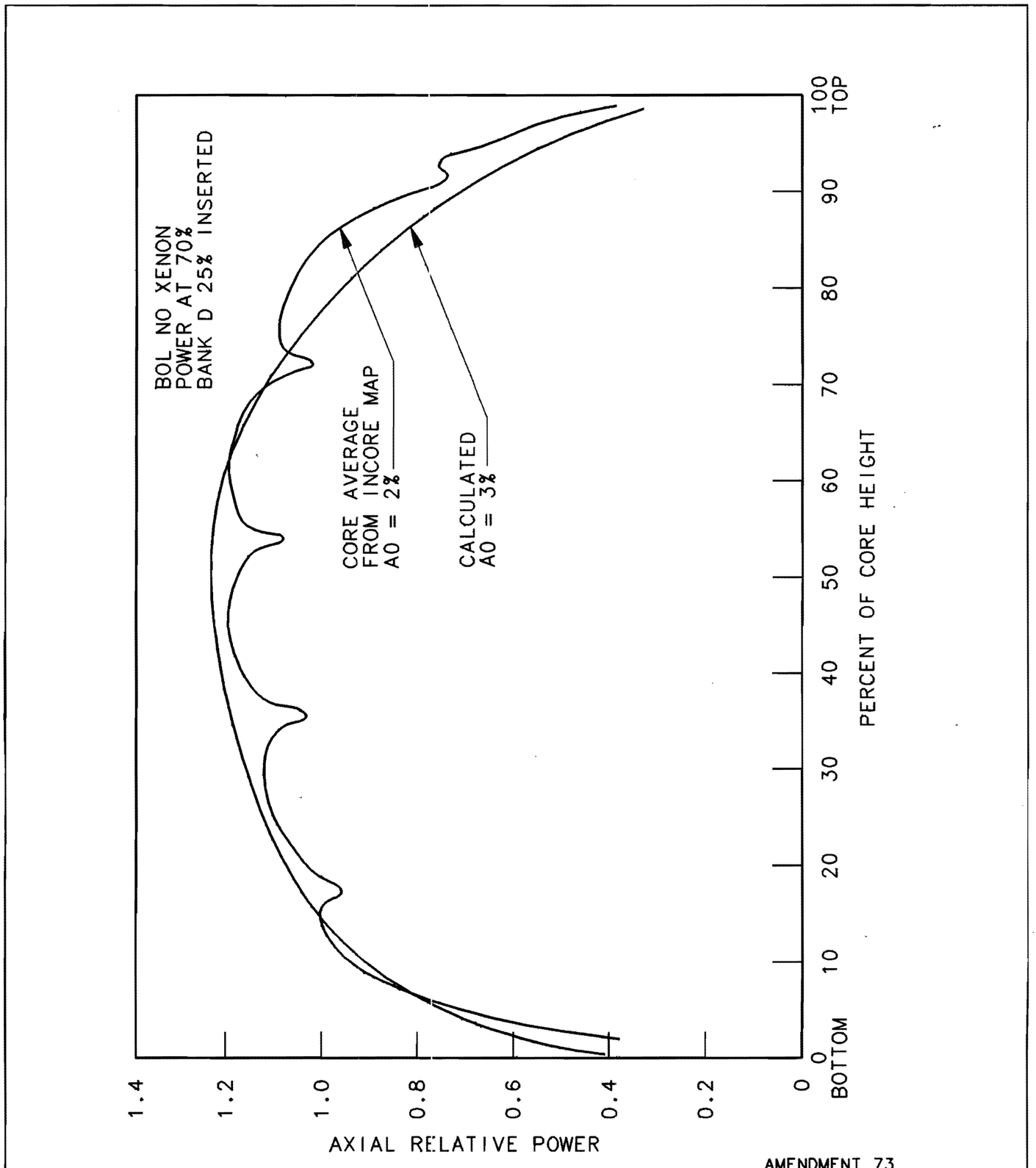


Figure 4.3-25 Comparison of Calculated and Measured Axial Shape (Typical)

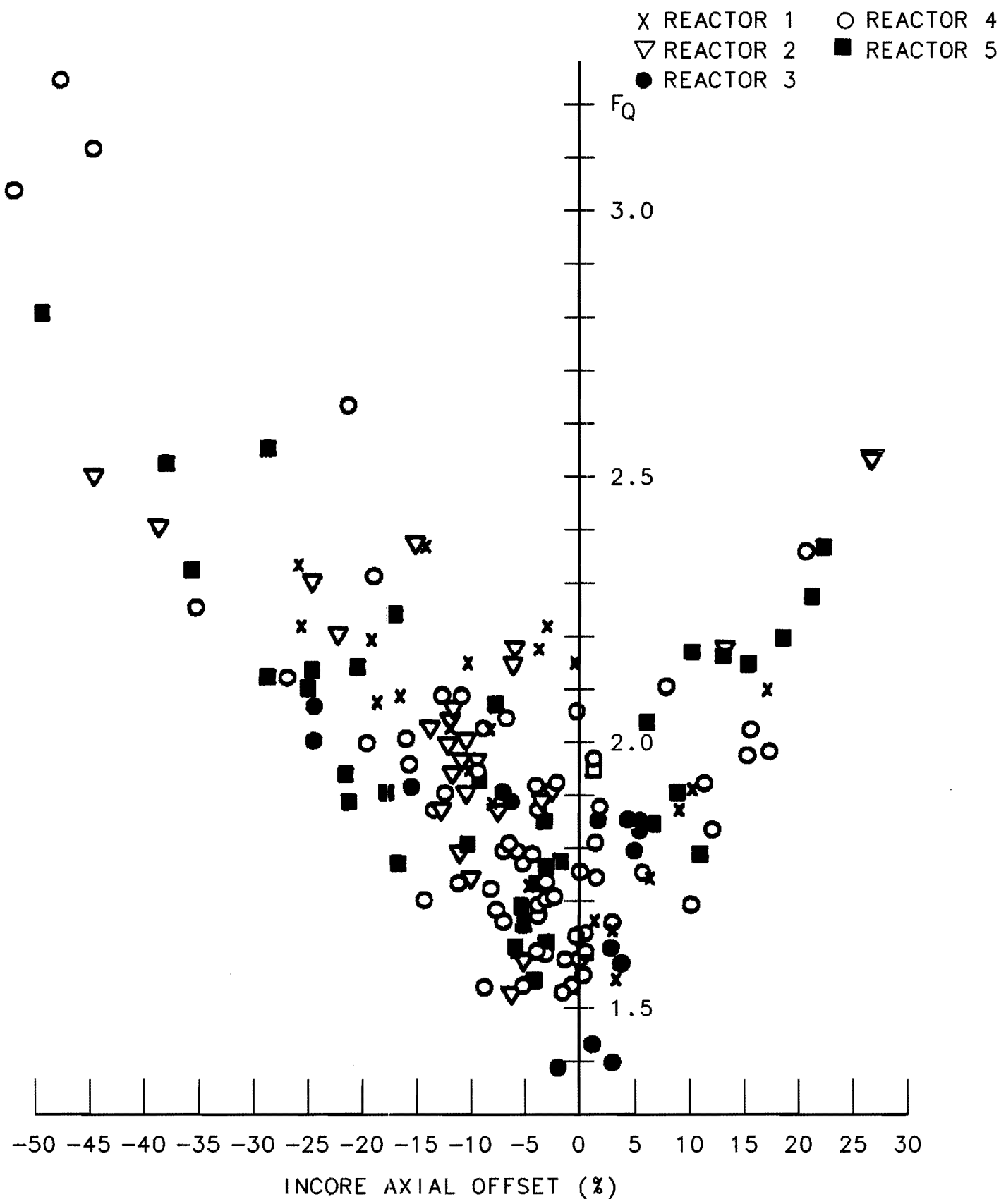


AMENDMENT 73

WATTS BAR NUCLEAR PLANT
FINAL SAFETY
ANALYSIS REPORT

MEASURED VALUES OF $F_Q$
FOR FULL POWER ROD
CONFIGURATIONS (TYPICAL)

FIGURE 4.3-26

**Figure 4.3-26 Measured Values of $F_Q$ for Full Power Rod Configurations (Typical)**

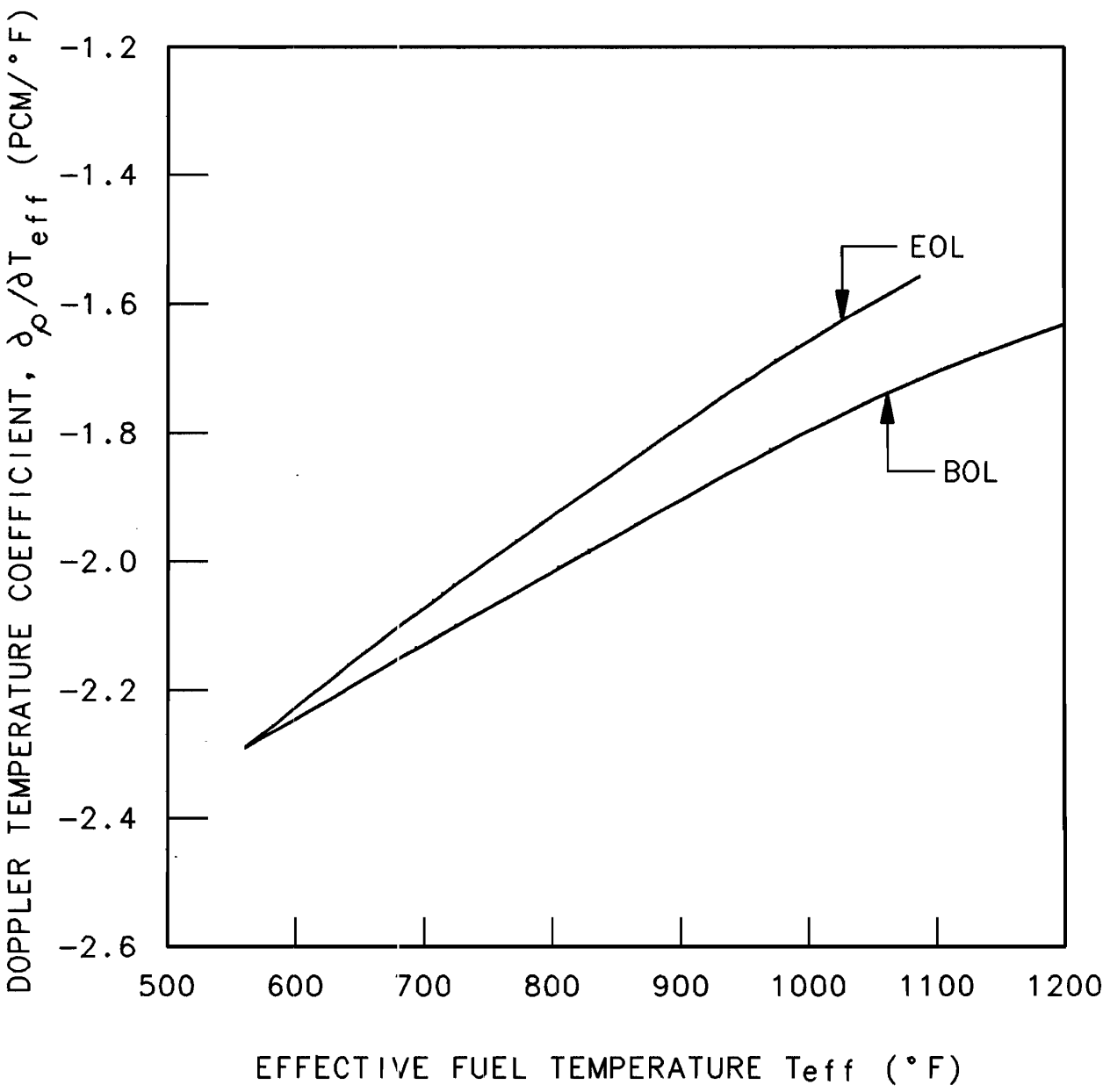


AMENDMENT 73

| WATTS BAR NUCLEAR PLANT FINAL SAFETY ANALYSIS REPORT |
|---|
| DOPPLER TEMPERATURE COEFFICIENT AT BOL AND EOL CYCLE 1, (TYPICAL)<br><br>FIGURE 4.3-27 |

**Figure 4.3-27 Doppler Temperature Coefficient at BOL and EOL Cycle 1, (Typical)**

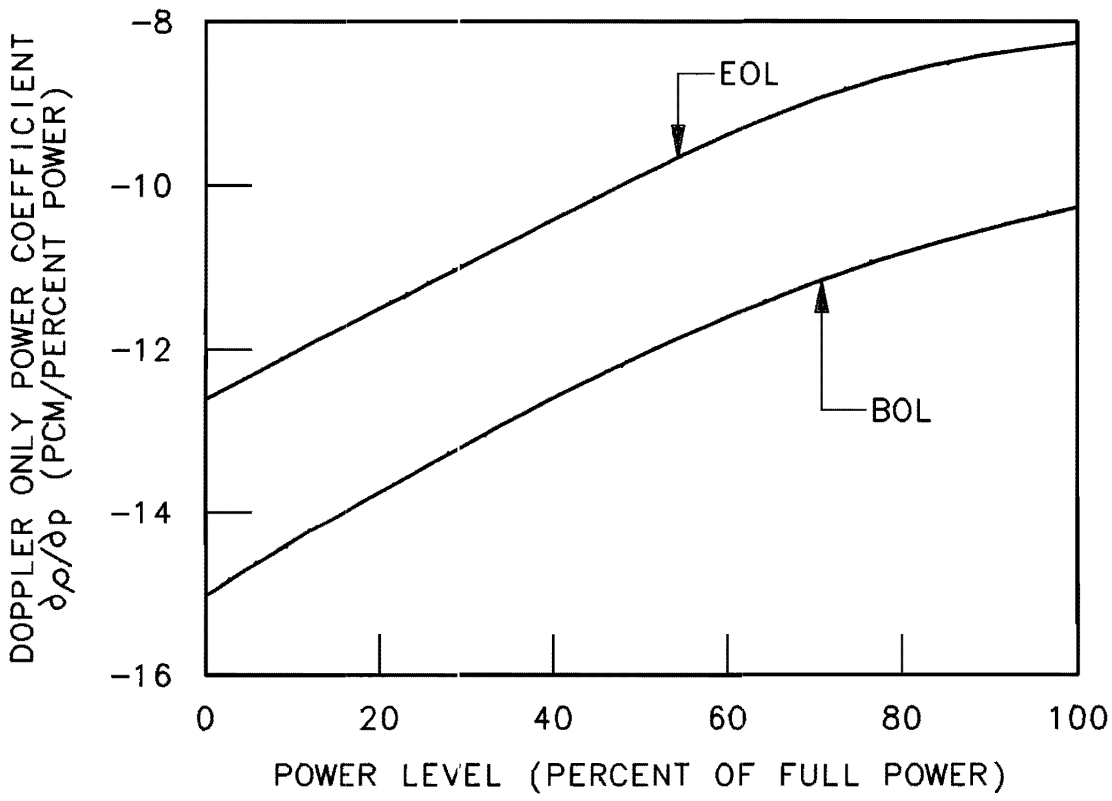


AMENDMENT 73

WATTS BAR NUCLEAR PLANT
FINAL SAFETY
ANALYSIS REPORT

DOPPLER - ONLY POWER
COEFFICIENT - BOL, EOL,
CYCLE 1, (TYPICAL)

FIGURE 4.3-28

**Figure 4.3-28 Doppler - Only Power Coefficient - BOL, EOL, Cycle 1, (Typical)**

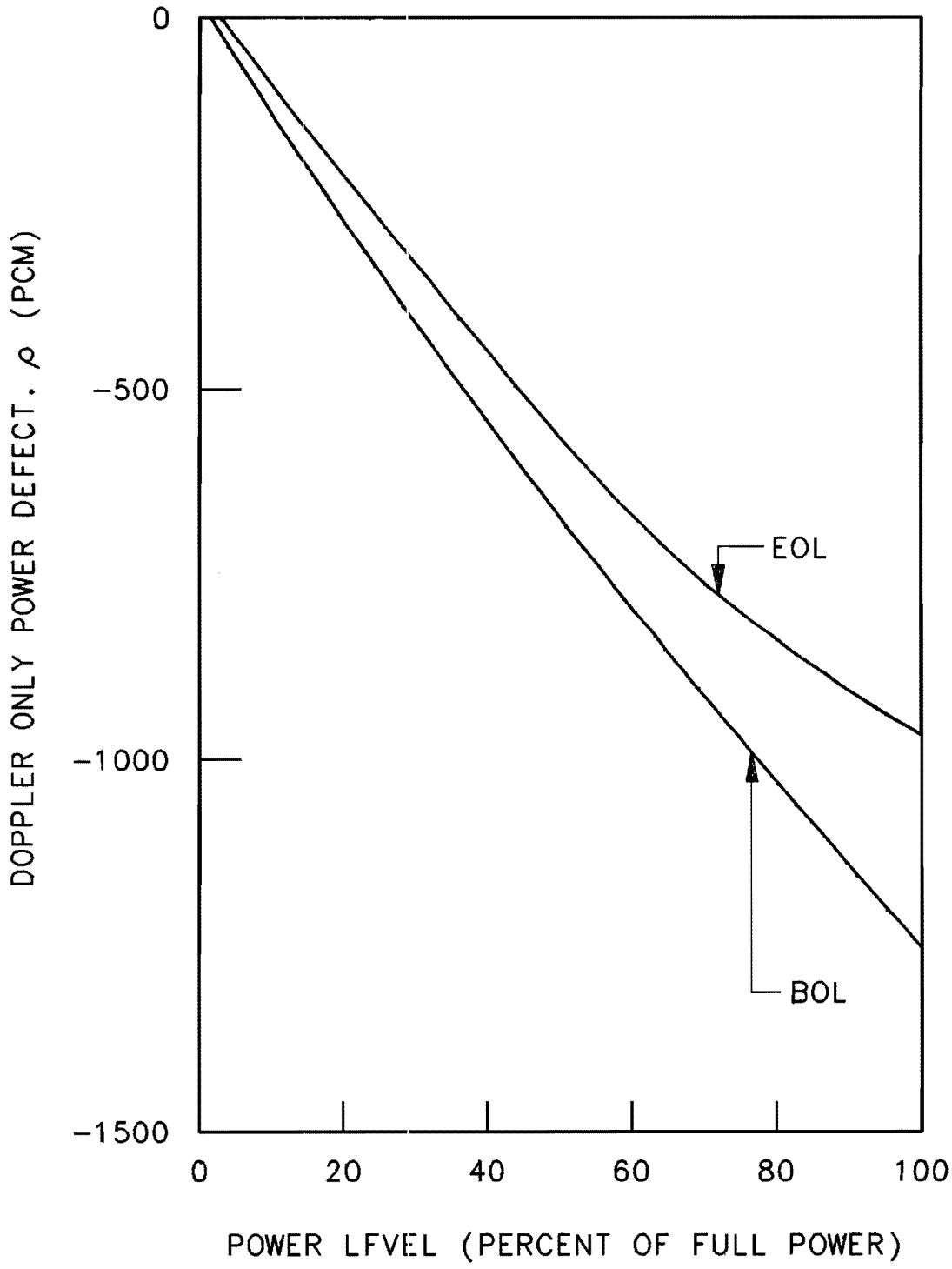


AMENDMENT 73

| WATTS BAR NUCLEAR PLANT<br>FINAL SAFETY<br>ANALYSIS REPORT |
|---|
| DOPPLER ONLY POWER<br>DEFECT - BOL, EOL,<br>CYCLE 1, (TYPICAL)<br><br>FIGURE 4.3-29 |

**Figure 4.3-29 Doppler - Only Power Defect - BOL, EOL, Cycle 1, (Typical)**

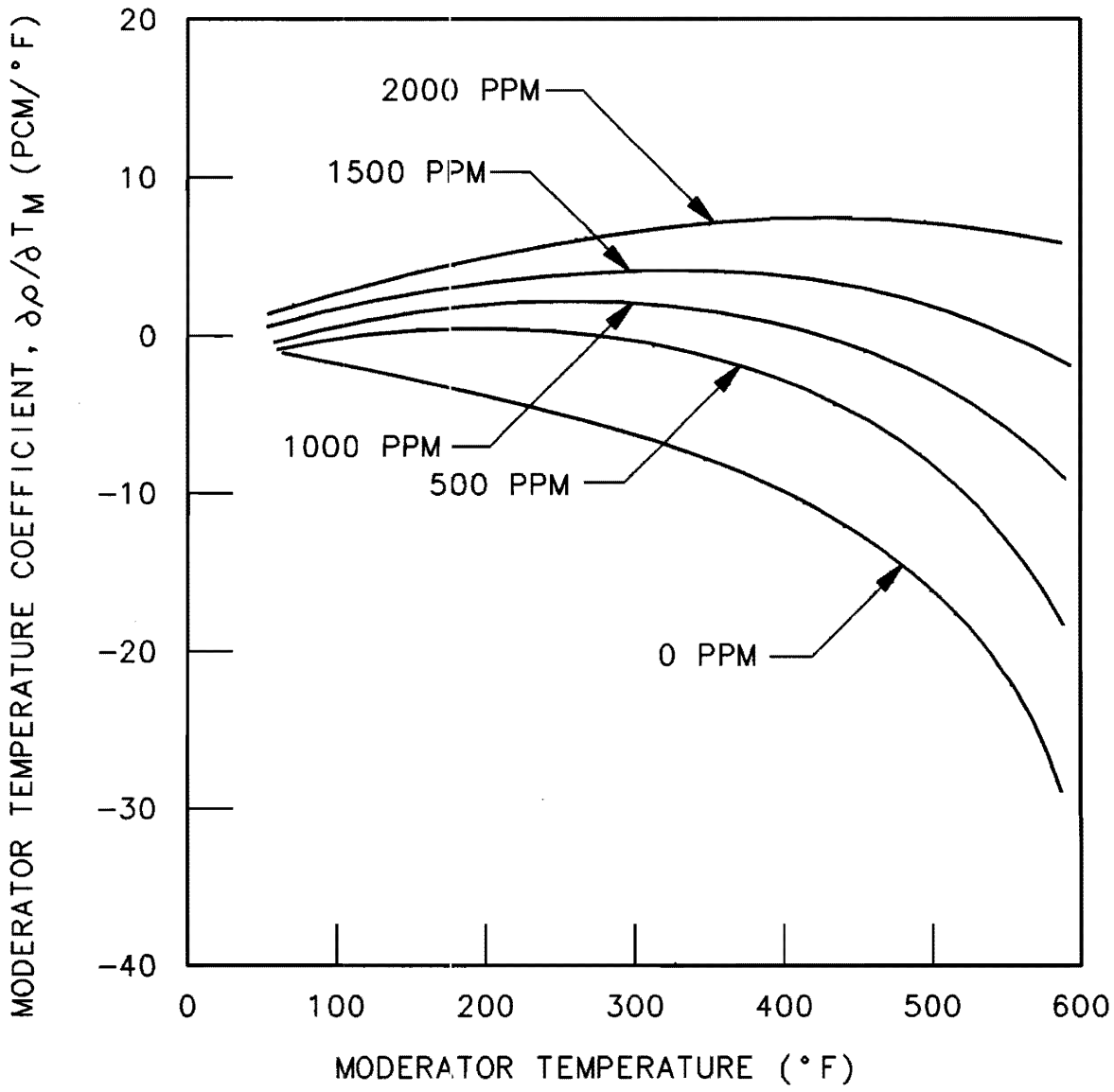


AMENDMENT 73

WATTS BAR NUCLEAR PLANT
FINAL SAFETY
ANALYSIS REPORT

MODERATOR TEMPERATURE
COEFFIEIENT – BOL, CYCLE 1
NO RODS, (TYPICAL)

FIGURE 4.3–30

**Figure 4.3-30 Moderator Temperature Coefficient - BOL, Cycle 1, No Rods, (Typical)**

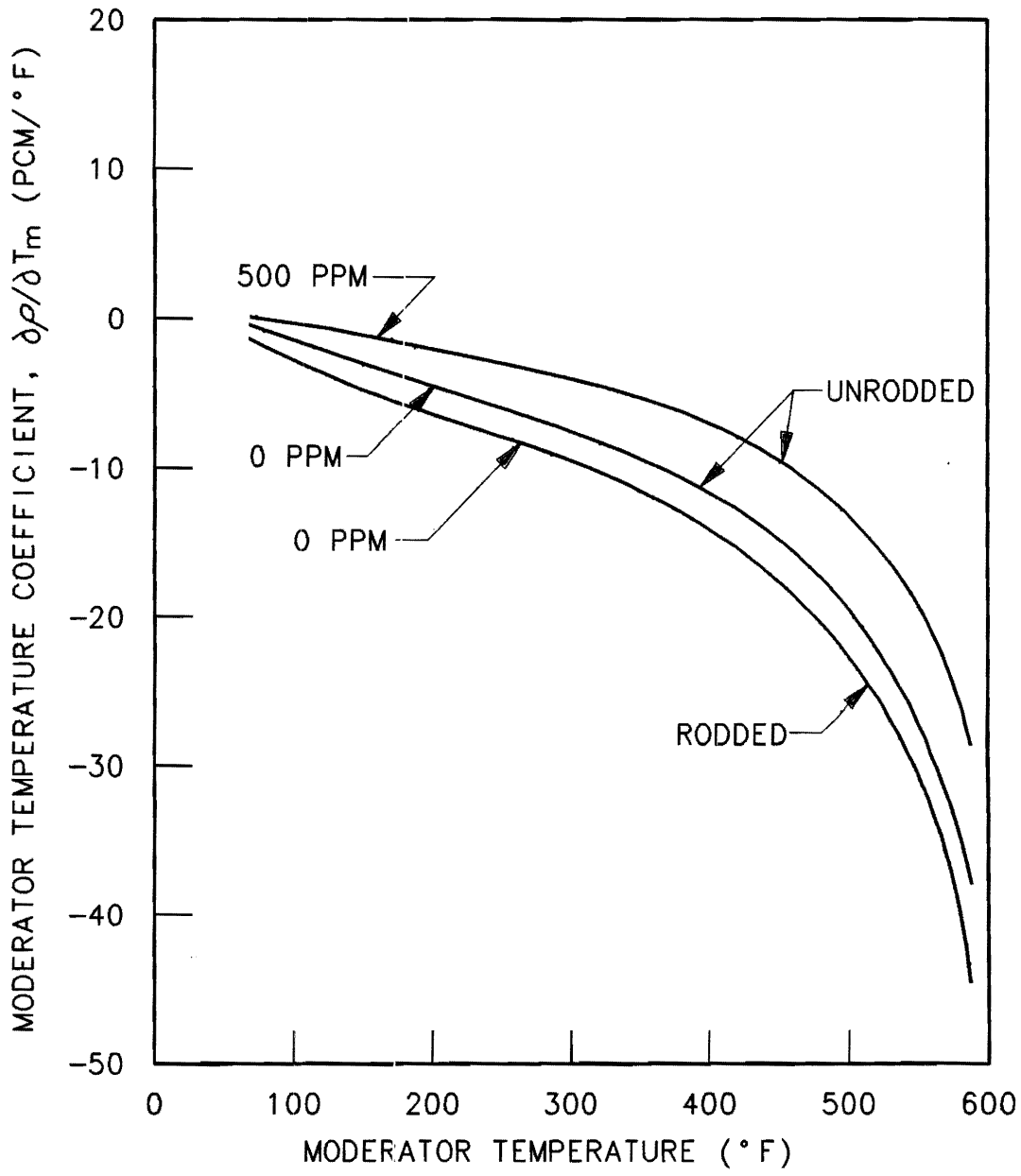


AMENDMENT 73

WATTS BAR NUCLEAR PLANT
FINAL SAFETY
ANALYSIS REPORT

MODERATOR TEMPERATURE
COEFFICIENT - EOL, CYCLE 1,
(TYPICAL)

FIGURE 4.3-31

**Figure 4.3-31 Moderator Temperature Coefficient - EOL, Cycle 1, (Typical)**

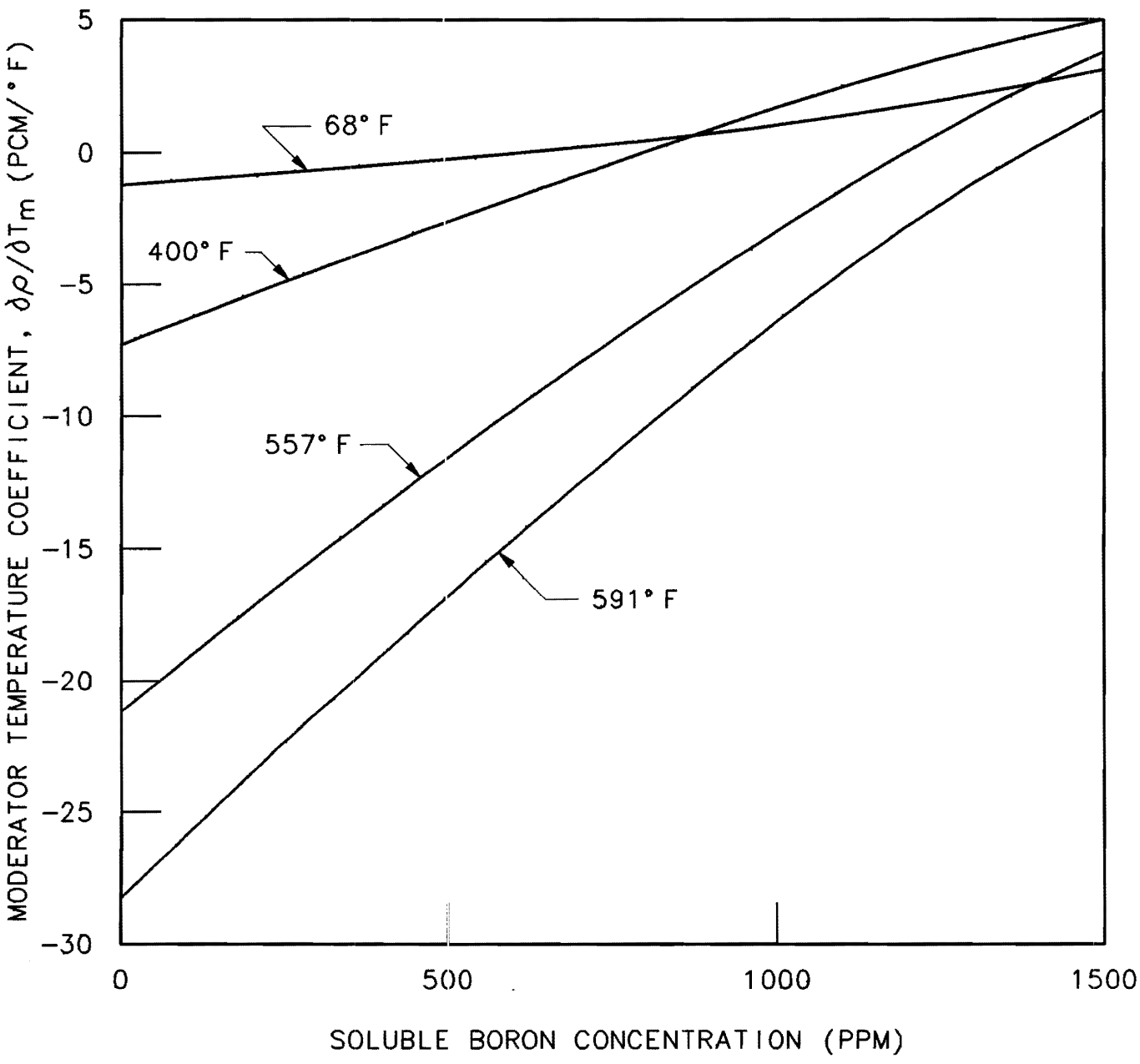


AMENDMENT 73

WATTS BAR NUCLEAR PLANT
FINAL SAFETY
ANALYSIS REPORT

MODERATOR TEMPERATURE
COEFFICIENT AS A FUNCTION
OF BORON CONCENTRATION –
BOL CYCLE 1, NO RODS,
(TYPICAL)

FIGURE 4.3–32

**Figure 4.3-32 Moderator Temperature Coefficient as a Function of Boron Concentration - BOL Cycle 1, No Rods, (Typical)**

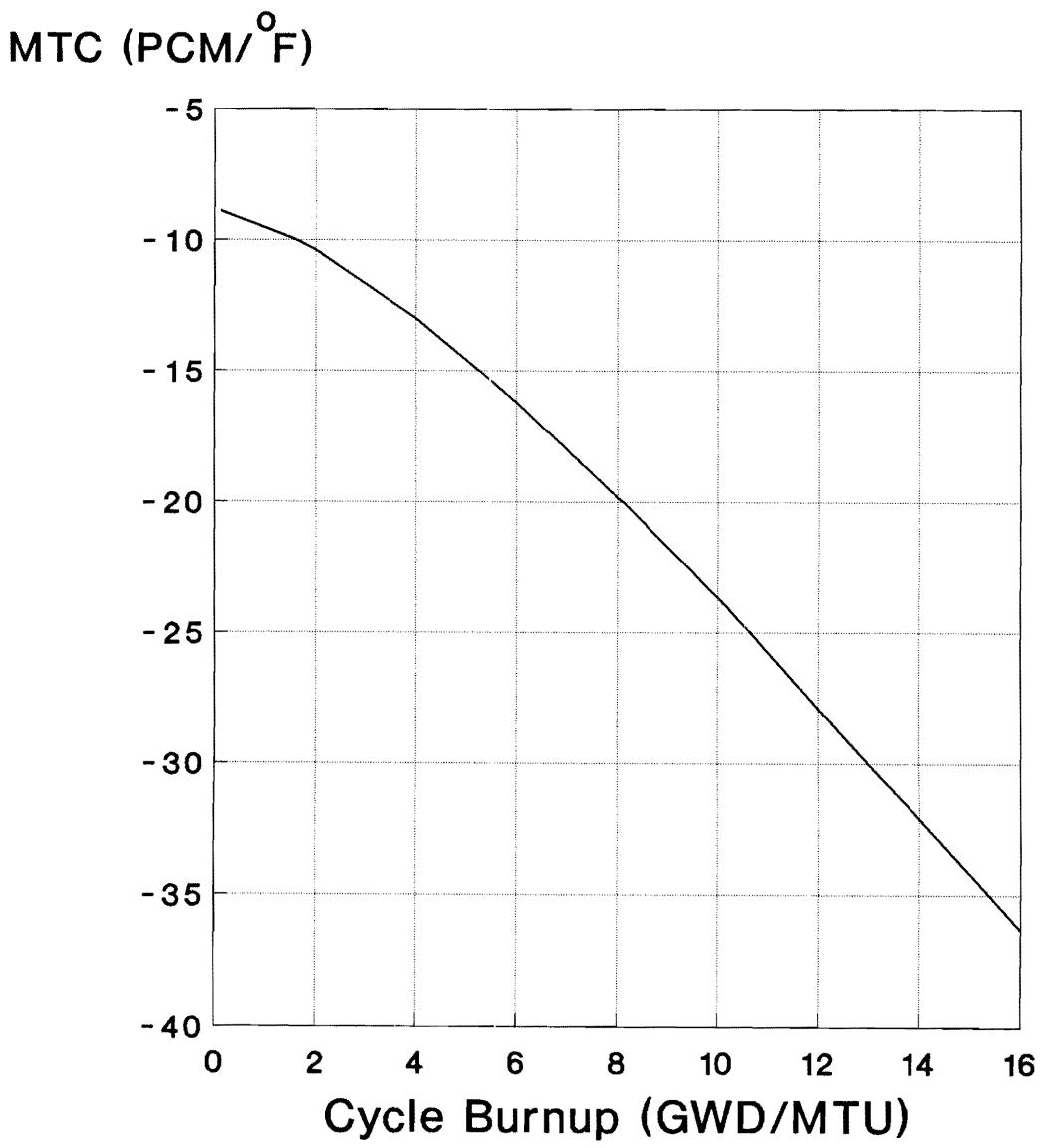


Amendment 73

| WATTS BAR<br>FINAL SAFETY ANALYSIS REPORT |
|---|
| MODERATOR TEMPERATURE COEFFICIENT DURING CYCLE 1 AT HFP, ARO EQUILIBRIUM XENON, CRITICAL BORON CONDITION, TYPICAL<br>FIGURE 4.3-33 |

**Figure 4.3-33 Moderator Temperature Coefficient During Cycle 1 at HFP, ARO Equilibrium Xenon, Critical Boron Condition, Typical**

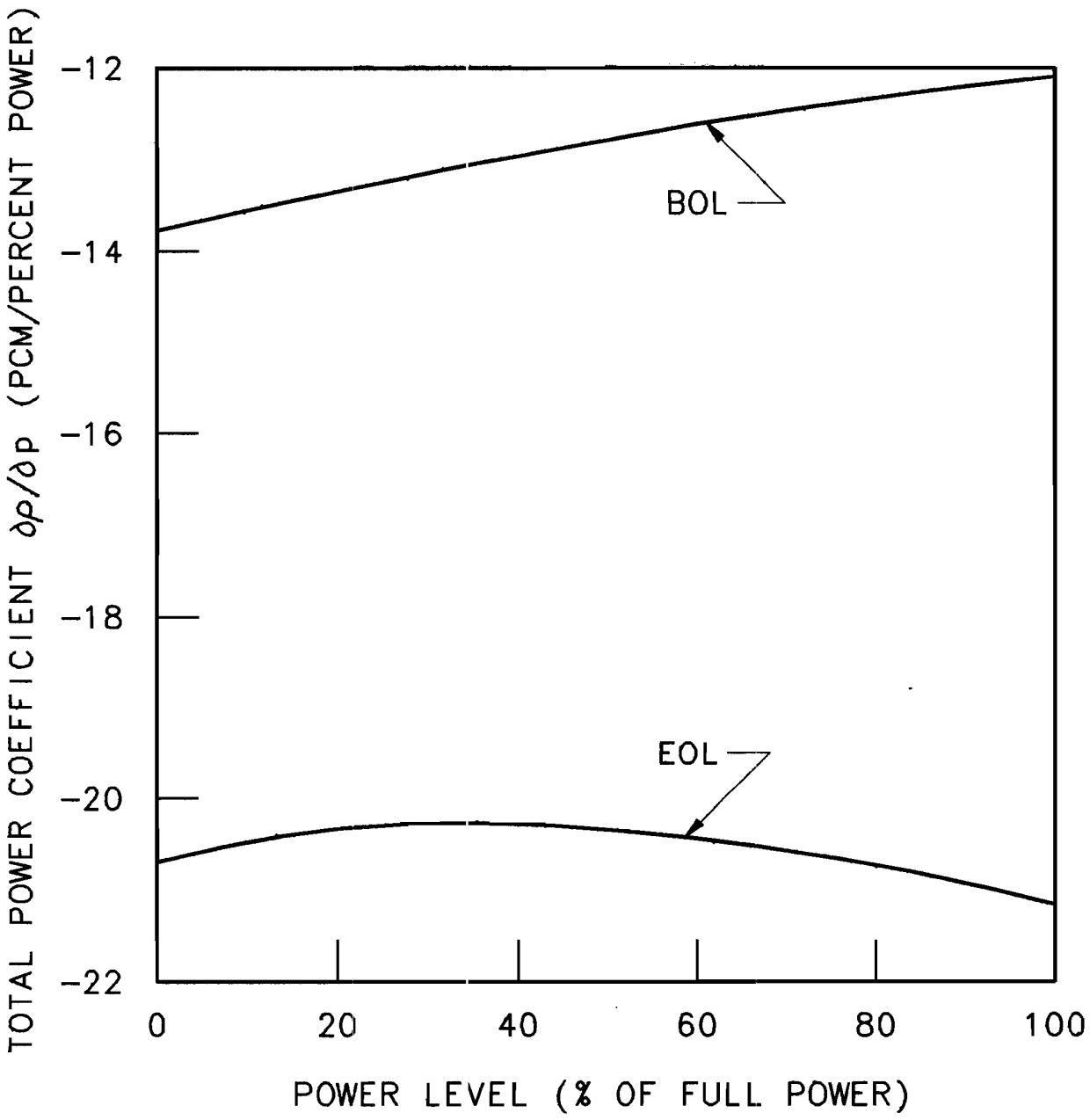


AMENDMENT 73

WATTS BAR NUCLEAR PLANT
FINAL SAFETY
ANALYSIS REPORT

TOTAL POWER COEFFICIENT-
BOL, EOL, CYCLE 1,
(TYPICAL)

FIGURE 4.3-34

**Figure 4.3-34 Total Power Coefficient - BOL, EOL, Cycle 1, (Typical)**

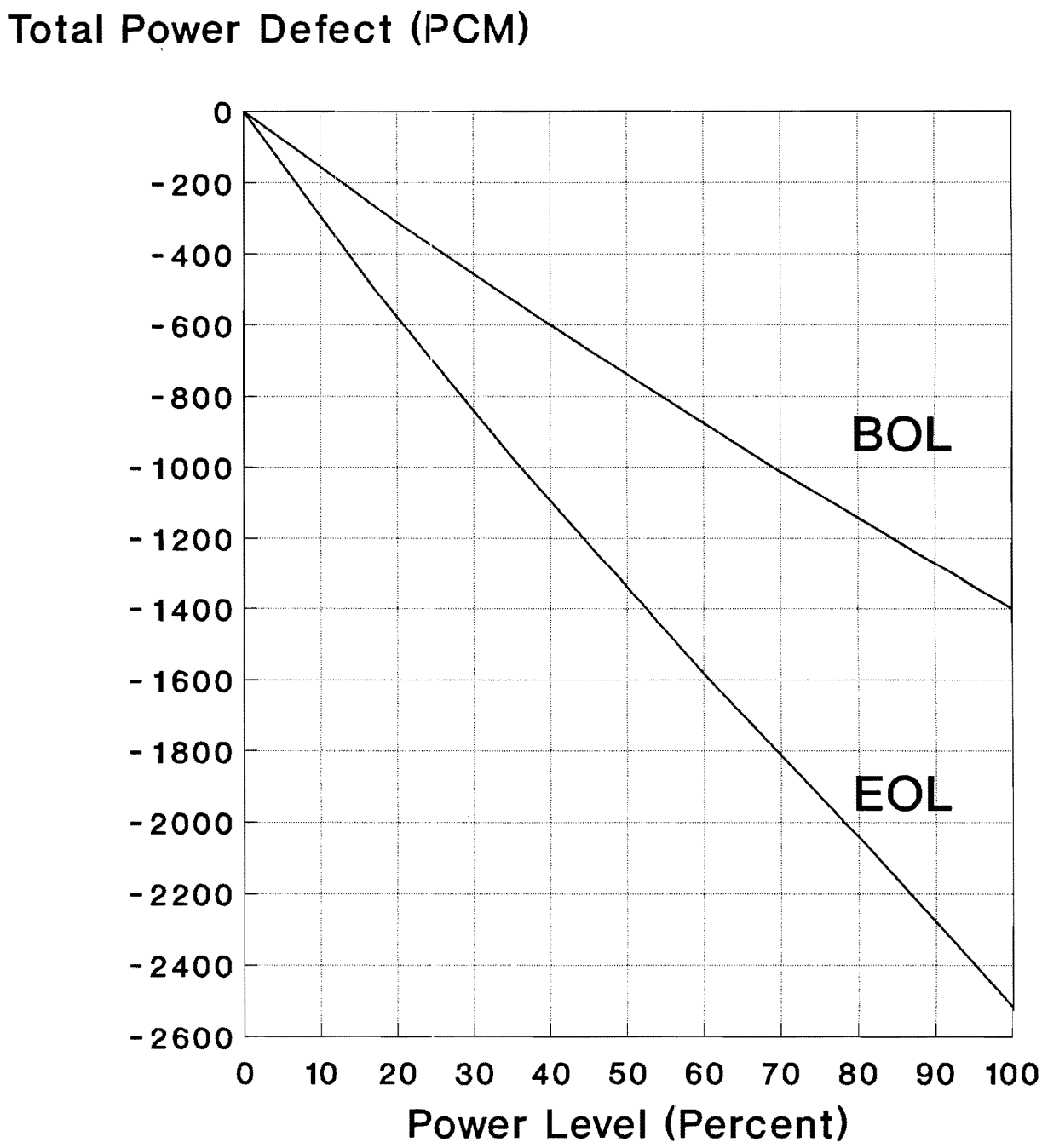


Amendment 73

| WATTS BAR<br>FINAL SAFETY ANALYSIS REPORT |
|---|
| TOTAL POWER DEFECT BOL, EOL,<br>CYCLE 1, TYPICAL<br>FIGURE 4.3-35 |

**Figure 4.3-35 Total Power Defect BOL, EOL, Cycle 1, Typical**

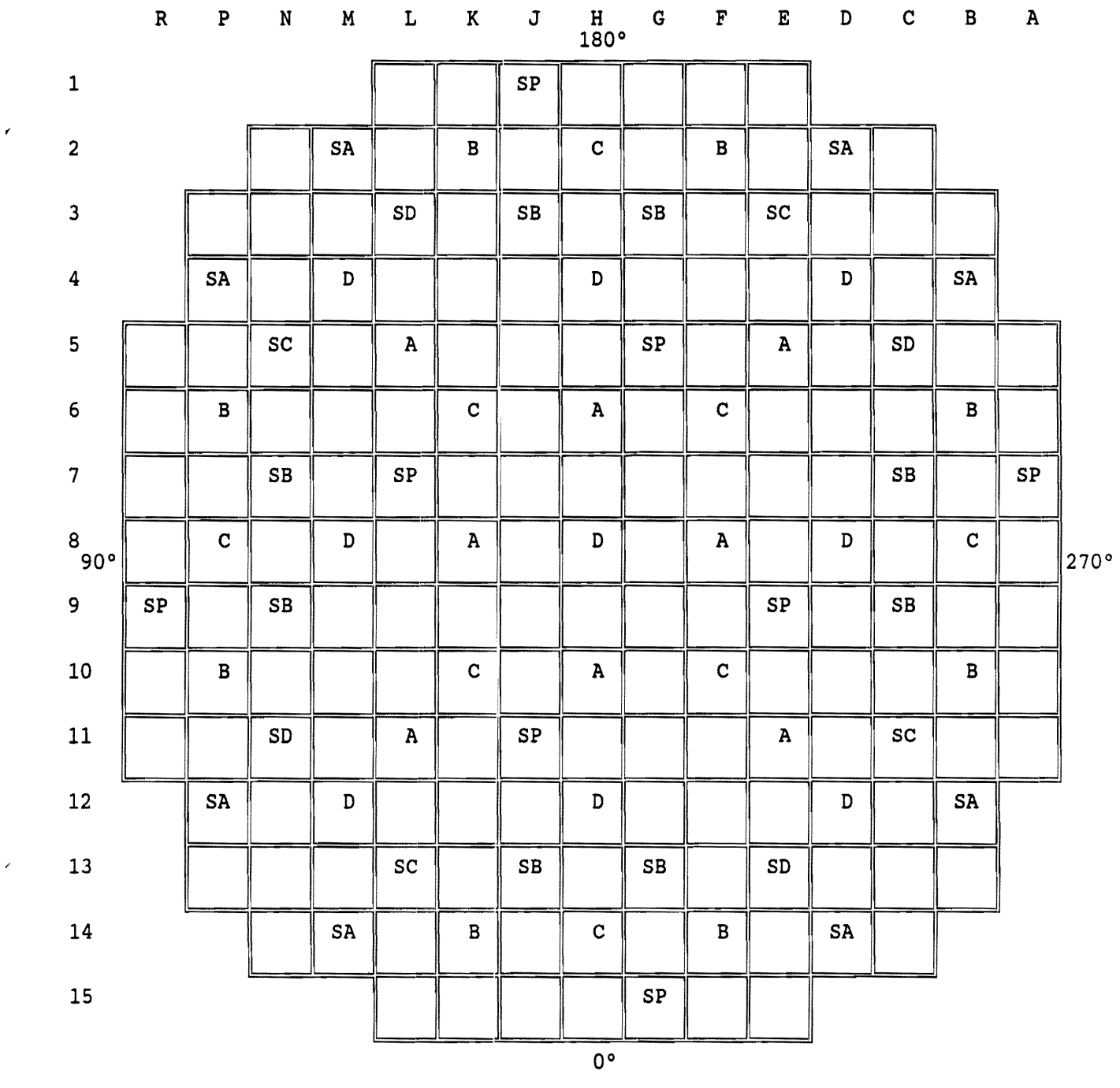


| BANK IDENTIFIER | NUMBER OF ROD CLUSTERS |
|---|---|
| CONTROL BANK A | 8 |
| CONTROL BANK B | 8 |
| CONTROL BANK C | 8 |
| CONTROL BANK D | 9 |
| SHUTDOWN BANK SA | 8 |
| SHUTDOWN BANK SB | 8 |
| SHUTDOWN BANK SC | 4 |
| SHUTDOWN BANK SD | 4 |
| SPARE SP | 8 |

Amendment 73

| WATTS BAR<br>FINAL SAFETY ANALYSIS REPORT |
|---|
| ROD CLUSTER CONTROL ASSEMBLY<br>PATTERN<br>FIGURE 4.3-36 |

**Figure 4.3-36 Rod Cluster Control Assembly Pattern**

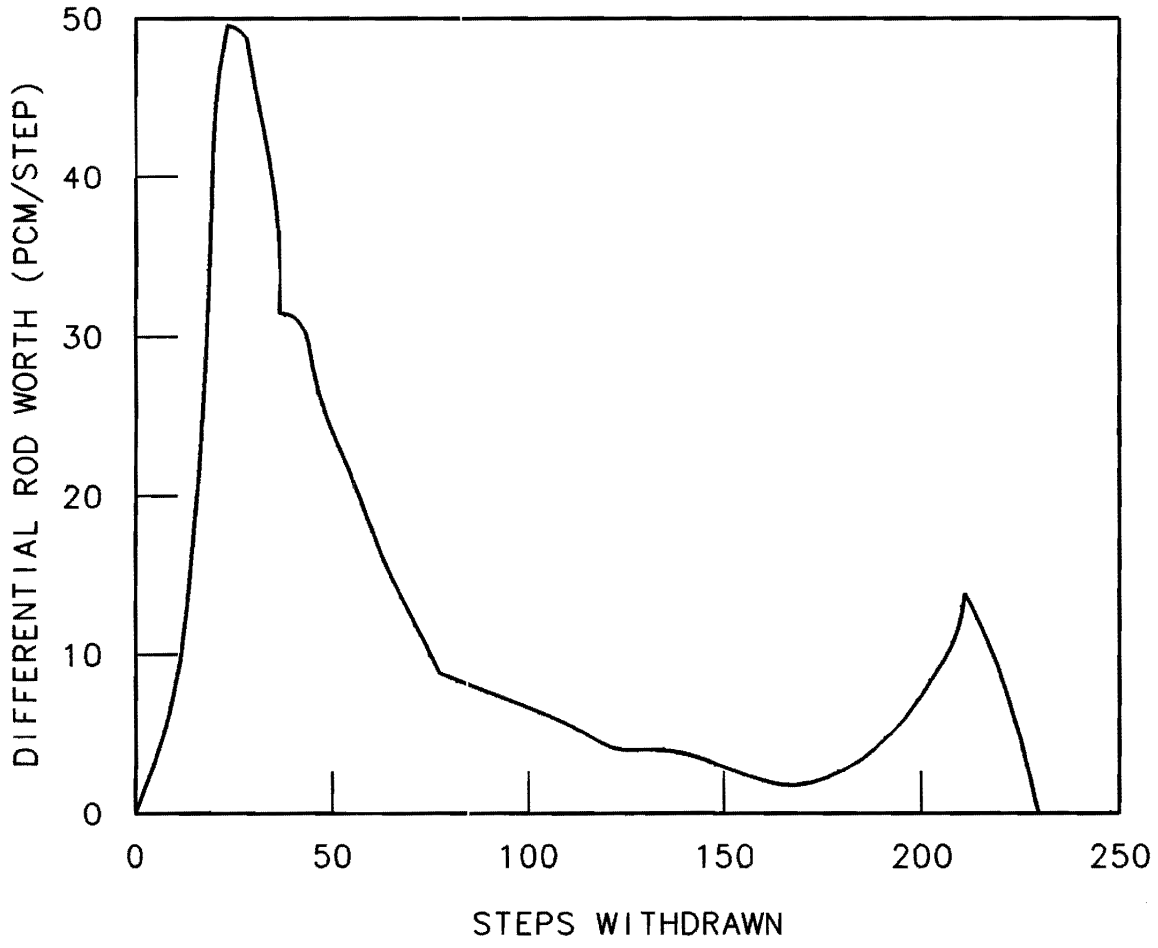


AMENDMENT 73

WATTS BAR NUCLEAR PLANT
FINAL SAFETY
ANALYSIS REPORT

ACCIDENTAL SIMULTANEOUS
WITHDRAWAL OF TWO CONTROL
BANKS EOL, HZP,
BANKS D AND B MOVING IN
THE SAME PLANE, (TYPICAL)

FIGURE 4.3-37

**Figure 4.3-37 Accidental Simultaneous Withdrawal of Two Control Banks EOL, HZP, Banks D and B Moving in the Same Plane, (Typical)**

**Figure 4.3-38 Deleted by Amendment 73**

**Figure 4.3-39 Deleted by Amendment 73**

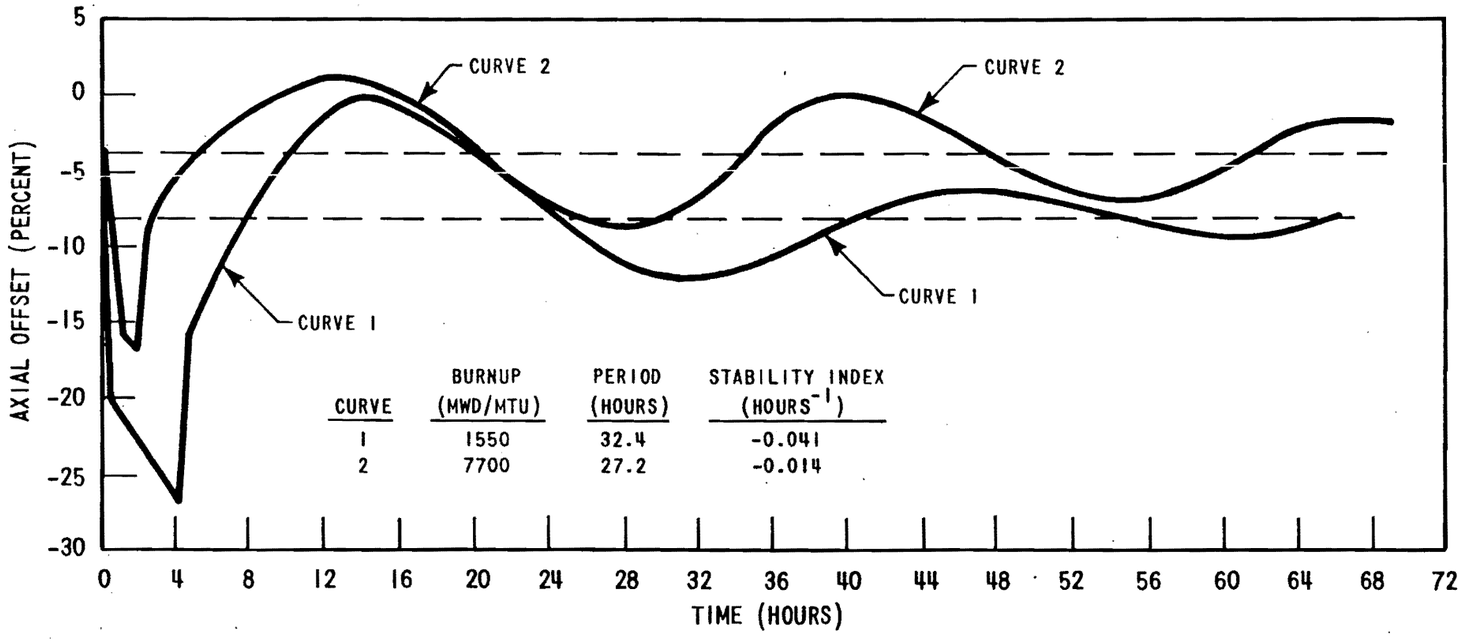


Figure 4.3-40 Axial Offset versus Time PWR Core with a 12-Ft Height and 121 Assemblies

Figure 4.3-40 Axial Offset versus Time PWR Core with a 12 ft. Height and 121 Assemblies

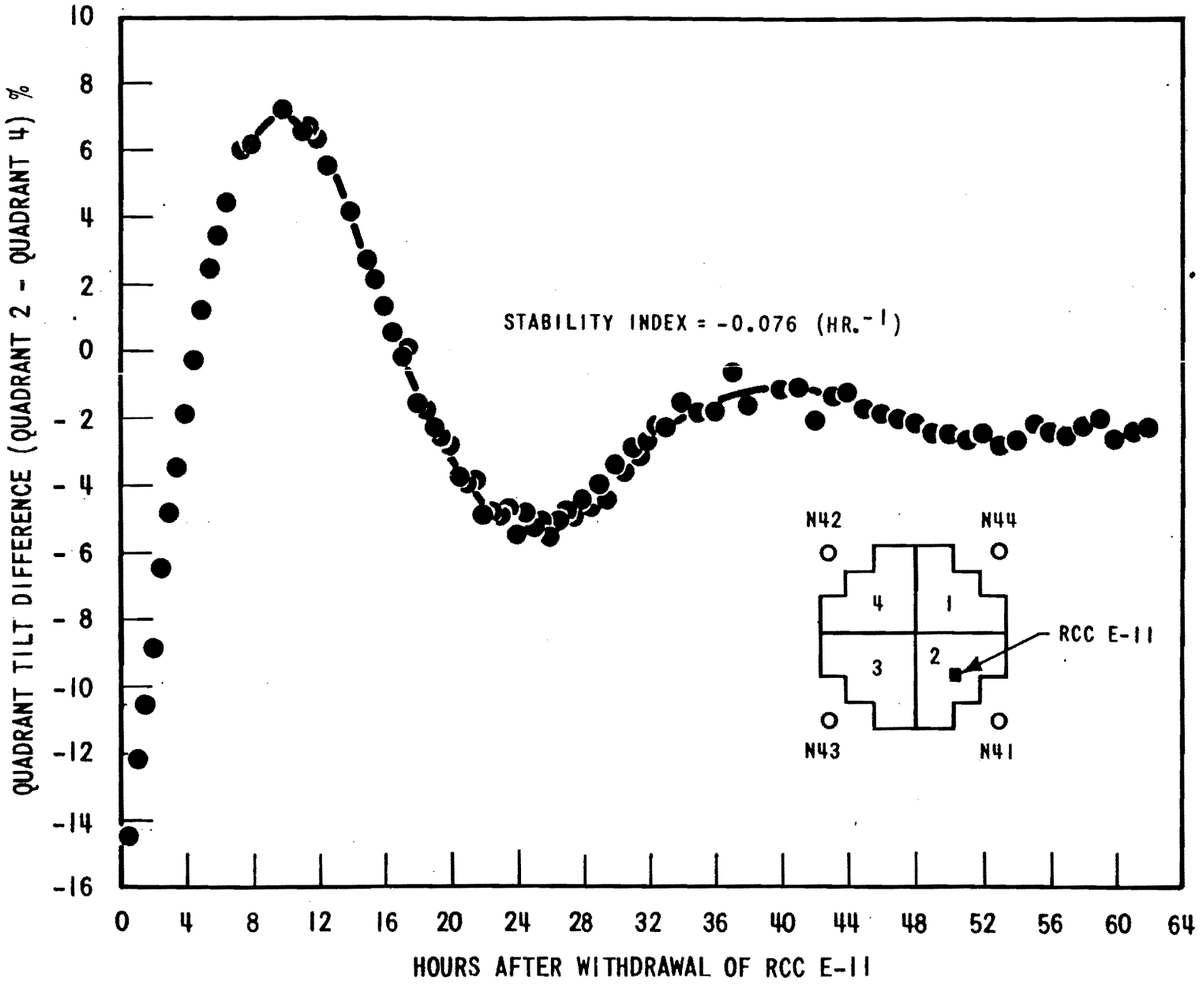


Figure 4.3-41 XY Xenon Test Thermocouple Response Quadrant Tilt Difference versus Time

**Figure 4.3-41 XY Xenon Test Thermocouple Response Quadrant Tilt Difference versus Time**

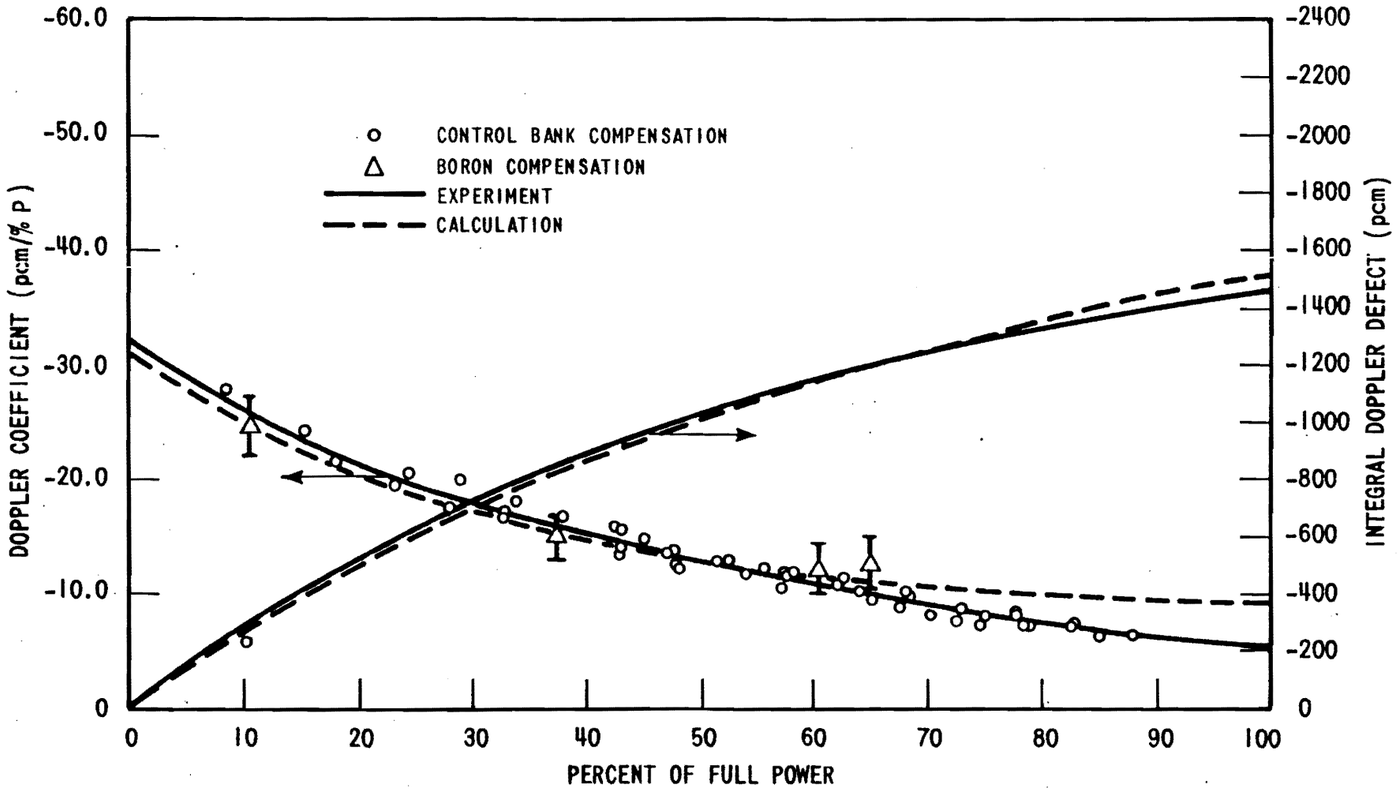


Figure 4.3-42 Calculated and Measured Doppler Defect and Coefficients at BOL, Two-Loop Plant, 121 Assemblies, 12-Foot Core

**Figure 4.3-42 Calculated and Measured Doppler Defect and Coefficients at BOL Two-Loop Plant, 121 Assemblies, 12 -felot Core**

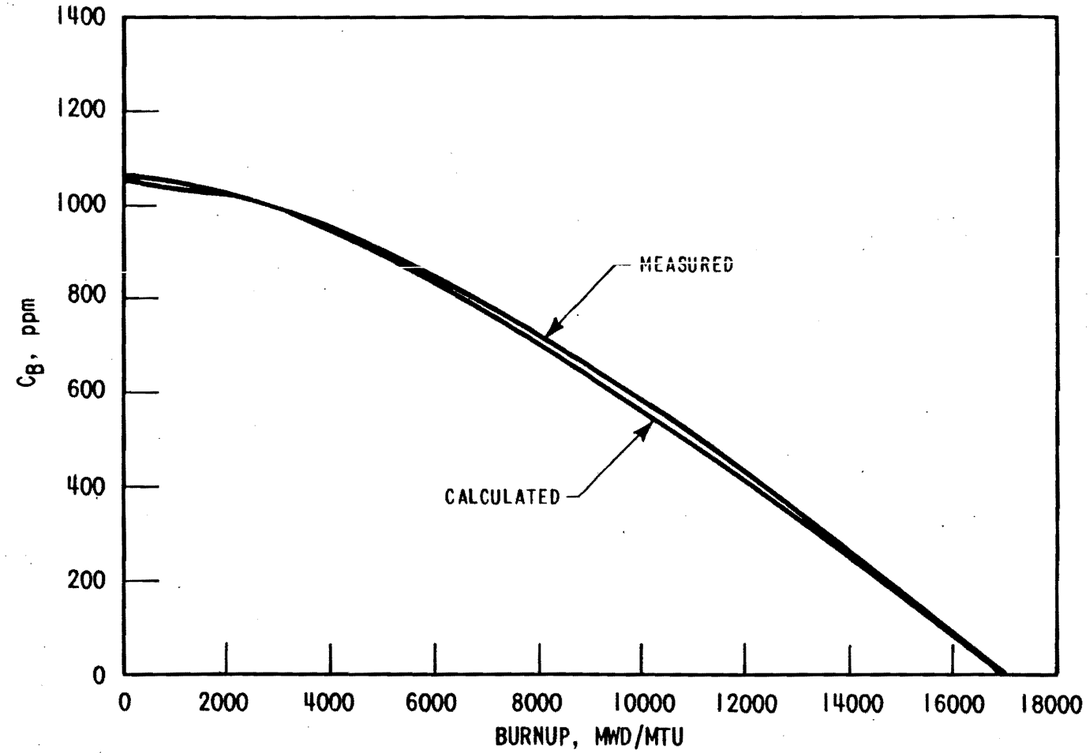


Figure 4.3-43 Comparison of Calculated and Measured Boron Concentration for 2-Loop Plant, 121 Assemblies, 12 Foot Core

**Figure 4.3-43 Comparison of Calculatedancl Measured Boron Concentration for 2-Loop Plant, 121 Assemblies, 12-foot Core**

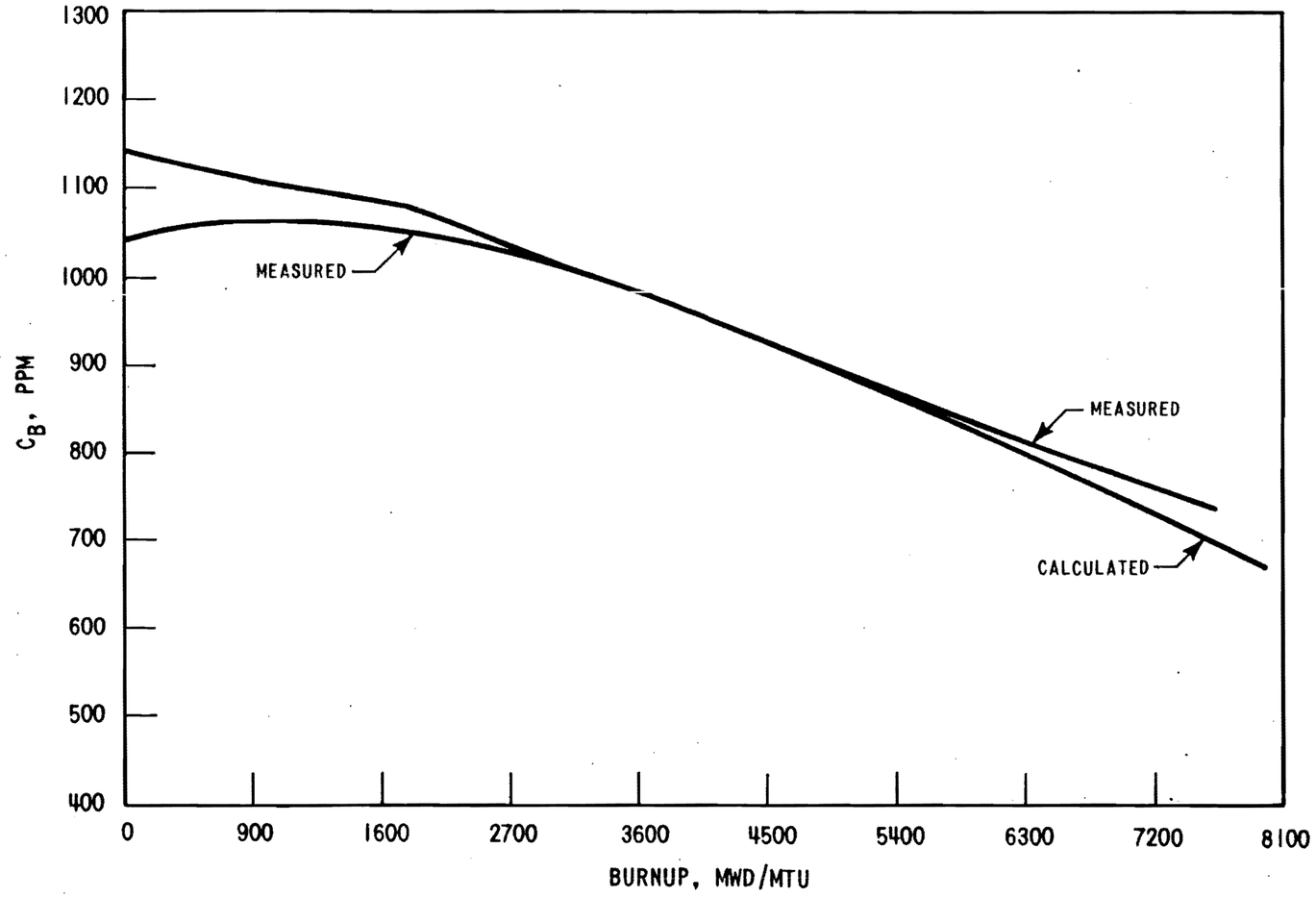


Figure 4.3-44 Comparison of Calculated and Measured $C_B$ 2-Loop with 121 Assemblies, 12 Foot Core

Figure 4.3-44 Comparison of Calculated and Measured $C_B$ 2-Loop with 121 Assemblies, 12-Foot Core

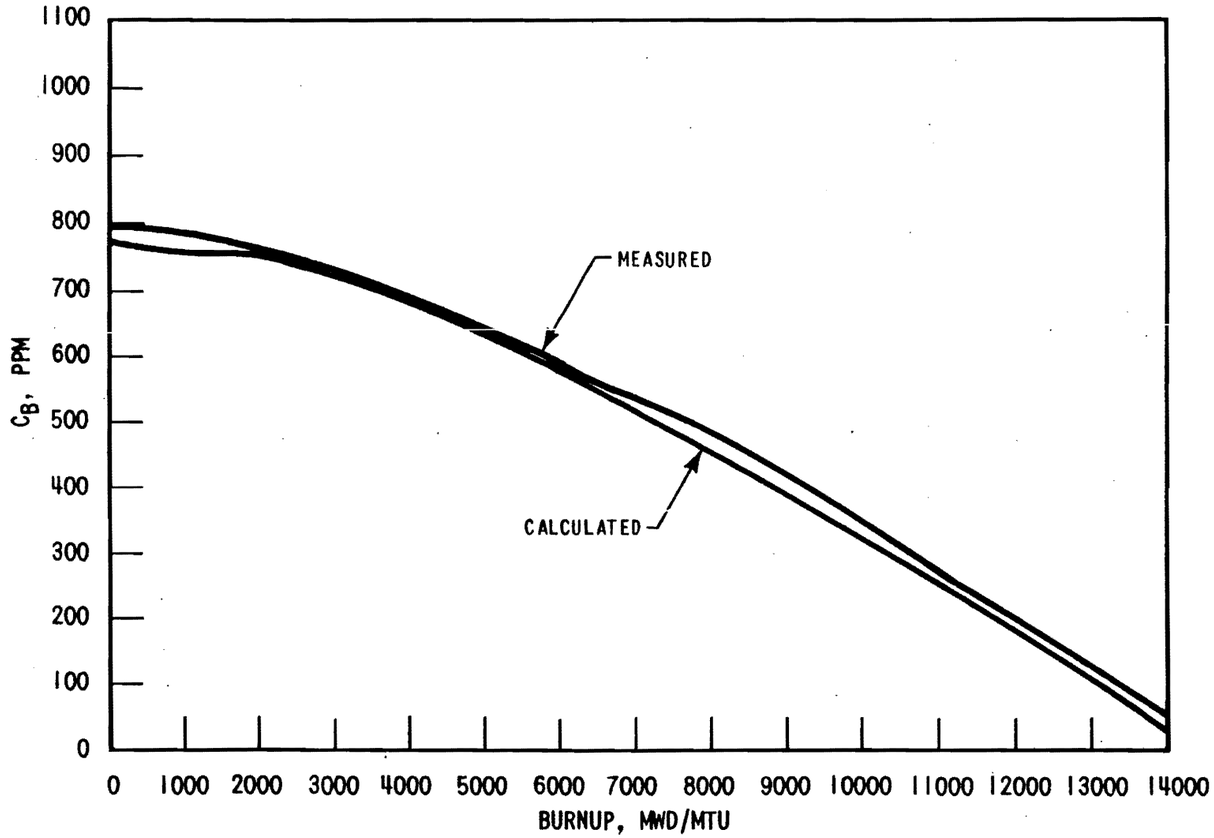


Figure 4.3-45 Comparison of Calculated and Measured $C_B$ in 3-Loop Plant, 157 Assemblies, 12 Foot Care

**Figure 4.3-45 Comparison of Calculated and Measured $C_B$ in 3-Loop Plant, 157 Assemblies, 12 -Foot Core**

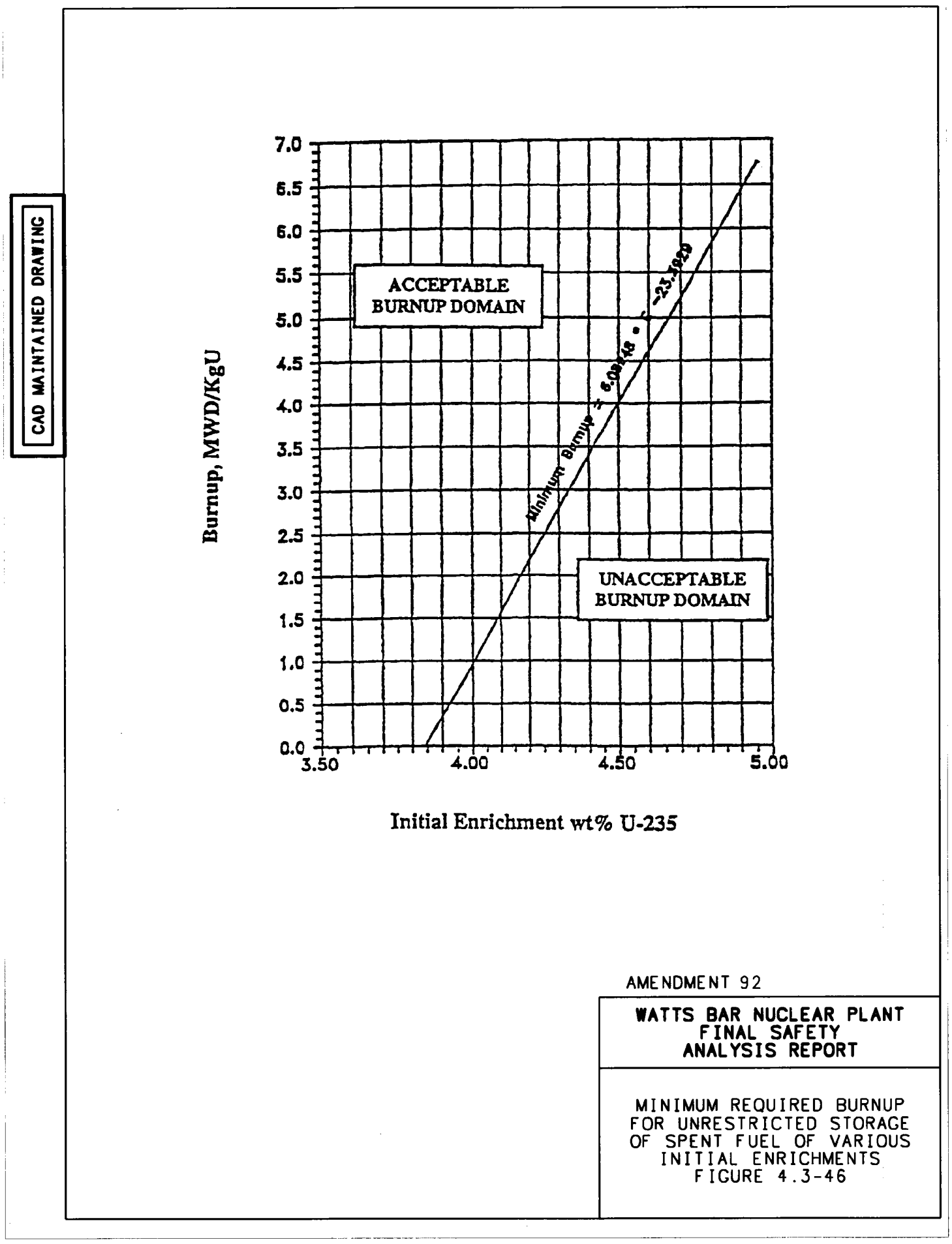


**Figure 4.3-46 Minimum Required Burnup for Unrestricted Storage of Spent Fuel of Various Initial Enrichments**

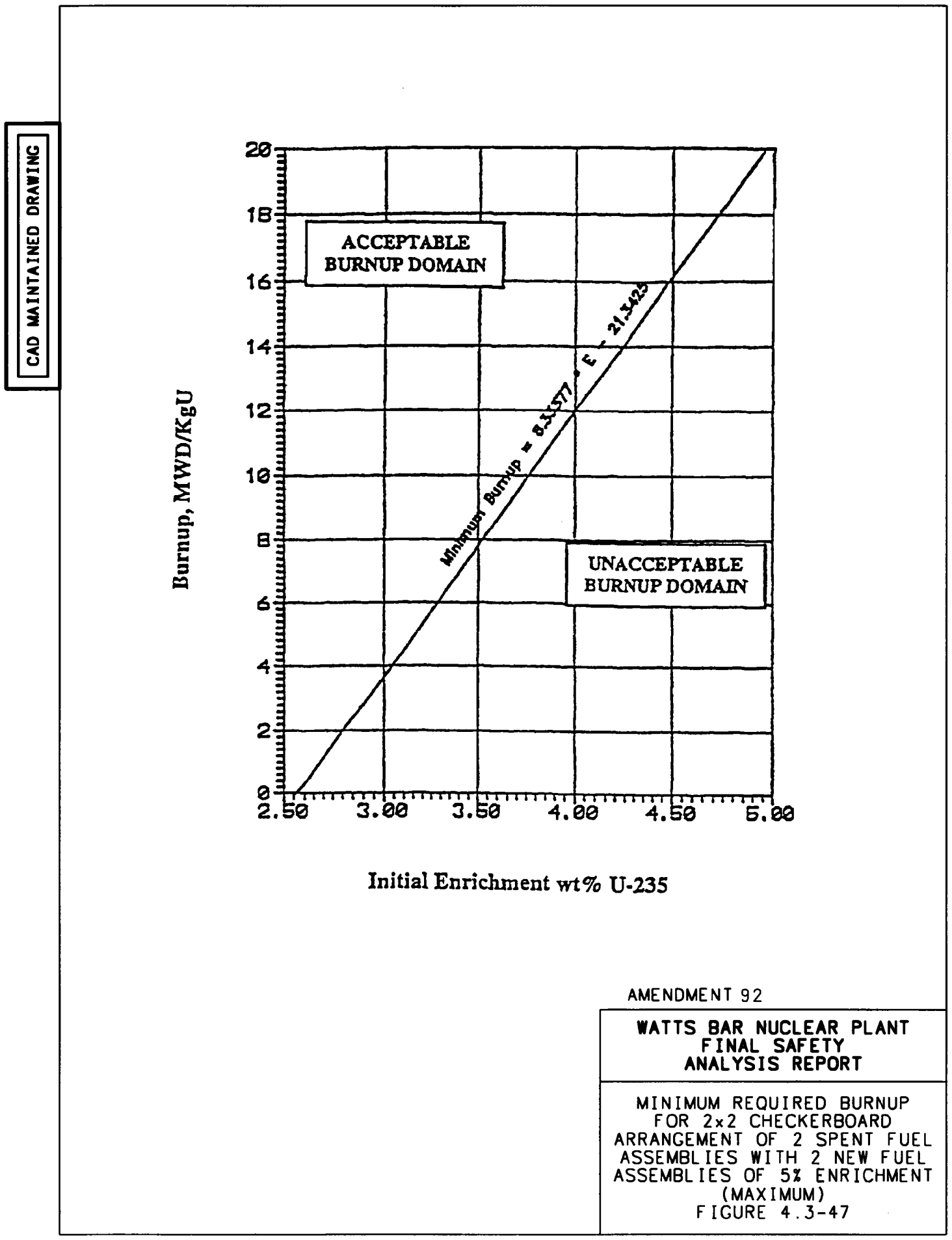


**Figure 4.3-47 Minimum Required Burnup for 2x2 Checkerboard Arrangement of 2 Spent Fuel Assemblies with 2 New Fuel Assemblies of 5% Enrichment (Maximum)**

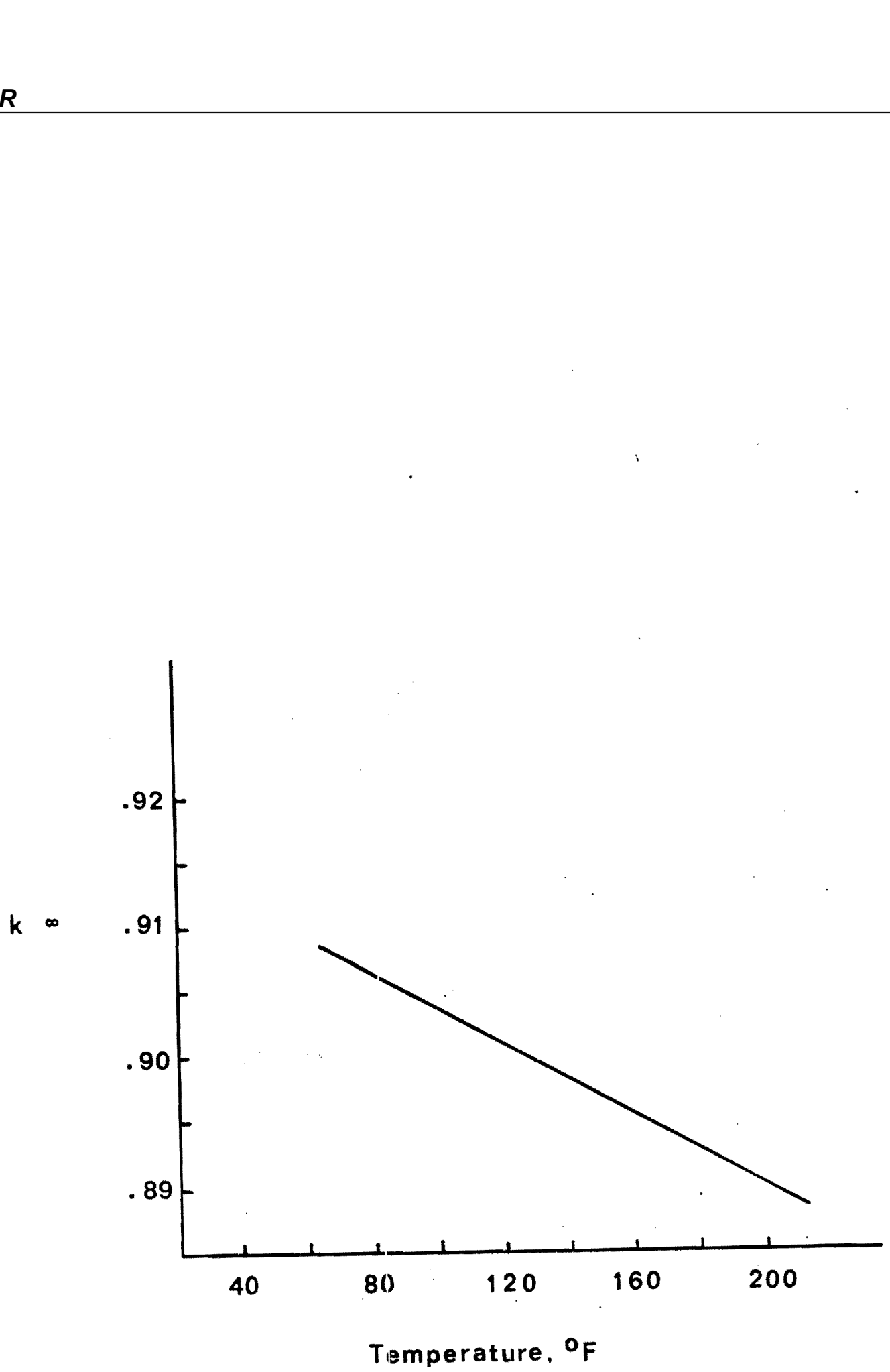


| WATTS BAR NUCLEAR PLANT<br>FINAL SAFETY<br>ANALYSIS REPORT |
|---|
| SPENT FUEL STORAGE RACK k∞<br>vs<br>TEMPERATURE<br>FIGURE 4.3-48<br>ADDED BY AMENDMENT 40 |

**Figure 4.3-48 Spent Fuel Storage Rack $k^{oo}$ vs Temperature**

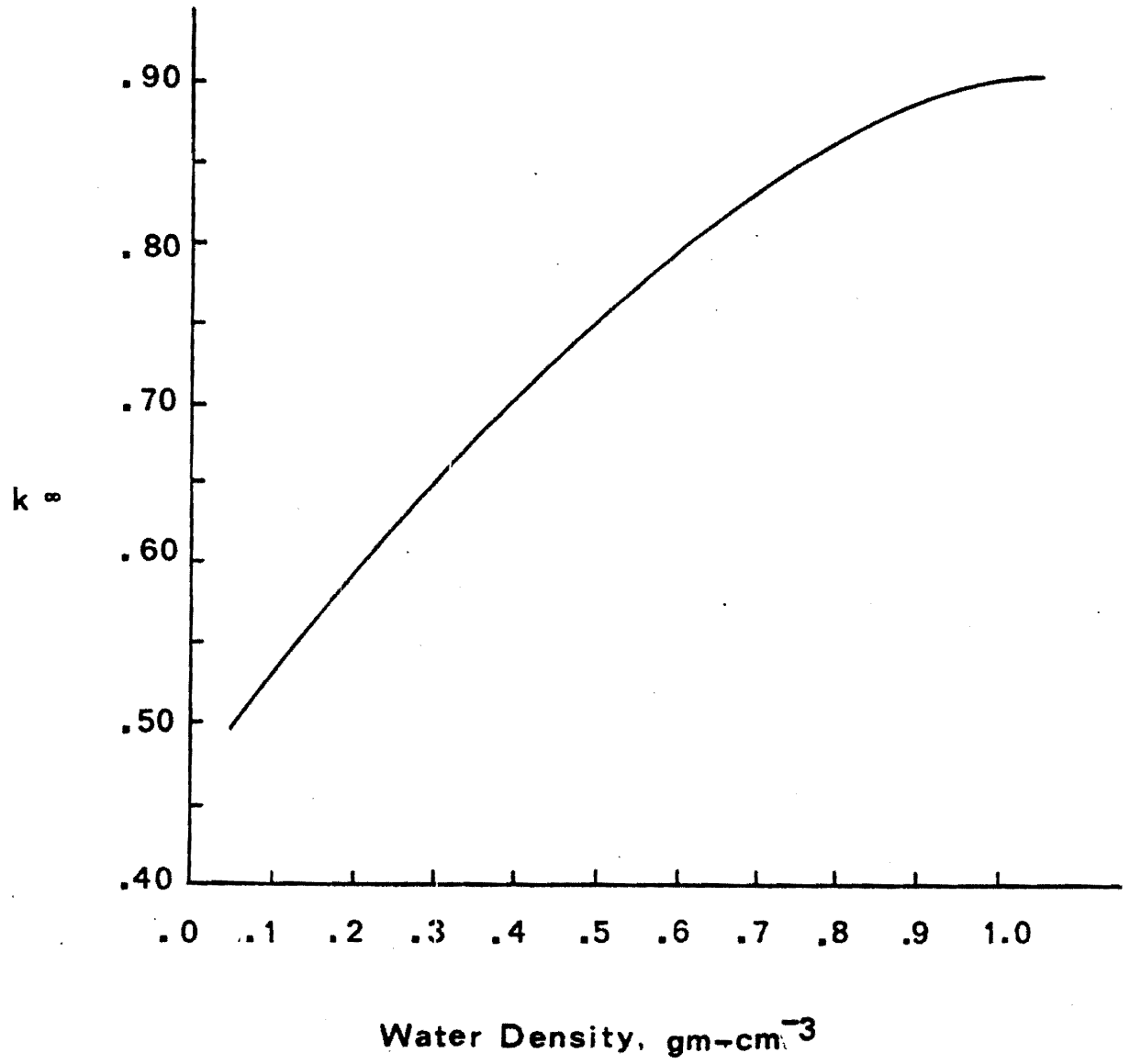


WATTS BAR NUCLEAR PLANT
FINAL SAFETY
ANALYSIS REPORT

SPENT FUEL STORAGE RACK k∞
vs
WATER DENSITY
FIGURE 4.3-49
ADDED BY AMENDMENT 40

**Figure 4.3-49 Spent Fuel Storage Rack $k^{oo}$ vs Water Density**

THIS PAGE INTENTIONALLY BLANK

## 4.4 THERMAL AND HYDRAULIC DESIGN

### 4.4.1 Design Bases

The overall objective of the thermal and hydraulic design of the reactor core is to provide adequate heat transfer which is compatible with the heat generation distribution in the core such that heat removal by the Reactor Coolant System or the Emergency Core Cooling System (when applicable) assures that the following performance and safety criteria requirements are met:

*(1)* Fuel damage (defined as penetration of the fission product barrier, i.e., the fuel rod clad) is not expected during normal operation and operational transients (Condition I) or any transient conditions arising from faults of moderate frequency (Condition II). It is not possible however, to preclude a very small number of rod failures. These will be within the capability of the plant cleanup system and are consistent with the plant design bases.

*(2)* The reactor can be brought to a safe state following a Condition III event with only a small fraction of fuel rods damaged (see above definition) although sufficient fuel damage might occur to preclude resumption of operation without considerable outage time.

*(3)* The reactor can be brought to a safe state and the core can be kept subcritical with acceptable heat transfer geometry following transients arising from Condition IV events.

In order to satisfy the above criteria, the following design bases have been established for the thermal and hydraulic design of the reactor core.

#### 4.4.1.1 Departure from Nucleate Boiling Design Basis

**Basis**

There will be at least a 95% probability that departure from nucleate boiling (DNB) will not occur on the limiting fuel rods during normal operation and operational transients and any transient conditions arising from faults of moderate frequency (Condition I and II events) at a 95% confidence level. Historically, this criterion has been met by adhering to the following thermal design basis: there must be at least a 95% probability that the minimum departure from nucleate boiling ratio (DNBR) of the limiting power rod during Condition I and II events is greater than or equal to the DNBR limit of the DNB correlation being used. The DNBR limit for the correlation is established based on the variance of the correlation such that there is a 95% probability with 95% confidence that DNB will not occur when the calculated DNBR is at the DNBR limit.

**Discussion**

Historically, the DNBR limit has been 1.30 for Westinghouse applications. In this application, the WRB-1 correlation [91] is employed. With the significant improvement in the accuracy of the critical heat flux prediction by using the WRB-1 correlation

instead of previous DNB correlations, a DNBR limit of 1.17 is applicable for the VANTAGE 5H fuel assembly [92].

DNBR margin is maintained for the VANTAGE 5H fuel by performing the DNB safety analysis which uses the WRB-1 correlation to a DNBR limit of 1.31. Comparing this safety analysis limit of 1.31 to the WRB-1 correlation limit of 1.17 results in 10.7% DNBR margin.

By preventing DNB, adequate heat transfer is assured between the fuel clad and the reactor coolant, thereby preventing clad damage as a result of inadequate cooling. Maximum fuel rod surface temperature is not a design basis as it will be within a few degrees of coolant temperature during operation in the nucleate boiling region. Limits provided by the nuclear control and protection systems are such that this design basis will be met for transients associated with Condition II events, including overpower transients. There is an additional large DNBR margin at rated power operation and during normal operating transients.

### 4.4.1.2 Fuel Temperature Design Basis

#### Basis

During modes of operation associated with Condition I and Condition II events, the maximum fuel temperature shall be less than the melting temperature of $UO_2$. The $UO_2$ melting temperature for at least 95% of the peak kW/ft fuel rods will not be exceeded at the 95% confidence level. The melting temperature of $UO_2$ is taken as 5080°F[1] unirradiated and decreasing 58°F per 10,000 MWD/MTU. By precluding $UO_2$ melting, the fuel geometry is preserved and possible adverse effects of molten $UO_2$ on the cladding are eliminated. To preclude center melting and as a basis for overpower protection system setpoints, a calculated centerline fuel temperature of 4700°F has been selected as the overpower limit. This provides sufficient margin for uncertainties in the thermal evaluations as described in Section 4.4.2.10.1.

#### Discussion

Fuel rod thermal evaluations are performed at rated power, maximum overpower and during transients at various burnups. These analyses assure that this design basis as well as the fuel integrity design bases given in Section 4.2 are met. They also provide input for the evaluation of Condition III and IV faults given in Chapter 15.

### 4.4.1.3 Core Flow Design Basis

#### Basis

A minimum of 91.0% of the thermal flow rate will pass through the fuel rod region of the core and be effective for fuel rod cooling. Coolant flow through the thimble tubes as well as the leakage from the core barrel-baffle region into the core are not considered effective for heat removal.

**Discussion**

Core cooling evaluations are based on the thermal flow rate (minimum flow) entering the reactor vessel. A maximum of 9.0% of this value is allotted as bypass flow. This includes guide thimble cooling flow, head cooling flow, baffle leakage, and leakage to the vessel outlet nozzle.

### 4.4.1.4 Hydrodynamic Stability Design Bases

**Basis**

Modes of operation associated with Condition I and II events shall not lead to hydrodynamic instability as defined in Section 4.4.3.5.

### 4.4.1.5 Other Considerations

The above design bases together with the fuel clad and fuel assembly design bases given in Section 4.2.1.1 are sufficiently comprehensive so additional limits are not required.

Fuel rod diametral gap characteristics, moderator-coolant flow velocity and distribution, and moderator void are not inherently limiting. Each of these parameters is incorporated into the thermal and hydraulic models used to ensure the above mentioned design criteria are met. For instance, the fuel rod diametral gap characteristics change with time (see Section 4.2.1.3.1) and the fuel rod integrity is evaluated on that basis. The effect of the moderator flow velocity and distribution (see Section 4.4.2.3) and moderator void distribution (see Section 4.4.2.5) are included in the core thermal (THINC) evaluation and thus affect the design bases.

Meeting the fuel clad integrity criteria covers possible effects of clad temperature limitations. As noted in Section 4.2.1.3.1, the fuel rod conditions change with time. A single clad temperature limit for Condition 1 or Condition II events is not appropriate since of necessity it would be overly conservative. A clad temperature limit is applied to the loss of coolant accident (Section 15.4.1), control rod ejection accident[2] and locked rotor accident[3].

## 4.4.2 Description

### 4.4.2.1 Summary Comparison

The design of the Watts Bar Units 1 and 2 have the following identical thermal and hydraulic parameters as the W. B. McGuire reactor design:

*(1)* Core power

*(2)* System pressure

*(3)* Open lattice fuel rod array

*(4)* Vessel average coolant temperatures.

Values of each parameter are presented in Table 4.4-1 for all coolant loops in service. It is also noted that in this power capability evaluation, there has not been any change in the design criteria. The reactor is designed to meet the DNB design basis as well as no fuel centerline melting during normal operation, operational transients and faults of moderate frequency.

### 4.4.2.2 Fuel and Cladding Temperatures

Consistent with the thermal-hydraulic design bases described in Section 4.4.1, the following discussion pertains mainly to fuel pellet temperature evaluation. A discussion of fuel clad integrity is presented in Section 4.2.1.3.1.

The thermal-hydraulic design assures that the maximum fuel temperature is below the melting point of $UO_2$ (melting point of 5080°F [1] unirradiated and decreasing by 58° F per 10,000 MWD /MTU). To preclude center melting and as a basis for overpower protection system setpoints, a calculated centerline fuel temperature of 4700°F has been selected as the overpower limit.

This provides sufficient margin for uncertainties in the thermal evaluations as described in Section 4.4.2.10.1. The temperature distribution within the fuel pellet is predominantly a function of the local power density and the $UO_2$ thermal conductivity. However, the computation of radial fuel temperature distributions combines crud, oxide, clad gap and pellet conductances. The factors which influence these conductances, such as gap size (or contact pressure), internal gas pressure, gas composition, pellet density, and radial power distribution within the pellet, etc., have been combined into a semiempirical thermal model (see Section 4.2.1.3.1) which includes the model modifications for time-dependent fuel densification given in Reference [93]. This thermal model enables the determination of these factors and their net effects on temperature profiles. The temperature predictions have been compared to in-pile fuel temperature measurements[7 - 13] and [93] and melt radius data[14,15] with good results.

Fuel rod thermal evaluations (fuel centerline, average and surface temperatures) are performed at several times during the fuel rod lifetime (with consideration of time dependent densification) to determine the maximum fuel temperatures. The maximum fuel average and surface temperatures, shown in Figure 4.4-1 as a function of linear power density (kW/ft) are peak values attained during the fuel lifetime. Figure 4.4-2 presents the peak value of fuel centerline temperature versus linear power density which is attained during the fuel lifetime.

The maximum pellet temperatures at the hot spot during full power steady state and at the peak linear power for determination of protection setpoints are shown in Table 4.4-1. The principal factors which are employed in the determination of the fuel temperature are discussed below.

#### 4.4.2.2.1 $UO_2$ Thermal Conductivity

The thermal conductivity of uranium dioxide was evaluated from data reported in References [16] through [28].

At the higher temperatures, thermal conductivity is best obtained by utilizing the integral conductivity to melt, which can be determined with more certainty.

From an examination of the data it has been concluded that the best estimate for the value of is $\int_{t=0°C}^{t=2800°C} K dt$ 93 watts/cm. This conclusion is based on the integral values reported by Gyllander[28], Lyons, et al.[29], Coplin, et al.[30], Duncan[14], Bain[31], and Stora[32].

The design curve for the thermal conductivity is shown in Figure 4.4-3. The section of the curve at temperatures between O°C and 1300°C is in excellent agreement with the recommendation of the IAEA panel[33]. The section of the curve above 1300°C is derived for an integral value of 93 watts/cm[14,28,32].

Thermal conductivity for $UO_2$ at 95% theoretical density can be represented best by the following equation:

$$K = \frac{1}{11.8 + 0.0238T} + 8.775 \times 10^{-13} T^3 \qquad (4.4\text{-}1)$$

where:

K = watts/cm-°C

T = °C

### 4.4.2.2.2 Radial Power Distribution in $UO_2$ Fuel Rods

An accurate description of the radial power distribution as a function of burnup is needed for determining the power level for incipient fuel melting and other important performance parameters such as pellet thermal expansion, fuel swelling and fission gas release rates.

This information on radial power distributions in $UO_2$ fuel rods is determined with the neutron transport theory code, LASER. The LASER Code has been validated by comparing the code predictions on radial burnup and isotopic distributions with measured radial microdrill data[34,35]. A 'radial power depression factor', f, is determined using radial power distributions predicted by LASER. The factor, f, enters into the determination of the pellet center line temperature, $T_c$, relative to the pellet surface temperature, $T_s$, through the expression:

$$\int_{T_s}^{T_c} k(T)dT = \frac{q'f}{4\pi} \qquad (4.4\text{-}2)$$

K(T) = the thermal conductivity for $UO_2$ with a uniform density distribution

q' = the linear power generation rate.

#### 4.4.2.2.3 Gap Conductance

The temperature drop across the pellet-clad gap is a function of the gap size and the thermal conductivity of the gas in the gap. The gap conductance model is selected such that when combined with the $UO_2$ thermal conductivity model, the calculated fuel centerline temperatures reflect the in-pile temperature measurements. A discussion of the gap conductance model is presented in Reference [93].

#### 4.4.2.2.4 Surface Heat Transfer Coefficients

The fuel rod surface heat transfer coefficients during subcooled forced convection and nucleate boiling are presented in Section 4.4.2.8.1.

#### 4.4.2.2.5 Fuel Clad Temperatures

The outer surface of the fuel rod at the hot spot operates at a temperature of approximately 660°F for steady state operation at rated power throughout core life due to the onset of nucleate boiling. Initially (beginning-of-life), this temperature is that of the clad metal outer surface.

During operation over the life of the core, the buildup of oxides and crud on the fuel rod surface causes the clad surface temperature to increase. Allowance is made in the fuel center melt evaluation for this temperature rise. Since the thermal-hydraulic design basis limits DNB, adequate-heat transfer is provided between the fuel clad and the reactor coolant so that the core thermal output is not limited by considerations of clad temperature.

#### 4.4.2.2.6 Treatment of Peaking Factors

The total heat flux hot channel factor, $F_Q$, is defined by the ratio of the maximum to core average heat flux and is presented in Table 4.3-2 and discussed in Section 4.3.2.2.6.

This results in a peak local power of 5.45 kW/ft X $F_Q$ at full-power conditions. As described in Section 4.3.2.2.6, the peak linear power for determination of protection setpoints is 21.1 kW/ft. The center line temperature at this kW/ft must be below the $UO_2$ melt temperature over the lifetime of the rod, including allowances for uncertainties. The fuel temperature design basis is discussed in Subsection 4.4.1.2 and results in a maximum allowable calculated centerline temperature of 4700 °F. The peak linear power for prevention of centerline melt is > 21.1 kW/ft. The centerline temperature at the peak linear power resulting from overpower transients/overpower errors (assuming a maximum overpower of 118%) is below that required to produce melting. Fuel centerline and average temperature at rated (100%) power and at the peak linear power for the determination of protection setpoints are presented in Table 4.4-1.

### 4.4.2.3 Critical Heat Flux Ratio or Departure from Nucleate Boiling Ratio and Mixing Technology

The minimum DNBR's for the rated power, design overpower and anticipated transient conditions are given in Table 4.4-1. The minimum DNBR in the limiting flow channel will be downstream of the peak heat flux location (hot spot) due to the increased down stream enthalpy rise.

DNBR's are calculated by using the correlation and definitions described in the following Sections 4.4.2.3.1 and 4.4.2.3.2. The THINC-IV computer code (discussed in Section 4.4.3.4.1) is used to determine the flow distribution in the core and the local conditions in the hot channel for use in the DNB correlation. The use of hot channel factors is discussed in Section 4.4.3.2.1 (nuclear hot channel factors) and in Section 4.4.2.3.4 (engineering hot channel factors).

### 4.4.2.3.1 Departure from Nucleate Boiling Technology

Early experimental studies of DNB were conducted with fluid flowing inside single heated tubes or channels and with single annulus configurations with one or both walls heated. The results of the experiments were analyzed using many different physical models for describing the DNB phenomenon, but all resultant correlations are highly empirical in nature. The evolution of these correlations is given by Tong[38,39] including the W-3 correlation which is in wide use in the PWR industry.

As testing methods progressed to the use of rod bundles, instead of single channels, it became apparent that the bundle average flow conditions cannot be used in DNB correlations. As outlined by Tong[40] test results showed that correlations based on average conditions were not accurate predictors of DNB heat flux. This indicated that a knowledge of the local subchannel conditions within the bundle is necessary.

In order to determine the local subchannel conditions, the THINC[41] computer code was developed. In the THINC code, a rod bundle is considered to be an array of subchannels each of which includes the flow area formed by four adjacent rods. The subchannels are also divided into axial steps such that each may be treated as a control volume. By solving simultaneously the mass, energy, and momentum equations, the local fluid conditions in each control volume are calculated. The W-3 correlation, developed from single channel data, can be applied to rod bundles by using the subchannel local fluid conditions calculated by the THINC code.

It was shown by Tong[40] that the above approach yielded conservative predictions particularly in rod bundles with mixing vane grid spacers.

The WRB-1 correlation [91] was developed based exclusively on the large bank of mixing vane grid rod bundle CHF data (over 1100 points) that Westinghouse has collected. The WRB-1 correlation, based on local fluid conditions, represents the rod bundle data with better accuracy over a wide range of variables than the previous correlation used in design. This correlation accounts directly for both typical and thimble cold wall cell effects, uniform and nonuniform heat flux profiles, and variations in rod heated length and in grid spacing.

The applicable range of parameters for the WRB-1 correlation is:

| | |
|---|---|
| Pressure: | $1440 \leq P \leq 2490$ psia |
| Local Mass Velocity: | $0.9 \times 10^6 \leq C_{loc} \leq 3.7 \times 10^6$ lb/ft$^2$-hr |
| Local Quality: | $-0.2 \leq X_{loc} \leq 0.3$ |
| Heated Length, Inlet to CHF Location: | $L_h \leq 14$ feet |
| Grid Spacing: | $13 \leq g_{sp} \leq 32$ inches |
| Equivalent Hydraulic Diameter: | $0.37 \leq d_e \leq 0.60$ inches |
| Equivalent Heated Hydraulic Diameter: | $0.46 \leq d_h \leq 0.59$ inches |

Figure 4.4-5 shows measured critical heat flux plotted against predicted critical heat flux using the WRB-1 correlation.

The WRB-1 correlation is the primary DNB correlation for the safety analysis of the VANTAGE 5H fuel in the Watts Bar Units. A correlation limit DNBR of 1.17 for the WRB-1 correlation has been approved by the NRC for VANTAGE 5H fuel [92].

The W-3 DNB correlation [39], [40] is used where the primary DNB correlation is not applicable. The WRB-1 correlation was developed based on mixing vane data and, therefore, is only applicable in the heated rod spans above the first mixing vane grid. The W-3 correlation, which does not take credit for mixing vane grids, is used to calculate DNBR values in the heated region below the first mixing vane grid. In addition, the W-3 correlation is applied in the analysis of accident conditions where the system pressure is below the range of the primary correlation. For system pressures in the range of 500 to 1000 psia, the W-3 correlation limit is 1.45 [94]. For system pressures greater than 1000 psia, the W-3 correlation limit is 1.30. A cold wall factor [43] is applied to the W-3 DNB correlation to account for the presence of the unheated thimble surfaces.

### 4.4.2.3.2 Definition of Departure from Nucleate Boiling Ratio

The DNB heat flux ratio (DNBR) as applied to typical cells (flow cells with all walls heated) and thimble cells (flow cells with heated and unheated walls) is defined as:

$$\mathrm{DNBR} = \frac{q_{D''NB,\,N}}{q_{loc}} \qquad 4.4\text{-}9$$

where:

$$q_{D''NB,N} = \frac{q_{D''NB,EU}}{F} \quad 4.4\text{-}10$$

and $q''_{DNB,EU}$ is the uniform DNB heat flux as predicted by the WRB-1 correlation or the W-3 DNB correlation (typical cell only).

F is the flux shape factor to account for nonuniform axial heat flux distributions[44] with the "C" term modified as in reference [39].

$q''_{loc}$ is the actual local heat flux.

The DNB heat flux ratio as applied to the W-3 DNB correlation when an unheated wall is present is:

$$DNBR = \frac{q_{D''NB,N,CW}}{q_{loc}} \quad 4.4\text{-}11$$

where:

$$q_{D''NB,N,CW} = \frac{q_{D''NB,EU,Dh} \text{ x } CWF}{F} \quad 4.4\text{-}12$$

where:

$q''_{DNB,EU,Dh}$ is the uniform DNB heat flux as predicted by the W-3 cold wall DNB correlation[39] when not all flow cell walls are heated (thimble cell).

$$CWF = 1.0 - R_u [13.76 - 1.372\, e^{1.78x} - 4.732 \left(\frac{G}{10^6}\right)^{-0.0535}$$

$$- 0.0619 \left[\frac{(P)}{1000}\right]^{0.14} - 8.509\, D_h^{0.107}] \quad 4.4\text{-}13$$

and $R_u = 1 - D_e/D_h$

The procedures used in the evaluation of DNB margin for this application show that the calculated minimum DNBR for the peak rod or rods in the core will be above the DNBR limit during Class I and II incidents, even when all the engineering hot channels factors described in Section 4.4.2.3.4 occur simultaneously in these channels. In reality the probability of this simultaneous occurrence is negligibly small and substantial increases in local heat flux or coolant temperature could be tolerated without violation of the design basis.

### 4.4.2.3.3 Mixing Technology

The rate of heat exchange by mixing between flow channels is proportional to the difference in the local mean fluid enthalpy of the respective channels, the local fluid density and flow velocity. The proportionality is expressed by the dimensionless thermal diffusion coefficient (TDC) which is defined as:

$$\mathrm{TDC} = \frac{W'}{\rho V A} \qquad 4.4\text{-}14$$

where:

W = flow exchange rate per unit length, lbm/ft-sec

ρ = fluid density, lbm/ft$^3$

V = fluid velocity, ft/sec

A = lateral flow area between channels per unit length ft$^2$/ft

The application of the TDC in the THINC analysis for determining the overall mixing effect or heat exchange rate is presented in reference [41].

As part of an ongoing research and development program, Westinghouse has sponsored and directed mixing tests at Columbia University[46]. These series of tests, using the "R" mixing vane grid design on 13, 26 and 32 inch grid spacing, were conducted in pressurized water loops at Reynolds numbers similar to that of a PWR core under the following single and two phase (subcooled boiling) flow conditions:

| | |
|---|---|
| Pressure | 1500 to 2400 psia |
| Inlet enthalpy | 303 to 638 Btu/lbm |
| Mass velocity | 0.954 to 3.8 x 10$^6$ lbm/hr-ft$^2$ |
| Reynolds number | 1.34 to 7.45 x 10$^5$ |
| Bulk outlet quality | -52.1 to -13.5% |

TDC is determined by comparing the THINC Code predictions with the measured subchannel exit temperatures. Data for 26 inch axial grid spacing are presented in Figure 4.4-8 where the thermal diffusion coefficient is plotted versus the Reynolds number. TDC is found to be independent of Reynolds number, mass velocity, pressure and quality over the ranges tested. The two phase data (local, subcooled boiling) fell within the scatter of the single phase data. The effect of two-phase flow on the value of TDC has been demonstrated by Cadek[46], Rowe and Angle[47,48], and Gonzalez - Santalo and Griffith[49]. In the subcooled boiling region the values of TDC were indistinguishable from the single phase values. In the quality region, Rowe and Angle show that in the case with rod spacing similar to that in PWR reactor core geometry, the value of TDC increased with quality to a point and then decreased, but never below the single phase value. Gonzalez - Santalo and Griffith showed that the mixing coefficient increased as the void fraction increased.

The data from these tests on the "R" grid showed that a design TDC value of 0.038 (for 26 inch grid spacing) can be used in determining the effect of coolant mixing in the THINC analysis.

A mixing test program similar to the one described above was conducted at Columbia University for the 17 x 17 geometry and mixing vane grids on 26 inch spacing[50]. The mean value of TDC obtained from these tests was 0.059, and all data was well above the current design value of 0.038.

Since the actual reactor grid spacing is approximately 20 inches, additional margin is available for this design, as the value of TDC increases as grid spacing decreases[46].

Zircaloy mixing vane grids are employed in the VANTAGE 5H fuel assembly. The VANTAGE 5H Zircaloy grid design is virtually identical to the 17x17 Inconel R-grid design in that the rod size, rod pitch, heated length and grid spacing are unchanged. Due to the change in grid material from Inconel to Zircaloy, the grid height and strap thickness have increased. However, the VANTAGE 5H Zircaloy grid was designed to preserve the important characteristics of the existing 17x17 type "R" mixing vane grid. Thus, the current conservative design value of TDC is applicable to the VANTAGE 5H fuel assembly design.

#### 4.4.2.3.4 Hot Channel Factors

The total hot channel factors for heat flux and enthalpy rise are defined as the maximum-to-core average ratios of these quantities. The heat flux hot channel factor considers the local maximum linear heat generation rate at a point (the hot spot), and the enthalpy rise hot channel factor involves the maximum integrated value along a channel (the hot channel).

Each of the total hot channel factors considers a nuclear hot channel factor (see Section 4.4.3.2) describing the neutron power distribution and an engineering hot channel factor, which allows for variations in flow conditions and fabrication tolerances. The engineering hot channel factors are made up of subfactors which account for the influence of the variations of fuel pellet diameter, density, enrichment and eccentricity, inlet flow distribution, flow redistribution, and flow mixing.

Heat Flux Engineering Hot Channel Factor, $F_Q^E$

The heat flux engineering hot channel factor is used to evaluate the maximum linear heat generation rate in the core. This subfactor is determined by statistically combining the fabrication variations for fuel pellet diameter, density, and enrichment and has a value of 1.03 at the 95-percent probability level with 95-percent confidence. As shown in Reference [87], no DNB penalty need be taken for the short, relatively low-intensity heat flux spikes caused by variations in the above parameters, as well as fuel pellet eccentricity and fuel rod diameter variation.

Enthalpy Rise Engineering Hot Channel Factor, $F_{\Delta H}^E$

The effect of variations in flow conditions and fabrication tolerances on the hot channel enthalpy rise is directly considered in the THINC core thermal subchannel analysis (see Section 4.4.3.4.1) under any reactor operating condition. The items considered contributing to the enthalpy rise engineering hot channel factor are discussed below:

*(1)* Pellet diameter, density and enrichment:

Design values employed in the THINC analysis related to the above fabrication variations are based on applicable limiting tolerances such that these design values are met for 95% of the limiting channels at a 95% confidence level. Measured manufacturing data on Westinghouse 17 x 17 fuel show the tolerances used in this evaluation are conservative. In addition, each fuel assembly is checked to assure the channel spacing design criteria are met. The effect of variations in pellet diameter and enrichment is employed in the THINC analysis as a direct multiplier on the channel enthalpy rise.

*(2)* Inlet Flow Maldistribution:

The consideration of inlet flow maldistribution in core thermal performances is discussed in Section 4.4.3.1.2. A design basis of 5% reduction in coolant flow to the hot assembly is used in the THINC-IV analysis.

*(3)* Flow Redistribution:

The flow redistribution accounts for the reduction in flow in the hot channel resulting from the high flow resistance in the channel due to the local or bulk boiling. The effect of the non-uniform power distribution is inherently considered in the THINC analysis for every operating condition which is evaluated.

*(4)* Flow Mixing:

The subchannel mixing model incorporated in the THINC Code and used in reactor design is based on experimental data[51] discussed in Section 4.4.3.4.1. The mixing vanes incorporated in the spacer grid design induce additional flow mixing between the various flow channels in a fuel assembly

as well as between adjacent assemblies. This mixing reduces the enthalpy rise in the hot channel resulting from local power peaking or unfavorable mechanical tolerances.

#### 4.4.2.3.5 Effects of Rod Bow on DNBR

The phenomenon of fuel rod bowing, as described in reference [88], must be accounted for in the DNBR safety analysis of Condition I and Condition II events. Applicable credits for margin resulting from retained conservatism in the evaluation of the DNBR and/or margin obtained from the measured plant operating parameters (such as $F_{\Delta H}^{E}$ or core flow) - which are less limiting than those required by the plant safety analysis - can be used to offset the effect of rod bow.

For the safety analysis of the Watts Bar Units, sufficient DNBR margin was maintained (see Section 4.4.1.1) to accommodate the full and low flow rod bow DNBR penalties identified in Reference [89]. The referenced penalties are applicable to VANTAGE 5H fuel assembly analyses using the WRB-1 DNB correlation.

The maximum rod bow penalties (< 1.5% DNBR) accounted for in the design safety analysis are based on an assembly average burnup of 24,000 MWD/MTU. At burnups greater than 24,000 MWD/MTU, credit is taken for the effect of $F_{\Delta H}^{N}$ burndown, due to the decrease in fissionable isotopes and the buildup of fission product inventory, and no additional rod bow penalty is required [95].

### 4.4.2.4 Flux Tilt Considerations

Significant quadrant power tilts are not anticipated during normal operation since this phenomenon is caused by some perturbation. For example, a dropped or misaligned RCCA could cause changes in the hot channel factors; however, these events are analyzed separately in Chapter 15. Other possible causes for quadrant power tilts include X-Y xenon transients, inlet temperature mismatches, enrichment variations within tolerances and so forth.

In addition to unanticipated quadrant power tilts as described above, other readily explainable asymmetries may be observed during calibration of the excore detector quadrant power tilt alarm. During operation, incore maps are taken at least once per month and, periodically, additional maps are obtained for calibration purposes. Each of these maps is reviewed for deviations from the expected power distributions. Asymmetry in the core, from quadrant to quadrant, is frequently a consequence of the design when assembly and/or component shuffling and rotation requirements do not allow exact symmetry preservation. In each case, the acceptability of an observed asymmetry, planned or otherwise, depends solely on meeting the required accident analyses assumptions.

In practice, once acceptability has been established by review of the incore maps, the quadrant power tilt alarms and related instrumentation are adjusted to indicate zero Quadrant Power Tilt Ratio as the final step in the calibration process. This action ensures that the instrumentation is correctly calibrated to alarm in the event an unexplained or unanticipated change occurs in the quadrant to quadrant relationships

between calibration intervals. Proper functioning of the quadrant power tilt alarm is significant because no allowances are made in the design for increased hot channel factors due to unexpected developing flux tilts since all likely causes are prevented by design or procedures or specifically analyzed. Finally, in the event that unexplained flux tilts do occur, the Technical Specifications provide appropriate corrective actions to ensure continued safe operation of the reactor.

### 4.4.2.5 Void Fraction Distribution

The calculated core average and the hot subchannel maximum and average void fractions are presented in Table 4.4-3 for operation at full power with design hot channel factors. The void fraction distribution in the core at various radial and axial locations is presented in Reference [52]. The void models used in the THINC-IV computer code are described in Section 4.4.2.8.3.

Since void formation due to subcooled boiling is an important promoter of interassembly flow redistribution, a sensitivity study was performed with THINC-IV using the void model referenced above.

The results of this study showed that because of the realistic crossflow model used in THINC-IV, the minimum DNBR in the hot channel is relatively insensitive to variations in this model. The range of variations considered in this sensitivity study covered the maximum uncertainty range of the data used to develop each part of the void fraction correlation.

### 4.4.2.6 Core Coolant Flow Distribution

Assembly average coolant mass velocity and enthalpy at various radial and axial core locations are given below. Coolant enthalpy rise and flow distributions are shown for the 4 foot elevation (1/3 of core height) in Figure 4.4-9, and 8 foot elevation (2/3 of core height) in Figure 4.4-10 and at the core exit in Figure 4.4-11. These distributions are representative of a Westinghouse 4-Loop plant at full power. The THINC Code analysis for this case utilized a uniform core inlet enthalpy and inlet flow distribution.

### 4.4.2.7 Core Pressure Drops and Hydraulic Loads

### 4.4.2.7.1 Core Pressure Drops

The analytical model and experimental data used to calculate the pressure drops shown in Table 4.4-1 are described in Section 4.4.2.8. The core pressure drop includes the fuel assembly, lower core plate, and upper core plate pressure drops. The full power operation pressure drop values shown in Table 4.4-1 are the unrecoverable pressure drops across the vessel, including the inlet and outlet nozzles, and across the core. These pressure drops are based on the best estimate flow for actual plant operating conditions as described in Section 5.1. Section 5.1 also defines and describes the thermal design flow (minimum flow) which is the basis for reactor core thermal performance and the mechanical design flow (maximum flow) which is used in the mechanical design of the reactor vessel internals and fuel assemblies. Since the best estimate flow is that flow which is most likely to exist in an operating plant, the

calculated core pressure drops in Table 4.4-1 are based on this best estimate flow rather than the thermal design flow.

Uncertainties associated with the core pressure drop values are discussed in Section 4.4.2.10.2.

### 4.4.2.7.2 Hydraulic Loads

The fuel assembly hold down springs, as shown in Figure 4.2-2, are designed to keep the fuel assemblies in contact with the lower core plate under all Condition I and II events with the exception of the turbine overspeed transient associated with a loss of external load. The hold down springs are designed to tolerate the possibility of an over deflection associated with fuel assembly lift off for this case and provide contact between the fuel assembly and the lower core plate following this transient. More adverse flow conditions can occur during a LOCA. These conditions are presented in Section 15.4.1.

Hydraulic loads at normal operations conditions are calculated considering the mechanical design flow which is described in Section 5.1 and accounting for the minimum core bypass flow based on manufacturing tolerances. Core hydraulic loads at cold plant startup conditions are adjusted to account for the coolant density difference. Conservative core hydraulic loads for a pump overspeed transient, which could possibly create flow rates 20% greater than the mechanical design flow, are evaluated to be approximately twice the fuel assembly weight. Full scale hydraulic test results for Vantage 5H fuel are presented in Reference [97].

### 4.4.2.8 Correlation and Physical Data

### 4.4.2.8.1 Surface Heat Transfer Coefficients

Forced convection heat transfer coefficients are obtained from the Dittus-Boelter correlation[53], with the properties evaluated at bulk fluid conditions:

$$\frac{hD_e}{K} = 0.023\left(\frac{D_e G}{\mu}\right)^{0.8}\left(\frac{C_p \mu}{K}\right)^{0.4} \quad 4.4\text{-}15$$

where:

h = heat transfer coefficient, BTU/hr-ft$^2$-°F

$D_e$ = equivalent diameter, ft

K = thermal conductivity, BTU/hr-ft-°F

G = mass velocity, lbm/hr-ft$^2$

μ = dynamic viscosity, lbm/ft-hr

$C_p$ = heat capacity, BTU/lbm-°F

This correlation has been shown to be conservative[54] for rod bundle geometries with pitch to diameter ratios in the range used by PWRs.

The onset of nucleate boiling occurs when the clad wall temperature reaches the amount of superheat predicted by Thom's[55] correlation. After this occurrence the outer clad wall temperature is determined by:

$$\Delta T_{sat} = [0.072 \exp(-P/1260)](q'')^{0.5} \quad 4.4\text{-}16$$

where:

$\Delta T_{sat}$ = wall superheat, $T_W - T_{sat}$ °F

q" = wall heat flux, BTU/hr-ft$^2$

P = pressure, psia

$T_W$ = outer clad wall temperature, °F

$T_{sat}$ = saturation temperature of coolant at P, °F

### 4.4.2.8.2 Total Core and Vessel Pressure Drop

Unrecoverable pressure losses occur as a result of viscous drag (friction) and/or geometry changes (form) in the fluid flow path. The flow field is assumed to be incompressible, turbulent, single-phase water. These assumptions apply to the core and vessel pressure drop calculations for the purpose of establishing the primary loop flow rate. Two-phase considerations are neglected in the vessel pressure drop evaluation because the core average void is negligible (see Section 4.4.2.5 and Table 4.4-3). Two-phase flow considerations in the core thermal subchannel analyses are considered and the models are discussed in Section 4.4.3.1.3. Core and vessel pressure losses are calculated by equations of the form:

$$\Delta P_L = \left(K + F\frac{L}{D_e}\right)\frac{\rho V^2}{2 g_c (144)} \quad 4.4\text{-}17$$

$\Delta P_L$ = unrecoverable pressure drop, $lb_f/in^2$

ρ = fluid density, $lb_m/ft^3$

L = length, ft

$D_e$ = equivalent diameter, ft

V = fluid velocity, ft/sec

$$g_c = 32.174 \frac{1b_m - ft}{1b_f - sec^2}$$

K = form loss coefficient, dimensionless

F = friction loss coefficient, dimensionless

Fluid density is assumed to be constant at the appropriate value for each component in the core and vessel. Because of the complex core and vessel flow geometry, precise analytical values for the form and friction lost coefficients are not available. Therefore, experimental values for these coefficients are obtained from geometrically similar models.

Values are quoted in Table 4.4-1 for unrecoverable pressure loss across the reactor vessel, including the inlet and outlet nozzles, and across the core. The results of full scale tests of core components and fuel assemblies were utilized in developing the core pressure loss characteristic. The pressure drop for the vessel was obtained by combining the core loss with correlation of 1/7th scale model hydraulic test data on a number of vessels[56,57] and form loss relationships[58]. Moody[59] curves were used to obtain the single phase friction factors.

Tests of the primary coolant loop flow rates are made (see Section 4.4.4.1 and Table 14.2-2) prior to initial criticality to verify that the flow rates used in the design, which were determined in part from the pressure losses calculated by the method described here, are conservative.

### 4.4.2.8.3 Void Fraction Correlation

There are three separate void regions considered in flow boiling in a PWR as illustrated in Figure 4.4-12. They are the wall void region (no bubble detachment), the subcooled boiling region (bubble detachment) and the bulk boiling region.

In the wall void region, the point where local boiling begins is determined when the clad temperature reaches the amount of superheat predicted by Thom's[55] correlation (discussed in Section 4.4.2.8.1). The void fraction in this region is calculated using a Maurer's[60] relationship. The bubble detachment point, where the superheated bubbles break away from the wall, is determined by using Griffith's[61] relationship.

The void fraction in the subcooled boiling region (that is, after the detachment point) is calculated from the Bowering[62] correlation. This correlation predicts the void fraction from the detachment point to the bulk boiling region.

The void fraction in the bulk boiling region is predicted by using homogeneous flow theory and assuming no slip. The void fraction in this region is therefore a function only of the thermodynamic quality.

### 4.4.2.9 Thermal Effects of Operational Transients

DNB core safety limits are generated as a function of coolant temperature, pressure, core power and axial power imbalance. Steady-state operation within these safety limits insures that the DNB design basis is met. Figure 15.1-1 shows the DNBR limit lines and the resulting overtemperature ΔT trip lines (which become part of the technical specifications), plotted as ΔT versus $T_{avg}$ for various pressures. This system provides adequate protection against anticipated operational transients that are slow with respect to fluid transport delays in the primary system. In addition, for fast transient, e.g., uncontrolled rod bank withdrawal at power incident (Section 15.2.2), specific protection functions are provided as described in Section 7.2 and the use of these protection functions are described in Chapter 15. (See Table 15.1-3). The thermal response of the fuel rod is discussed in Section 4.4.3.7.

### 4.4.2.10 Uncertainties in Estimates

### 4.4.2.10.1 Uncertainties in Fuel and Clad Temperatures

As discussed in Section 4.4.2.2, the fuel temperature is a function of crud, oxide, clad, gap, and pellet conductances. Uncertainties in the fuel temperature calculation are essentially of two types: fabrication uncertainties such as variations in the pellet and clad dimensions and the pellet density; and model uncertainties such as variations in the pellet conductivity and the gap conductance. These uncertainties have been quantified by comparison of the thermal model to the in-pile thermocouple measurements[7-13] by out-of-pile measurements of the fuel and clad properties[16 - 27] and by measurements of the fuel and clad dimensions during fabrication. The resulting uncertainties are then used in all evaluations involving the fuel temperature. The effect of densification on fuel temperature uncertainties is also included in the calculation of the total uncertainty.

In addition to the temperature uncertainty described above, the measurement uncertainty in determining the local power, and the effect of density and enrichment variations on the local power are considered in establishing the heat flux hot channel factor. These uncertainties are described in Section 4.3.2.2.1.

Reactor trip setpoints, as specified in the Technical Specifications, include allowance for instrument and measurement uncertainties, such as calorimetric error, instrument drift and channel reproducibility, temperature measurement uncertainties, noise, and heat capacity variations.

Uncertainty in determining the cladding temperature results from uncertainties in the crud and oxide thicknesses. Because of the excellent heat transfer between the surface of the rod and the coolant, the film temperature drop does not appreciably contribute to the uncertainty.

### 4.4.2.10.2 Uncertainties in Pressure Drops

Core and vessel pressure drops based on the best estimate flow, as described in Section 5.1, are quoted in Table 4.4-1. The uncertainties quoted are based on the

uncertainties in both the test results and the analytical extension of these values to the reactor application.

A major use of the core and vessel pressure drops is to determine the primary system coolant flow rates as discussed in Section 5.1. In addition, as discussed in Section 4.4.4.1 and Table 14.2-2, tests on the primary system prior to initial criticality are made to verify that a conservative primary system coolant flow rate has been used in the design and analyses of the Watts Bar Units 1 and 2.

### 4.4.2.10.3 Uncertainties Due to Inlet Flow Maldistribution

The effects of uncertainties in the inlet flow maldistribution criteria used in the core thermal analyses are discussed in Section 4.4.3.1.2.

### 4.4.2.10.4 Uncertainties in DNB Correlation

The uncertainty in the DNB correlation (Section 4.4.2.3) can be written as a statement on the probability of not being in DNB based on the statistics of the DNB data. This is discussed in Section 4.4.1.1.

### 4.4.2.10.5 Uncertainties in DNBR Calculations

The uncertainties in the DNBR's calculated by THINC analysis (see Section 4.4.3.4.1) due to uncertainties in the nuclear peaking factors are accounted for by applying conservatively high values of the nuclear peaking factors and including measurement error allowances. In addition, conservative values for the engineering hot channel factors are used as discussed in Section 4.4.2.3.4. The results of a sensitivity study[52] with THINC-IV show that the minimum DNBR in the hot channel is relatively insensitive to variations in the core-wide radial power distribution (for the same value of $F^N_{\Delta H}$).

The ability of the THINC-IV computer code to accurately predict flow and enthalpy distributions in rod bundles is discussed in Section 4.4.3.4.1 and in reference [63]. Studies have been performed[52] to determine the sensitivity of the minimum DNBR in the hot channel to the void fraction correlation (see also Section 4.4.2.8.3); the inlet velocity and exit pressure distributions assumed as boundary conditions for the analysis; and the grid pressure loss coefficients. The results of these studies show that the minimum DNBR in the hot channel is relatively insensitive to variations in these parameters. The range of variations considered in these studies covered the range of possible variations in these parameters.

### 4.4.2.10.6 Uncertainties in Flow Rates

The uncertainties associated with loop flow rates are discussed in Section 5.1. For core thermal performance evaluations, a thermal design loop flow is used which is less than the best estimate loop flow (approximately 4.0%). In addition, another 9.0% of the thermal design flow is assumed to be ineffective for core heat removal capability because it bypasses the core through the various available vessel flow paths described in Section 4.4.3.1.1.

### 4.4.2.10.7 Uncertainties in Hydraulic Loads

As discussed in Section 4.4.2.7.2, hydraulic loads on the fuel assembly are evaluated for a pump overspeed transient which creates flow rates 20% greater than the mechanical design flow. The mechanical design flow as stated in Section 5.1 is greater than the best estimate or most likely flow rate value for the actual plant operating condition (by approximately 4.5%).

### 4.4.2.10.8 Uncertainties in Mixing Coefficient

The value of the mixing coefficient, TDC, used in THINC analyses for this application is 0.038. The results of the mixing tests done on 17 x 17 geometry, as discussed in Section 4.4.2.3.3, had a mean value of TDC of 0.059 and standard deviation of $\sigma$ = 0.007. Hence, the current design value of TDC is almost 3 standard deviations below the mean for 26 inch grid spacing.

### 4.4.2.11 Plant Configuration Data

Plant configuration data for the thermal hydraulic and fluid systems external to the core are provided in the appropriate Chapters 5, 6, and 9. Implementation of the Emergency Core Cooling System (ECCS) is discussed in Chapter 15. Some specific areas of interest are the following:

*(1)* Total coolant flow rates for the Reactor Coolant System (RCS) and each loop are provided in Table 5.1-1. Flow rates employed in the evaluation of the core are presented in Section 4.4.

*(2)* Total RCS volume including pressurizer and surge line, RCS liquid volume including pressurizer water at steady state power conditions are given in Table 5.1-1.

*(3)* The flow path length through each volume may be calculated from physical data provided in the above referenced tables.

*(4)* The height of fluid in each component of the RCS may be determined from the physical data presented in Section 5.5. The components of the RCS are water filled during power operation with the pressurizer being approximately 60% water filled.

*(5)* Components of the ECCS are to be located so as to meet the criteria for net positive suction head described in Section 6.3.

*(6)* Line lengths and sizes for the Safety Injection System are determined so as to guarantee a total system resistance which will provide, as a minimum, the fluid delivery rates assumed in the safety analyses described in Chapter 15.

*(7)* The minimum flow areas for components of the RCS are presented in Section 5.5, component and subsystem design.

*(8)* The steady state pressure drops and temperature distributions through the RCS are presented in Table 5.1-1.

## 4.4.3 EVALUATION

### 4.4.3.1 Core Hydraulics

#### 4.4.3.1.1 Flow Paths Considered in Core Pressure Drop and Thermal Design

The following flow paths or core bypass flow are considered:

*(1)* Flow through the spray nozzles into the upper head for head cooling purposes.

*(2)* Flow entering into the RCC guide thimbles to cool the control rods.

*(3)* Leakage flow from the vessel inlet nozzle directly to the vessel outlet nozzle through the gap between the vessel and the barrel.

*(4)* Flow introduced between the baffle and the barrel for the purpose of cooling these components, and which is not considered available for core cooling.

*(5)* Flow in the gaps between the fuel assemblies on the core periphery and the adjacent baffle wall.

The above contributions are evaluated to confirm that the design value of the core bypass flow is met. The design value of core bypass flow for the Watts Bar Units 1 and 2 is equal to 9.0% of the total vessel flow. Of the total allowance, 7.0% is associated with the internals (items 1, 3, 4, and 5 above) and 2.0% for the core. Calculations have been performed using drawing tolerances on a worst case basis and accounting for uncertainties in pressure losses. Based on these calculations, the core bypass flow for the Watts Bar units 1 and 2 is < 9.0%. This design bypass value is also used in the evaluation of the core pressure drops quoted in Table 4.4-1, and the determination of reactor flow rates in Section 5.1.

Flow model test results for the flow path through the reactor are discussed in Section 4.4.2.8.2.

#### 4.4.3.1.2 Inlet Flow Distributions

Data has been considered from several 1/7 scale hydraulic reactor model tests[56,57,64] in arriving at the core inlet flow maldistribution criteria to be used in the THINC analyses (see Section 4.4.3.4.1). THINC I analyses made, using this data, have indicated that a conservative design basis is to consider 5% reduction in the flow to the hot assembly[65]. The same design basis of 5% reduction to the hot assembly inlet is used in THINC IV analyses.

The experimental error estimated in the inlet velocity distribution has been considered as outlined in Reference [52] where the sensitivity of changes in inlet velocity distributions to hot channel thermal performance is shown to be small. Studies[52]

made with THINC-IV show that it is adequate to use the 5% reduction in inlet flow to the hot assembly for a loop out of service based on the experimental data in References [56] and [57].

The effect of the total flow rate on the inlet velocity distribution was studied in the experiments of Reference [56]. As was expected, on the basis of the theoretical analysis, no significant variation could be found in inlet velocity distribution with reduced flow rate.

#### 4.4.3.1.3 Empirical Friction Factor Correlations

Two empirical friction factor correlations are used in the THINC-IV computer code (described in Section 4.4.3.4.1).

The friction factor in the axial direction, parallel to the fuel rod axis, is evaluated using the Novendstern-Sandberg correlation[66]. This correlation consists of the following:

*(1)* For isothermal conditions, this correlation uses the Moody[59] friction factor including surface roughness effects,

*(2)* Under single-phase heating conditions a factor is applied based on the values of the coolant density and viscosity at the temperature of the heated surface and at the bulk coolant temperature, and

*(3)* Under two-phase flow conditions the homogeneous flow model proposed by Owens[67] is used with a modification to account for a mass velocity and heat flux effect.

The flow in the lateral directions, normal to the fuel rod axis, views the reactor core as a large tube bank. Thus, the lateral friction factor proposed by Idel'chik[58] is applicable. This correlation is of the form:

$$F_L = A\, Re_L^{-0.2} \qquad 4.4\text{-}18$$

where:

A is a function of the rod pitch and diameter as given in reference [58].

$Re_L$ is the lateral Reynolds number based on the rod diameter.

Extensive comparisons of THINC-IV predictions using these correlations to experimental data are given in reference [63], and verify the applicability of these correlations in PWR design.

### 4.4.3.2 Influence of Power Distribution

The core power distribution, which is largely established at beginning-of-life by fuel enrichment, loading pattern, and core power level, is also a function of variables such as control rod worth and position, and fuel depletion throughout lifetime. Radial power distributions in various planes of the core are often illustrated for general interest, however, the core radial enthalpy rise distribution as determined by the integral of power up each channel is of greater importance for DNB analyses. These radial power distributions, characterized by $F^N_H$ (defined in Section 4.3.2.2.1) as well as axial heat flux profiles are discussed in the following two sections.

#### 4.4.3.2.1 Nuclear Enthalpy Rise Hot Channel Factor, $F^N_{\Delta H}$

Given the local power density q' (kW/ft) at a point x, y, z in a core with N fuel rods and height H,

$$F^N_{\Delta H} = \frac{\text{hot rod power}}{\text{average rod power}} = \frac{\text{Max} \int_o^H q'(x_o, y_o, z)\,dz}{\frac{1}{N} \sum_{\text{allrods}} \int_o^H q'(x, y, z)\,dz} \qquad (4.4\text{-}19)$$

The way in which $F_H$ is used in the DNB calculation is important. The location of minimum DNBR depends on the axial profile and the value of DNBR depends on the enthalpy rise to that point. Basically, the maximum value of the rod integral is used to identify the most likely rod for minimum DNBR. An axial power profile is obtained which, when normalized to the design value of $F_H$, recreates the axial heat flux along the limiting rod. The surrounding rods are assumed to have the same axial profile with rod average powers which are typical distributions found in hot assemblies. In this manner worst case axial profiles can be combined with worst case radial distributions for reference DNB calculations.

It should be noted again that $F_H$ is an integral and is used as such in DNB calculations. Local heat fluxes are obtained by using hot channel and adjacent channel explicit power shapes which take into account variations in horizontal power shapes throughout the core. The sensitivity of the THINC-IV analysis to radial power shapes is discussed in reference [52].

For operation at a fraction, P, of full power, the design $F_H$ used is given by:

$$F_H = 1.55\,[1 + 0.3\,(1\text{-}P)] \qquad (4.4\text{-}20)$$

The permitted relaxation of $F_H$ is included in the DNB protection setpoints and allows radial power shape changes with rod insertion to the insertion limits [68], thus allowing greater flexibility in the nuclear design.

#### 4.4.3.2.2 Axial Heat Flux Distributions

As discussed in Section 4.3.2.2. the axial heat flux distribution can vary as a result of rod motion, power change, or due to spatial xenon transients which may occur in the axial direction. Consequently, it is necessary to measure the axial power imbalance by means of the excore nuclear detectors (as discussed in Section 4.3.2.2.7) and protect the core from excessive axial power imbalance. The Reactor Trip System provides automatic reduction of the trip setpoint in the overtemperature ΔT channels on excessive axial power imbalance; that is, when an extremely large axial offset corresponds to an axial shape which could lead to a DNBR which is less than that calculated for the reference DNBR design axial shape.

The reference DNB design axial shape used is a chopped cosine shape with a peak average value of 1.55.

The course of those accidents in which DNB is a concern is analyzed in Chapter 15 assuming that the protection setpoints have been set on the basis of the reference shape. In many cases, the axial power distribution in the hot channel changes throughout the course of the accident due to rod motion, coolant temperature, and power level changes.

The initial conditions for the accidents for which DNB protection is required are assumed to be those permissible within the specified axial offset control limits described in 4.3.2.2. In the case of the loss-of-flow accident, the hot channel heat flux profile is very similar to the power density profile in normal operation preceding the accident. It is therefore possible to illustrate the calculated minimum DNBR for conditions representative of the loss-of-flow accident as a function of the flux difference initially in the core. A typical plot of this type is provided in Figure 4.4-23. The power shapes are evaluated with the design full-power radial peaking factor ($F^N_\Delta$ H). The radial contribution to the hot rod power shape is conservative both for the initial condition and for the condition at the time of minimum DNBR during the loss of flow transient. Also shown is the minimum DNBR calculated for the design power shape for non-overpower/overtemperature DNB events. It can be seen that this design shape results in calculated DNBR that bounds all the normal operation shapes.

### 4.4.3.3 Core Thermal Response

A general summary of the steady-state, thermal-hydraulic design parameters, including thermal output, flow rates, etc., is provided in Table 4.4-1 for all loops in operation.

As stated in Section 4.4.1, the design bases of the application are to prevent DNB and to prevent fuel melting for Condition I and II events. The protective systems described in Chapter 7 are designed to meet these bases. The response of the core to Condition II transients is given in Chapter 15.

## 4.4.3.4 Analytical Techniques

### 4.4.3.4.1 Core Analysis

The objective of reactor core thermal design is to determine the maximum heat removal capability in all flow subchannels and show that the core safety limits, as presented in the technical specifications, are not exceeded while compounding engineering and nuclear effects. The thermal design takes into account local variations in dimensions, power generation, flow redistribution, and mixing. THINC-IV is a realistic three-dimensional matrix model which has been developed to account for hydraulic and nuclear effects on the enthalpy rise in the core[52, 63] and [96]. The behavior of the hot assembly is determined by superimposing the power distribution among the assemblies upon the inlet flow distribution while allowing for flow mixing and flow distribution between assemblies. The average flow and enthalpy in the hottest assembly is obtained from the core-wide, assembly by assembly analysis. The local variations in power, fuel rod and pellet fabrication, and mixing within the hottest assembly are then superimposed on the average conditions of the hottest assembly in order to determine the conditions in the hot channel.

The following sections describe the use of the THINC Code in the thermal-hydraulic design evaluation to determine the conditions in the hot channel and to assure that the safety related design bases are not violated.

**Steady State Analysis**

The THINC-IV computer program as approved by the NRC, references [90] and [96], is used to determine coolant density, mass velocity, enthalpy, vapor void, static pressure, and DNBR distributions along parallel flow channels within a reactor core under all expected operating conditions. The THINC-IV code is described in detail in references [52] and [63], including models and correlations used. In addition, a discussion on experimental verification of THINC-IV is given in reference [63]. The effect of crud on the flow and enthalpy distribution in the core is accounted for directly in the THINC-IV evaluations by assuming a crud thickness several times that which would be expected to occur. This results in slightly conservative evaluations of the minimum DNBR.

Estimates of uncertainties are discussed in Section 4.4.2.10.

**Experimental Verification**

Extensive additional experimental verification of THINC-IV is presented in Reference [63].

The THINC-IV analysis is based on a knowledge and understanding of the heat transfer and hydrodynamic behavior of the coolant flow and the mechanical characteristics of the fuel elements. The use of the THINC-IV analysis provides a realistic evaluation of the core performance and is used in the thermal analyses as described above.

**Transient Analysis**

The THINC-IV thermal-hydraulic computer code does not have a transient capability. Since the third version of the THINC-I program[41] does have this capability, this version (THINC-III) continues to be used for transient DNB analysis.

The conservation equations needed for the transient analysis are included in THINC-III by adding the necessary accumulation terms to the conservation equations used in the steady-state (THINC-I) analysis. The input description must now include one or more of the following time dependent arrays:

*(1)* Inlet flow variation,

*(2)* Heat flux distribution,

*(3)* Inlet pressure history.

At the beginning of the transient, the calculation procedure is carried out as in the steady state analysis. The THINC-III Code is first run in the steady state mode to ensure conservatism with respect to THINC-IV and in order to provide the steady state initial conditions at the start of the transient. The time is incremented by an amount determined either by the user or by the program itself. At each new time step the calculations are carried out with the addition of the accumulation terms which are evaluated using the information from the previous time step. This procedure is continued until a preset maximum time is reached.

At preselected intervals, a complete description of the coolant parameter distributions within the array as well as DNBR are printed out. In this manner the variation of any parameter with time can be readily determined.

At various times during the transient, steady state THINC-IV is applied to show that the application of the transient version of THINC-I is conservative.

The THINC-III Code does not have the capability for evaluating fuel rod thermal response. This is treated by the methods described in Section 15.1.9.

### 4.4.3.4.2 Fuel Temperatures

As discussed in Section 4.4.2.2, the fuel rod behavior is evaluated utilizing a semi-empirical thermal model which considers, in addition to the thermal aspects, such items as clad creep, fuel swelling, fission gas release, release of absorbed gases, cladding corrosion and elastic deflection, and helium solubility.

A detailed description of the thermal model can be found in Reference [93].

### 4.4.3.4.3 Hydrodynamic Instability

The analytical methods used to assess hydraulic instability are discussed in Section 4.4.3.5.

### 4.4.3.5 Hydrodynamic and Flow Power Coupled Instability

Boiling flows may be susceptible to thermohydrodynamic instabilities[73]. These instabilities are undesirable in reactors since they may cause a change in thermohydraulic conditions that may lead to a reduction in the DNB heat flux relative to that observed during a steady flow condition or to undesired forced vibrations of core components. Therefore, a thermohydraulic design was developed which states that modes of operation under Condition I and II events shall not lead to thermohydrodynamic instabilities.

Two specific types of flow instabilities are considered for W PWR operation. These are the Ledinegg or flow excursion type of static instability and the density wave type of dynamic instability.

A Ledinegg instability involves a sudden change in flow rate from one steady state to another. This instability occurs[73] when the slope of the reactor coolant system pressure drop-flow rate curve $\left(\left.\frac{\partial \Delta P}{\partial G}\right|_{internal}\right)$

becomes algebraically smaller than the loop supply (pump head) pressure drop-flow rate curve $\left.\frac{\partial \Delta P}{\partial G}\right|_{external}$

The criterion for stability is thus $\left.\frac{\partial \Delta P}{\partial G}\right|_{internal} > \left.\frac{\partial \Delta P}{\partial G}\right|_{external}$

The W pump head curve has a negative slope $(\partial \Delta P|_{external} < 0)$ whereas the reactor coolant system pressure drop-flow curve has a positive slope $(\partial \Delta P|_{internal} > 0)$ over the Condition I and Condition II operational ranges. Thus, the Ledinegg instability will not occur.

The mechanism of density wave oscillations in a heated channel has been described by Lahey and Moody[74]. Briefly, an inlet flow fluctuation produces an enthalpy perturbation. This perturbs the length and the pressure drop of the single phase region and causes quality or void perturbations in the two-phase regions which travel up the channel with the flow. The quality and length perturbations in the two-phase region create two-phase pressure drop perturbations. However, since the total pressure drop across the core is maintained by the characteristics of the fluid system external to the core, then the two-phase pressure drop perturbation feeds back to the single phase region. These resulting perturbations can be either attenuated or self-sustained.

A simple method has been developed by Ishii[75] for parallel closed channel systems to evaluate whether a given condition is stable with respect to the density wave type of dynamic instability. This method had been used to assess the stability of typical W reactor designs[76,77,78], including Virgil C. Summer, under Condition I and II operation. The results indicate that a large margin to density wave instability exists, e.g.,

increases on the order of 200 percent of rated reactor power would be required for the predicted inception of this type of instability.

The application of the method of Ishii[75] to W reactor designs is conservative due to the parallel open channel feature of Westinghouse PWR cores. For such cores, there is little resistance to lateral flow leaving the flow channels of high power density. There is also energy transfer from channels of high power density to lower power density channels. This coupling with cooler channels has led to the opinion that an open channel configuration is more stable than the above closed channel analysis under the same boundary conditions. Flow stability tests[79] have been conducted where the closed channel systems were shown to be less stable than when the same channels were cross connected at several locations. The cross connections were such that the resistance to channel to channel cross flow and enthalpy perturbations would be greater than that which would exist in a PWR core which has a relatively low resistance to cross flow.

Flow instabilities which have been observed have occurred almost exclusively in closed channel systems operating at low pressures relative to the W PWR operating pressures. Kao, Morgan, and Parker[80] analyzed parallel closed channel stability experiments simulating a reactor core flow. These experiments were conducted at pressures up to 2200 psia. The results showed that for flow and power levels typical of power reactor conditions, no flow oscillations could be induced above 1200 psia.

Additional evidence that flow instabilities do not adversely affect thermal margin is provided by the data from the rod bundle DNB tests. Many W rod bundles have been tested over wide ranges of operating conditions with no evidence of premature DNB or of inconsistent data which might be indicative of flow instabilities in the rod bundle.

In summary, it is concluded that thermohydrodynamic instabilities will not occur under Condition I and II modes of operation for W PWR reactor designs. A large power margin, greater than doubling rated power, exists to predicted inception of such instabilities. Analysis has been performed which shows that minor plant to plant differences in W reactor designs such as fuel assembly arrays, core power to flow ratios, fuel assembly length, etc. will not result in gross deterioration of the above power margins.

### 4.4.3.6 Temperature Transient Effects Analysis

Waterlogging damage of a fuel rod could occur as a consequence of a power increase on a rod after water has entered the fuel rod through a clad defect. Water entry will continue until the fuel rod internal pressure is equal to the reactor coolant pressure. A subsequent power increase raises the temperature and, hence, could raise the pressure of the water contained within the fuel rod. The increase in hydrostatic pressure within the fuel rod then drives a portion of the water from the fuel rod through the water entry defect. Clad distortion and/or rupture can occur if the fuel rod internal pressure increase is excessive due to insufficient venting of water to the reactor coolant. This occurs when there is both a rapid increase in the temperature of the water within the fuel rod and a small defect. Zircaloy clad fuel rods which have failed due to waterlogging[81,82] indicate that very rapid power transients are required for fuel

failure. Normal operational transients are limited to about 40 cal/gm-min. (peak rod) while the Spert tests[81] indicate that 120 to 150 cal/gm is required to rupture the clad even with very short transients (5.5 msec. period). Release of the internal fuel rod pressure is expected to have a minimal effect on the Reactor Coolant System[81] and is not expected to result in failure of additional fuel rods[82]. Ejection of fuel pellet fragments into the coolant stream is not expected[81,82]. A clad breech due to waterlogging is thus expected to be similar to any fuel rod failure mechanism which exposes fuel pellets to the reactor coolant stream. Waterlogging has not been identified as the mechanism for clad distortion or perforation of any Westinghouse Zircaloy-4 fuel rods.

High fuel rod internal gas pressure could cause clad failure. One of the fuel rod design bases (Section 4.2.1.1.1) is that the fuel rod internal gas pressure is limited to a value below that which could cause (1) the diametral gap to increase due to outward cladding creep during steady-state operation, and (2) extensive DNB propagation to occur. During operational transients, fuel rod clad rupture due to high internal gas pressure is precluded by meeting the above design basis.

### 4.4.3.7 Potentially Damaging Temperature Effects During Transients

The fuel rod experiences many operational transients (intentional maneuvers) during its residence in the core. A number of thermal effects must be considered when analyzing the fuel rod performance.

The clad can be in contact with the fuel pellet at some time in the fuel lifetime. Clad-pellet interaction occurs if the fuel pellet temperature is increased after the clad is in contact with the pellet. Clad-pellet interaction is discussed in Section 4.2.1.3.1.

The potential effects of operation with waterlogged fuel are discussed in Section 4.4.3.6 which concluded that waterlogging is not a concern during operational transients.

Clad flattening, as noted in Section 4.2.1.3.1, has been observed in some operating power reactors. Thermal expansion (axial) of the fuel rod stack against a flattened section of clad could cause failure of the clad. This is no longer a concern because clad flattening is precluded during the fuel residence in the core (see Section 4.2.1.3.1).

There can be a differential thermal expansion between the fuel rods and the guide thimbles during a transient. Excessive bowing of the fuel rods could occur if the grid assemblies did not allow axial movement of the fuel rods relative to the grids. Thermal expansion of the fuel rods is considered in the grid design so that axial loads imposed on the fuel rods during a thermal transient will not result in excessively bowed fuel rods (see Section 4.2.1.2.2).

### 4.4.3.8 Energy Release During Fuel Element Burnout

As discussed in Section 4.4.2.3, the core is protected from going through DNB over the full range of possible operating conditions. In the extremely unlikely event that DNB should occur, the clad temperature will rise due to the steam blanketing at the rod

surface and the consequent degradation in heat transfer. During this time there is a potential for chemical reaction between the cladding and the coolant. However, because of the relatively good film boiling heat transfer following DNB, the energy release resulting from this reaction is insignificant compared to the power produced by the fuel.

DNB With Physical Burnout - Westinghouse[72] has conducted DNB tests in a 25 rod bundle where physical burnout occurred with one rod. After this occurrence, the 25 rod test section was used for several days to obtain more DNB data from the other rods in the bundle. The burnout and deformation of the rod did not affect the performance of neighboring rods in the test section during the burnout or the validity of the subsequent DNB data points as predicted by the W-3 correlation. No occurrences of flow instability or other abnormal operation were observed.

DNB With Return to Nucleate Boiling - Additional DNB tests have been conducted by Westinghouse[83] in 19 and 21 rod bundles. In these tests, DNB without physical burnout was experienced more than once on single rods in the bundles for short periods of time. Each time, a reduction in power of approximately 10 percent was sufficient to re-establish nucleate boiling on the surface of the rod. During these and subsequent tests, no adverse effects were observed on this rod or any other rod in the bundle as a consequence of operating in DNB.

### 4.4.3.9 Deleted

### 4.4.3.10 Fuel Rod Behavior-Effects from Coolant Flow Blockage

Coolant flow blockages can occur within the coolant channels of a fuel assembly or external to the reactor core. The effects of fuel assembly blockage within the assembly on fuel rod behavior is more pronounced than external blockages of the same magnitude. In both cases the flow blockages cause local reductions in coolant flow. The amount of local flow reduction, where it occurs in the reactor, and how far along the flow stream the reduction persists are considerations which will influence the fuel rod behavior. The effects of coolant flow blockages in terms of maintaining rated core performance are determined both by analytical and experimental methods. The experimental data are usually used to augment analytical tools such as computer programs similar to the THINC-IV program. Based on the DNB correlation (Section 4.4.2.3), the predicted DNBR is dependent upon the local values of quality and mass velocity.

The THINC-IV Code is capable of predicting the effects of local flow blockages on DNBR within the fuel assembly on a sub-channel basis, regardless of where the flow blockage occurs. In reference [63], it is shown that for a fuel assembly similar to the Westinghouse design, THINC-IV accurately predicts the flow distribution within the fuel assembly when the inlet nozzle is completely blocked. Full recovery of the flow was found to occur about 30 inches downstream of the blockage. With the reference reactor operating at the nominal full power conditions specified in Table 4.4-1, the effects of an increase in enthalpy and decrease in mass velocity in the lower portion of the fuel assembly would not result in the reactor violating the DNB design basis.

From a review of the open literature it is concluded that flow blockage in 'open lattice cores' similar to the Westinghouse cores cause flow perturbations which are local to the blockage. For instance, A. Oktaubo[84], et al., show that the mean bundle velocity is approached asymptotically about 4 inches downstream from a flow blockage in a single flow cell. Similar results were also found for 2 and 3 cells completely blocked. P. Basmer[85], et al., tested an open lattice fuel assembly in which 41% of the subchannels were completely blocked in the center of the test bundle between spacer grids. Their results show the stagnant zone behind the flow blockage essentially disappears after 1.65 L/De or about 5 inches for their test bundle. They also found that leakage flow through the blockage tended to shorten the stagnant zone or, in essence, the complete recovery length. Thus, local flow blockages within a fuel assembly have little effect on subchannel enthalpy rise. The reduction in local mass velocity is then the main parameter which affects the DNBR. If the Watts Bar units 1 and 2 were operating at full power and nominal steady state conditions as specified in Table 4.4-1, a reduction in local mass velocity greater than 85% would be required to reduce the DNBR to the safety analysis DNBR limit. The above mass velocity effect on the DNB correlation was based on the assumption of fully developed flow along the full channel length. In reality a local flow blockage is expected to promote turbulence and thus would not adversely affect DNBR at all[87].

Coolant flow blockages induce local crossflows as well as promote turbulence. Fuel rod behavior is changed under the influence of a sufficiently high crossflow component. Fuel rod vibration could occur, caused by this crossflow component, through vortex shedding or turbulent mechanisms. If the crossflow velocity exceeds the limit established for fluid elastic stability, large amplitude whirling results. The limits for a controlled vibration mechanism are established from studies of vortex shedding and turbulent pressure fluctuations. The crossflow velocity required to exceed fluid elastic stability limits is dependent on the axial location of the blockage and the characterization of the crossflow (jet flow or not). These limits are greater than those for vibratory fuel rod wear. Crossflow velocity above the established limits can lead to mechanical wear of the fuel rods at the grid support locations. Fuel rod wear due to flow induced vibration is considered in the fuel rod fretting evaluation (Section 4.2).

## 4.4.4 Testing and Verification

### 4.4.4.1 Tests Prior to Initial Criticality

A reactor coolant flow test, as noted in Table 14.2-2, is performed following fuel loading but prior to initial criticality. Reactor coolant loop elbow tap differential pressures are measured with all four reactor coolant pumps in operation with reactor temperatures and pressure at normal operating conditions. This data is used to calculate the coolant flow rates. This test verifies, within the accuracy of elbow tap measurements, that proper coolant flow rates have been used in the core thermal and hydraulic analysis.

### 4.4.4.2 Initial Power and Plant Operation

Core power distribution measurements are made during the ascent to power. These tests are used to ensure that conservative peaking factors are used in the core thermal and hydraulic analysis.

Additional demonstration of the overall conservatism of the THINC analysis was obtained by comparing THINC predictions to incore thermocouple measurements. These measurements were performed on the Zion reactor[86]. No further in-reactor testing is planned.

#### 4.4.4.3 Component and Fuel Inspections

Inspections performed on the manufactured fuel are delineated in Section 4.2.1.4. Fabrication measurements critical to thermal and hydraulic analysis are obtained to verify that the engineering hot channel factors employed in the design analyses (Section 4.4.2.3.4) are met.

### 4.4.5 Instrumentation Application

#### 4.4.5.1 Incore Instrumentation

Instrumentation is located in the core to obtain radial, axial, and azimuthal core characteristics for all core quadrants by correlating movable neutron detector information with fixed thermocouple information.

The incore instrumentation system is comprised of thermocouples, positioned to measure fuel assembly coolant outlet temperatures at preselected positions, and fission chamber detectors positioned in instrument thimbles which run the length of selected fuel assemblies to measure the neutron flux distribution. Figure 4.4-22 shows the number and location of instrumented assemblies in the core.

The core-exit thermocouples provide a backup to the flux monitoring instrumentation for monitoring power distribution. The routine, systematic collection of thermocouple readings by the operator provides a data base. From this data base, abnormally high or abnormally low readings, quadrant temperature tilts, or systematic departures from a prior reference map can be deduced.

The movable incore neutron detector system would be used for more detailed mapping if the thermocouple system were to indicate an abnormality. These two complementary systems are more useful when taken together than either system alone would be. The incore instrumentation system is described in more detail in Section 7.7.1.9.

The incore instrumentation is provided to obtain data from which fission power density distribution in the core, coolant enthalpy distribution in the core, and fuel burnup distribution may be determined.

#### 4.4.5.2 Overtemperature and Overpower ▲T Instrumentation

The overtemperature ▲T trip protects the core against low DNBR. The overpower ▲T trip protects against excessive power (fuel rod rating protection).

As discussed in Section 7.2.1.1.2, factors included in establishing the overtemperature ▲T and overpower ▲T trip setpoints include the reactor coolant temperature in each

loop and the axial distribution of core power (for overtemperature ΔT only) through the use of the two-section excore neutron detectors.

### 4.4.5.3 Instrumentation to Limit Maximum Power Output

The output of the three ranges (source, intermediate, and power) of detectors, with the electronics of the nuclear instruments, are used to limit the maximum power output of the reactor within their respective ranges.

There are six radial locations containing a total of six neutron flux detectors installed around the reactor in the primary shield, two fission chamber detectors for the source range and intermediate installed on opposite "flat" portions of the core containing the primary startup sources; four dual section uncompensated ionization chamber assemblies for the power range installed vertically at the four corners of the core and located equidistant from the reactor vessel at all points and, to minimize neutron flux pattern distortions, within one foot of the reactor vessel. Each power range detector provides two signals corresponding to the neutron flux in the upper and in the lower sections of a core quadrant. The three ranges of detectors are used as inputs to monitor neutron flux from a completely shutdown condition up to 200% of full power.

The difference in neutron flux between the upper and lower sections of the power range detectors are used to limit the overtemperature ΔT trip setpoint and to provide the operator with an indication of the core power axial offset. In addition, the output of the power range channels are used for:

*(1)* The rod speed control function,

*(2)* To alert the operator to an excessive power unbalance between the quadrants,

*(3)* Protect the core against rod ejection accidents, and

*(4)* Protect the core against adverse power distributions resulting from dropped rods.

Details of the neutron detectors and nuclear instrumentation design and the control and trip logic are given in Chapter 7. The limits on neutron flux operation and trip setpoints are given in the Technical Specifications.

**REFERENCES**

*(1)* Christensen, J. A., Allio, R. J. and Biancheria, A., "Melting Point of Irradiated $UO_2$," WCAP-6065, February 1965.

*(2)* Risherl, D. H., "An Evaluation of the Rod Ejection Accident in Westinghouse Pressurized Water Reactors Using Spatial Kinetics Methods," WCAP-7588, Revision 1-A, January 1975.

*(3)* Supplemental information on fuel design transmitted from R. Salvatoril, Westinghouse NES, to D. Knuth, AEC, as attachments to letter NS-SL-518 (12/22/72), NS-SL-521 (12/29/72), NS-SL-524 (12/29/72) and NS-SL-543 (1/12/73), (Westinghouse Proprietary), and supplemental information on fuel design transmitted from R. Salvatore, Westinghouse NES, to D. Knuth, AEC, as attachments to letters NS-SL-527 (1/12/73) and NS-SL-544 (1/12/73).

*(4)* Deleted by Amendment 73

*(5)* Deleted by Amendment 73

*(6)* Deleted by Amendment 73

*(7)* Kjaerheim, G. and Rolstad, E., "In Pile Determination of $UO_2$ Thermal Conductivity, Density Effects and Gap Conductance," HPR-80, December 1967.

*(8)* Kjaerheim, G., "In-Pile Measurements of Center Fuel Temperatures and Thermal Conductivity Determination of Oxide Fuels," paper IFA-175 presented at the European Atomic Energy Society Symposium on Performance Experience of Water-Cooled Power Reactor Fuel, Stockholm, Sweden (October 21-22, 1969).

*(9)* Cohen, I., Lustman, B. and Eichenberg, D., "Measurement of the Thermal Conductivity of Metal-Clad Uranium Oxide Rods during Irradiation," WAPD-228, 1960.

*(10)* Clough, D. J. and Sayers, J. B., "The Measurement of the Thermal Conductivity of $UO_2$ Under Irradiation in the Temperature Range 150-1600°C," AERE-R-4690, UKAEA Research Group, Harwell, December 1964.

*(11)* Stora, J. P., Debernardy, DeSigoyer, B., Delmas, R., Deschamps, P., Ringot, C. and Lavaud, B., "Thermal Conductivity of Sintered Uranium Oxide Under In-Pile Conditions." EURAEC-1095, 1964.

*(12)* Devold, I., "A Study of the Temperature Distribution in $UO_2$ Reactor Fuel Elements," AE-3183 Aktiebolaget Atomenergi, Stockholm, Sweden, 1968.

*(13)* Balfour, M. G., Christensen, J. A. and Ferrari., H. M., "In-Pile Measurement of $UO_2$ Thermal Conductivity," WCAP-2923, 1966.

*(14)* Duncan, R. N., "Rabbit Capsule Irradiation of $UO_2$", CVTR Project, CVNA-142, June 1962.

*(15)* Nelson, R. C., Coplin, D. H., Lyons, M. F. and Weidenbaum, B., "Fission Gas Release from $UO_2$ Fuel Rods with Gross Central Melting," GEAP-4572, July 1964.

*(16)* Howard, V. C., and Gulvin, T. G., "Thermal Conductivity Determinations on Uranium Dioxide by a Radial Flow Method", UKAEA IG-Report 51, November 1960.

*(17)* Lucks, C. F., and Deem, H. W., "Thermal Conductivity and Electrical Conductivity of $UO_2$," In-Progress Reports Relating to Civilian Applications, BMI-1448 (Rev.) for June 1960; BMI-1489 (Rev.) for December 1960 and BMI-1518 (Rev.) for May 1961.

*(18)* Daniel, J. L., Matolich, Jr., J., and Deem, H. W., "Thermal Conductivity of $UO_2$," HW-69945, September 1962.

*(19)* Feith, A. D., "Thermal Conductivity of $UO_2$ by a Radial Heat Flow Method" TID-21668, 1962.

*(20)* Vogt, J., Grandell L. and Runfors, U., "Determination of the Thermal Conductivity of Unirradiated Uranium Dioxide," AB Atomenergi Report RMB-527, 1964, Quoted by IAEA Technical Report Series No. 59, "Thermal Conductivity of Uranium Dioxide"

*(21)* Nishijima, T., Kawada, T. and Ishihata, A., "Thermal Conductivity of Sintered $UO_2$ and $Al_2O_3$, at High Temperatures," J. American Ceramic Society, 48, 31-34 (1965).

*(22)* Ainscough, J. B. and Wheeler, M. J., "The Thermal Diffusivity and Thermal Conductivity of Sintered Uranium Dioxide," in Proceedings of the Seventh Conference of Thermal Conductivity, p. 467, National Bureau of Standards, Washington, 1968.

*(23)* Godfrey, T. G., Fulkerson, W., Killie, T. G., Moore, J. P. and McElroy, D. L. "Thermal Conductivity of Uranium Dioxide and Armco Iron by an Improved Radial Heat Flow Technique," ORNL-3556, June 1964.

*(24)* Stora, J. P., et al., "Thermal Conductivity of Sintered Uranium Oxide Under In-Pile Conditions," EURAEC-1095, August 1964.

*(25)* Bush, A. J., "Apparatus for Measuring Thermal Conductivity to 2500°C," Westinghouse Research Laboratories Report 64-lP6-4Ol-R3, February 1965. (Proprietary)

*(26)* Asamoto, R. R., Anselm, F. L. and Conti, A. E., "The Effect of Density on the Thermal Conductivity of Uranium Dioxide," GEAP-5493, April 1968.

*(27)* Kruger, O. L . "Heat Transfer Properties of Uranium and Plutonium Dioxide," Paper 11-N-68F presented at the Fall meeting of Nuclear Division of the American Ceramic Society, September, 1968, Pittsburgh.

*(28)* Gyllander, J. A., "In-Pile Determination of the Thermal Conductivity of $UO_2$ in the Range 500-2500°C," AE-411, January 1971.

*(29)* Lyons, M. F., et al., $U0_2$ Powder and Pellet Thermal Conductivity During Irradiation," GEAP-5100-1, March 1966.

*(30)* Coplin, D. H., et al., "The Thermal Conductivity of $UO_2$ by Direct In-reactor Measurements," GEAP-5100-6, March 1968.

*(31)* Bain, A. S., "The Heat Rating Required to Produce Center Melting in Various $UO_2$ Fuels," ASTM Special Technical Publication, No. 306, pp. 30-46, Philadelphia, 1962.

*(32)* Stora, J. P., "In-Reactor Measurements of the Integrated Thermal Conductivity of $UO_2$ - Effect of Porosity," Trans. ANS, 13, 137-138 (1970).

*(33)* International Atomic Energy Agency, "Thermal Conductivity of Uranium Dioxide," Report of the Panel held in Vienna, April 1965, IAEA Technical Reports Series, No. 59, Vienna, The Agency, 1966.

*(34)* Poncelet, C. G., "Burnup Physics of Heterogeneous Reactor Latices, WCAP-6069, June 1965.

*(35)* Nodvick, R. J., "Saxton Core II Fuel Performance Evaluation," WCAP-3385-56, Part II, "Evaluation of Mass Spectrometric and Radiochemical Analyses of Irradiated Saxton Plutonium Fuel," July 1970.

*(36)* Deleted by Amendment 73

*(37)* Deleted by Amendment 73

*(38)* Tong, L. S., "Boiling Heat Transfer and Two-Phase Flow," John Wiley & Sons, New York, 1965.

*(39)* Tong, L. S., "Boiling Crisis and Critical Heat Flux," AEC Critical Review Series, TID-25887, 1972.

*(40)* Tong, L. S., "Critical Heat Fluxes on Rod Bundles," in "Two-Phase Flow and Heat Transfer in Rod Bundles," pp. 31-41, American Society of Mechanical Engineers, New York, 1969.

*(41)* Chelemer, H., Weisman, J. and Tong, L. S., "Subchannel Thermal Analysis of Rod Bundle Cores," WCAP-7015., Revision 1, January 1969.

*(42)* Deleted by Amendment 73

*(43)* Motley, F. E. and Cadek, F. F., "DNB Test Results for R Grid Thimble Cold Wall Cells," WCAP-7695-Addendum 1-P-A (Proprietary) and WCAP-7958-Addendum 1-A (Non-Proprietary), January 1975.

*(44)* Tong, L. S., "Prediction of Departure from Nucleate Boiling for an Axially Non-Uniform Heat Flux Distribution," J. Nucl. Energy, 21, 241-248 (1967).

*(45)* Deleted by Amendment 73

*(46)* Cadek, F. F., Motley, F. E. and Dominicis, D. P., "Effect of Axial Spacing on Interchannel Thermal Mixing with the R Mixing Vane Grid," WCAP-7941-P-A (Proprietary), and WCAP-7959-A (Non-Proprietary), January 1975.

*(47)* Rowe, D. S., Angle, C. W., "Crossflow Mixing Between Parallel Flow Channels During Boiling, Part II Measurement of Flow and Enthalpy in Two Parallel Channels," BNWL-371, part 2, December 1967.

*(48)* Rowe, D. S., Angle, C. W., "Crossflow Mixing Between Parallel Flow Channels During Boiling, Part III Effect of Spacers on Mixing Between Two Channels," BNWL-371, part 3, January 1969.

*(49)* Gonzalez-Santalo, J. M. and Griffith, P., "Two-Phase Flow Mixing in Rod Bundle Subchannels," ASME Paper 72-WA/NE-19.

*(50)* Motley, F. E., Wenzel, A. H., Cadek, F. F., "The Effect of 17 x 17 Fuel Assembly Geometry on Interchannel Thermal Mixing," WCAP-8298-P-A (Proprietary) and WCAP-8299-A, January 1975.

*(51)* Cadek, F. F., "Interchannel Thermal Mixing with Mixing Vane Grids," WCAP-7667-P-A (Proprietary) and WCAP-7755-A (Non-Proprietary), January 1975.

*(52)* Hochreiter, L. E., "Application of the THINC IV Program to PWR Design," WCAP-8054 (Proprietary) and WCAP-8195 (Non-Proprietary), October 1973.

*(53)* Dittus, F. W., and Boelter, L. M. K., "Heat Transfer in Automobile Radiators of the Tubular Type," Calif. Univ. Publication in Eng., 2, No. 13, 443-461 (1930).

*(54)* Weisman, J., "Heat Transfer to Water Flowing Parallel to Tube Bundles" Nucl. Sci. Eng., 6, 78-79 (1959).

*(55)* Thom, J. R. S., Walker, W. M., Fallon, T. A. and Raising, G. F. S., "Boiling in Subcooled Water During Flow up Heated Tubes or Annuli," Prc. Instn. Mech. Engrs., 180, Pt. 3C, 226-46 (1965-66).

*(56)* Hetsroni, G., "Hydraulic Tests of the San Onofre Reactor Model," WCAP-3269-8, June 1964.

*(57)* Hetsroni, G., "Studies of the Connecticut-Yankee Hydraulic Model," NYO-3250-2, June 1965.

*(58)* Idel'chik, I. E., "Handbook of Hydraulic Resistance," AEC-TR-6630, 1960.

*(59)* Moody, L. F., "Friction Factors for Pipe Flow, "Transaction of the American Society of Mechanical Engineers, 66, 671-684 (1944).

*(60)* Maurer, G. W., "A Method of Predicting Steady State Boiling Vapor Fractions in Reactor Coolant Channels," WAPD-BT-19, pp. 59-70, June 1960.

*(61)* Griffith, P., Clark, J. A. and Rohsenow, W. M., "Void Volumes in Subcooled Boiling Systems," ASHE Paper No. 58-HT-19.

*(62)* Bowering, R. W., "Physical Model, Based on Bubble Detachment, and Calculation of Steam Voidage in the Subcooled Region of a Heated Channel," HPR-10, December 1962.

*(63)* Hochreiter, L. E., Chelemer H. and Chu, P. T., "THINC-IV An Improved Program for Thermal-Hydraulic Analysis of Rod Bundle Cores," WCAP-7956, June 1973.

*(64)* Carter, F. D., "Inlet Orificing of Open PWR Cores," WCAP-9004 (Proprietary), January 1969 and WCAP-7836 (Non-Proprietary), January 1972.

*(65)* Shefcheck, J., "Application of the THINC Program to PWR Design," WCAP-7359-L (Proprietary), August 1969, and WCAP-7638 (Non-Proprietary), January 1972.

*(66)* Novendstern, E. H. and Sandberg, R. O., "Single Phase Local Boiling and Bulk Boiling Pressure Drop Correlations," WCAP-2850 (Proprietary), April 1966 and WCAP-7916 (Non-Proprietary), June 1972.

*(67)* Owens, Jr., W. L., "Two-Phase Pressure Gradient," in International Developments in Heat Transfer, Part II, pp 363-368, ASME, New York, 1961.

*(68)* McFarlane, A. F., "Power Peaking Factors," WCAP-7912-P-A (Proprietary) and WCAP-7912-A (Non-Proprietary), January 1975.

*(69)* Deleted by Amendment 73

*(70)* Deleted by Amendment 73

*(71)* Deleted by Amendment 73

*(72)* Weisman, J., Wenzel, A. H., Tong L. S., Fitzsimmons, D., Thorne, W. and Batch, J., "Experimental Determination of the Departure from Nucleate Boiling in Large Rod Bundles at High Pressures," Chem. Eng. Prog. Symp. Ser. 64, No. 82, 114-125 (1968).

*(73)* Boure, J. A., Bergles, A. E., and Tong, L. S., "Review of Two-Phase Flow Instability," ASME Paper 71-HT-42, August 1971.

*(74)* Lahey, R. T., and Moody, F. J., "The Thermal Hydraulics of a Boiling Water Reactor," American Nuclear Society, 1977.

*(75)* Saha, P., Ishii, B., and Zuber, N., "An Experimental Investigation of the Thermally Induced Flow Oscillations in Two-Phase Systems," J. of Heat Transfer, November 1976, pp. 616-622.

*(76)* Virgil C. Summer FSAR, Docket No. 50-395.

*(77)* Braidwood/Byron FSAR, Docket No. 50-456.

*(78)* South Texas FSAR, Docket No. 50-498.

*(79)* Kakac, S., Veziroglu, T. N., Akyuzlu, K., and Berkol, O., "Sustained and Transient Boiling Flow Instabilities in a Cross-Connected Four-Parallel-Channel Upflow System," Proc. of 5th International Heat Transfer Conference, Tokyo, Sept. 3-7, 1974.

*(80)* Kao, H. S., Morgan, C. D., and Parker, W. B., "Prediction of Flow Oscillation in Reactor Core Channel," Trans. ANS, Vol. 16, 1973, pp. 212-213.

*(81)* Stephan, L. A., "The Effects of Cladding Material and Heat Treatment on the Response of Waterlogged $UO_2$ Fuel Rods to Power Bursts," IN-ITR-III, January 1970.

*(82)* Western New York Nuclear Research Center correspondence with the AEC on February 11 and August 27, 1971, Docket 50-57.

*(83)* Tong, L. S., et al., "Critical Heat Flux (DNB) in Square and Triangular Array Rod Bundles," presented at the Japan Society of Mechanical Engineers Semi-International Symposium held at Tokyo, Japan, September 4-8, 1967, pp. 25-34.

*(84)* Ohtsubo, A., and Uruwashi, S., "Stagnant Fluid Due to Local Flow Blockage," J. Nucl. Sci. Technol., 9, No. 7, 433-434, (1972).

*(85)* Basmer, P., Kirsh, D. and Schultheiss, G. F., "Investigation of the Flow Pattern in the Recirculation Zone Downstream of Local Coolant Blockages in Pin Bundles," Atomwirtschaft, 17, No. 8, 416-417, (1972). (In German).

*(86)* Burke, T. M., Meyer, C. E. and Shefcheck J., "Analysis of Data from the Zion (Unit 1) THINC Verification Test," WCAP-8453-P-A (Proprietary) and WCAP-8454-A (Non-Proprietary), December 1974.

*(87)* Hill, K. W., Motley, F. E., Cadek, F. F., and Castulin, J. E., "Effects on Critical Heat Flux of Local Heat Flux spikes on Local Flow Blockage in Pressurized Water Reactor Rod Bundles," ASME Paper 74-WA/BT-54, August 12, 1974.

*(88)* Skaritka, J. (Ed.), "Fuel Rod Bow Evaluation," WCAP-8691 Revision 1, July 1979.

*(89)* "Partial Response to Request Number 1 for Additional Information on WCAP-8691, Revision 1" letter, E. P. Rahe, Jr., (Westinghouse) to J. R. Miller (NRC) , NS-EPR-2515, dated October 9, 1981; "Remaining Response to Request Number 1 for Additional Information on WCAP-8691, Revision 1" letter, E. P. Rahe, Jr., (Westinghouse) to J. R. Miller (NRC), NS-EPR-2572, dated March 16, 1982.

*(90)* Letter from J. F. Stolz (NRC) to C. Eicheldinger (Westinghouse); Subject: Staff Evaluation of WCAP-7956, WCAP-8054, WCAP-8567, and WCAP-8762; dated April 19, 1978.

*(91)* Motley, F. E., Hill, K. W., Cadek, F. F., and Shefcheck, J., "New Westinghouse Correlation WRB-1 for Predicting Critical Heat Flux in Rod Bundles with Mixing Vane Grids," WCAP-8762-P-A, July 1984.

*(92)* Davidson, S. L., ed., et. al., "VANTAGE 5H Fuel Assembly," WCAP-10444-P-A, Addendum 2A, April 1988.

*(93)* Leech, W.J., et. al, "Revised PAD Code Thermal Safety Model," WCAP-8720, Addendum 2, October 1982.

*(94)* Letter from A. C. Thadani (NRC) to W. J. Johnson (Westinghouse), January 31, 1989, Subject: Acceptance for Referencing of Licensing Topical Report, WCAP-9226-P/9227-NP, "Reactor Core Response to Excessive Secondary Steam Releases."

*(95)* Letter from C. Berlinger (NRC) to E. P. Rahe, Jr. (Westinghouse), Subject: "Request for Reduction in Fuel Assembly Burnup Limit for Calculation of Maximum Rod Bow Penalty," June 18, 1986.

*(96)* Friedland, A. J., Ray, S., "Improved THINC-IV Modeling for PWR Core Design," WCAP-12330-A, September 1991.

*(97)* Davidson, S. L., (ed.), et.al., "VANTAGE 5 Fuel Assembly," WCAP-10444-P-A, Appendix A, September, 1985.

**Table 4.4-1 Thermal and Hydraulic Comparison Table**
**(Page 1 of 2)**

| Design Parameters | Watts Barr Units 1 and 2 | W.B McGuire Units 1 and 2 |
|---|---|---|
| Reactor Core Heat Output, MWt | 3411 | 3411 |
| Reactor Core Heat Output, $10^6$ BTU/hr | 11,641.7 | 11,641.7 |
| Heat Generated in Fuel, % | 97.4 | 97.4 |
| System Pressure, Nominal, psia | 2250 | 2250 |
| System Pressure, Minimum Steady State, psia | 2204 | 2220 |
| Minimum DNBR at Nominal Conditions | | |
| Typical Flow Channel | 2.21 | 2.05 |
| Thimble (Cold Wall) Flow Channel | 2.13 | 1.72 |
| Minimum DNBR for Design Transients | >1.31 | >1.30 |
| DNB Correlation "R" | WRB-1 | (W-3 with modified spacer factor) |
| **Coolant Flow** | | |
| Total Thermal Flow Rate, $10^6$ lb/hr | 144.7 | 144.8 |
| Effective Flow Rate for Heat Transfer, $10^6$ lb/hr | 131.7 | 133.9 |
| Effective Flow Area for Heat Transfer, $ft^2$ | 51.3 | 51.1 |
| Average Velocity Along Fuel Rods, ft/sec | 15.4 | 16.6 |
| Average Mass Velocity, $10^6$ lb/hr-$ft^2$ | 2.57 | 2.62 |
| **Coolant Temperature** | | |
| Nominal Inlet,°F | 559.0 | 559.1 |
| Average Rise in Vessel, °F | 58.4 | 58.2 |
| Average Rise in Core, °F | 63.5 | 62.5 |
| Average in Core, °F | 592.5 | 592.0 |
| Average in Vessel, °F | 588.2 | 588.2 |
| **Heat Transfer** | | |
| Active Heat Transfer, Surface Area, $ft^2$ | 59,700 | 59,700 |
| Average Heat Flux, BTU/hr-$ft^2$ | 189,800 | 189,800 |
| Maximum Heat Flux for Normal Operation, BTU/hr-$ft^2$ | 455,520[e] | 440,300[c] |
| Average Thermal Output, kW/ft | 5.45[d] | 5.44 |
| Maximum Thermal Output for Normal Operation, kW/ft | 13.1[e] | 12.6[c] |
| Peak Linear Power for Determination of Protection Setpoints, kW/ft[b] | 21.1 | 18.0 |

**Table 4.4-1 Thermal and Hydraulic Comparison Table**
**(Page 2 of 2)**

| Design Parameters | Watts Barr Units 1 and 2 | W.B McGuire Units 1 and 2 |
|---|---|---|
| **Fuel Central Temperature** | | |
| Peak at 100% Power, °F | 3160 | 3250 |
| Peak at Thermal Output Maximum for Maximum Overpower Trip Point, °F | 4500 | 4150 |
| **Pressure Drop[a]** | | |
| Across Core, psi | 24.4 + 2.4 | 25.8 + 3.9 |
| Across Vessel, including nozzle, psi | 44.5 + 6.7 | 46.7 + 7.0 |

[a] Based on best estimate reactor flow rate as discussed in Section 5.1

[b] See Section 4.3.2.2.6

[c] This limit is associated with the value of FQ = 2.32

[d] Based on densified active fuel length (143.7 inches).

[e] This limit is associated with the value of $F_Q$ = 2.40

[f] Cycle 1

**Table 4.4-2 Deleted by Amendment 73**

**Table 4.4-3 Void Fractions At Nominal Reactor Conditions With Design Hot Channel Factors**

| | Average | Maximum |
|---|---|---|
| Core | 0.31 | -- |
| Hot Subchannel | 7.9 | 23.6 |

**Table 4.4-4 Deleted by Amendment 73**

THIS PAGE INTENTIONALLY BLANK

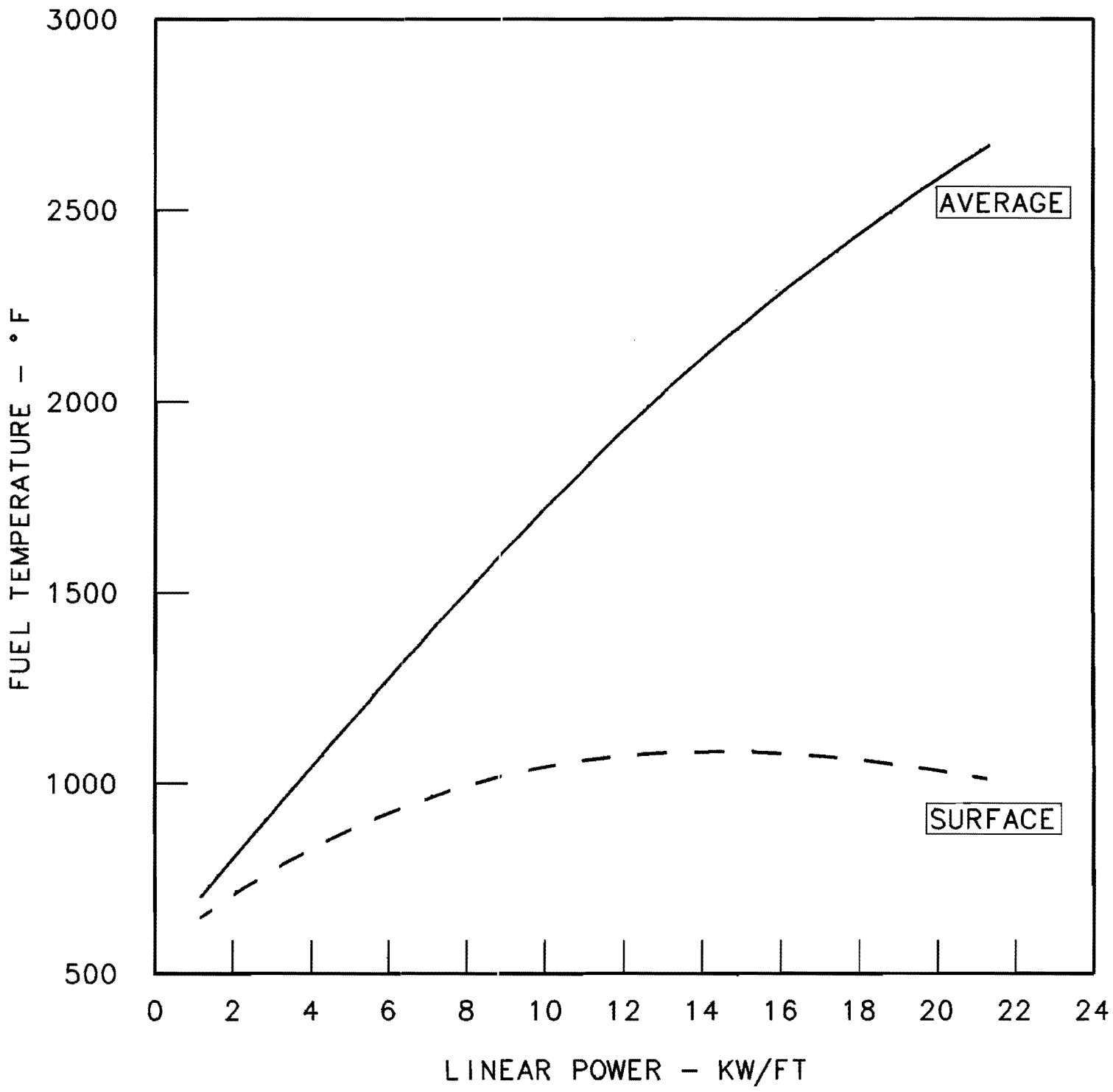


AMENDMENT 73

WATTS BAR NUCLEAR PLANT
FINAL SAFETY
ANALYSIS REPORT

PEAK FUEL AVERAGE AND
SURFACE TEMPERATURES
DURING FUEL ROD LIFE-
TIME VS. LINEAR POWER

FIGURE 4.4-1

**Figure 4.4-1 Peak Fuel Average and Surface Temperatures During Fuel Rod Lifetime versus Linear Power**

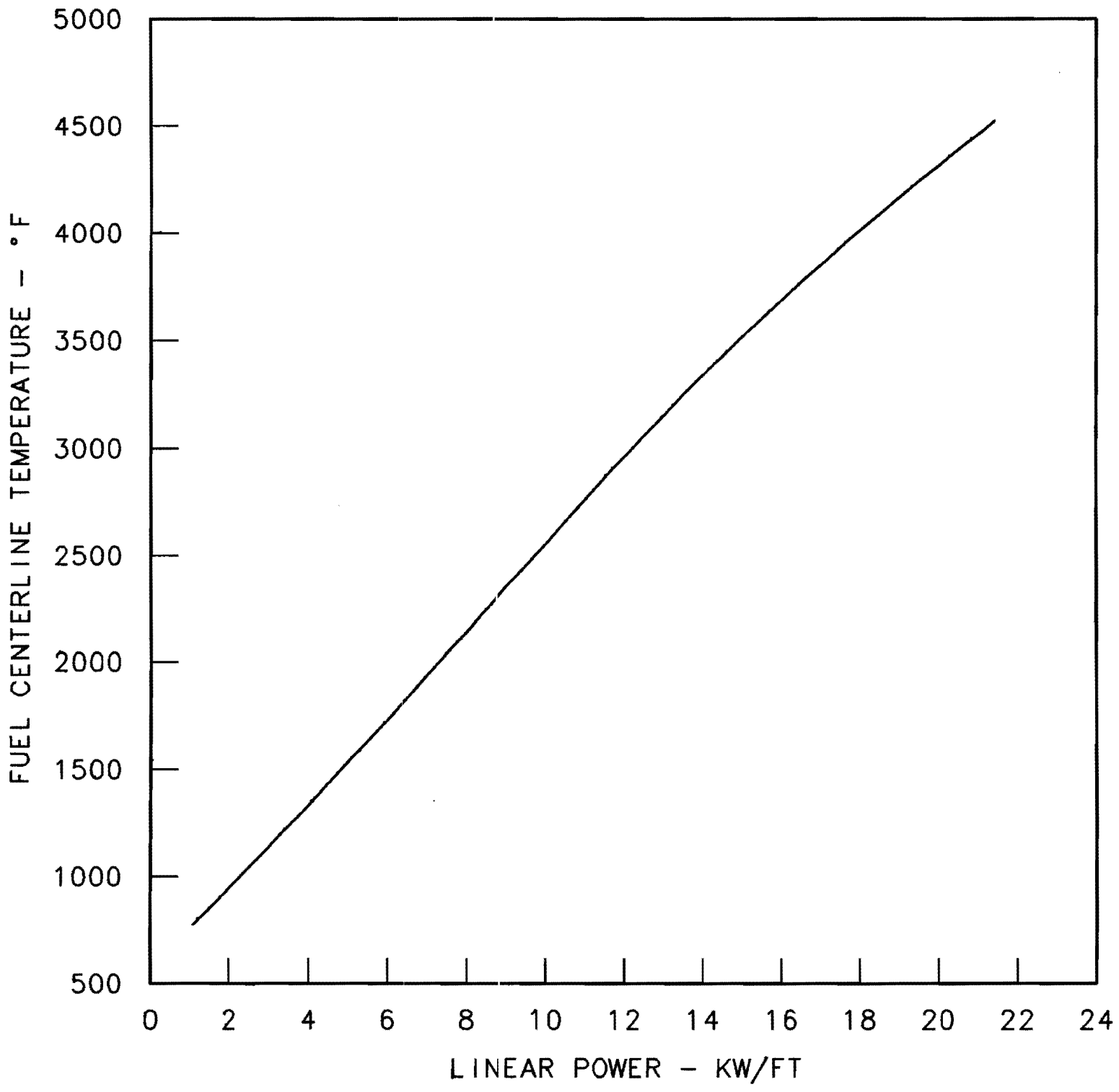


AMENDMENT 73

WATTS BAR NUCLEAR PLANT
FINAL SAFETY
ANALYSIS REPORT

PEAK FUEL CENTERLINE TEMPERATURE DURING FUEL ROD LIFETIME VS LINEAR POWER

FIGURE 4.4–2

**Figure 4.4-2 Peak Fuel Centerline Temperature During Fuel Rod Lifetime versus Linear Power**

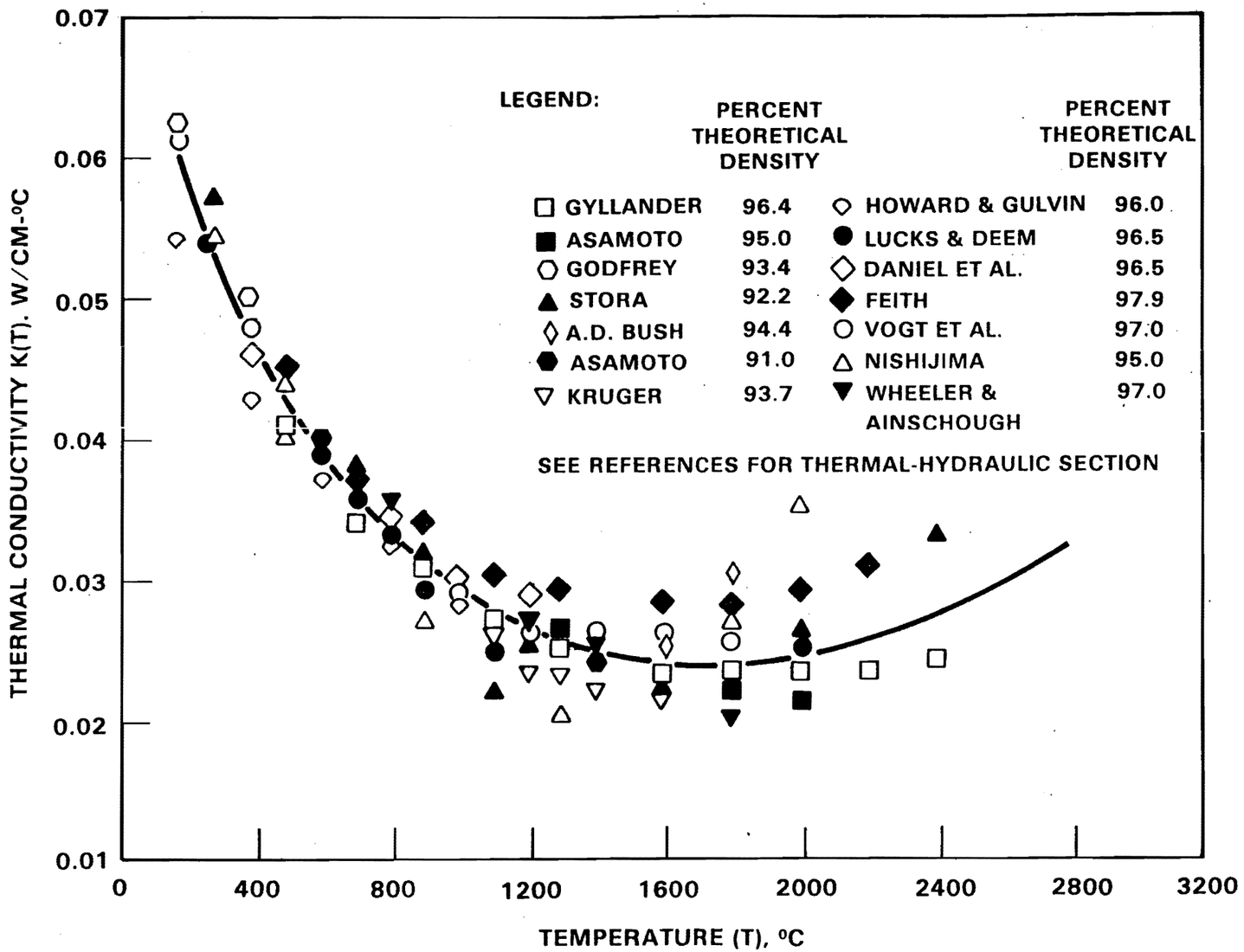


Figure 4.4-3. Thermal Conductivity of $UO_2$ (Data Corrected to 95% Theoretical Density)

Revised by Amendment 45

**Figure 4.4-3 Thermal Conductivity of $UO_2$ (Data Corrected to 95% Theoretical Density)**

**Figure 4.4-4 Deleted by Amendment 73**

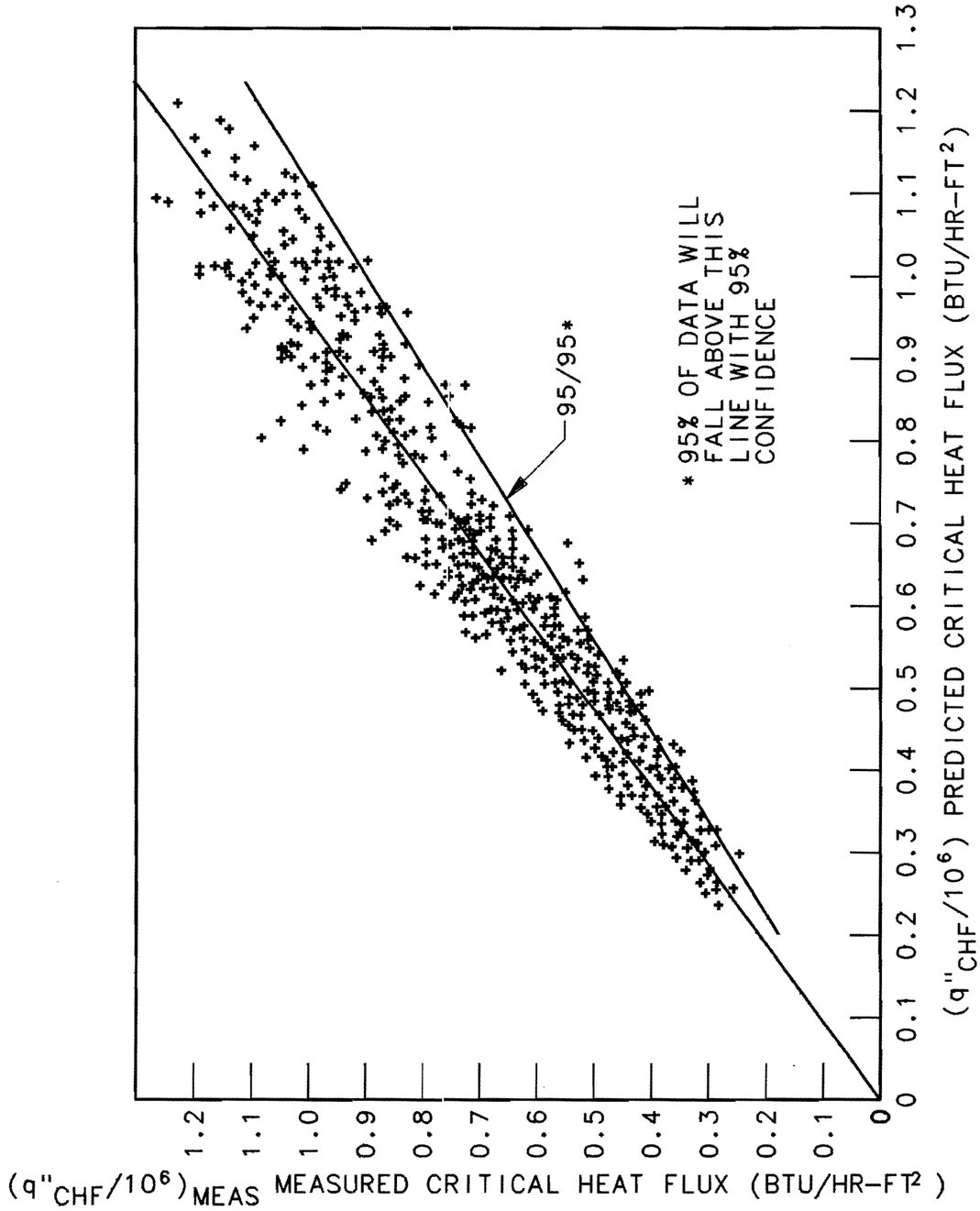


AMENDMENT 73

WATTS BAR NUCLEAR PLANT
FINAL SAFETY
ANALYSIS REPORT

COMPARISON OF MEASURED VERSUS PREDICTED CRITICAL HEAT FLUX FOR THE WRB-1 CORRELATION

FIGURE 4.4-5

**Figure 4.4-5 Comparison of Measured versus Predicted Critical Heat Flux for the WRB-1 Correlation**

**Figure 4.4-6 Deleted by Amendment 73**

**Figure 4.4-7 Deleted by Amendment 73**

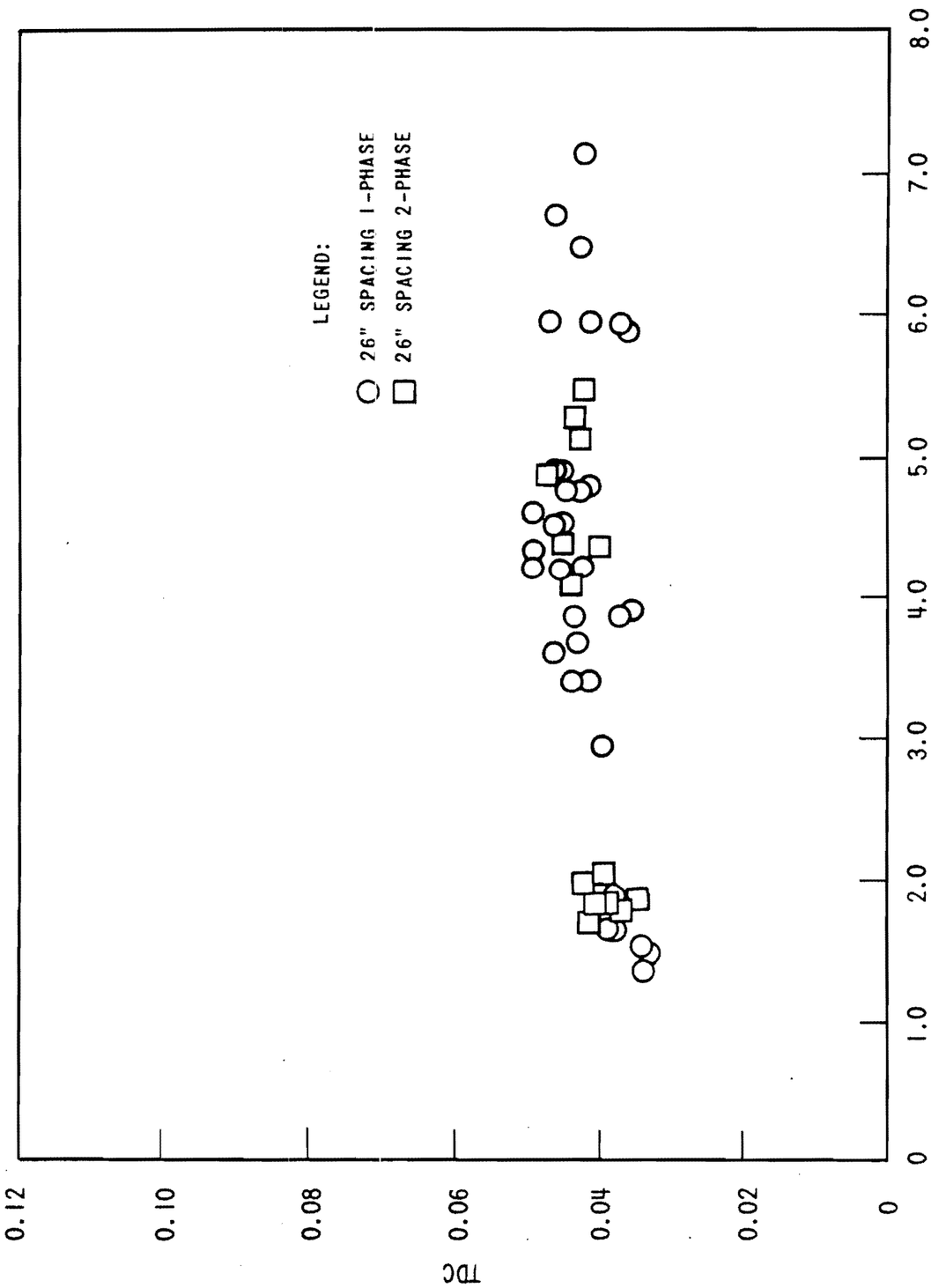


Figure 4.4-8 TDC Versus Reynolds Number for 26" Grid Spacing

**Figure 4.4-8 TDC Versus Reynolds Number for 26" Grid Spacing**

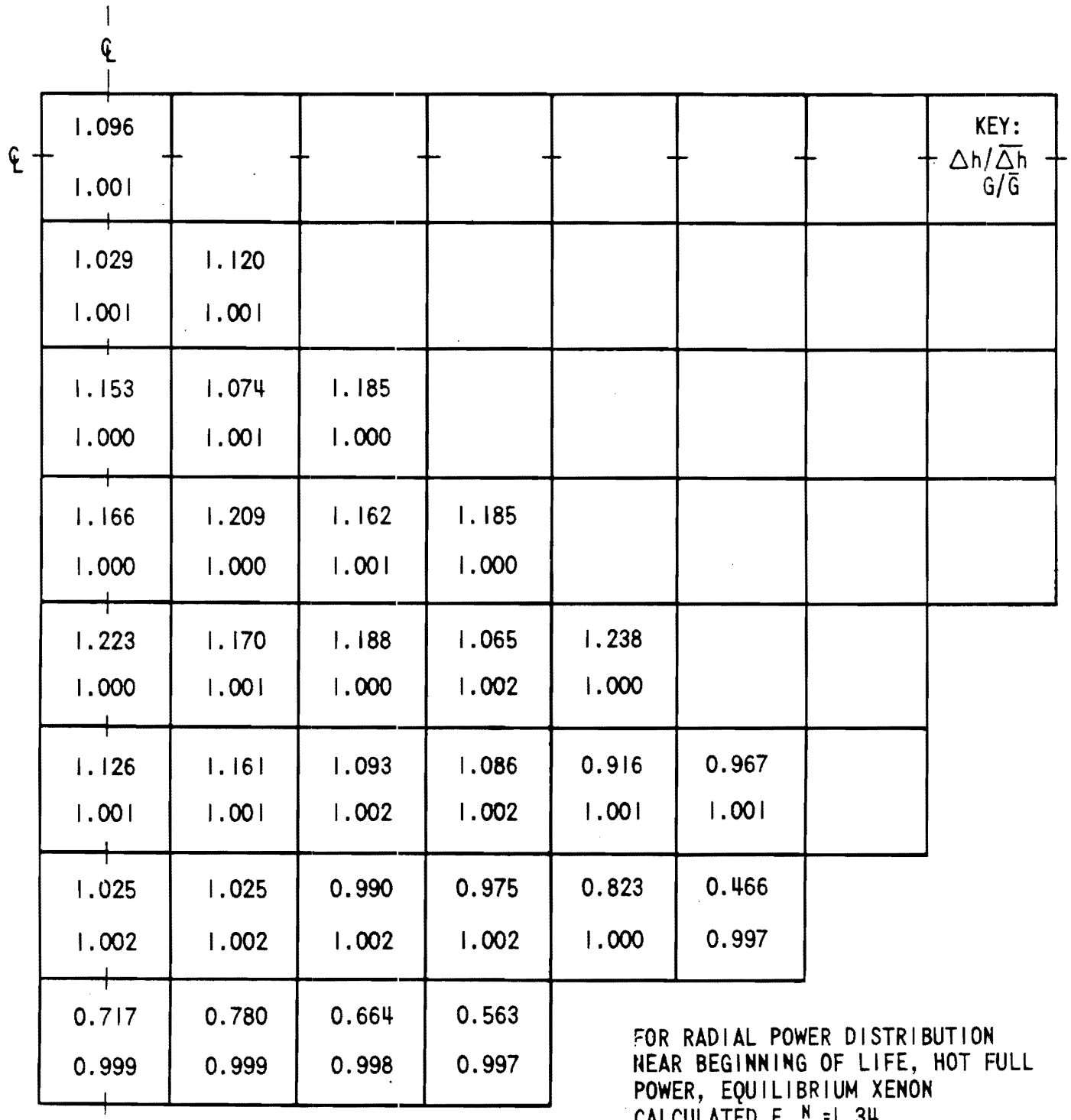


Figure 4.4-9 Normalized Radial Flow and Enthalpy Distribution at 4-Ft Elevation

**Figure 4.4-9 Normalized Radial Flow and Enthalpy Distribution at 4-ft. Elevation**

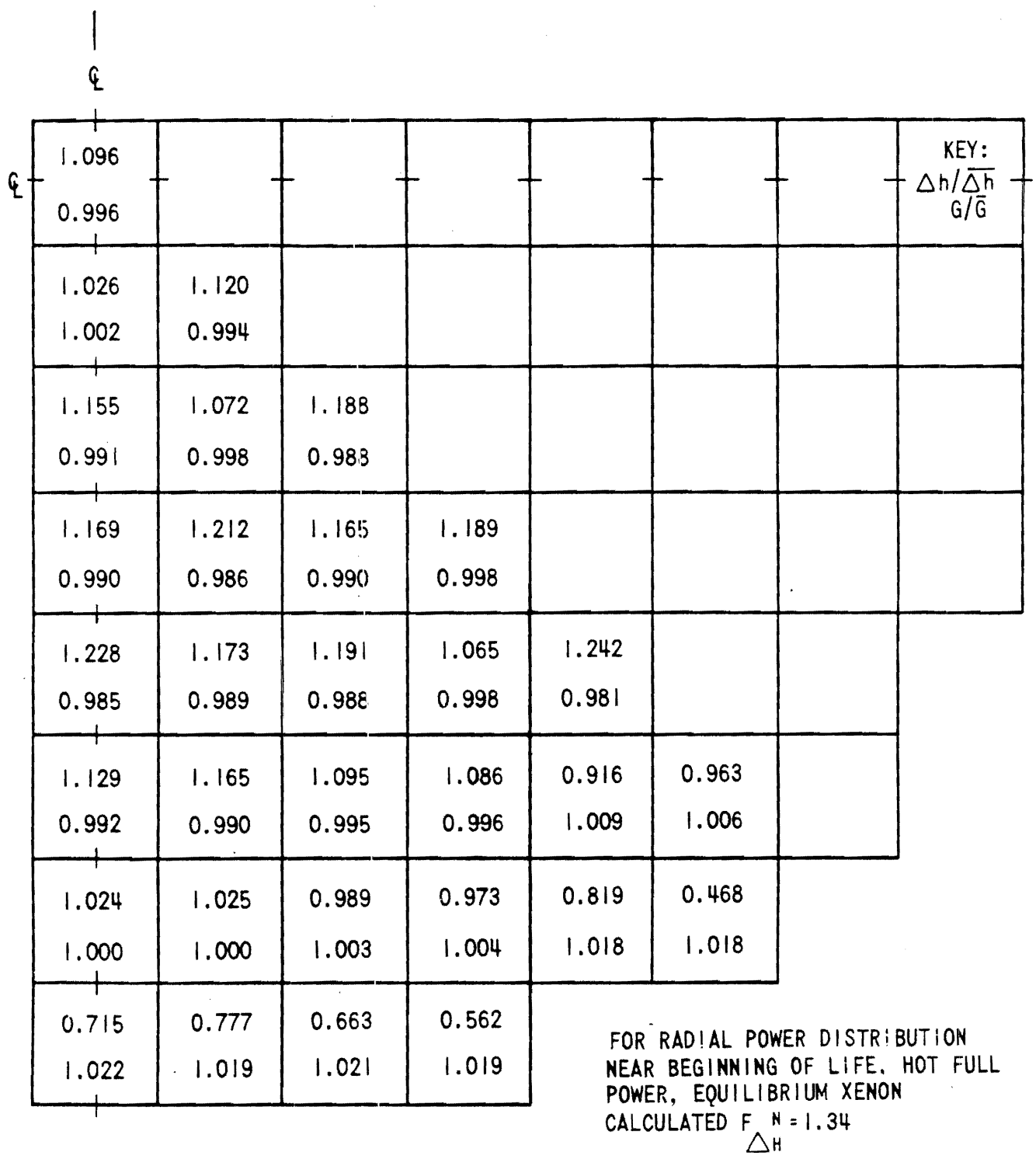


Figure 4.4-10 Normalized Radial Flow and Enthalpy Distribution at 8-Ft Elevation

**Figure 4.4-10 Normalized Radial Flow and Enthalpy Distribution at 8-ft. Elevation**

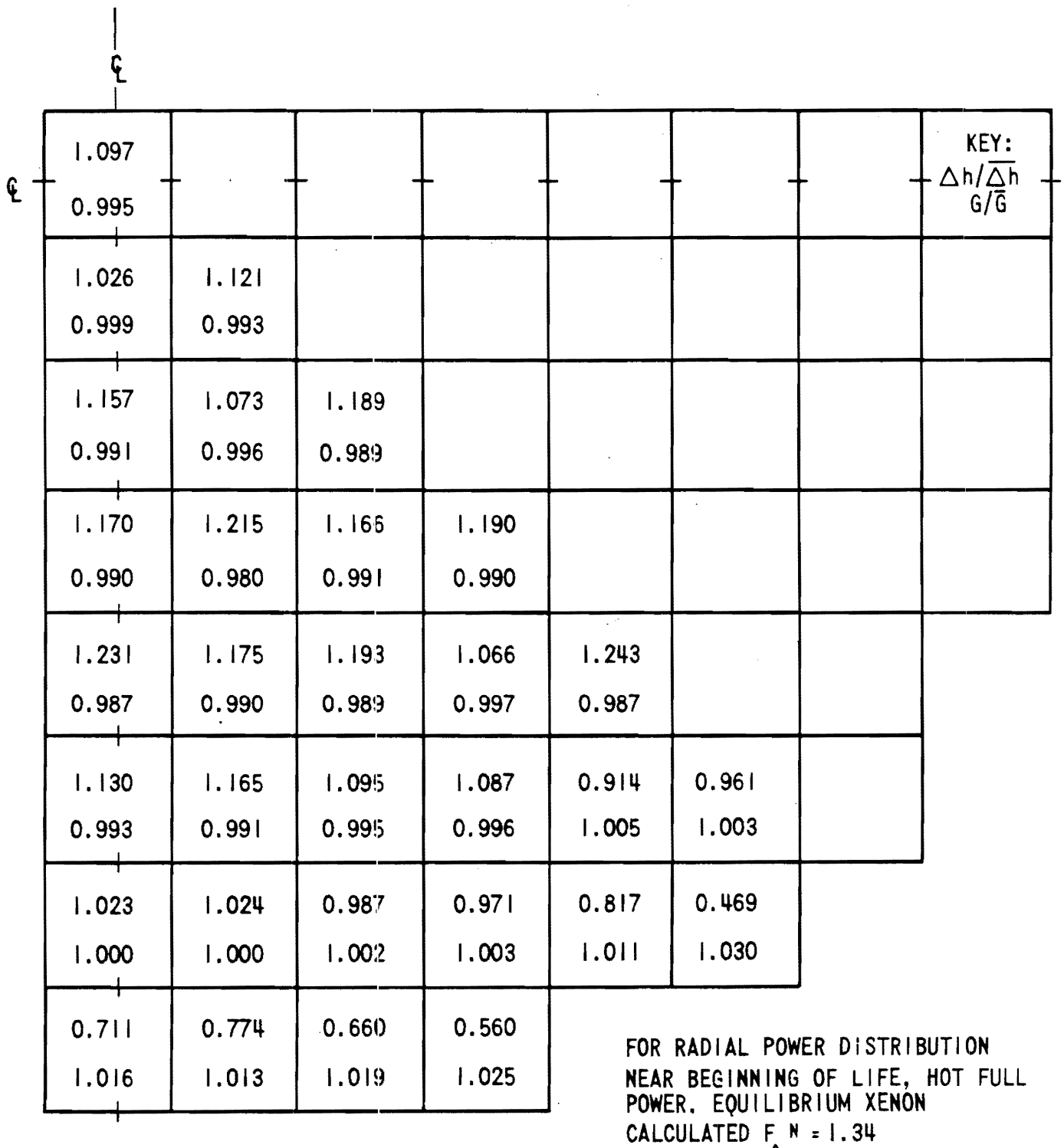


Figure 4.4-11 Normalized Radial Flow and Enthalpy Distribution at 12-Ft Elevation - Core Exit

**Figure 4.4-11 Normalized Radial Flow and Enthalpy Distribution at 12-ft. Elevation Core Exit**

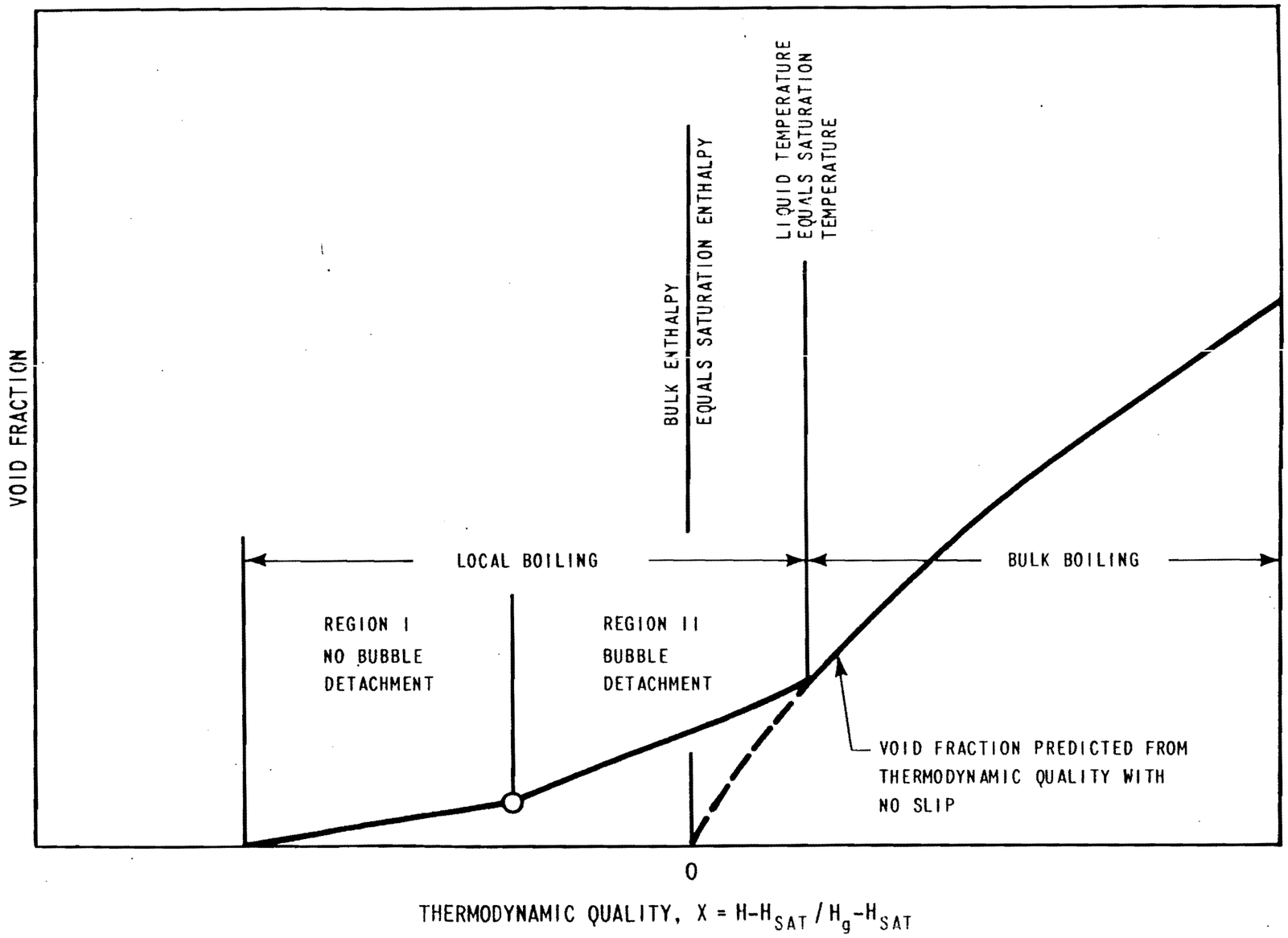


Figure 4.4-12 Void Fraction Versus Thermodynamic Quality H-H$_{SAT}$/Hg-H$_{SAT}$

**Figure 4.4-12 Void Fraction Versus Thenoodynamic Quality H-H $_{SAT}$/Hg-H$_{SAT}$**

**Figure 4.4-13 Deleted by Amendment 73**

**Figure 4.4-14 Deleted by Amendment 73**

**Figure 4.4-15 Deleted by Amendment 73**

**Figure 4.4-16 Deleted by Amendment 73**

**Figure 4.4-17 Deleted by Amendment 46**

**Figure 4.4-18 Deleted by Amendment 46**

**Figure 4.4-19 Deleted by Amendment 46**

**Figure 4.4-20 Deleted by Amendment 63**

**Figure 4.4-21 Deleted by Amendment 63**

10.103-3

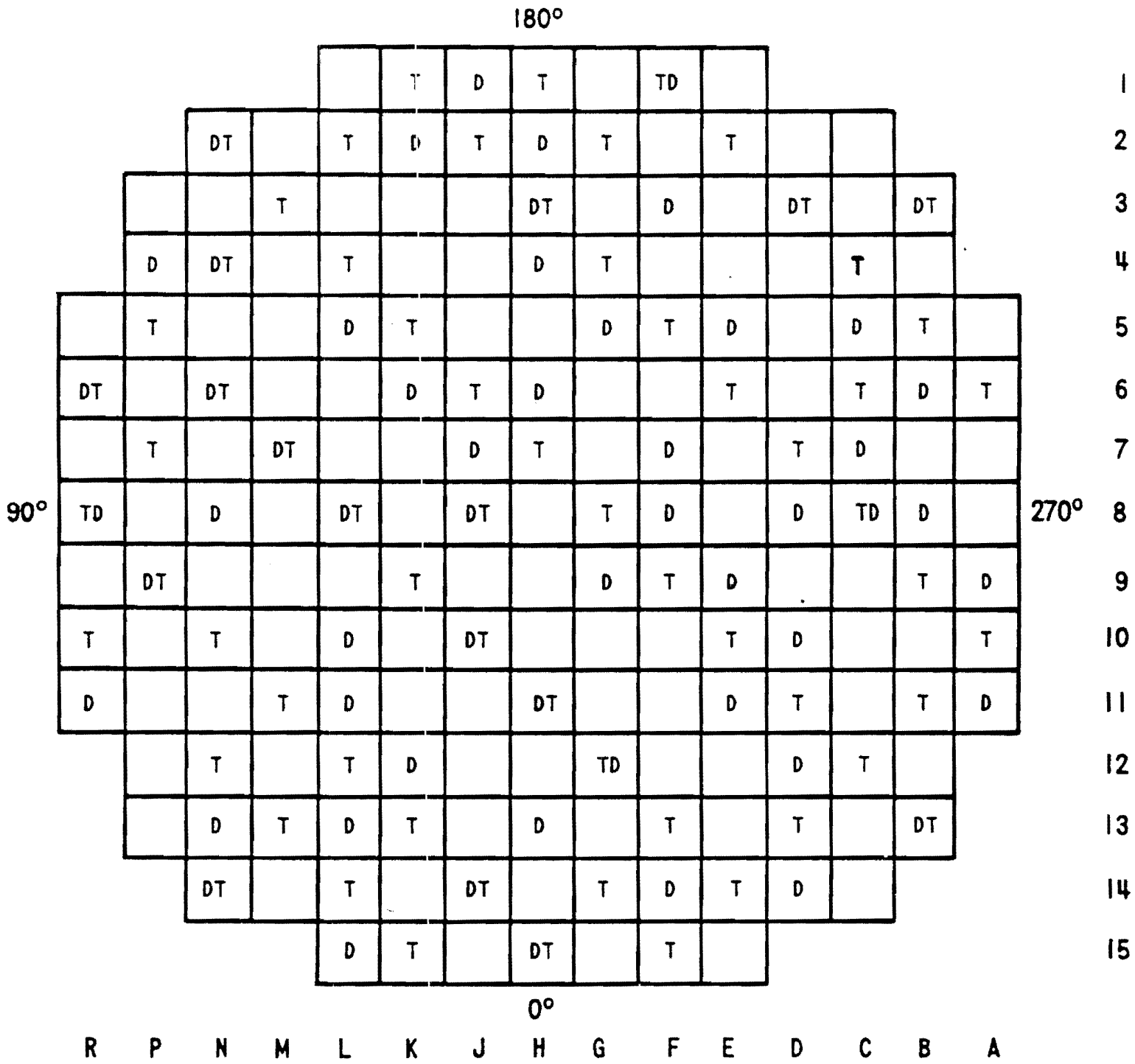


Figure 4.4-22. Distribution of In-Core Instrumentation.

Amendment 63

**Figure 4.4-22 Distribution of In-Core Instrumentation**

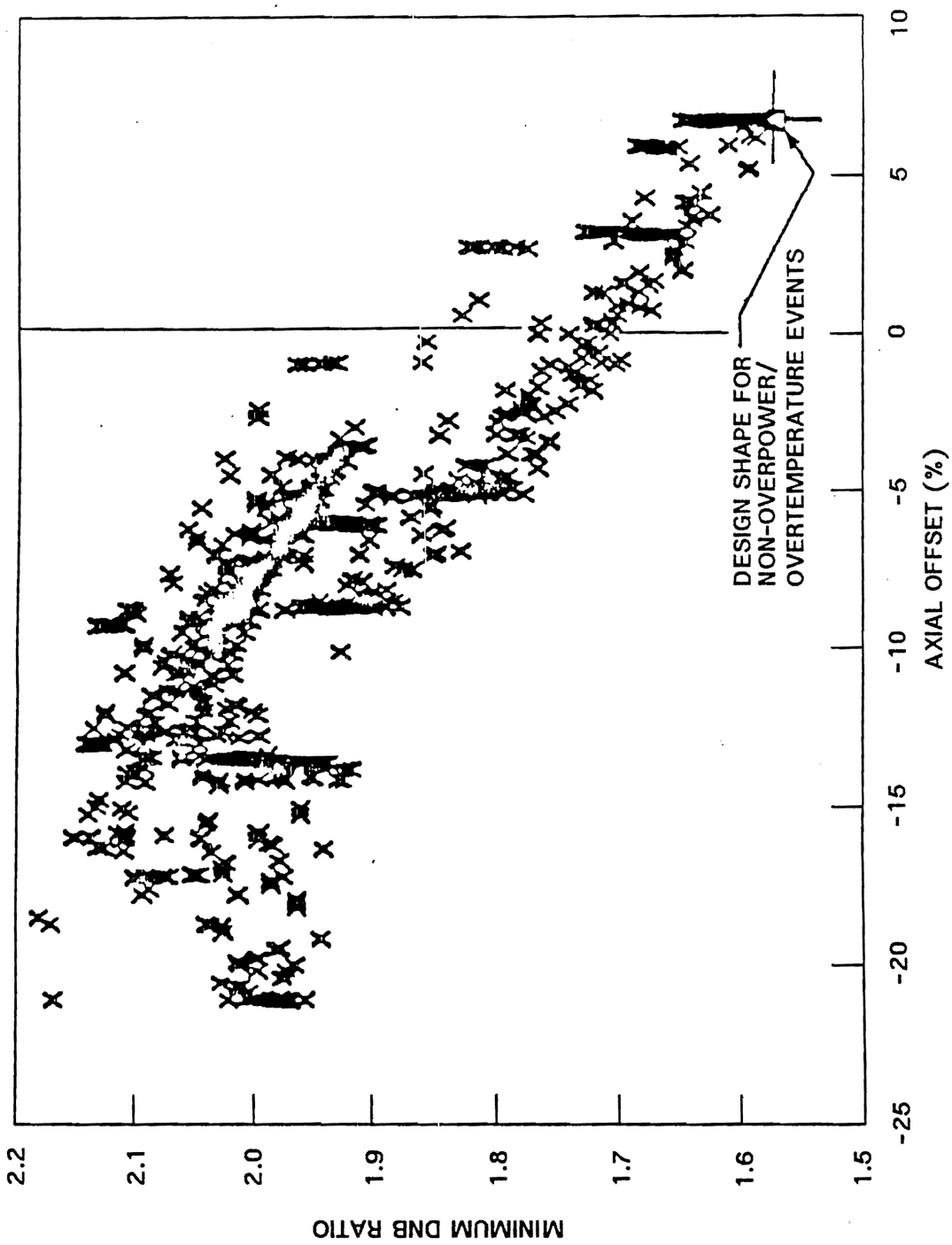


Figure 4.4-23 Typical DNBR Evaluation of 100% Power Shapes at Conditions Representative of Loss of Flow

REVISED BY AMENDMENT 89

WATTS BAR NUCLEAR PLANT
FINAL SAFETY
ANALYSIS REPORT

TYPICAL DNBR EVALUATION OF 100% POWER SHAPES AT CONDITIONS REPRESENTATIVE OF LOSS OF FLOW
FIGURE 4.4-23

SCANNED DOCUMENT
THIS IS A SCANNED DOCUMENT MAINTAINED ON THE WBNP OPTIGRAPHICS SCANNER DATABASE

THIS PAGE INTENTIONALLY BLANK